Contribution of dissolved gases to the understanding of groundwater hydrobiogeochemical dynamics

Eliot Chatton

ANNÉE 2017

THÈSE / UNIVERSITÉ DE RENNES 1
sous le sceau de l'Université Bretagne Loire

pour le grade de

DOCTEUR DE L'UNIVERSITÉ DE RENNES 1

Mention : Sciences de la Terre

Ecole doctorale Ecologie Géosciences Agronomie Alimentation

Eliot Chatton

Préparée à l'unité de recherche UMR6118 – Géosciences Rennes
OSUR – UFR Sciences et Propriétés de la Matière

Contribution of Dissolved Gases to the Understanding of Groundwater Hydrobiogeochemical Dynamics

Thèse soutenue à Rennes le 05/12/2017

devant le jury composé de :

Hélène CELLE JEANTON
Professeur - Université de Franche-Comté/ *rapporteuse*

René LEFEBVRE
Professeur - INRS / *rapporteur*

Emmanuelle PETELET GIRAUD
Chargée de Recherche - BRGM / *examinatrice*

Véronique DE MONTETY
Maître de Conférence – Université de Montpellier / *examinatrice*

Jean-Raynald DE DREUZY
Directeur de Recherche – CNRS / *examinateur*

Werner AESCHBACH HERTIG
Professor - University of Heidelberg / *examinateur*

Luc AQUILINA
Professeur – Université de Rennes 1 / *directeur de thèse*

Thierry LABASQUE
Ingénieur de Recherche – CNRS / *encadrant*

Cher lecteur,

Tu fais désormais parti de la liste plus ou moins longue des personnes qui ont osé tourner les premières pages de ce manuscrit sans avoir été suffisamment repoussées par son titre. Avant d'aller plus loin dans ta lecture, je souhaite tout d'abord ajouter quelques mots pour tenter d'allonger ce manuscrit scandaleusement court vu le travail abattu et plaider pour ton indulgence car, après tout, ce ne sont que mes premiers écrits.

Dans ce qui suit, tu iras peut-être le voir, il sera question de capteurs, d'instruments d'analyse, de données et de modèles dont l'ensemble se trouve lié par une forme d'écriture impersonnelle dans la langue de Shakespeare, qui se trouve, d'ailleurs, être aussi celle des Monty Python. Jusque-là, pas de quoi transpirer de la moustache malgré les nombreuses images en couleur qui viennent égayer le manuscrit.

J'en viens donc à mon propos en affirmant que si la Science n'était faite que de cela, il n'y aurait que des chercheurs/chercheuses masochistes et psychorigides à s'y intéresser. Sans pour autant négliger cette catégorie dans la profession, je profite de ces quelques lignes pour me recentrer sur l'humain et exprimer ma gratitude aux personnes qui ont accompagné et partagé mon aventure pendant ces trois années de doctorat.

Si la recherche académique peut parfois être une usine à gaz (dissous ?) avec ses nombreux travers régulièrement mis en évidence dans la presse, il existe néanmoins en Armorique un petit laboratoire qui résiste encore et toujours, et pourvu que cela dure (dans la bonne humeur !). Là je parle bien sûr de l'OSUR, enfin aussi de Géosciences Rennes et plus particulièrement de l'équipe Transfert devenue l'équipe Eau puis DIMENV@RISC et qui n'a vraiment pas fini de changer de nom à force d'intégration ! Bref, c'est dans cet océan d'entités et d'acronymes qu'il m'a été possible d'apporter ma petite pierre à l'édifice et cela grâce aux conditions humaines, scientifiques, matérielles et financières qui sont réunies à l'OSUR. A ce titre j'aimerais remercier en particulier Jean-Raynald, Olivier, Tanguy et Laurent pour leur soutient, leurs conseils, les échanges passionnants que nous avons pu entretenir ces dernières années. C'est aussi l'occasion de remercier les anciens du labo (les grands frères et grandes sœurs) Nicolas, Clément, Antoine, Maria et Pietro qui nous ont fait profiter avec bienveillance de leurs expériences passées et présentes.

Ce manuscrit n'aurait pas pu voir le jour sans trois projets scientifiques qui m'ont chacun permit de travailler dans de très bonnes conditions. Pour cela je dois remercier les partenaires du projet ANR Stock-en-Socle notamment Luc, Olivier, Jean-Raynald, Jérôme, Lorine pour Géosciences Rennes mais aussi le BRGM avec Hélène, Marie, Emmanuelle, Bruno, Benoît et surtout mes compagnons de terrain Alexandre et Florian. Je suis également très heureux et reconnaissant d'avoir pu prendre part au projet CRITEX qui, comme le manuscrit le démontre, a été une source d'inspiration et un élément structurant dans mon travail de doctorat. Pour cela je remercie tout particulièrement Thierry, Laurent et Jérôme. Enfin je voudrais saluer l'aventure humaine et scientifique passionnante que j'ai eu la chance de partager dans le cadre du projet ANR Coqueiral aux côtés d'Emmanuelle, Lise, Hélène, Géraldine, Wolfram, Gilles, Ricardo, Veridiana, Armelle, Paul, Suzana, Mélissa, Axel, Jonathan, Raiane mais aussi et surtout mes compagnons d'euphorie Guillaume, Rebecca et bien sûr Thierry.

Ce manuscrit n'aurait pas non plus vu le jour sans l'indispensable travail des trop rares techniciens et ingénieurs du labo. Essentiels à la conception et à la mise en œuvre des expériences de terrain et des dispositifs de mesure pendant mon doctorat, ils sont le précieux soutient quotidien de nos projets scientifiques. Au-delà du partage de leurs inestimables compétences et expériences professionnelles je voudrais aussi saluer leurs qualités humaines exceptionnelles qui crée une atmosphère de franche camaraderie au labo, sur le terrain ou même en conf' ou en école d'été. Pour tout cela un énorme merci à Thierry, Virginie, Nicolas, Christophe, Aurélie, MaF, Isa, Patrice, Annick, Catherine et Anne.

Ces cinq dernières années, j'ai pu compter sur le soutien sans failles et les conseils avisés de Luc qui après avoir été mon tuteur de stage m'a permis de poursuivre mon parcours en thèse sous sa direction. J'ai notamment pu évoluer dans mon projet avec son entière confiance et avec l'autonomie et la liberté de cette précieuse « carte blanche » qui m'a été accordé tout en sollicitant son regard expérimenté dans les moments cruciaux. J'ai adoré cette ambiance de travail, cette relation humaine avec mon directeur de thèse et puis aussi ces moments sur le terrain à Guidel, à Naizin ou à Ribeauvillé. Merci Luc !

Thierry ! Ce jeune finistérien poivre-et-sel qui, fidèle à ses origines, vire de plus en plus sur le sel sans rien lâcher sur ses temps au semi. Que dire de Thierry le basque ? TOUT et RIEN en même temps, puisque les plus belle choses ne se disent rarement aussi bien qu'elles se vivent. De manière très motivante et inspirante, ce sont à la fois le dynamisme et la curiosité qui caractérisent le mieux le bonhomme dans ce qui a pu être mon projet de stage ou de thèse. C'est sa contagieuse culture de l'empirisme, de l'expérimentation et de l'observation qui nous a permis de pousser les instruments de labo sur le terrain au-delà des limites imaginées par leurs concepteurs (souvent à leur grande surprise). Grâce à cela, nous nous sommes embarqués au plus proche de la Zone Critique dans de belles aventures qui nous ont permis de progresser rapidement et agréablement vers une meilleure connaissance des milieux aquatiques. Monsieur Thierry, avec son enthousiasme et son incroyable gentillesse a été de la partie tout au long de mon projet de thèse et c'est tant mieux ! Trugarez vras dit Thierry!

Malgré la déco austère, l'obscurité et l'isolation thermique défaillante, le labo a toujours été pour moi une seconde maison où il faisait bon vivre grâce à l'ambiance chaleureuse animé par les jeunes autochtones comme : la cuisine légèrement aillée de La Cheul, la sagesse de La Queue, les bonjours personnalisés de Youss, la modération de Marie, le zèle végétarien de La Bab', la bonne humeur de La Deul, l'exubérance de JPP, la joie de vivre de Jéjé, la bienséance de La Lotte, la philosophie poétique de Dani, la sobriété d'Aurélie, l'intermittence de MaF ou la nervosité de Riccard. Dans cette ambiance, je ne voudrais pas non plus oublier Sarah la grande sœur, Maya la karatékette et les fou-rires dans le bureau des microbiologistes déglingos avec Alix, Kévin, Nathan et Lorine. Et, bien sûr, il y a eu ces terrains, ces confs, ces formations, ces séances de foot, de volley, ces pauses au soleil avec les compères de l'équipe DIMENV notamment Camille, Julien, Loulou, Luca, Madeleine, Nat, Tristan, La Hube, Jean.

Je voudrais remercier tout particulièrement mes compagnons de bureau Hugo, Jonathan, La Boche, Fanfan La Turube, La Burte avec qui nous avons TOUT partagé pour le meilleur et pour le pire durant ce doctorat à commencer par :

- un espace de travail à la déco digne des premiers hôpitaux psychiatriques (accessoires fournis).
- un éventail d'odeurs oscillant entre les vieilles chaussures de sport mouillées qui sèchent depuis plusieurs jours dans un sac plastique fermé ayant transporté le poisson du marché et, les croûtes d'une grande variété de fromages au lait de vache moisissant ensemble pour couvrir le mélange des exhalaisons du sac de chasubles de l'équipe de foot et le fumet du vinaigre qui fuit systématiquement sur le bureau lorsque le pot des cornichons est stocké à l'horizontale.
- les « HOLA QUE TAL?! » assourdissants d'un Hugo fatigué dès 9h30 le matin.
- l'accueil quotidien à partir de 16h30 (14h le vendredi) des joies et des peines des jeunes travailleurs autochtones dans le canapé.
- les arrivées plus ou moins matinales et plus ou moins justifiées de Redj'.
- les entraînements effrénés au jonglage.
- les pauses quotidiennes pain-fromage.
- les emprunts parfois de très longue durée du matériel informatique (chargeur de batterie, souris et clé USB).
- les canulars variés.
- l'accueil quotidien et chaleureux réservé à Dani l'exubérant affamé.
- les nombreux appels téléphoniques.
- les concerts de Mozart et des Beatles à fond les manettes à partir de 18h.
- l'inévitable naufrage sportif de l'En Avant Guingamp.
- les succès, les échecs, les « raz-le-bol », les espoirs quotidiens.

Il y en a avec qui nos chemins se sont suivis avec plaisir tout au long de ces trois années. Je veux bien sûr parler de mon ami Nanard aussi appelé « JérÔÔÔÔÔme !!! » par son directeur de thèse. A la fois comédien hippie, musicien improvisible, philosophe des marchés bio et parfois même géothermicien alternatif à ses heures ; il a pour habitude de déambuler avec sa démarche chaloupée au bureau comme au milieu des champs de génisses fredonnant des petits airs de sa composition très personnelle, laissant au passage tous types de spectateurs ébaubis et captivés par l'énergumène. S'il y a pu avoir sur le terrain des moments de concentration excédentaire, de sérieux superflu ou même de nervosité latente, l'entrée en scène du Nanard, tantôt comique, tantôt distrait, rappelait à toute la galerie que la vie n'est qu'une comédie qui peut se jouer dans n'importe quel décor. Merci Nanardo pour tous ces moments de légèreté au labo, à Ploemeur, à Naizin sous la neige et sous le cagnard et puis à Cargèse !

Il me reste à remercier tout spécialement Diana, curieusement appelée Didi, qui a partagé ma vie de thésard au-delà des horaires du labo et qui n'a jamais cessé de me soutenir jusque dans les moments les plus tendus où j'adorais me mettre à râler. La période de rédaction de nos thèses respectives aurait même presque paru rapide et douce tant il m'a été agréable de partager avec ma généreuse transalcopine ces rires, ces histoires passionnées et ces repas décidément trop riches « pour ne pas perdre le moral ». Merci La Berthe, tu as probablement sauvé ma santé mentale !

Enfin que serait le petit Chatton seul sans le reste de sa portée ?! Je remercie bien sûr ma famille de m'avoir soutenu avec une grande générosité, un humour toujours fin, un optimisme sans faille et surtout avec compréhension et indulgence dans les derniers moments. Merci à tous !

Table of Contents

Chapter I: General introduction

1. The Critical Zone

Emergence of a new concept

In the beginning of the 21st century, the concept of the "Critical Zone" emerged in the United States of America to define the near-surface environment supporting terrestrial life (Ashley 1998; National Research Council 2001). In regard of the overall rising concern related to the impact of global change and human activities on the environment and the inhabitants of the planet, the National Research Council recommended an integrated study of the Critical Zone (CZ) as one of the most compelling research areas in Earth sciences (National Research Council 2001; Giardino & Houser 2015). From a geopolitical perspective, Latour (Latour 2014) emphasised the significance of the notion of CZ for both the scientific community and the layperson. He pointed out the advantage of the CZ concept to deconstruct the planet into much smaller pieces which turns to be essential given the importance of the concept of scale for humans to understand and accept the responsibility for the stewardship of Earth.

Although sometimes debated, the extension of the CZ ranges vertically from the top of the canopy down to the bottom of the aquifers (i.e. freely circulating fresh groundwater) and covers horizontally the entire surface of the continents (Giardino & Houser 2015). The CZ is the very home of the "living planet" (figure 1) where the biosphere, the atmosphere, the hydrosphere, the lithosphere and the pedosphere interact at all scales of space and time, from the atom to the globe and from a second to several million years (Brantley et al. 2007).

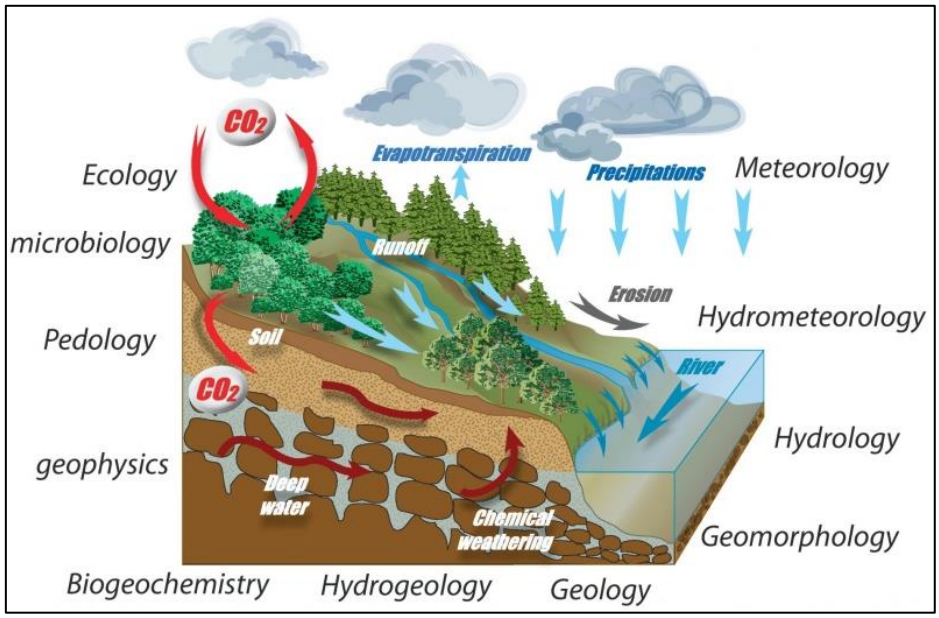

Figure 1: Schematic view of the Critical Zone (https://www.critex.fr/what-is-critex/la-zone-critique-en/).

The structure and dynamics of the CZ evolves in response to natural and anthropogenic forcing that involve a combination of complex biogeochemical-physical processes interconnected at various scales of space and time (figure 1 and 2). Their study requires scientific expertise from a large array of disciplines such as biology, ecology, soil science, hydrology, geology, geochemistry, geomorphology, atmospheric science, and many more (National Research Council 2001). Therefore, the CZ implies to reconsider our way of conducting our research to support a true interdisciplinary science. This CZ science require the integration of various types of observations at all spatial and temporal scales at stake in the CZ which are produced from specifically selected locations i.e. the Critical Zone Observatories (CZOs) (Brantley et al. 2017). Eventually, the emergence of a CZ science relies intrinsically on our innovative capacity in sensing technologies, spatial statistics and modelling (Giardino & Houser 2015). In this project, we will focus our efforts of innovation and observation on a very essential molecule in the CZ: Water.

Water as the link connecting all components of the Critical Zone

On Earth, water can either take the form of a solid, a liquid or a gas. This characteristic is the reason of its ubiquity in the CZ (hydrosphere, biosphere, atmosphere, pedosphere and lithosphere). Besides, the water molecule comprises many other interesting properties that are essential to the functioning of our "living planet". For instance, water is a dipolar solvent with a low viscosity and a high surface tension which makes it a sustainer of life, a weathering agent and vector of matter flows. Furthermore, with a high heat capacity, a high latent heat of vaporisation and a capacity of infrared and ultraviolet rays absorption, water ensures the transport and storage of energy essential in the regulation of the Earth's climate. Therefore, as both a vector and an agent of the flows and storage of energy and matter, water is the central link connecting all components of the CZ (Giardino & Houser 2015; Schuite 2016). As a result, the characterisation and quantification of the flows and stocks of water in the CZ constitute a major scientific challenge.

Among the water resources of the CZ, groundwater is and may have long been one the most important for humans (Döll et al. 2012; Cuthbert et al. 2017). Groundwater reservoirs also referred to as aquifers, supply about one third of the total water withdrawn from the environment for human activities such as agriculture, households and industry (Shiklomanov 2000; Döll et al. 2012). Given its relative isolation from the surface as well as its slow flow in the geosphere, groundwater is the most sustainable water resource in terms of quality. Furthermore, groundwater is the largest freshwater resource on Earth and remains, despite its slow response time, an active component of the hydrologic system(Leung et al. 2011; Aeschbach-Hertig & Gleeson 2012). For instance, groundwater sustains river flows, controls the chemical weathering of rocks and therefore, supplies water and chemical elements essential to maintain the ecosystems (Sophocleous 2002; Giardino & Houser 2015). Also, in the new perspective of CZ science, recent investigations were able to describe the strong interactions of groundwater with

land surface processes and climate change (Leung et al. 2011; Condon et al. 2013). This example shows that the connection of groundwater with the upper components of the CZ is not unilateral (natural groundwater dynamics depends on surface and atmospheric inputs) but leads to more complex exchanges where groundwater also influences the surface and climate responses (figure 1).

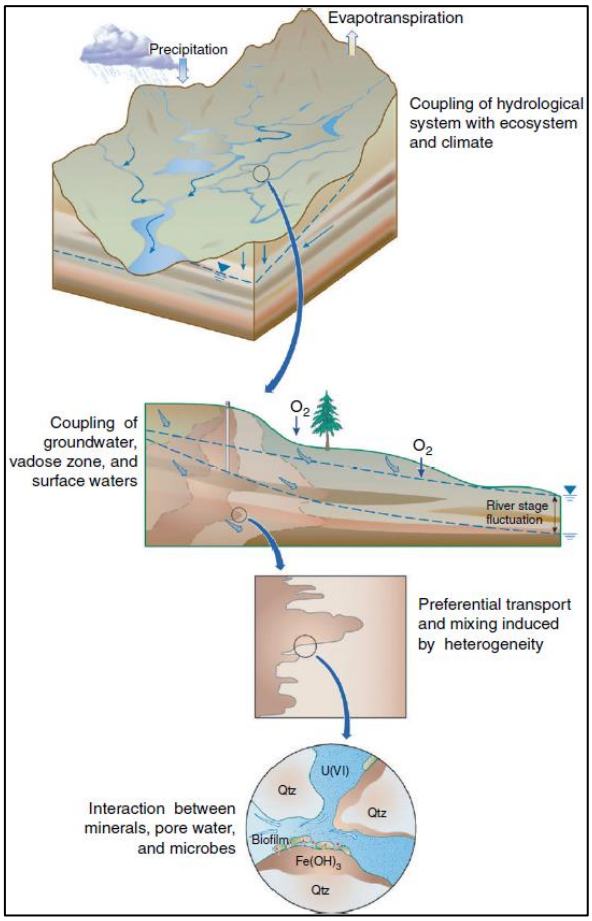

Figure 2: Subsurface flow and transport is impacted by coupled processes and properties that preferentially exert influence over a wide range of spatial scales (Hubbard & Linde 2010).

However, the CZ and thus groundwater resources are already facing expanding threats due to the last decades intensification of human activities and global change (Foster & Chilton 2003; Aeschbach-Hertig & Gleeson 2012; Gleeson et al. 2012). Besides, both the ongoing climate change and the projected human population growth are expected to increase further the pressures on natural resources (Banwart et al. 2013). Recently, large scale studies on groundwater attempted to assess of the global situation (decline of groundwater quantity and quality) and pointed out both the need for global management strategies and the lack of observations that limits our understanding on the dynamic interactions of groundwater with the surface and the atmosphere (Gleeson et al. 2010; Aeschbach-Hertig & Gleeson 2012; Taylor et al. 2012). In this context, the emergence of the CZ science gives the opportunity to observe and understand the life sustaining systems of the planet as a whole for an efficient stewardship of the Earth.

The Critical Zone in this project

This project is part of the CRITEX program consisting in a shared fleet of mobile equipment bringing together different scientific communities (5 research organisations, 21 laboratories) from the French CZOs (SOERE RBV and H+ networks) to develop new monitoring prototypes and to produce holistic observations of the CZ at different scales. Within CRITEX (WP 7.3 & 8.1), this PhD project has been dedicated to the development of an innovative instrument for the continuous monitoring of the dissolved gases of the CZ and to the implementation of interdisciplinary field experiments at different scales for the investigation of groundwater systems.

In this approach, one could find some similarities with the work of James Lovelock before becoming famous for its contribution to the Gaïa hypothesis. Aware of the importance of sensing innovation in environmental sciences, Lovelock's first major contribution to science was the Electron Capture Detector (ECD) for gas chromatography (Lovelock 1958). This technique (figure 3) is the most sensitive for the measurement of halogenated hydrocarbons and is well-known of our scientific community for enabling the measurement of dissolved chlorofluorocarbons and sulphur hexafluoride (CFCs and SF_6) which are used as groundwater dating tools (see section 1.5 and chapter 2).

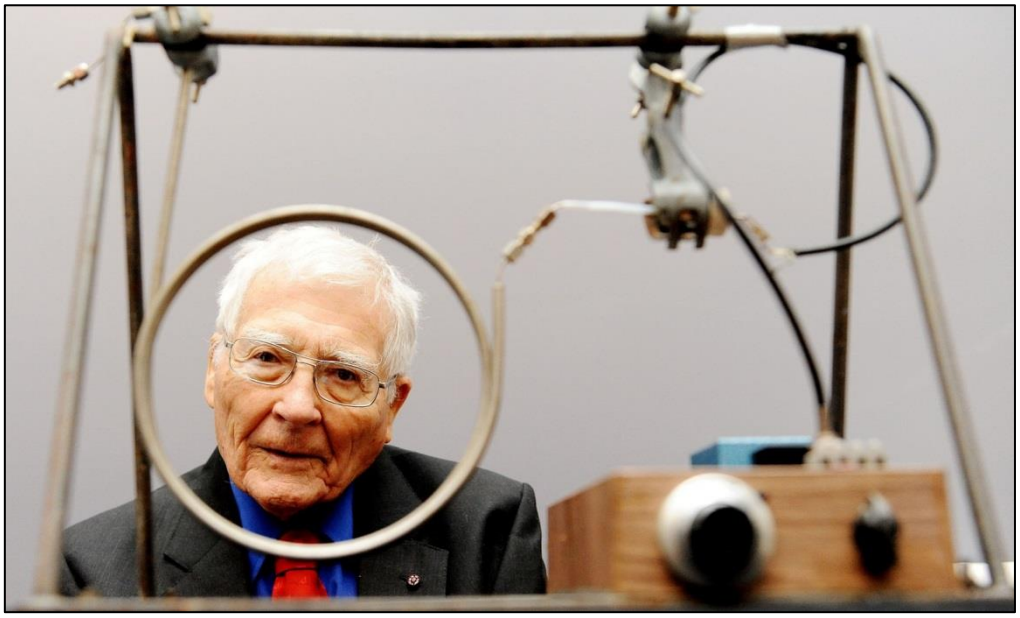

Figure 3: Scientist and inventor James Lovelock, 94, sits with one of his early inventions, a homemade gas chromatography device (https://www.theguardian.com/environment/georgemonbiot/2014/apr/24/james-lovelocks-book-genius-defence).

At the time, Lovelock embarked with his GC-ECD aboard the research vessel *RRS Shackleton* to measure atmospheric gases over the Atlantic Ocean (Montevideo-UK and UK-Antarctica-UK between 1971 and 1972). His distributed observations demonstrated the role of biogenic dimethyl sulphide (DMS) in the global sulphur cycle (Lovelock et al. 1972) as well as the persistence of the CFCs in the atmosphere (Lovelock et al. 1973). The latter ultimately assisted in the Nobel prized discovery of the

role of CFCs in stratospheric ozone depletion (Molina & Rowland 1974). Subsequently, Lovelock's career reached a decisive turning point when he and his colleagues discovered that the DMS produced by oceanic phytoplankton was the major source of cloud condensation and therefore capable of a climate regulation (Charlson et al. 1987). This evidence of biological control of the climate became the basis of the controversial Gaïa hypothesis and eventually lead to the emergence of the Earth Science System (Lovelock 1972; Margulis & Lovelock 1974; Doolittle 1981; Dawkins 2006; Kirchner 1989; Kirchner 2002; Lovelock 2003).

In other words, Lovelock's career started with a gas sensing innovation, continued with distributed atmospheric observations and finally ended with a new conception of Earth sciences that probably favoured the emergence of the CZ concept today. Inspired by James Lovelock's approach, this manuscript is about the first adventures of a wee critical zonist* (in Latour's parlance) committed to the measurement of gases in groundwater as a starting point for the investigation of the CZ.

**May they last as long as Lovelock's.*

2. Groundwater flow and solute transport in porous media

As described earlier, groundwater plays an important part in CZ dynamics and human development. Understanding the origins of its occurrence, movement as well as the factors affecting its quantity and quality appear to be indispensable in order to be able to face the challenges awaiting this threatened resource. In this respect, the present section introduces some useful concepts and definitions so as to establish a basis to the understanding of groundwater systems.

2.1. Hydrodynamic properties of porous media

The existence and flow of groundwater rely intrinsically on the hydrodynamic properties of the geological formations also approached in terms of porous media (Singhal & Gupta 2010). There are three basic types of geological formations: (1) the **igneous formations** formed during the crystallisation of magmas like granites or basalts; (2) the **sedimentary formations** formed at the surface of the Earth consisting either in clastic rocks (fragments of pre-existing rocks) or biochemogenic rocks (formed by the precipitation of ions in solution or composed of dead organisms) such as carbonates, conglomerates, sandstones or clays; (3) the **metamorphic formations** formed by the solid transformation of any rock type (protolith) due to a change in the temperature or pressure conditions resulting in gneisses, schists or marbles for instance.

These geological formations comprise different physical structures affecting their hydrodynamic properties such as the porosity and the permeability (figure 4). The **total porosity** (φ) consists in the ratio of the volume of pore contained in a rock (Vp) on the volume of the rock itself (Vr):

$$\varphi = \frac{V_p}{V_r}$$

[-] (Eq. 1)

In other words, the total porosity gives the proportion of pores in a rock. However, the total porosity does not inform on pore interconnection which is a critical information for the characterisation of reservoirs (a porous formation is not necessarily a good reservoir). For instance, in the perspective of the exploitation of groundwater reservoirs we are only interested in the connected pores (saturated with water). They are either characterised by the **kinematic/effective porosity** (contributing to groundwater flow) or the **diffusive porosity** (where immobile groundwater is accessible by diffusion). In geological formations, the connected porosity can be attributed to the intergranular spaces of the rock matrix (**primary porosity**) and/or the porosity acquired during the rock history (**secondary porosity**: porosity formed by dissolution, fissures, fractures or joints). Geological formations presenting both a primary and a secondary porosity are referred as **double porosity** formations.

a)

Geological formation	φ(%)
Unconsolidated deposits	
Gravel	28–34
Sand	35–50
Silt	40–50
Clay	40–60
Dune Sand	40–45
Loess	45–50
Rocks	
Sandstone	15–30
Limestone, dolomite	10–25
Shale	0–10
Siltstone	5–20
Till	30–35
Dense crystalline rock	0–5
Fractured crystalline rock	5–10
Weathered crystalline rock	20–40
Basalt	5–30

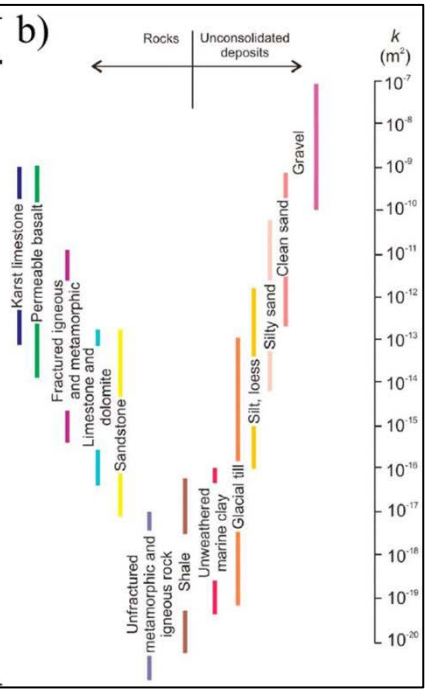

Figure 4: Hydraulic properties of common geological formations: a) porosity φ (modified from Singhal and Gupta, 2010) and b) permeability k modified from (Freeze & Cherry 1979; Gleeson et al. 2011).

The other hydrodynamic property of the geological formations relies in their capacity to conduct fluids and is referred as the **permeability** (k). Expressed in darcys [L^2], the permeability is a characteristic of the porous media which depends only on the structure and connectivity of the porosity. According to their permeability, geological formations are classified either as **aquifers** (permeable formations saturated with water i.e. groundwater reservoirs), **aquitard** (formations with a low permeability) or **aquiclude** (formations with a very low permeability). Subsequently, an aquifer overlain and underlain by a confining layer (aquiclude or aquitard) is referred as a **confined aquifer** where the groundwater

pressure is greater than the atmospheric pressure (figure 5). On the other hand, an aquifer exposed to the surface and underlain by a confining layer is denoted as an **unconfined aquifer** (Singhal & Gupta 2010). Unconfined aquifers are not totally saturated with groundwater. Therefore, these aquifers comprise a **water-saturated zone** overlain by an **unsaturated zone** and separated by a surface at atmospheric pressure called the **water-table**. Determining the distribution of groundwater pressure in confined or unconfined aquifers is important to understand groundwater movements in the subsurface. The evaluation of the groundwater pressure in a well (piezometer) consists in the measurement the **piezometric/hydraulic head** h [L] which is the groundwater elevation above a geodetic datum.

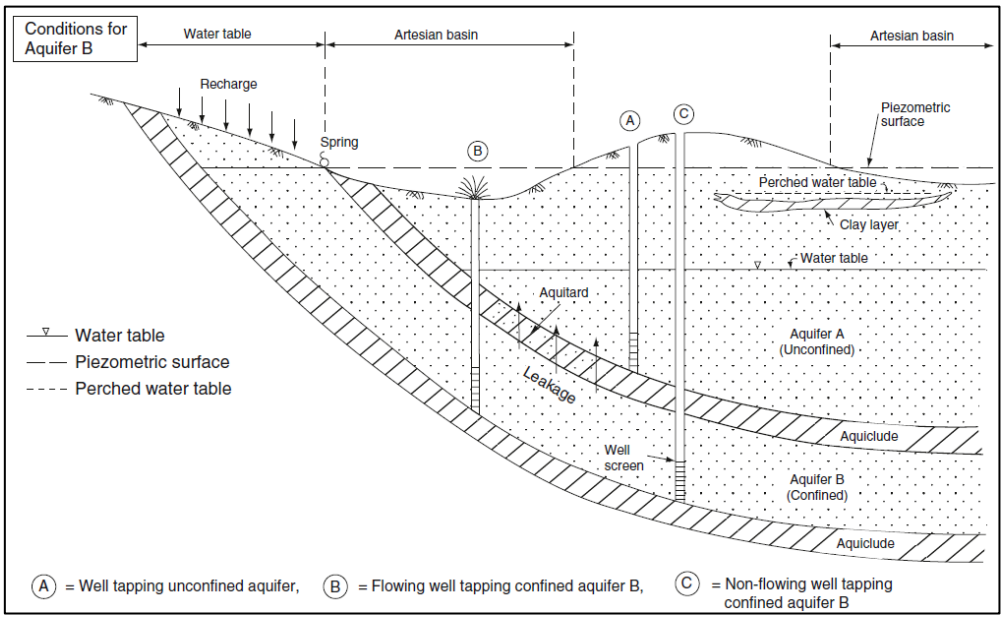

Figure 5: Types of aquifers (Singhal & Gupta 2010).

This section exposed how the porosity and permeability of the subsurface enable water to enter and be stored in some geological formations called aquifers. It is now interesting to focus our attention on the mechanisms controlling groundwater dynamics in these porous media.

2.2. Groundwater flow in porous media

In 1856, Henry Darcy observed that the water flow (Q) through a porous medium (a sandbox in Darcy's experiment) was proportional to the **hydraulic gradient** and to a constant called the **hydraulic conductivity** related to the permeability (equation 2). The hydraulic gradient refers here to the linear hydraulic head loss while the hydraulic conductivity is a measure of the capacity of a porous medium to conduct fluids depending both on the medium and fluid properties. Therefore, the description of macroscopic fluid flows in porous media comes from Darcy's law presented in equation 3 below (Darcy 1856):

$$K = \left(\frac{\rho \cdot g}{\mu}\right) \cdot k$$

$[L^2.T^{-1}]$ (Eq. 2)

$$Q = -K \cdot A \cdot \nabla h$$

$[L^3.T^{-1}]$ (Eq. 3)

Where Q is the fluid flow $[L^3.T^{-1}]$, K is the hydraulic conductivity $[L.T^{-1}]$, A is the cross sectional area of the porous media perpendicular to the fluid flow $[L^2]$, ∇h is the hydraulic gradient [-], ρ is the fluid volumetric mass density $[M.L^{-3}]$, g is the gravitational acceleration $[L.T^{-2}]$, μ is the fluid dynamic viscosity $[M.L^{-1}.T^{-1}]$ and k is the permeability $[L^2]$. It is important to note that Darcy's law applies under some conditions that are often but not always met in natural porous media. This empirical law applies for the laminar flow (for a sufficiently low flow or a sufficiently viscous fluid) occurring in a single fluid saturated porous medium which is sufficiently homogeneous (same properties everywhere) and isotropic (properties do not depend on the direction). In this case, it is possible to define a **Representative Elementary Volume** (REV) which refers to the smallest portion of the porous medium where heterogeneities do not significantly affect its average hydrodynamic properties.

At the **catchment** (drainage basin) scale, Darcy's law describes groundwater flow from areas with high hydraulic heads (high groundwater pressure) to areas with low hydraulic heads. In natural conditions, hydraulic heads generally follow the topography of the catchment. Therefore, the elevated zones of a catchment consist in **recharge areas** where water (usually rainfall) infiltrates the soil and the unsaturated zone to reach the saturated zone. In these areas groundwater movements are structured in downward diverging flows. On the contrary, **discharge areas** consist in the low-elevation zones of a catchment where groundwater leaves the aquifer to reach the surface (wetlands, rivers, lakes, ocean). In these areas groundwater movements are structured in upward converging flows. This general structuration of groundwater flows in water catchments leads to a more or less important **partitioning of flow paths** from the local to the regional scale (figure 6). This partitioning intensifies with the observation scale and the heterogeneity of porous media.

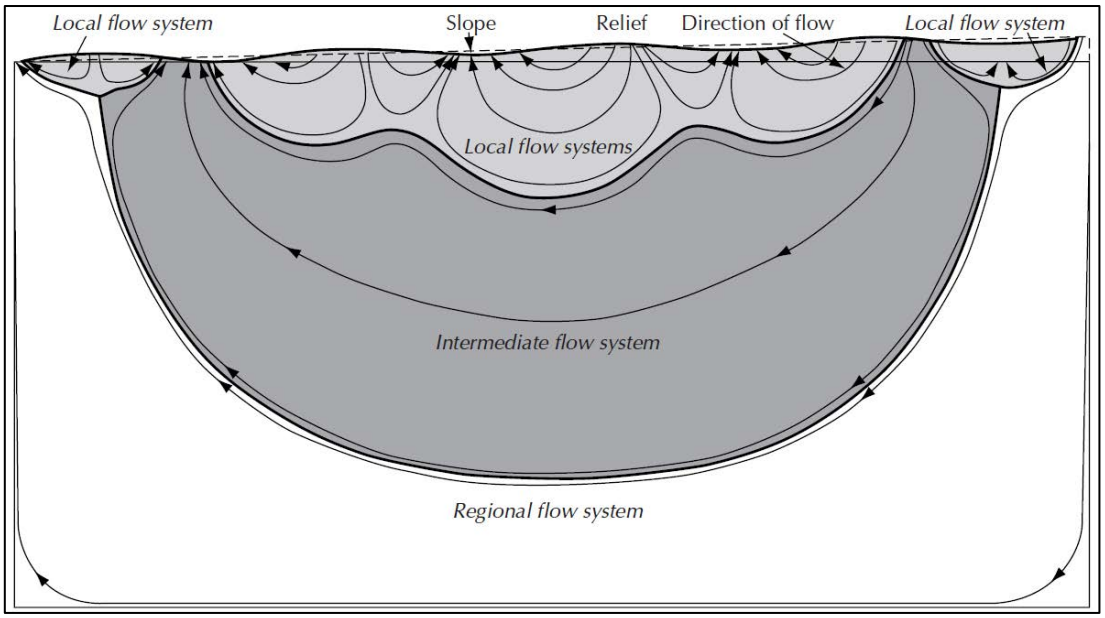

Figure 6: Partitioning of groundwater flow paths (Fetter 2014).

Groundwater flows are generally slow and imply relatively large resource turnover times (from decades to thousands of years or more) which require proper groundwater management practices to ensure the resource sustainability. Therefore, understanding groundwater flows in an aquifer is important in the perspective of an exploitation of groundwater resources. For instance, determining the influence of the pumping rate is essential as an overexploitation of the aquifer would lead to the drop of piezometric levels (aquifer drying) and could potentially turn discharge areas into recharge areas (potentially conducting to groundwater contamination or salinisation) thus threatening the sustainability of both the quantity and quality of the groundwater resource.

2.3. Solute transport in porous media

During its movement through aquifer formations groundwater transports solutes (dissolved substances) and small particles such as chemical elements coming from soil and rock weathering, dissolved atmospheric gases or micro-organisms. This transport capability is a vector of life for ecosystems but also a vector of contamination. The latter has received great attention in the perspective of the remediation of contaminated sites (Fetter 1993), the exploitation of insular or coastal groundwater resources (Vengosh & Rosenthal 1994; Werner et al. 2013; L. Cary, Petelet-Giraud, et al. 2015) or the geological storage of carbon dioxide or nuclear waste (de Marsily et al. 1977; Neretnieks 1980; Neretnieks & Rasmuson 1984; Moreno & Neretnieks 1993a; Kharaka et al. 2006; Juanes et al. 2010). The study of the combined physical and biogeochemical processes controlling the solute transport is therefore a major stake. In this respect, the present section exposes the main transport processes encountered in porous media.

The most efficient solute transport process is called **advection** and occurs when the solute is driven by fluid flow. The advective transport of solute can be described by the mass balance equation 4 below:

$$\frac{\partial C}{\partial t} = -v \cdot \nabla C$$

(Eq. 4)

Where C is the solute concentration [$M.L^{-3}$], ∇C is the concentration gradient [$M.L^{-2}$], t is the time [T] and v is the pore fluid velocity [$L.T^{-1}$].

During the advection of a solute in porous media, the pore fluid velocity fluctuates around the average velocity due to microscopic heterogeneities (figure 7) and/or macroscopic heterogeneities (nature and structure of subsurface formations, contrasts of permeability) affecting the velocity field. These fluctuations lead to the progressive solute spreading and is called the **kinematic/mechanical dispersion** (D_m). The latter depends on the average pore fluid velocity v and on the **dispersivity** α [L] which is the characteristic length of the porous medium heterogeneities (equation 5). The mechanical dispersion is commonly described by the fickian law below (equation 6):

$$D_m = \alpha \cdot v$$

[$L^2.T^{-1}$] (Eq. 5)

$$\frac{\partial C}{\partial t} = D_m \cdot \nabla^2 C$$

(Eq. 6)

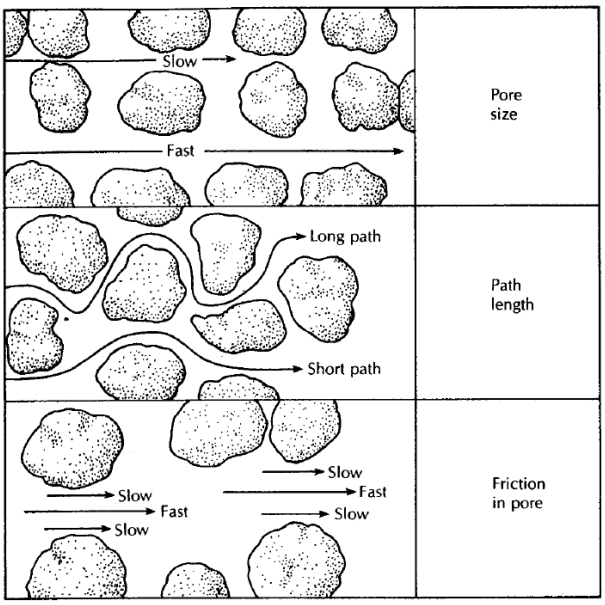

Figure 7: Factors producing mechanical dispersion at the pore-scale (Fetter 2014).

In resting or flowing fluids, solutes spread and migrate from concentrated areas to less concentrated areas. This process of homogenisation of the concentration is called **molecular diffusion** and occurs in the presence of a concentration gradient. The diffusion is independent of the flow velocity and its role in solute transport is significant especially in weakly permeable media.

The efficiency of the diffusion process in free water depends on the diffusivity of the solute which is measured by the diffusion coefficient. This coefficient ranges from around 5×10^{-10} to 1×10^{-8} m^2/s depending both on the considered solute and the water temperature. In porous media, the diffusion process is (around ten times) slower as the solute needs to follow longer migration paths due to the shape of the porosity measured by κ the geometric factor. Therefore, the diffusion coefficient of a solute in a saturated porous media is denoted as the effective diffusion coefficient D_e which depends on the free water diffusion coefficient D_w as well as the tortuosity τ and the constrictivity δ_D of the porosity (equation 7).

$$D_e = D_w\left(\frac{\delta_D}{\tau^2}\right) = D_w \cdot \kappa$$

$[L^2.T^{-1}]$ (Eq. 7)

The diffusive transport of a solute in a porous media is described by the equation 8 below (second Fick's law):

$$\frac{\partial C}{\partial t} = D_e \cdot \nabla^2 C$$

(Eq. 8)

In groundwater flows, the processes of mechanical dispersion and molecular diffusion cannot be separated and are usually gathered in a single process called the **hydrodynamic dispersion** D $[L^2{*}T^{-1}]$ and described in equation 9 and 10:

$$D_L = \alpha_L \cdot + D_w \cdot \kappa$$

$[L^2.T^{-1}]$ (Eq. 9)

$$D_T = \alpha_T \cdot + D_w \cdot \kappa$$

$[L^2.T^{-1}]$ (Eq. 10)

Where the subscripts L and T used for the hydrodynamic dispersion and the dispersivity refer respectively to their longitudinal (parallel to the flow direction) and transversal (perpendicular to the flow direction) components in anisotropic porous media.

Advection, mechanical dispersion and molecular diffusion therefore result in the movement of the solutes with groundwater and their spreading along flow path. The aforementioned solute transport

processes can be combined in the Advection Dispersion Equation (ADE) to describe the conservative transport of a solute in a porous media where Darcy's law applies (equation 11, figure 8).

$$\frac{\partial C}{\partial t} = D \cdot \nabla^2 C - v \cdot \nabla \mathrm{C}$$

(Eq. 11)

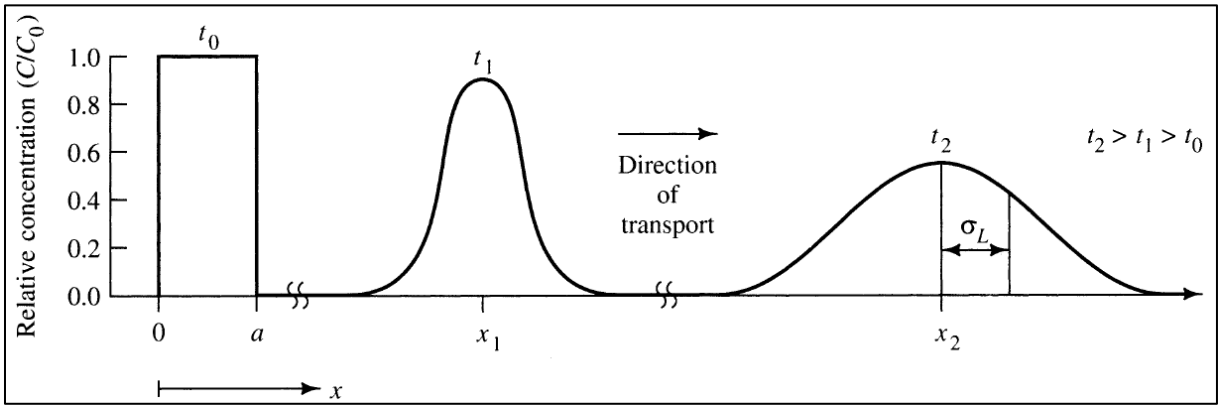

Figure 8: Transport and spreading of a solute slug with time due to advection and dispersion (Fetter 1993).

Additionally, physical processes such as **density effects** (buoyancy effects) can, in some cases, affect significantly groundwater flow as well as conservative and reactive solute transports (Istok & Humphrey 1995; Becker 2003). For instance, many problems of groundwater contamination (with Non-Aqueous Phase Liquids, NAPLs, figure 9a) or salinisation (with seawater or brines, figure 9b and 9c) must couple density effects and fluid flow to predict solute spatial distribution and migration either at the top of the saturated zone or at the bottom of the aquifer according to the contrasts of fluid densities.

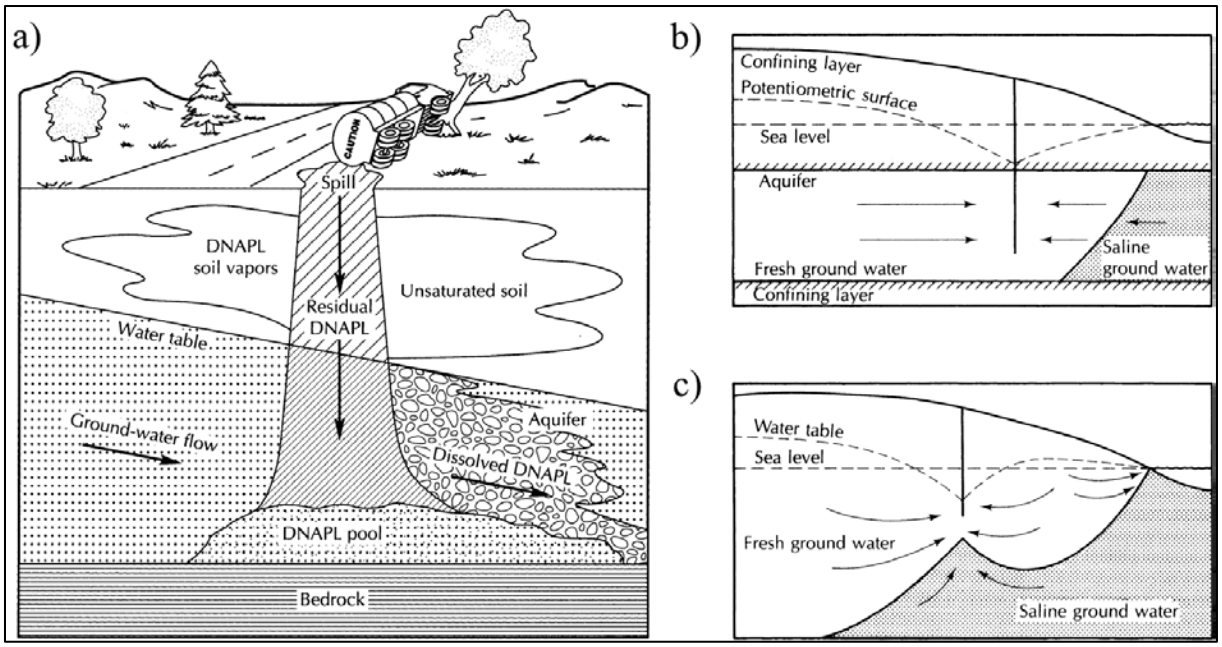

Figure 9: Groundwater transport of dense solutes a) Dense Non-Aqueous Phase Liquids (DNAPLs) sink to the bottom of an aquifer when a spill occurs. The same behaviour applies for saline groundwater when pumping in coastal confined b) and unconfined aquifers modified from (Fetter 2014).

In groundwater, some solutes are inert with respect to biogeochemical processes. These solutes are referred as **conservative elements** and their transport can be described by the ADE. On the contrary, many solutes are commonly involved in various biogeochemical reactions occurring during their transport. Therefore, the transport of these **reactive elements** in porous media cannot be described by the ADE alone and additional reactive terms might be needed.

2.4. Hydrobiogeochemical processes affecting solute transport

Groundwater quality is the result of many different biogeochemical reactions integrated over groundwater flow paths. These reactions can be biotic or abiotic (whether the reaction is mediated by microorganisms or not), slow or fast (relative to groundwater flow), reversible or irreversible, homogeneous or heterogeneous (whether the reaction takes place within the dissolved phase alone or involve also a solid phase i.e. minerals) as well as superficial or classical (heterogeneous reactions occurring at the surface of the solid phase or modifying its extent). Biogeochemical processes result either in the **retardation** (compared to the transporting groundwater), the partial/total **attenuation** or the **production** of solutes depending on the reaction nature (Fetter 1993).

For instance, **sorption** reactions are heterogeneous and involve either the reversible partitioning of the solute between the dissolved phase and the surface of the solid phase (**adsorption** or **ion exchanges**) or the incorporation of the solute in rock surfaces or micro-organisms (**chemisorption** or **absorption**). Sorption reduces the solute velocity in the aquifer and complicates contaminated site remediation.

Some solutes called **radionuclides** (parent nuclei) undergo **radioactive decay** resulting in the decrease of their concentration along groundwater flow path (IAEA 2001). The extent of the concentration decline depends on the radionuclide half-life (period of time in which half of the radionuclides have disappeared). For instance, radioactive decay starts to be significant in the radionuclide transport (a decay of 5%) when its half-life is about fifteen times its residence time in the groundwater system. On the contrary, some solutes called **radiogenic elements** (daughter nuclei) are produced through **radioactive growth**. This reaction can result in an increase of the solute concentration along groundwater flow path if the formed radiogenic elements are stable (no decay). Otherwise, the evolution of solute concentration depends on the equilibrium between the processes of radioactive growth and decay (IAEA 2001).

Solute transport can also be affected by **association and dissociation reactions** consisting in the dissociation of ionic bonds and the formation and exchange of ions along groundwater flow path (Clark 2015). For instance, these processes can consist in **acid-base reactions** involving water (H_2O), carbonic acid (H_2CO_3), sulfuric acid (H_2SO_4), nitric acid (HNO_3) or organic acids (like acetic acid, CH_3COOH). Association and dissociation reactions also include the **dissolution or precipitation of soluble minerals** (carbonates or evaporites) such as calcite ($CaCO_3$), dolomite ($CaMg(CO_3)_2$) gypsum ($CaSO_4$,$2H_2O$) or halite (NaCl). The bipolar nature of water and its capability of autoprotolysis ($2H_2O \rightleftharpoons OH^- + H_3O^+$) make water a good solvent responsible of the reactions of **ion hydration** and **ion hydrolysis** (formation of aqueous complexes with ions in solution). The last group of association and dissociation reactions consist in the **incongruent dissolution** of minerals (also called mineral hydrolysis) leading to the production of both solutes and secondary mineral phases. For instance, these reactions are involved in the **weathering** of silicate minerals such as the hydrolysis of feldspars ($(K,Na,Ca)(Si,Al)_4O_8$) which produces cations (K^+, Na^+ or Ca^{2+}) and kaolinites ($Al_2Si_2O_5(OH)_4$). Association and dissociation reactions can result in the retardation of the solute and can substantially affect aquifer porosity and permeability.

At last, solute transport can be affected by **redox reactions** (reduction and oxidation solutes or minerals) consisting in a biotic or abiotic exchange of one or more electrons between a reducer (**electron donor**) and an oxidant (**electron acceptor**). These reactions rely on the availability of redox couples (oxidant/reducer) such as O_2/H_2O for the reaction of aerobic respiration which consist in the oxidation of organic matter (CH_2O) by oxygen (O_2) to produce carbon dioxide (CO_2) and water (H_2O). As aerobic respiration, redox reactions produce output of energy that can be exploited by the microorganisms of the groundwater for their metabolism and growth. Nonetheless, many other redox reactions can take place in absence of oxygen (anaerobic environments) or organic matter (autotrophic reactions) and their successive occurrence depends on the electromotive potential of each of the couples (Clark 2015). As a result, some microorganisms possess a metabolic flexibility and thus a veritable adaptation capacity enabling them to use several electron acceptors (O_2, NO_3^-, MnO_2,

FeOOH, SO_4^{2-} or CO_2) for their respiration. In groundwater systems, redox conditions vary along flow path and depth due to the successive consumption of electron acceptors as groundwater isolates from the surface. This phenomenon is summarised in figure 10 as a theoretical vertical redox sequence in aquifers. Similarly to association and dissociation reactions, redox reactions can result in the retardation of the solute and can substantially affect aquifer porosity and permeability (mineral oxidation, biotic and abiotic precipitation, biofilm growth).

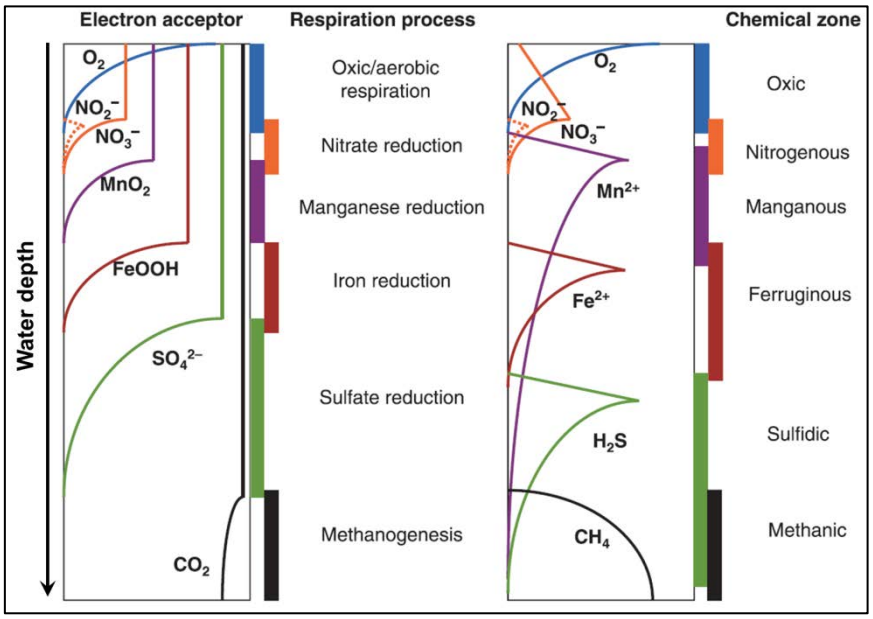

Figure 10: Vertical redox sequence in aquifers modified from (Canfield & Thamdrup 2009).

Biogeochemical reactions exert therefore a significant control on reactive solutes transport (retardation, attenuation, release) but also on the groundwater flow itself (precipitation, dissolution, biofilm growth).

Groundwater flow and solute transport in porous media are therefore the result of a combination of geological, physical, chemical and biological processes taking place in a continuum of scales of space and time. These processes are becoming quite well understood in relatively homogeneous media. However, some porous media such as fractured crystalline rocks are characterised by strong heterogeneities which complicate considerably the interactions between the processes controlling groundwater flow and solute transport. Among porous media, the characterisation of fractured geological reservoirs is therefore considered as one of the greatest challenge for hydrogeologists (Faybishenko et al. 2000).

3. Fractured geological reservoirs

Crystalline rocks encompass both igneous and metamorphic geological formations and form the basement of the Earth's crust. Mostly formed of plutonic rocks (granitoids), this crystalline basement

occurs in about 35% of the continents surface (Amiotte Suchet et al. 2003) and in some regions outcrops on most of the territory including Eastern Canada, Eastern South-America, Western Australia, India, Scandinavia and many regions of Africa (figure 11).

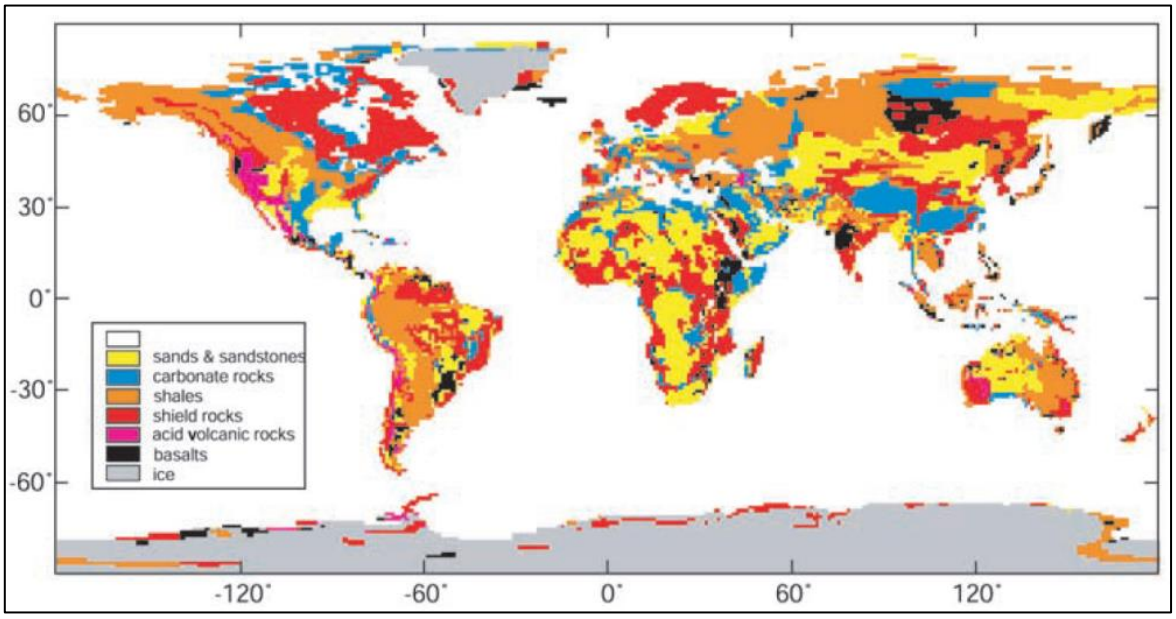

Figure 11: Present-day exposures of the six major rock types on land area (Amiotte Suchet et al. 2003).

Over the last decades, fractured geological reservoirs received great attention in the perspective of the exploitation of oil resources (Petford & Mccaffrey 2003), of geothermal energy (Aquilina et al. 2004), the storage of nuclear waste (de Marsily et al. 1977; Neretnieks 1980; Neretnieks & Rasmuson 1984; Neretnieks 2013; Moreno & Neretnieks 1993a) as well as the exploitation of groundwater resources (Touchard 1999; Roques 2013; Guihéneuf 2014). For all these applications, it is essential to identify the structures and hydrodynamic properties that enable the storage and the circulation of fluids in these fractured geological reservoirs.

Crystalline rocks and more particularly plutonic rocks are formed during the deep and slow crystallisation of magmas which favours the formation of very joined centimetre-sized minerals (phenocrysts). As a result, crystalline rocks possess a very weakly permeable matrix (low primary porosity) of the order of 0.5% for granites (Ohlsson & Neretnieks 1995). Over their geological history, crystalline rocks subjected to mechanical stresses acquire a second porosity induced by the formation of fractures. This secondary porosity is typically structured in fracture networks which geometry conditions their hydraulic properties. For instance, the figure 12 illustrates the structure of a fractured network which is conditioned by the spatial distribution of fracture density, length, orientation, shape and aperture.

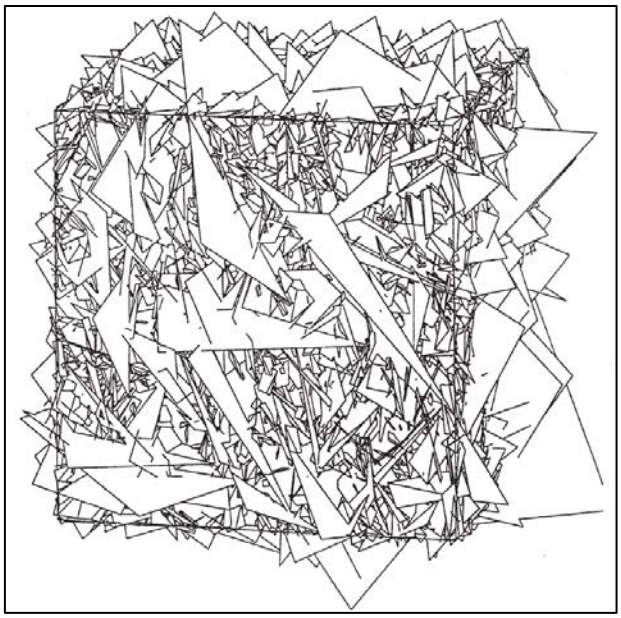

Figure 12: Fracture network generated to compute equivalent hydraulic properties of the crystalline rocks at the Stripa Mine in Sweden (Neuman 2005).

The porosity and permeability of fracture networks are significantly higher than those of the rock matrix. Therefore, fractures are the main vector of underground flows in crystalline rocks. For instance, observations in the Stripa Mine (Olsson 1992) indicate that only on a few fractures concentrate most of fluid flows (figure 13) where more than 99% of the water emerged from a 6 m long intersection with the most densely fractured zone (H-zone).

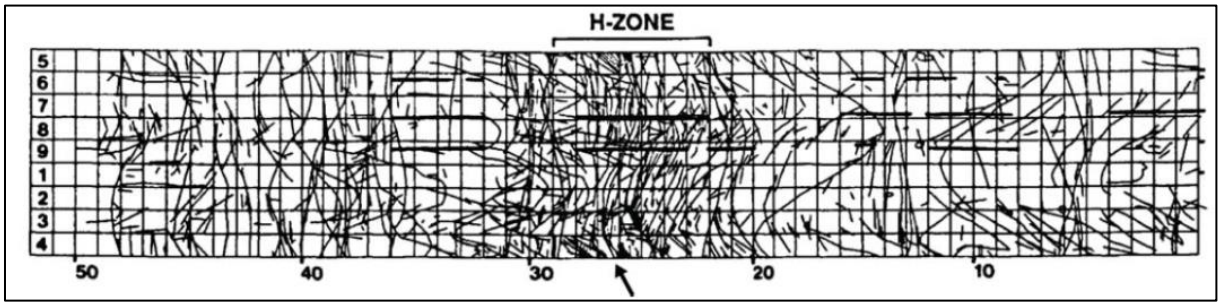

Figure 13: Fractures referenced in the Stripa Mine in Sweden where 99% of the flux is concentrated in the fractured "H-zone" (Olsson 1992). The arrow indicates the location where the fracture flow arises.

This phenomenon of flow **channelling** illustrates the role of fracture networks as permeable structures ensuring the pore **connectivity** and therefore the fluid **percolation** within crystalline media. Over the last decades, many studies based on field observations and modelling have been dedicated to the description of the key properties of fractured networks (percolation threshold) and their influence on fluid flows in fractured media (Adler et al. 2012; Berkowitz et al. 2000; Bour & Davy 1997; Bour & Davy 1998; Bour & Davy 1999; Bonnet et al. 2001; J.-R. de Dreuzy et al. 2001; J. R. de Dreuzy et al. 2001; de Dreuzy et al. 2002; Bour et al. 2002; Darcel et al. 2003; Davy et al. 2006; Davy et al. 2010; de Dreuzy et al. 2012; Mongstad Hope et al. 2015). These investigations indicate that densely

fractured media where small fractures dominate can behave as relatively homogeneous media at all spatial scales. Conversely, fractured networks where large fractures preponderate are highly heterogeneous and can typically concentrate most of the flows of the system in a few wide structures. In naturally fractured crystalline media, large and small structures coexist with decreasing fracture density through depth and contribute to the heterogeneous organisation of subsurface flows. Therefore, in many cases, the structure of fractured geological reservoirs does not allow the definition of a REV and classical theories on groundwater flow and solute transport cannot apply to crystalline rocks.

The complex structure of fracture networks and the particularly localised character of fractured rock permeability generate very heterogeneous hydraulic properties that are scale dependent. For instance, observations in the site of Mirror Lake indicate that rock hydraulic conductivities can vary over several orders of magnitude and over the observation scale (figure 14). The scale dependence of hydraulic properties of rocks is nonetheless discussed for the lack of measurements at large scale (Neuman 1990; Clauser 1992; Sánchez-Vila et al. 1996; Hsieh 1998; Le Borgne et al. 2006).

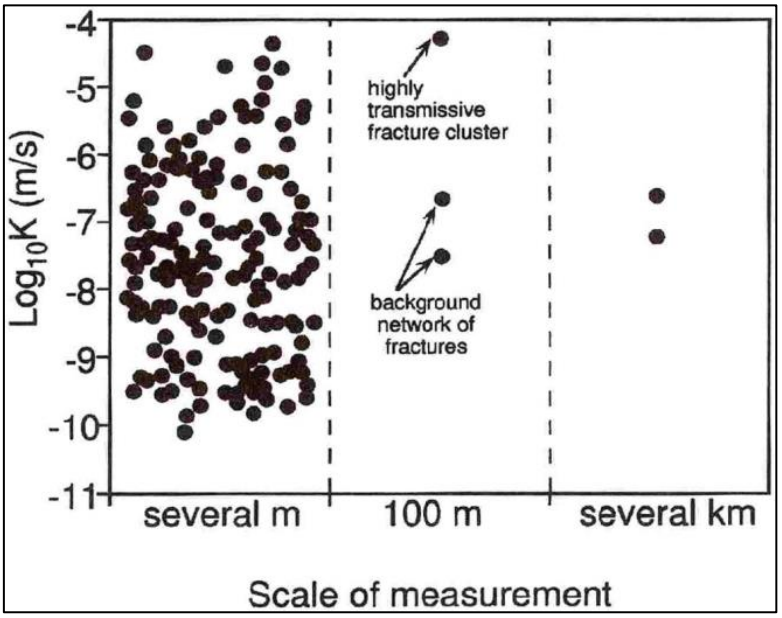

Figure 14: Variability of hydraulic conductivity measurement as a function of the observation scale (Hsieh 1998).

The heterogeneous structure of fractured crystalline media also implies heterogeneous transport properties (Tsang & Neretnieks 1998). For example, at the fracture scale, the fluid flow between fracture walls create a parabolic profile of fluid velocities resulting in a solute spreading called the Taylor-Aris dispersion (figure 15a). In addition, the roughness of fracture walls and the distribution of fracture apertures (figure 15b) generate a highly heterogeneous velocity field with preferential paths and stagnant areas that are responsible of important solute dispersion in fractures (Bodin et al. 2003). Therefore, the hydrodynamic dispersion of a solute flowing in a fracture is the result of the combined

action of these three mechanisms (**Taylor–Aris dispersion**, **roughness dispersion** and **aperture-variation dispersion**) and is called the **microdispersion**.

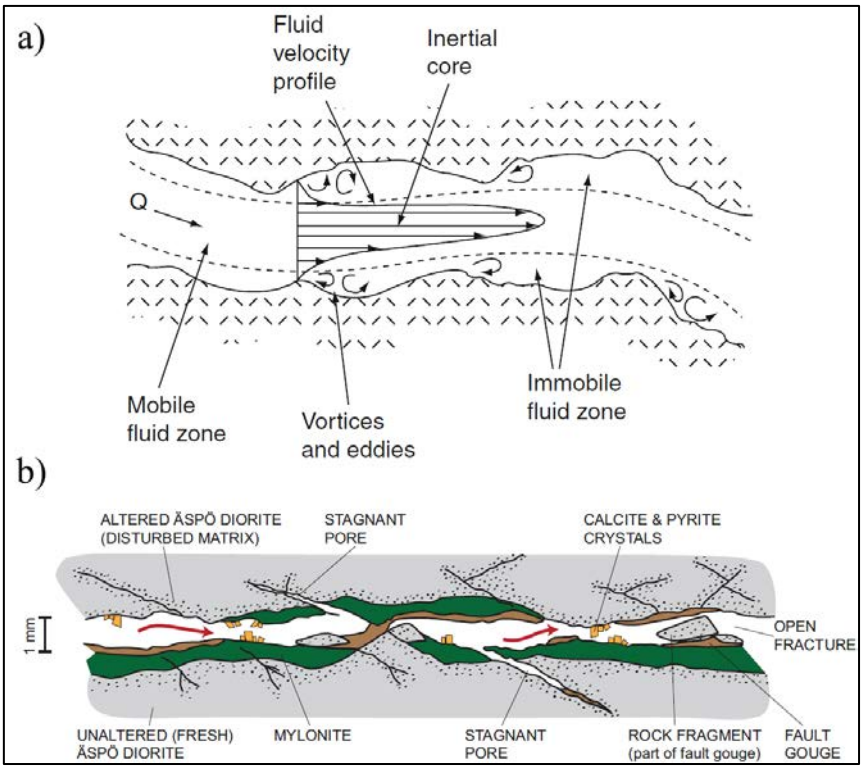

Figure 15: Mechanisms of dispersion at the fracture scale: a) Taylor-Aris dispersion (Raven et al. 1988) and b) roughness and aperture variation of a fracture (Winberg et al. 2000).

Solute microdispersion in fractures is naturally enhanced by physico-biogeochemical processes such as rock weathering, precipitation of secondary minerals on fracture walls (fracture coating, fracture skin) or the development of biofilms (figure 16) that typically increase flow heterogeneity.

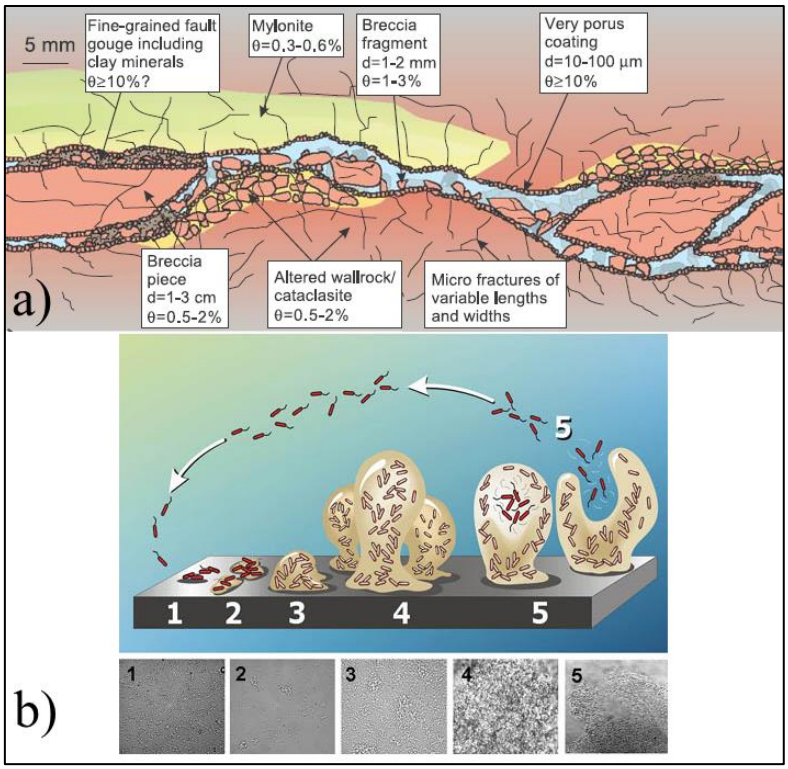

Figure 16: a) Impact of physical and biogeochemical weathering on fracture walls (Andersson et al. 2004) and b) Scheme and pictures of a biofilm growth (http://www.genomenewsnetwork.org/articles/06_02/biofilms_image1.shtml).

At the fracture network scale, the large distribution of fluid velocities over the different flow paths generate a **macrodispersion** which is superimposed on the effects of hydrodynamic dispersion in single fractures (Fetter 1993; Bodin et al. 2003). In addition, experimental observations and theoretical studies have shown that the partitioning of preferential flow paths is a common phenomenon in fractured media that impacts significantly solute dispersion (Neretnieks et al. 1982; Tsang et al. 1988; Moreno et al. 1988; Moreno & Neretnieks 1993b; Abelin et al. 1994; Tsang & Neretnieks 1998). Arising both in single fractures and in fracture networks, this heterogeneous advection referred as **flow channelling** enables solutes to take almost independent flow paths of contrasting velocities, which in turn, enhances the solute dispersion (Fetter 1993; Bodin et al. 2003). In practice, this phenomenon takes the form of **multimodal curves** (induced by independent channels) and **tailing effects** (induced by slow channels) during tracer tests in fractured media (see section 1.4). Nevertheless, the phenomenon of channelling is rarely taken into account in the interpretation of the field data (Bodin et al. 2003).

In crystalline media, the coexistence of fracture and rock matrix porosity is also an important factor controlling solute transport (Grisak & Pickens 1981; Neretnieks 1980). This double porosity does not necessarily affect groundwater flow (crystalline rock matrix porosity is usually conceptualised as a diffusive porosity) but act as a vector of retardation and spreading of the transported solutes (Bodin et al. 2003). Over the last decades, many field and laboratory investigations in fractured media pointed

out the impact of **matrix diffusion** on solute travel times over several spatial and temporal scales (Sudicky & Frind 1982; Novakowski & Lapcevic 1994; Novakowski et al. 1995; Novakowski & Bogan 1999; Zhou et al. 2007). In practice, the tailing effects produced by matrix diffusion are difficult to distinguish from those generated by channelling and their discrimination requires the implementation of several tracer tests (Bodin et al. 2003).

As the diffusive flux to the rock matrix depends on the surface of interaction between the fluid and the fracture walls, it has been shown that the matrix diffusion strongly depends on channelling (Neretnieks 1980; Rasmuson & Neretnieks 1981; Rasmuson & Neretnieks 1986; Moreno et al. 1988; Dykhuizen 1992; Moreno & Neretnieks 1993b). As a result of flow channelling, solutes tend to explore smaller surfaces thus decreasing the influence of diffusive fluxes on the solute transport. On the other hand, biogeochemical reactions leading to the coating of fracture walls appear to have little influence on matrix diffusion (Ohlsson & Neretnieks 1995).

As for hydraulic properties, different literature reviews on the transport properties of porous media including fractured media (Neuman 1990; Gelhar et al. 1992; Zhou et al. 2007) demonstrated that dispersivity and matrix diffusion varies over several orders of magnitude and over the observation scale (figure 17).

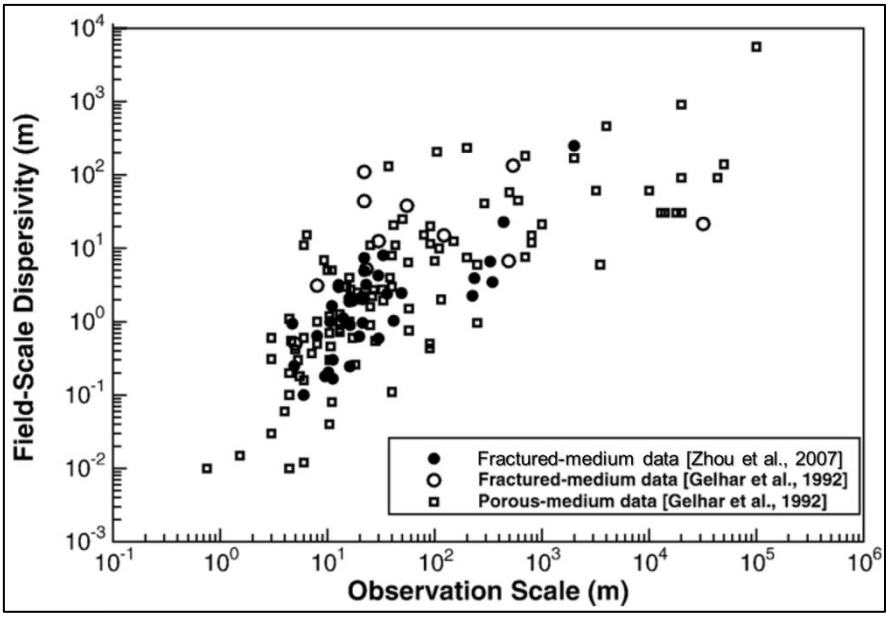

Figure 17: Variability of hydraulic conductivity measurement as a function of the observation scale modified from (Zhou et al. 2007).

In essence, the classical advection-dispersion theory cannot effectively describe transport in heterogeneous media. As a result, capturing the heterogeneity and the scale dependence of solute transport properties has become one of the greatest concerns of scientists interested in the migration of contaminants such as radionuclides in fractured crystalline media (Bodin et al. 2003).

At the catchment scale, the characteristic contrasts of porosity and permeability observed in fractured crystalline media trigger the heterogeneity of groundwater flow and solute transport in these aquifers. Such heterogeneity leads to the enhanced **partitioning of groundwater flows** from the pore to the catchment scale (figure 18).

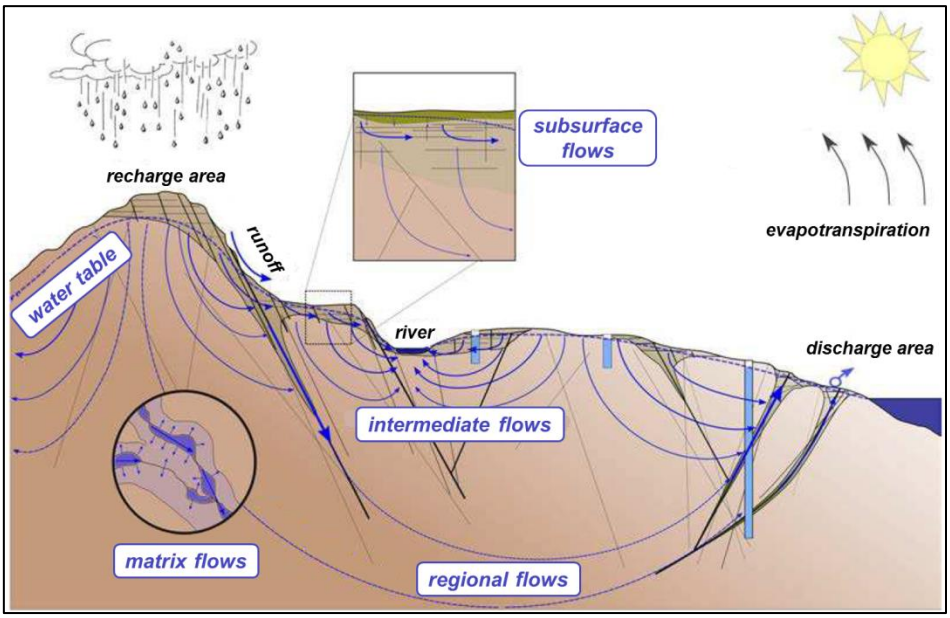

Figure 18: Partitioning of groundwater flow path in fractured media modified from (Roques 2013).

In turn, the phenomenon of flow partitioning controls the distribution of water residence times in aquifers, and contributes to the progressive differentiation of water biogeochemical composition along the segregated flow paths. Over time, reactions and mixing; groundwater acquires different biogeochemical signatures characterising both groundwater origins and aquifer dynamics (meteoric, lithologic, anthropogenic, saline, marine, modern, old, etc.). For instance, the heterogeneity of crystalline media favours the mixing of converging groundwater flows of distinct biogeochemical signatures which sustains the development of dynamic microbiological hotspots (Ben Maamar et al. 2015; Bochet et al. 2017).

These observations illustrate the complexity of groundwater flows and solute transport in fractured media. Their exceptional heterogeneity highlights the need to develop particular approaches to capture aquifer hydrobiogeochemical dynamics at different scales and their interactions with other components of the CZ (pedosphere, biosphere, atmosphere and the rest of the hydrosphere). The characterisation of fractured aquifers at different scales can be performed using preferentially a combination of various methods that are summarised in figure 19 (Bense et al. 2013; Schuite 2016).

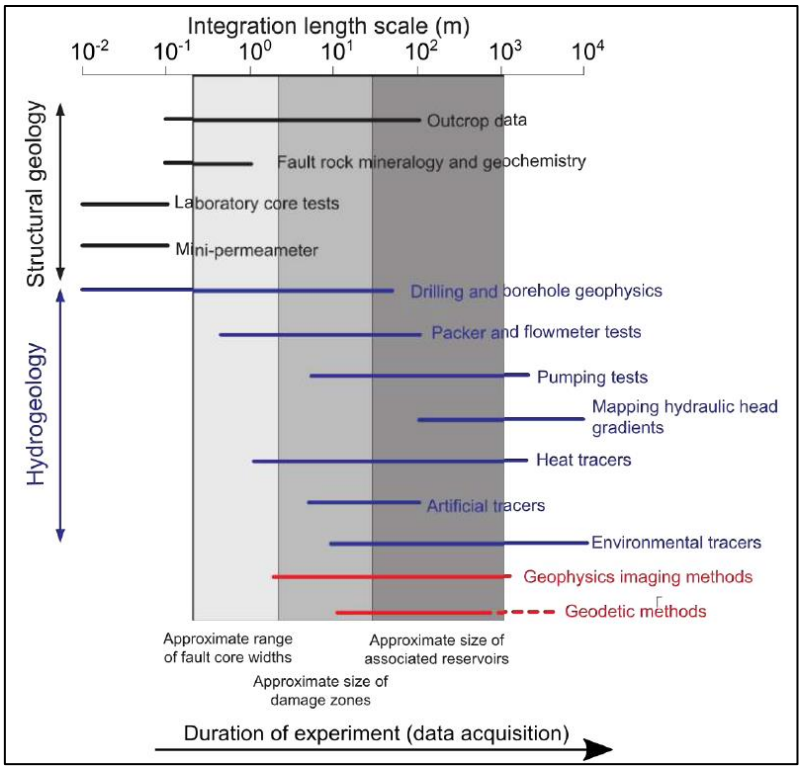

Figure 19: Investigation scales of characterisation methods in fractured media (Bense et al. 2013; Schuite 2016).

During this project, two approaches have been employed to characterise groundwater dynamics using dissolved gas tracers. The first one uses the natural dissolved gas signature of groundwater to infer the natural dynamics of an aquifer system and the anthropogenic impact of its exploitation ("environmental tracers" in figure 19). The second consist in introducing artificially dissolved gas tracers in aquifers to characterise their solute transport properties ("artificial tracers" in figure 19). These two approaches are detailed in the following section.

4. Environmental tracers

Over the past, the natural biogeochemical signature of groundwater has been widely used to determine groundwater residence times, groundwater sources, the mixing of groundwater bodies as well as the origin and pathways of groundwater contaminants. Therefore, characterising groundwater biogeochemical signature is very informative in subsurface hydrology and can be achieved using certain specific solutes. These environmental tracers are defined as natural or anthropogenic compounds or isotopes that are widely distributed in the environment, such that variations in their composition can be used to determine the origin, the pathways and the timescales of environmental processes (Cook & Böhlke 2000).

For instance, the simple study of major cations (K^+, Na^+, Mg^{2+}, Ca^{2+}), major anions (Cl^-, HCO_3^-, NO_3^-, SO_4^{2-}) but also trace elements (Li^+, Sr^{2+}, F^-, Br^-) inform on recharge and discharge rates, recharge

history, the origin of salinisation, rock weathering fluxes and mixing of water bodies (Herczeg & Edmunds 2000).

In the environment, many physical and biogeochemical processes are mass-dependent and lead to measurable changes in the isotopic composition of the water. This phenomenon of isotopic fractionation (isotopes are elements with the same number of protons but a different number of neutrons) can be driven by changes of physical state (evaporation, condensation, crystallisation, melting or sublimation), chemical reactions (ion exchange, sorption and desorption), biological processes (assimilation, respiration, dissimilatory redox reactions), or diffusion (Cook & Böhlke 2000). Therefore, mass-dependent fractionations of the stable isotopes ($^{2}H/^{1}H$, $^{7}Li/^{6}Li$, $^{10}B/^{11}B$, $^{13}C/^{12}C$, $^{15}N/^{14}N$, $^{18}O/^{16}O$, $^{34}S/^{32}S$, $^{37}Cl/^{35}Cl$, $^{87}Sr/^{86}Sr$) have been commonly used in subsurface hydrology to determine the sources of water, the origin of its dissolved constituents and the mechanisms of biogeochemical reactions taking place along flow paths(Cook & Herczeg 2000; IAEA 2001).

One of the principal uses of environmental tracers is for determining the timescales of water hydrobiogeochemical dynamics (Cook & Böhlke 2000). Information on groundwater residence times and mixing of water bodies can be obtained from:

- the decay of radioactive tracers which have a constant and well-known input history (^{3}H, ^{14}C, ^{35}S, ^{32}Si, ^{36}Cl, ^{129}I, $^{234}U/^{238}U$, ^{39}Ar, ^{81}Kr). Depending on their half-lives (i.e. rate of decay), these radioactive tracers are used for dating modern to very old groundwater systems (figure 20).
- accumulating tracers that are produced in the subsurface by chemical reactions (Si^{4+}) or radioactive decay (^{36}Cl, ^{4}He, ^{21}Ne, ^{40}Ar) of other compounds. Depending on their production rates, these tracers are used for dating modern to very old groundwater systems (figure 20).
- conservative tracers which have a variable but well-known input history (^{3}H, ^{14}C, ^{36}Cl, CFCs, SF_6, $^{3}H/^{3}He$, ^{85}Kr). These event markers are used for dating modern groundwater fractions (figure 20).
- radioactive tracers that are produced by other radionuclides but which do not accumulate owing to their own decay (^{226}Ra, ^{37}Ar, ^{222}Rn). These tracers are used to measure infiltration rates, aquifer discharge into surface water bodies, flow rates through fractured rock aquifers or as partitioning tracers in contaminant studies.

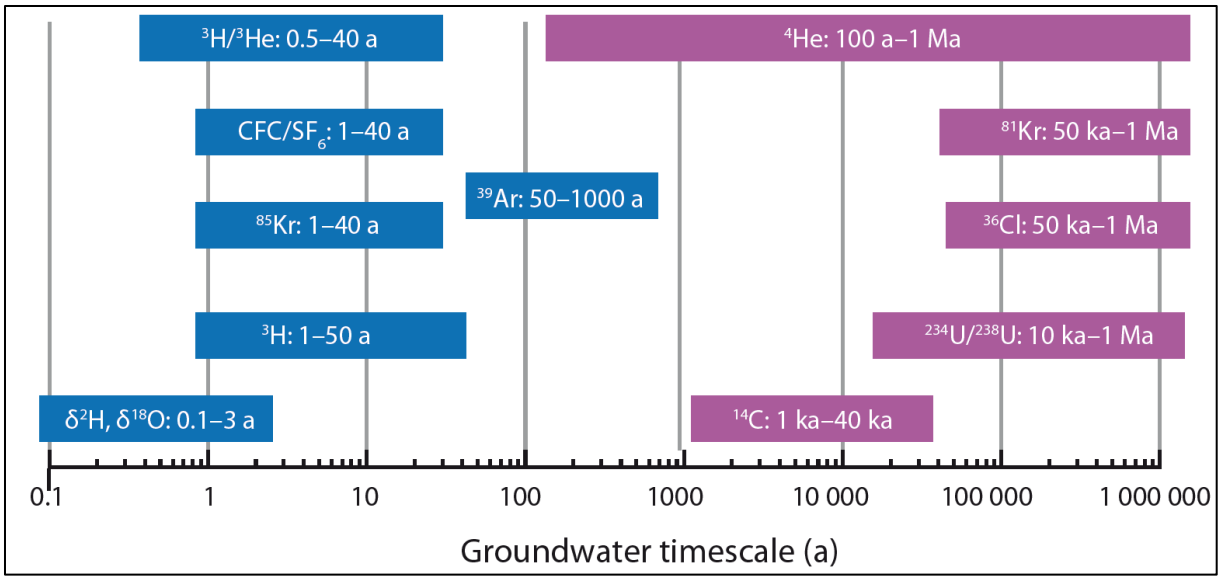

Figure 20: Environmental tracers used for estimating groundwater age (IAEA 2013).

Owing to the diversity of information they integrate, environmental tracers are essential to the study of hydrological and hydrogeological systems. Their combined use is very useful and enables to constrain the timescale of environmental processes. For instance, the combination of different groundwater dating methods allows the determination of the full groundwater residence time distribution which is a valuable information for water resource management. In addition to dating methods, stable isotopes can be used to determine the pathways and rates of biogeochemical reactions (rock weathering, contaminant degradation, etc.), to infer contaminant input histories (fertiliser application, industrial or domestic leakages, etc.) or to characterise changes in contaminant sources over time.

Thereafter, this section will focus on dissolved gas tracers owing to the diversity of their physical and chemical properties that allow the determination of groundwater residence times, groundwater origins, the mixing of water bodies as well as the mechanisms of biogeochemical reactions.

4.1. Groundwater origin and recharge conditions

Atmosphere is the main source of dissolved gases in natural waters through equilibria described by Henry's law. The latter defines the proportionality between the partial pressure of a gas to its concentration in water according to equation 12 below:

$$p_i = k_i(T,S) \cdot x_i$$

[-] (Eq. 12)

Where p_i is the partial pressure of the gas i in the gas phase and x_i is the mole fraction of the gas i dissolved in the aqueous phase (equilibrium concentration). The Henry constant k_i depends on the temperature T and the salinity S of the aqueous phase.

Consequently, atmosphere is responsible for most of the nitrogen (N_2), oxygen (O_2), carbon dioxide (CO_2) and noble gases (He, Ne, Ar, Kr, Xe) observed in natural waters. Nevertheless, as water isolates from the atmosphere (infiltration in the subsurface), the water dissolved gas signature evolve along flow path through biogeochemical reactions (respiration, denitrification, rock weathering), radioactive decay or production.

Owing to their conservative behaviour, the concentrations of dissolved noble gases are only affected by the physical parameters controlling their solubility (temperature, pressure, salinity) and the physical processes governing water flow and transport (advection, dispersion, diffusion). Therefore, the measurement of noble gas concentrations in groundwater enables the determination of recharge conditions (recharge temperature and elevation) as well as the transport properties of aquatic systems (aquifers, rivers, lakes, oceans, etc.). The latter is beyond the scope of this section and will be addressed in the section 1.5.

Many equations enable to calculate the equilibrium noble gas concentrations as a function of the temperature, pressure and salinity of the recharging water (Clever 1979a; Clever 1979b; Clever 1980; Smith & Kennedy 1983). However, groundwater noble gas concentrations often differ from these atmospheric equilibria and appear to be altered by an additional ubiquitous phenomenon. Although not totally well understood, this phenomenon is commonly referred as “excess air” and is intrinsically related to the structure of the unsaturated zone (thickness, porosity), the processes of aquifer recharge (frequency, amplitude, infiltration rate) and the biogeochemical processes affecting soil air composition (O_2 consumption, CO_2 production).

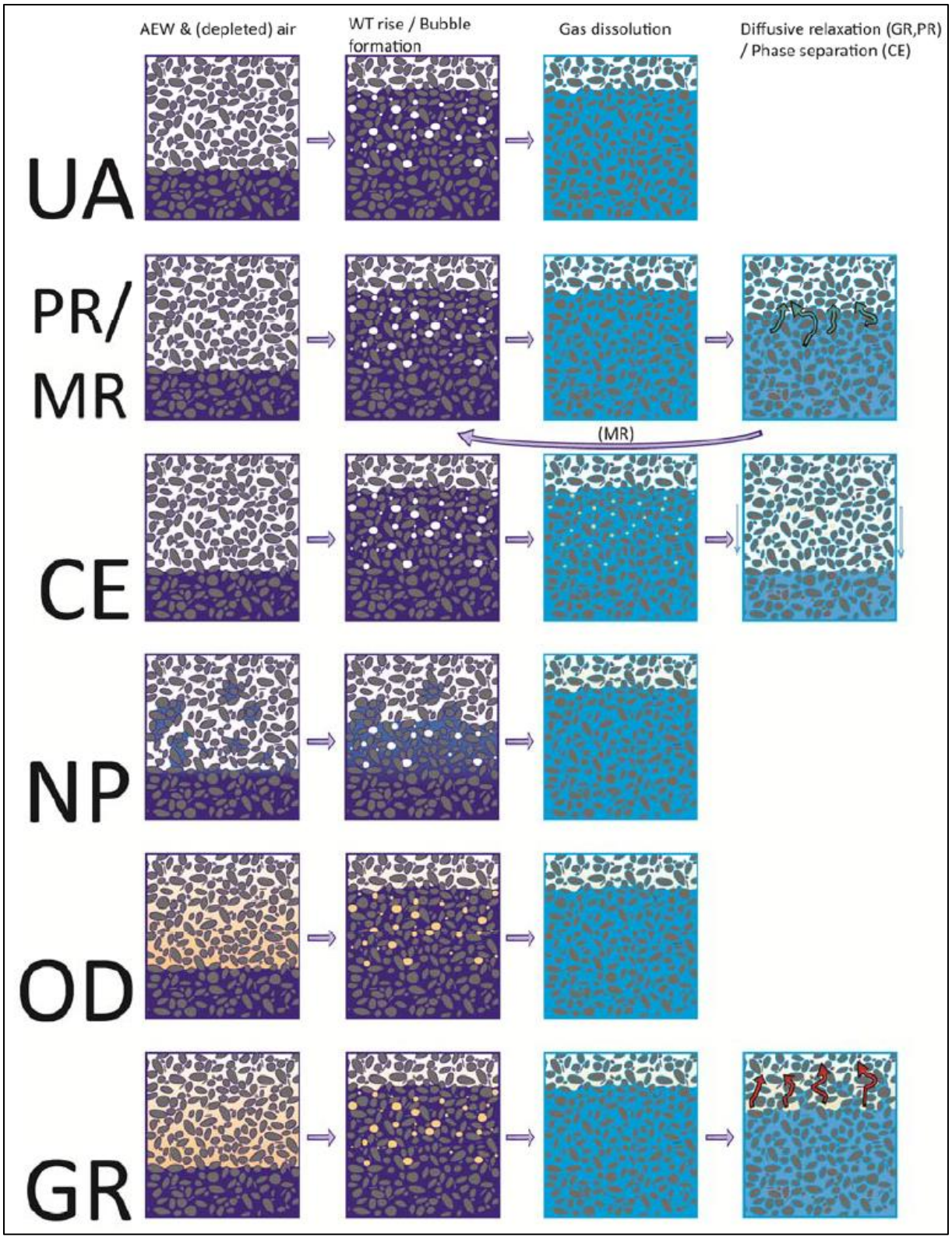

Figure 21: Illustration of the processes conceptualised in the different excess air models (Aeschbach-Hertig & Solomon 2013). Excess air in groundwater can be obtained by the total dissolution of unfractionated excess air (UA) that can be affected by oxygen depletion (OD) or partially re-equilibrate with the soil atmosphere by diffusion using one (PR and GR) or multiple steps (MR). Excess air can also form under negative pressure (NP) or in equilibration with a closed system (CE).

Figure 21 shows that there are currently different conceptual models of excess air available to propose an interpretation of groundwater noble gas contents using their equilibrium concentrations with soil air, and various assumptions on the excess air component in terms of amounts, fractionation or composition (Andrews & Lee 1979; Heaton & Vogel 1981; Stute, Forster, et al. 1995; Kipfer et al. 2002; Aeschbach-Hertig et al. 2002; Lippmann et al. 2003; Mercury et al. 2004; Hall et al. 2005; Sun et al. 2008). When implemented in inverse models, these concepts of excess air formation have enabled the use noble gases as tracers of aquifer recharge conditions (temperature, elevation, frequency and amplitude of recharge) and therefore of groundwater origins (Stute & Schlosser 1993; Aeschbach-Hertig et al. 1999; Aeschbach-Hertig & Solomon 2013). Combined with dating methods, noble gas tracers have made possible the study of the evolution of the recharge temperature (also called the Noble Gas Temperature, NGT) through time thus, paving the way for the use of groundwater as archives of past climates (Stute, Clark, et al. 1995; Stute, Forster, et al. 1995; Beyerle et al. 1998; Aeschbach-Hertig et al. 2000; Castro et al. 2007; Castro et al. 2012; Corcho Alvarado et al. 2009; Corcho Alvarado et al. 2011; Plummer et al. 2012).

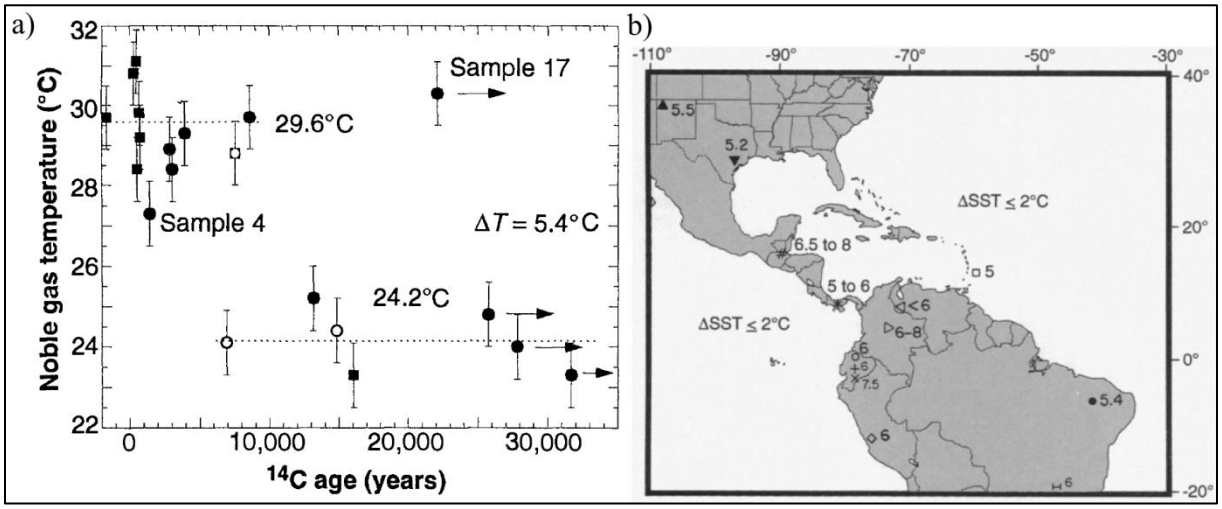

Figure 22: Noble gas temperatures and other climate proxies allowing the investigation of past climates in tropical South-America (Stute, Forster, et al. 1995).

These past climate investigations (figure 22) produce important input data for regional climate models and require precise timescale constrains as much as groundwater flow studies.

4.2. Groundwater dating

As mentioned earlier, one of the principal applications of environmental tracers is for groundwater dating, dissolved gas tracers having a large contribution to this task. Over the last decades, human activities lead to the more or less homogeneous release in the atmosphere of various gaseous compounds and isotopes which partly dissolved in natural waters as a result of atmospheric equilibria. Thereafter, these event markers have been largely used from the 1980s to determine groundwater

residence times. The "events" responsible of the release of these tracers are relatively recent, limiting thus these dating methods to the characterisation of modern groundwater fractions.

Dating methods based on anthropogenic dissolved gas tracers rely on different basic principles. Firstly, according to Henry's law, the evaluation of groundwater recharge conditions (using dissolved noble gases) and the measurement of these tracers in groundwater allow to calculate their theoretical atmospheric partial pressure at the time of recharge (before the system closed). Secondly, the available global atmospheric chronicles of their concentrations allow to link the partial pressures of the tracers to the year of the last groundwater equilibration with the atmosphere. Finally, this leads to an "apparent groundwater age" which assumes that the sampled groundwater originates from only one flow line following a piston flow and that the environmental tracers did not undergo mixing nor dispersion in the subsurface.

Naturally, most of groundwater flows are usually more complex than the piston flow model (PFM) and the interpretation of the tracer concentrations is usually performed using different lumped parameter models (LPMs). In these models, groundwater flow characteristics and tracer physical properties (i.e. radioactive decay) are taken into account to evaluate the groundwater residence time distribution (IAEA 2001). For instance, the main parameter of all LPMs for a single-porosity media is the water mean transit time (T) through the system, which is connected to the mobile water volume (Vm) in the system and the volumetric flow rate (Q) according to equation 13 below:

$$T = \frac{Q}{V_m}$$

[T] (Eq. 13)

where T can be determined through different LPMs using measured tracer input concentration $C_{in}(t)$ (concentration at the time of aquifer recharge) to calculate the theoretical tracer output concentration $C_{out}(t)$ (concentration at the observation point) which is then compared to the actual measured tracer concentration. The relationship between input and output concentrations is given by the convolution integral shown in the equation 14 below (Małoszewski & Zuber 1982):

$$C_{out}(t) = \int_0^\infty C_{in}(t-\tau)g(\tau)\, e^{-\lambda\tau} d\tau$$

(Eq. 14)

where λ is the decay constant of the radioactive tracers and $g(\tau)$ is the transit time distribution function. The most common transit time distribution functions used for single-porosity media are (Leibundgut et al. 2009):

Piston Flow Model (PFM)

$$g(\tau) = \delta(\tau - T)$$

(Eq. 15)

Exponential Model (EM)

$$g(\tau) = \frac{1}{T} e^{-\left(\frac{\tau}{T}\right)}$$

(Eq. 16)

Combined Exponential Piston Flow Model (EPM)

$$g(\tau) = \frac{\eta}{T} e^{-\left(\frac{\eta\tau}{T}+\eta-1\right)}$$

for $\tau \geq (\eta-1)\cdot T/\eta$ (Eq. 17)

$$g(\tau) = 0$$

for $\tau \leq (\eta-1)\cdot T/\eta$

Dispersion-Model (DM)

$$g(\tau) = \frac{1}{\tau\sqrt{4\pi P_D \frac{\tau}{T}}} e^{-\left[\frac{\left(1-\frac{\tau}{T}\right)^2}{4P_D\frac{\tau}{T}}\right]}$$

(Eq. 18)

where P_D is the dispersion parameter and η is the ratio of the total water volume in the system to volume of that part of the water characterized by the exponential transit time distribution (V/V_{EM}). The EPM model is a combination of the PFM and EM models in series; the order in which these models are applied is not important. Examples of the transit time distribution functions are shown in figure 23.

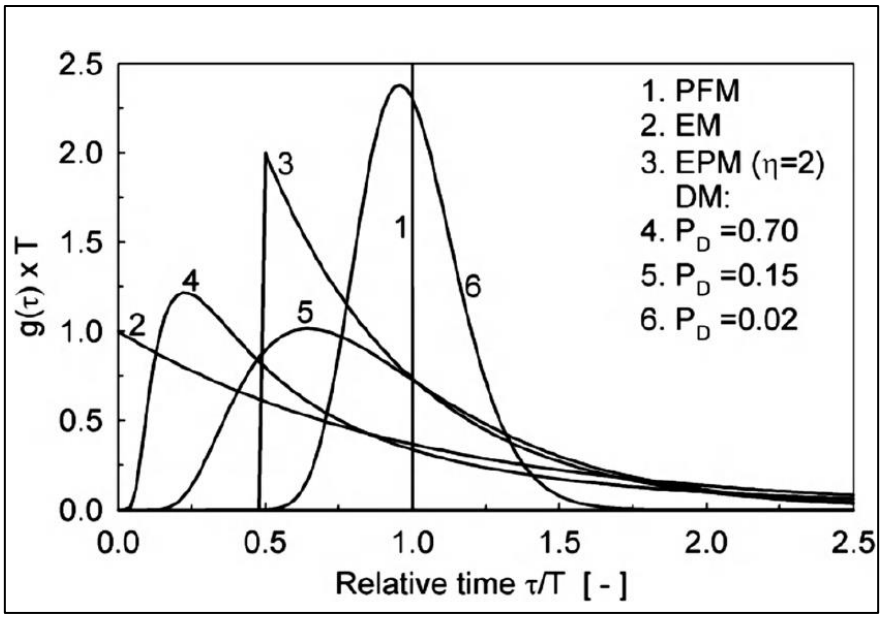

Figure 23: Examples of the transit time distribution functions (Leibundgut et al. 2009).

Other kinds of LPMs also exist for double-porosity media characterised by fracture networks where there is both mobile water in the fractures and immobile water in the microporous matrix such as the Parallel Fissure Dispersion Model (PFDM) (Małoszewski & Zuber 1985).

Groundwater dating methods based on event markers use the anthropogenic release of various tracers (figure 24 and table 1). For instance, the global atmospheric concentrations in chlorofluorocarbons (CFCs) and sulphur hexafluoride (SF_6) have been increasing since the beginning of the 1950s as a result of the releases of the industry (figure 24). While SF_6 contents are still increasing, the atmospheric concentrations of the CFCs began to stagnate in the mid-1990s until ultimately decrease on the basis of the Montreal protocol on ozone layer depleting substances (1987). Aside from some cases of CFC-11 degradation, CFC-113 retardation or SF_6 geogenic production, the three CFCs (CFC-11, CFC-12 and CFC-113) and SF_6 have been largely used in subsurface hydrology to characterise the contribution of post-1950 groundwater to the overall aquifer dynamics (Busenberg & Plummer 1992; Busenberg & Plummer 2000; Bohlke & Denver 1995; Cook et al. 1995; Maiss et al. 1996; Oster & Sonntag 1996; Ayraud et al. 2008).

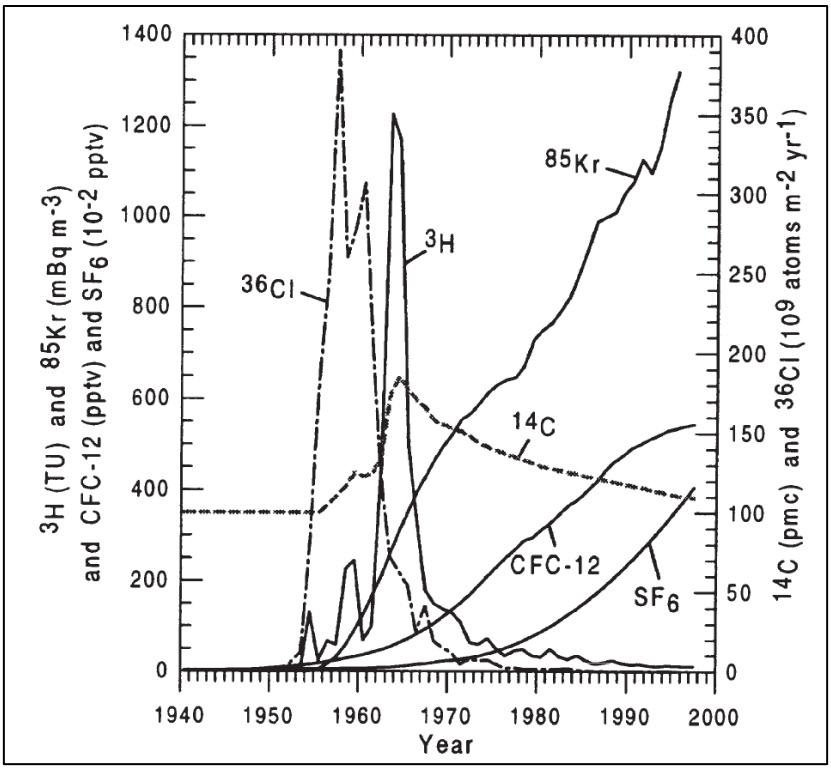

Figure 24: Evolution of atmospheric concentrations of the event markers ^{3}H, ^{36}Cl, ^{14}C, ^{85}Kr, CFC-12 and SF_6 (Cook & Böhlke 2000).

Similarly, atmospheric activities of ^{85}Kr, tritium (^{3}H) and radiocarbon (^{14}C) isotopes increased in the 1950s as a result of the nuclear industry releases (^{85}Kr) and nuclear weapons testing (^{3}H and ^{14}C). While ^{85}Kr atmospheric activity is still increasing, ^{3}H and ^{14}C activities have dropped exponentially after the atom bomb moratorium (figure 24). The global monitoring of atmospheric levels of these radioactive tracers enable to characterise the modern groundwater fraction in aquifers (post-1950 water) through the measurement of ^{3}H, ^{85}Kr and ^{14}C activities in wells (Smethie et al. 1992; Ekwurzel et al. 1994; Cook & Solomon 1997; Loosli 2000; Stewart & Morgenstern 2016). The activity of these tracers decreases exponentially following the law of radioactive decay:

$$A = A_0 \cdot e^{-\lambda t}$$

$[L^{-3}]$ (Eq. 19)

Where t is the time elapsed since the last atmospheric equilibrium, A_0 and A are respectively the initial (atmospheric) and the sample activities, λ is the radioactive isotope decay constant ($\lambda = \ln(2)/t_{1/2}$) which is associated to $t_{1/2}$ the isotope half-life (time required for a radioactive isotope activity to reduce to half its initial value).

In recharge areas, dissolved radioactive tracer activities are maintained by atmospheric equilibria (A_0) as long as groundwater can exchange with the atmosphere. However, when groundwater flows and isolates from the atmosphere, the system closes (atmospheric equilibration is no longer possible) and

the hydrochronometer starts. Then, the "apparent groundwater age" t can then be inferred from the equation 20 below:

$$t = \frac{1}{\lambda} \cdot ln\left(\frac{A}{A_0}\right)$$

[T] (Eq. 20)

Due to the relatively short ^{3}H half-life ($t_{1/2}$), the tritium dating method has now been replaced by $^{3}H/^{3}He$ dating method that give better precisions when measuring both the parent ^{3}H and daughter ^{3}He activities in groundwater (Schlosser et al. 1988; Solomon et al. 1992; Solomon & Cook 2000).

Table 1: Origin and timescales of different dating methods

Tracer	Origin	Half-Life	Dating Timescale
^{3}H	Mainly Anthropogenic	12.43 a	1 to 50 a
^{3}He	Atmospheric, Geogenic & ^{3}H decay	stable	1 to 50 a
^{4}He	Atmospheric & Geogenic	stable	50 a to 1 Ma
^{14}C	Atmospheric & Anthropogenic	5730 a	1 to 40 ka
^{37}Ar	Geogenic	35.04 d	-
^{39}Ar	Atmospheric	269 a	50 a to 1 ka
^{40}Ar	Atmospheric & Geogenic	stable	200 ka to 1 Ma
^{81}Kr	Atmospheric	229 ka	50 ka to 1 Ma
^{85}Kr	Atmospheric	10.76 a	1 to 50 a
^{222}Rn	Geogenic	3.824 d	-
CFCs	Anthropogenic	stable	1 to 50 a
SF_6	Anthropogenic	stable	1 to 40 a

In addition to anthropogenic dissolved gas tracers (tracers of modern groundwater), other dating methods based on natural atmospheric of dissolved gases have been developed (table 1). Contrary to the event markers, the radioactive isotopes ^{39}Ar, ^{81}Kr and ^{14}C enable the characterisation of old to very old groundwater (50 a to 1 Ma). These dating methods (as for ^{3}H and ^{85}Kr,) are based on the exponential decay of these radioactive isotopes with time once groundwater is isolated from the atmosphere. This time, the initial tracer activity A_0 is a constant (no need for atmospheric chronicles) and, as for ^{85}Kr, the determination of recharge conditions is not necessary as the measured $^{39}Ar/Ar$, $^{81}Kr/Kr$ and $^{85}Kr/Kr$ ratios are insensitive to recharge temperature, excess air or degassing (IAEA 2013).

Alike anthropogenic tracers, the interpretation of ^{39}Ar, ^{81}Kr and ^{14}C activities can be affected by subsurface mixing processes and would require the use of the previously mentioned LPMs. Regarding the timescales at stake (several hundreds or thousands years), diffusion processes can also

substantially modify tracer transport and therefore lead to the overestimation groundwater residence time due to the tracer retardation (Neretnieks, 1980 and 1981). In addition, due to the carbon element biogeochemical reactivity, radiocarbon dating must often take into account different processes affecting its activity such as carbonate and gypsum dissolution, soil gas dissolution, soil gas-aqueous isotopic exchange, calcite-aqueous isotopic exchange or Ca/Na exchange (IAEA 2013).

Despite the complexity of the interpretation of the ^{14}C activities, the radiocarbon dating method is one of the most implemented for dating old groundwater (Fontes 1992; Kalin 2000; Plummer & Sprinkle 2001). The great progresses achieved with the atom trap trace analysis for very low abundant radioactive isotopes (see Chapter 2) have now increased the interests on ^{85}Kr, ^{39}Ar and ^{81}Kr dating methods and their combined use for a thorough characterisation of groundwater residence time distribution (Loosli 1992; Loosli 2000; Chen 1999; Collon et al. 2000; Du et al. 2003; Sturchio et al. 2004; Lehmann et al. 2003; Corcho Alvarado et al. 2007; Corcho Alvarado et al. 2013; Delbart et al. 2014; Lu et al. 2014).

At last, noble gas stable radiogenic isotopes such as ^4He and ^{40}Ar can be used for groundwater dating as they accumulate with time in the subsurface through the respective decay of uranium-thorium (U-Th) and potassium (^{40}K) radioactive isotopes of the aquifer rocks (Andrews & Lee 1979; Andrews et al. 1982; Andrews 1985; Torgersen & Clarke 1985; Torgersen & Ivey 1985; Torgersen & Clarke 1987; Stute et al. 1992; Solomon et al. 1996; Castro, Jambon, et al. 1998; Castro, Goblet, et al. 1998; Castro et al. 2000; Morikawa et al. 2005; Mahara et al. 2009; Wei et al. 2015; Méjean et al. 2016). These accumulative tracers have both atmospheric (from equilibrium concentrations and excess air) and radiogenic (from U-Th of ^{40}K radionuclide decay) origins that can be distinguished on the basis of dissolved noble gas isotopic and absolute measurements (^3He, ^4He, ^{36}Ar, ^{40}Ar, Ne, Kr and Xe). For instance, the ^4He dating method consequently require the determination of (i) the amount of the radiogenic component ($^4He_{rad}$) by subtraction of the atmospheric component ($^4He_{atm}$) from the total measured concentration ($^4He_{mes}$) and, (ii) the tracer production rate depending on the in situ production of radiogenic ^4He (A_{He}) and the ^4He external flux J_0 (Stute et al. 1992). The determination of groundwater "apparent age" (τ_{He}) using ^4He accumulation rate is based on the following equations 21 and 22 below:

$$A_{He} = \rho_r \cdot \Lambda \cdot \{1.19 \times 10^{-13} \cdot [U] + 2.88 \times 10^{-14} \cdot [Th]\} \cdot \frac{1-\varphi}{\varphi}$$

$[M.L^{-3}.T^{-1}]$ (Eq. 21)

$$\tau_{He} = \frac{{}^4He_{rad}}{\left(\frac{J_0}{\varphi \cdot Z_0 \cdot \rho_w} + A_{He}\right)}$$

[T] (Eq. 22)

Where φ is the effective rock porosity, [U] and [Th] are the rock U and Th contents, ρ_r and ρ_w are respectively the rock and water density, Λ the ^{4}He release factor and Z_0 is the aquifer thickness.

As a result of its relatively rapid accumulation in the subsurface, radiogenic ^{4}He is a very interesting groundwater dating tool which covers timescales from several decades to several million years being the dating method with the largest temporal coverage. However, ^{4}He production rate is not always well constrained due to the complexity of the assessment of the spatial variability of φ, [U], [Th], Λ and J_0 parameters. Therefore, ^{4}He dating is often compared to other methods for an accurate constrain of groundwater timescales (Castro et al. 2000; Lehmann et al. 2003; Plummer et al. 2012; Corcho Alvarado et al. 2013).

In essence, groundwater dating methods are very powerful tools for the study and the management of subsurface water resources. The diversity of sources and behaviours of the different tracers allow the evaluation of various hydrological timescales and transit time distribution. In this regard, the combined use of different dating methods is definitely an asset.

4.3. Water-rock interactions and groundwater interfaces

Due to their short half-lives, groundwaters show almost no atmospheric ^{37}Ar and ^{222}Rn activities (Loosli et al, C&H 2000). However, these two noble gas radioisotopes are continuously produced in the subsurface by the respective decay of rock matrix ^{40}Ca and ^{226}Ra (coming from ^{238}U decay chain) of the rock matrix. The ^{37}Ar and ^{222}Rn activities in groundwater therefore reflect both their subsurface production rate and the efficiency of their transfer from rocks to water (DeWayne Cecil & Green 2000; Loosli 2000). The latter depends on the structural geometry of the rock-water interface and on the distribution of the parent isotopes ^{226}Ra and ^{40}Ca in the rocks (DeWayne Cecil & Green 2000; Torgersen et al. 1990). Therefore, groundwater ^{37}Ar and ^{222}Rn are interesting tracers water-rock interactions (Loosli 1992; Le Druillennec et al. 2010) and groundwater recharge and discharge in rivers (DeWayne Cecil & Green 2000; Bourke et al. 2014; Cranswick et al. 2014).

4.4. Biogeochemical reactivity

Similarly to noble gases, groundwater dissolved reactive gases such as N_2, O_2 and CO_2 have an atmospheric origin. Yet, their concentrations in groundwater can be significantly affected (consumption or production) by biogeochemical processes in which other reactive gases can be produced (CO, CH_4, N_2O, NO, NH_3, SO_2, H_2S, H_2). Most of these dissolved gases can be analysed with the same analytical instrument and allow the understanding of the subsurface reactivity affecting the carbon, nitrogen and sulphur cycles (Vogel et al. 1981; Solomon & Cerling 1987; Lovley et al. 1994; Van Stempvoort et al. 2005).

Among environmental tracers, dissolved gas tracers enable the understanding of various physical, chemical and biological processes occurring at different spatial and temporal scales in subsurface

hydrology. Nevertheless, this integrative (large scale) approach can be completed by field scale experiments enabling the thorough characterisation of these transport processes at smaller scales. This second approach is detailed in the following section.

5. Field characterisation of aquifer transport properties

Understanding the processes controlling the solute transport in aquifer systems is essential in order to predict the subsurface transfer of contaminants or to remediate contaminated systems (Berkowitz 2002; Bodin et al. 2003). Solute transport in aquifer systems can be investigated in the field from a few to several hundreds of meters through the implementation of groundwater tracer tests. Generally, these experiments involve the injection of **tracers** (solutes chosen for their specific characteristics) into one or more **injection wells** and their migration in the subsurface is monitored in one or more **observation wells**. The analysis of tracer transport in aquifers can be performed using two approaches (Bodin et al. 2003). The first approach takes advantage of the existence of several observation wells to monitor the **spatial moments** of the tracer plume (spatial distribution of tracer concentrations) at a given time (Lapcevic et al. 1999). The second approach consists in monitoring the tracer **breakthrough curves** (BTC) at a given location (temporal distribution of tracer concentrations).

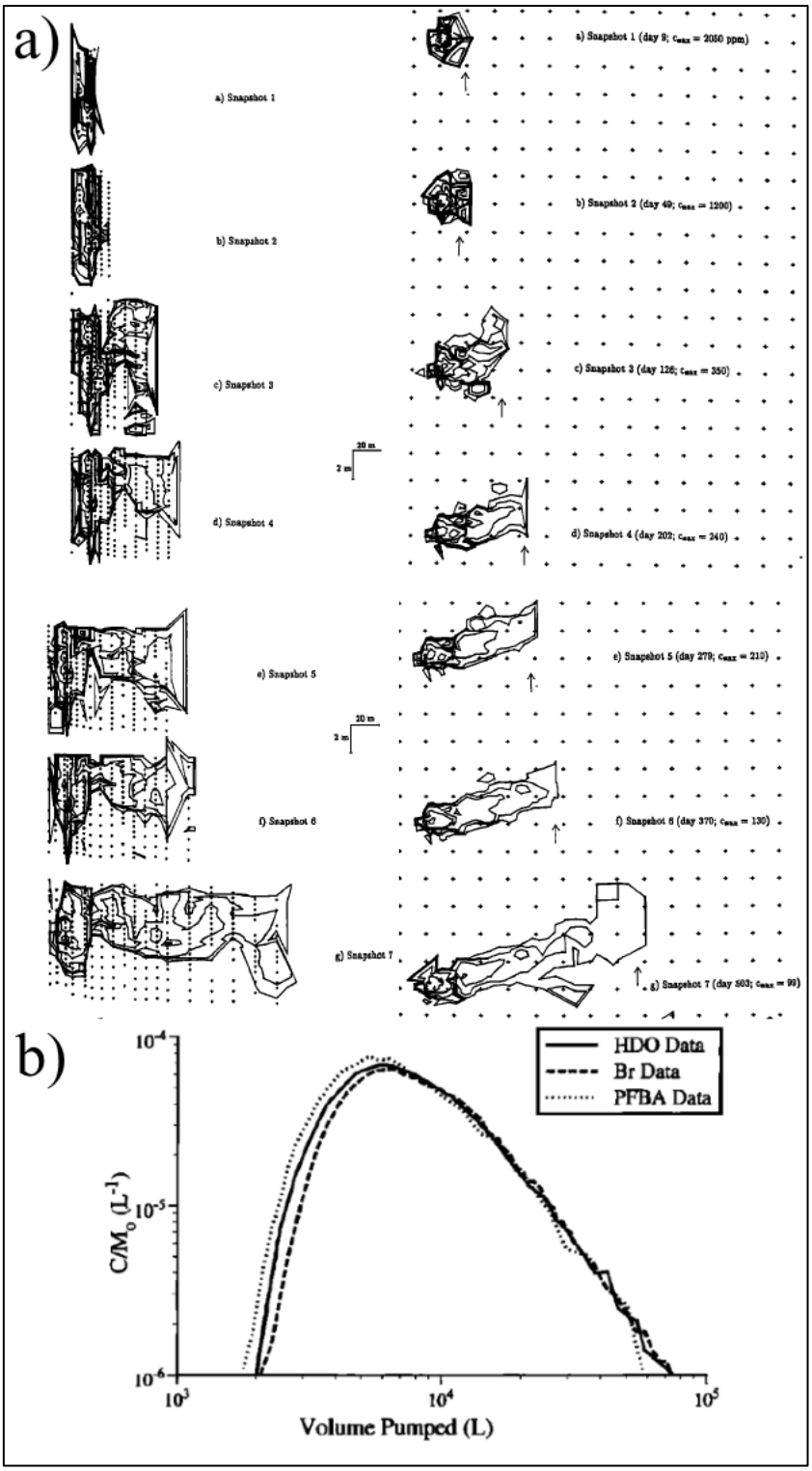

Figure 25: Example of a) the spatial moments approach (Adams & Gelhar 1992) and b) the breakthrough curve approach (Becker & Shapiro 2000).

The spatial moments approach (figure 25a) enables the characterisation of the effective tracer dispersion over time while the BTC approach (figure 25b) only informs on the apparent dispersion at a given time as the analysis generally assumes the spatial homogeneity of the dispersion mechanisms along the travel distance (Bodin et al. 2003). However, for economic reasons, facilities providing

dense networks of observation wells are scarce and thus, the spatial moments approach is only applicable for specific experimental sites (Bodin et al. 2003). As a result, the BTC approach is the most frequently applied tracer test enabling the implementation of various experimental configurations (figure 26). For instance, **cross-borehole tests** (figure 26a) investigate the tracer migration between an injection well and an observation well using either the natural hydraulic gradient or a forced gradient using a pump to constrain the local groundwater flow in the observation well (**convergent test**). If the injection is maintained throughout the experiment, the test is called either a **dipole convergent** or a **dipole divergent** test depending on the ratio of the injection rate on the pumping rate. When the injection rate matches the pumping rate in the observation well, the experiment is called a **perfect dipole** test. Nevertheless, the BTC approach can also be implemented using a single well for the injection and the observation of the tracers (figure 26b). These experiments are called **push-pull tests** and sequentially involve an injection phase (tracer injection) and a pumping phase (tracer monitoring) that can be separated both by a chasing phase (tracer-free groundwater injection) and a resting phase (no injection) of different durations.

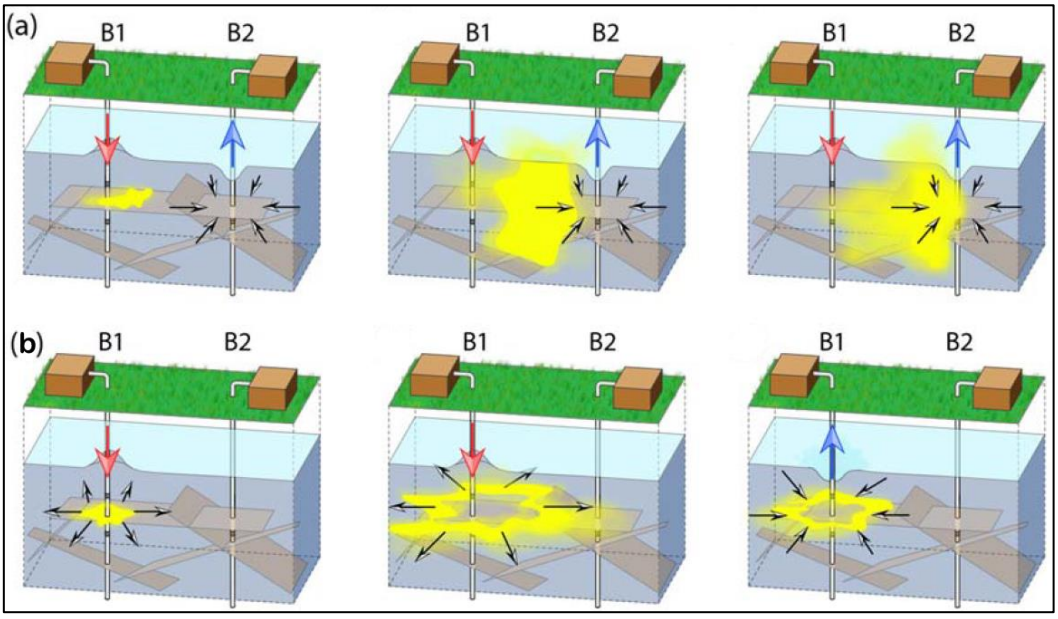

Figure 26: Example of the different configurations of tracer test experiments: a) dipole convergent test and b) push-pull test modified from (Kang et al. 2015).

In fractured media, field tracer tests are often implemented over short travel distances (<30 m) and fractures are usually isolated with packers to minimize possible dilution effects in the wells (figure 27).

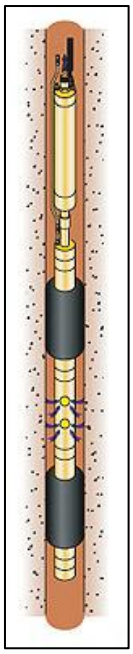

Figure 27: Example of double packer equipped with a pump allowing for groundwater extraction from the isolated zone (usually a fractured zone in the well) placed between the two inflatable elements in black (http://www.geopro.be/images/ill/pumpacker02.jpg).

These various tracer test configurations allow the characterisation of the different solute transport processes in homogeneous and heterogeneous media. As mentioned earlier, some transport processes in fractured media such as matrix diffusion and flow channelling can produce similar BTCs (tailing effects) making these mechanisms difficult to distinguish. As a result, many studies choose to combine various experimental designs (cross-borehole, push-pull) implemented with different tracers (with different diffusivities, chemical properties, etc.) to allow a better understanding of the transport processes at stake. For instance, Becker and Shapiro (Becker & Shapiro 2000) implemented multiple tracer tests using tracers of different diffusivities to observe the effects of matrix diffusion in a fractured geological media. The authors observed BTCs with similar power law slopes associated to tailing effects for all the tracers (figure 25b). Therefore, Becker and Shapiro concluded that strong breakthrough tailing in fractured geologic media may rather be caused by advective transport processes than matrix diffusion. In a second study, Becker and Shapiro (Becker & Shapiro 2003) demonstrate that the observed tailing effects show a -2 power law slope that can be explained by flow channelling (figure 28). On the contrary, breakthrough tailings displaying -3/2 power law slopes characterise matrix diffusion processes (Hadermann & Heer 1996). However, the subsequent attempt of the two authors to separate the effects of flow channelling from hydrodynamic dispersion turned to be unsuccessful.

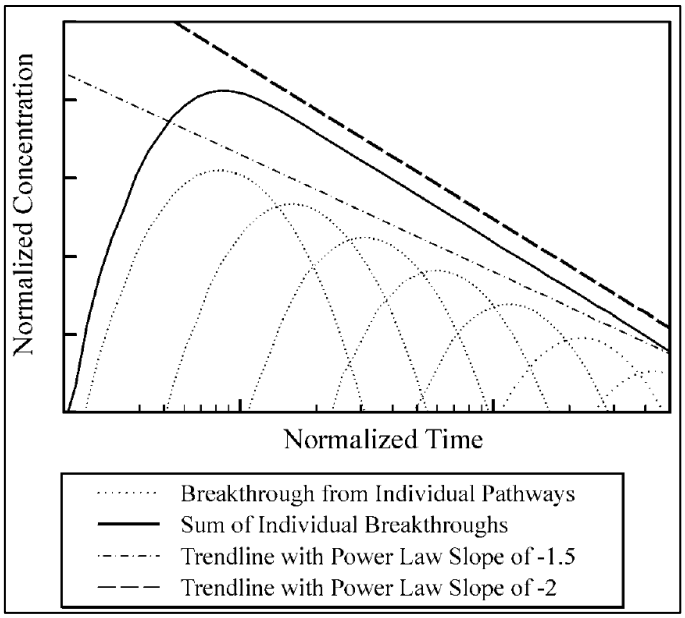

Figure 28: Example of breakthrough curve representing an addition of mass transport along individual flow paths (Becker & Shapiro 2000).

The solute transport analysis from tracer BTCs is often performed by fitting an analytical solution to the tracer test data. Over the last decades, many analytical models have been developed to describe tracer behaviour (Tang et al. 1981; Maloszewski & Zuber 1990; Maloszewski & Zuber 1993; Moench 1995; Haggerty & Gorelick 1995; Haggerty et al. 2000; Reimus et al. 2003; Berkowitz et al. 2008; Roubinet et al. 2012). Each of these models takes into account different transport processes and provides good fit to environmental data. However, a single BTC can be explained by several models holding different assumptions on the processes governing solute transport (Becker & Shapiro 2000). Therefore, single tracer test data do not always allow the identification of the controlling transport mechanisms. Furthermore, Becker and Shapiro (Becker & Shapiro 2003) show that it is possible to obtain very different estimates of transport parameters under different tracer experiment designs. As a result, the authors advise the implementation of several tracer tests under different forced-gradient configurations using different tracers in order to evaluate the uniqueness and the validity of a model and its associated set of transport parameters.

The choice of the tracer to be injected is obviously very important and conditions the results of the groundwater tracer experiments. Tracers could either be conservative (transport only controlled by physical processes) or reactive (transport also affected by biogeochemical processes). Conservative tracers are therefore used to characterise the earlier mentioned advection, dispersion and diffusion processes controlling solute transport in porous media. In addition, reactive tracers can be used to investigate the biogeochemical processes affecting solute transport but also informs on fracture matrix interactions (sorbing tracers and diffusive traces). Usually, conservative tracer tests are implemented with anions (Cl^-, Br^-), dyes (fluorescein/uranine, eosin, rhodamine WT, rhodamine B, sulfo-rhodamine B, amino-G acid, pyranine, lissamine FF), stable isotopes (^2H, ^{13}C, ^{15}N, ^{18}O, ^{34}S), dissolved noble

gases (He, Ne, Kr, Xe), dissolved halogenated compounds (CFCs, SF_6, PFBA) or else, heat. Depending on the investigated processes, reactive tracer tests can be implemented with anions (NO_3^-, SO_4^{2-}, F^-, I^-), cations (Li+, K^+, Sr^{2+}), radioactive isotopes (^3H, ^{14}C, ^{51}Cr, ^{60}Co, ^{82}Br, ^{99}Tc, ^{131}I), dissolved gases (O_2, CO_2, CH_4, N_2, N_2O, H_2, H_2S), dyes (FDA, Resazurin-Resorufin), colloids or else micro-organisms.

Over the past, groundwater tracer tests were implemented using dissolved gas tracers owing to the several advantages they encompass (Eikenberg et al. 1992; Gupta, Moravcik, et al. 1994; Gupta, Stephen Lau, et al. 1994; McNeill et al. 2001). Although little used so far in tracer experiments, dissolved noble gases (He, Ne, Ar, Kr, Xe) are soluble in water and can be injected at saturation without changing significantly the physical (density) and chemical (pH, redox potential, conductivity) properties of the injected water. Noble gases are biogeochemically inert (non-reactive), non-toxic and do not change water taste, smell or colour. They have a low natural background (except Ar and sometimes He) and multiple noble gas tracers can be injected together and analysed with the same equipment (Sanford et al. 1996).

Therefore, where classical tracers may possibly entail flaws (toxicity, sorption, degradation, density effects), noble gas tracers can represent a valuable alternative especially when implementing tracer tests in drinking water supply areas (Uddin et al. 1999; Richter et al. 2008; Visser et al. 2014). Also, dissolved noble gases (particularly He and Ne) were specifically used because their relatively high diffusion coefficients allow the investigation of diffusive transport in fractured heterogeneous media (Sanford et al. 1996; Jardine et al. 1999). Therefore, dissolved noble gases are interesting tracers for the investigation of the physical processes involved in groundwater flow and solute transport in porous media. The reason of the scarce use of noble gases in tracer tests lied so far in the lack of available measurement techniques for these purposes.

On the other hand, dissolved reactive gases such as O_2, CO_2, CH_4, N_2, N_2O, H_2 and H_2S can be used as tracers of biogeochemical reactions occurring in the subsurface. For instance, the injection of these dissolved reactive gases or their biogeochemical production as a consequence of a reactive tracer injection allowed the in-situ investigation of reactions such as aerobic respiration, denitrification or sulphate reduction (Trudell et al. 1986; Smith et al. 1996; Istok et al. 1997; Smith et al. 2004; Kim et al. 2005; Boisson et al. 2013).

In essence, the use dissolved reactive and noble gas tracers comprise many advantages owing to the versatility of their physical and biogeochemical properties. The implementation of dissolved gas tracer tests has therefore a good potential for the field investigation of groundwater flow and solute transport in porous media. However, the development of such experiments is conditioned to the development of suitable dissolved gas measurement techniques.

6. Objectives

This general introduction shows that the forthcoming social and environmental challenges contributed to the emergence of the CZ concept, which intends to increase efforts on field high-frequency observations and multidisciplinary research for a more thorough understanding of our environment and its resilience. In this manuscript these efforts concentrate on water as a central constituent of the CZ and more particularly on ground water. Through the study of aquifer systems, the approaches developed in thesis consist in the implementation of both an innovative instrumentation and original tracers to characterise groundwater hydrobiogeochemical dynamics.

The general objective of this thesis is to describe the potentials and the versatility of dissolved gases as tracers of physical and biogeochemical processes that are taking place at different scales of space and time in groundwater systems.

On the one hand, capturing the information conveyed by dissolved gases relies on the acquisition of reliable data by means of different analytical techniques. However, in the perspective of a high-frequency temporal and spatial exploration of the CZ, the available analytical techniques cannot properly serve the purposes of these investigations. As a result, the first objective of this thesis (Chapter 2) consisted in developing an innovative instrument enabling the continuous field measurements of several dissolved gases.

On the other hand, the analysis of the information behind dissolved gas data relies on our ability to conceptualise and model environmental systems and on our capacity to constrain these models with data. Therefore, this thesis also consisted in collecting multiple tracer data (including dissolved gases) with the objective of (1) characterising the natural dynamics of groundwater systems and the anthropogenic footprint of their exploitation at the catchment scale (Chapter 3) and (2) characterise the physical and biogeochemical processes controlling solute transport in heterogeneous aquifers at the fracture scale (Chapter 4).

Chapter II: Development of an innovative analytical tool for the characterisation of dissolved gases in natural waters

1. State of the art of dissolved gas analysis

Among environmental tracers, dissolved gases have a large contribution to the understanding of various physical, chemical and biological processes occurring at different spatial and temporal scales in the Hydrosphere. The currently available sampling and analytical techniques for dissolved gas measurements imply the acquisition of datasets of varying costs, precisions, exhaustiveness (gas specific or multi-gas analysis), spatio-temporal distribution, representativeness uncertainty and also various lab-time requirements. The choice of a suitable analytical technique conditions thus the investigation outcomes.

The available methods can base their sensing strategies on different properties of the gaseous species for the sampling, extraction, purification, separation and detection of the analytes (gaseous species to be analysed). For instance, there are many gas-specific sensors developed for the direct measurement of dissolved gases (no need for sampling). These techniques are based on the sensor immersion in the water to be analysed where the analyte diffusion through a semi-permeable membrane produces electrochemical reactions between two electrodes enabling thus the analyte detection and measurement of O_2, CO_2, H_2 or H_2S. These electrochemical sensors display very fast response times but are also associated to analyte consumption (water flow is required), gradual drifts (electrolyte consumption) or limited lifetimes (anode consumption). Similarly, dissolved O_2, or CH_4 can also be measured by fiber-optic or other optical sensors based on the near infrared technology (NIR) using either the phenomena of O_2 fluorescence quenching or CH_4 absorption (Wolfbeis 2008). Despite longer response times and higher power consumptions, these optical sensors comprise many advantages over the electrochemical ones and display little maintenance, little analytical drifts and no analyte consumption.

Recently, other spectroscopic methods have been developed for the measurement of gases. Among them, the cavity ring-down spectroscopy (CRDS) is now becoming popular for the use of the analyte laser absorption property enabling the individual measurement of N_2O, CO, CO_2, CH_4, NH_3, H_2S, H_2O and some stable isotopes in gas phases. This novel field deployable technique gives similar results to classical methods such as chromatographic techniques (Christiansen et al. 2015).

As a matter of fact, the most implemented method for dissolved gas analysis is the gas chromatography (GC) (Wilde & Engewald 2014). Firstly, this analytical method is based on the selective retardation (separation) of the different analytes (of the analysed gas phase) that are transported by a carrier gas (mobile phase, usually H_2 or He) in a heated column (stationary phase). Secondly, the separated analytes arrive successively at the end of the column to be detected using a

thermal conductivity (TCD), flame ionization (FID), nitrogen–phosphorus (NPD), flame photometric (FPD) or electron capture (ECD) detector. Additionally, some applications require the GC method to be complemented by one or more mass spectrometric segments (GC-MS) for a better identification of the analytes (Sparkman 2011; Brennwald et al. 2013).

Mass spectrometers have been widely used for absolute and isotopic measurements of gases (Burnard 2013; Sparkman 2011). Firstly, this technique is based on the ionisation of the different analytes (of the analysed gas phase) using different ionisation techniques such as electron ionisation (EI), chemical ionisation (CI), electron capture negative ionization (ECNI), field ionization (FI) or atmospheric pressure chemical ionization (APCI). Secondly, these freshly formed ions are separated according to their mass-to-charge ratios (m/z) using different separation techniques such as quadrupole mass filters (QMF), quadrupole ion traps (QIT), time of flight (TOF), magnetic or electric sectors. Finally, the separated ions are directed towards the detector consisting either in a faraday cup (FC) for abundant analytes or in a secondary electron multiplier (SEM) for low abundant analytes. As the ions travel from the ion source through the m/z filter into the detector they are in free motion. Their path and direction of travel must be determined only by the electrical or magnetic fields which require the mass spectrometer to be operated under vacuum (Sparkman 2011). Today, most noble gas absolute and isotopic measurements use mass spectrometers with EI sources, magnetic sector mass filters and the detection by FCs and SEMs (Beyerle et al. 2000; Burnard 2013). For dissolved noble gases, this method is based on the sampling of water in copper pinch-off tubes from which dissolved gases are extracted at the laboratory under static vacuum. Before analysis, the different extracted gases are purified and separated by an advanced combination of chemical and physical methods (Burnard 2013). This technique therefore requires the field sampling of a few decilitres of water and a few hours for handling each sample preparation and analysis to deliver very precise noble gas data.

Some radioactive gases are naturally occurring in the environment and can be found in natural waters (^{222}Rn for instance). Their measurement can be performed using different techniques in which the radioactive sample is an intrinsic part (internal source) of the counting method (IAEA 2001). For instance, gas counters (ionisation chamber IC or proportional gas counter PGC) are based on the capacity of radioactive analytes to produce radiations colliding with the particles present in the gas counter that are ionised. These collisions (and ionisations) yield electrons which are accelerated by a high-voltage wire (positively charged) to produce a measureable current as electrons reach the wire. This measured current is representative for the number of produced electrons and thus of the energy of the incoming particle that allows recording the radioactive decay event from which they originate. On the other hand, liquid scintillation spectrometers (LSS) are based on the capability of certain liquids placed in the instrument to emit light after being excited by collisions with high-energy particles (electrons). Similarly to gas counters, the measured light allows the quantification of the decay event of interest (IAEA 2001).

Due to their high interest in environmental science and to their very low abundance, gas trace isotopes benefit from dedicated analytical techniques (Lu & Wendt 2003) including resonance ionisation mass spectrometry (RIMS), photon burst mass spectrometry (PBMS), low-level counting (LLC) and accelerator mass spectrometry (AMS). Among these advanced techniques, atom trap trace analysis (ATTA) is a recent atom-counting method developed notably for the measurement of radiokrypton isotopes (^{85}Kr and ^{81}Kr) in natural atmospheric and water samples (Chen 1999; Du et al. 2003). The ATTA enables atoms of a particular isotope to be selectively captured by a magneto-optical trap (tuned diode lasers holding atoms) and detected by observing their fluorescence. This technique comprises many advantages over the others including a higher signal/noise ratio, a higher selectivity and no signal interference. All gas trace isotopes analysis require the sampling of large volumes of water (hundreds to thousands of litres) as well as the dedication of quite large amounts of time to produce the analysis at the laboratory (from several hours to several days).

All these analytical techniques (CRDS, GC, MS, PGC, ATTA …) require the collection of various volumes water from which dissolved gases are subsequently extracted for analysis. Classically, this procedure consist first in a sampling phase carried out in the field where water is collected from lakes, rivers, oceans or boreholes with or without the aid of (submersible or surface) pumps or samplers (Niskin bottles). The subsequent extraction phase occurs at the laboratory using for instance a head space equilibration (Kampbell et al. 1989) or the purge and trap method (Busenberg & Plummer 1992). However, in some cases, the collection and transport of water samples is impractical and the gas extraction phase takes place directly in the field. For instance, this can be achieved with passive samplers which consist in gas-permeable membranes whose gas phase equilibrate with the surrounding water after tens of hours of immersion (Gardner & Solomon 2009; Spalding & Watson 2006; Spalding & Watson 2008). Another example arises from the measurement of ultra-trace noble gas radioisotope abundances such as ^{85}Kr and ^{81}Kr which now require the collection of "only" 5 to10 µL of pure Kr equivalent to the amounts of Kr dissolved in several hundreds of litres of water. As a result, advanced field gas extraction devices were recently developed in order to avoid the collection and transport of such large volumes of water to the laboratory (Yokochi 2016).

All these water or gas samples are collected under some assumptions concerning their representativeness whose veracity is quite uncertain. This applies particularly when sampling water in heterogeneous porous media where groundwater dissolved gas signatures can be very different and much localised. Furthermore, sampling in heterogeneous media can intrinsically induce complex mixing processes in the wells when pumping or when moving sampling devices downhole. Representativeness can also be questioned due to inappropriate sample collection (contamination) or preservation (leaking container, modification of reactive gas concentrations during storage). It is therefore essential to minimise the uncertainties related to the sampling process since they could be misleading when interpreting of the data.

Finally, the spatio-temporal distribution of datasets is obviously conditioned by the cost, the analytical throughput and the complexity inherent to each analytical technique. Therefore, absolute and isotopic measurements of noble gases and trace radioisotopes do not in practice allow a significant spatio-temporal resolution of these very informative data. From a broader perspective, when environmental investigations increasingly require both high-frequency and spatially distributed data, classical analytical procedures still rely on the sampling, storage, transport and analysis of dissolved gases. Suffering from the time, cost and energy necessary to obtain a great number of representative data (several gas species, observation sites, hydrological periods...), classical methods need to be complemented by more appropriate techniques for a thorough spatial and temporal investigation of the Hydrosphere.

2. Context of the analytical development

Over the last century, the Critical Zone faced remarkable climate and land use changes increasing the pressures on the Hydrosphere and giving rise to numerous environmental consequences in terms of water quantity and quality. From now on, the Critical Zone must face the challenge to supply 9 billion people with quality food and safe drinking water in a context of global warming. For the Hydrosphere, this challenge could be addressed with a better understanding of the dynamics and resilience of aquatic environments (rivers, lakes, groundwaters, oceans).

In view of the spatial and temporal variety and variability of flow dynamics and biogeochemical reactions occurring in the Hydrosphere, new investigation methods are needed. This challenge has recently been taken up by the CRITEX project (French excellence equipment program) which aims to develop and share innovative equipment and methods for the investigation of the Critical Zone.

Within this project and in the perspective of a temporal and spatial exploration of aquatic environments (surface and ground water), this chapter presents the development of an original technique for the continuous measurements of several dissolved gases (N_2, O_2, CO_2, CH_4, N_2O, H_2, He, Ne, Ar, Kr, Xe). In addition, the present chapter illustrates the capabilities of this innovative instrument called CF-MIMS (Continuous Flow Membrane Inlet Mass Spectrometer) through two field applications in groundwater systems.

3. Article: Field continuous measurement of dissolved gases with a CF-MIMS: applications to the physics and biogeochemistry of groundwater flow

Environmental Science & Technology

Article

pubs.acs.org/est

Field Continuous Measurement of Dissolved Gases with a CF-MIMS: Applications to the Physics and Biogeochemistry of Groundwater Flow

Eliot Chatton,*[,†] Thierry Labasque,[†] Jérôme de La Bernardie,[†] Nicolas Guihéneuf,[†,‡] Olivier Bour,[†] and Luc Aquilina[†]

[†]OSUR-UMR6118 Géosciences Rennes, Université de Rennes 1 and Centre National de la Recherche Scientifique, Rennes, France
[‡]University of Guelph, 50 Stone Road East, Guelph, Ontario Canada

Supporting Information

ABSTRACT: In the perspective of a temporal and spatial exploration of aquatic environments (surface and groundwater), we developed a technique for field continuous measurements of dissolved gases with a precision better than 1% for N_2, O_2, CO_2, He, Ar, 2% for Kr, 8% for Xe, and 3% for CH_4, N_2O and Ne. With a large resolution (from 1×10^{-9} to 1×10^{-2} ccSTP/g) and a capability of high frequency analysis (1 measure every 2 s), the CF-MIMS (Continuous Flow Membrane Inlet Mass Spectrometer) is an innovative tool allowing the investigation of a large panel of hydrological and biogeochemical processes in aquatic systems. Based on the available MIMS technology, this study introduces the development of the CF-MIMS (conception for field experiments, membrane choices, ionization) and an original calibration procedure allowing the quantification of mass spectral overlaps and temperature effects on membrane permeability. This study also presents two field applications of the CF-MIMS involving the well-logging of dissolved gases and the implementation of groundwater tracer tests with dissolved ^{4}He. The results demonstrate the analytical capabilities of the CF-MIMS in the field. Therefore, the CF-MIMS is a valuable tool for the field characterization of biogeochemical reactivity, aquifer transport properties, groundwater recharge, groundwater residence time and aquifer-river exchanges from few hours to several weeks experiments.

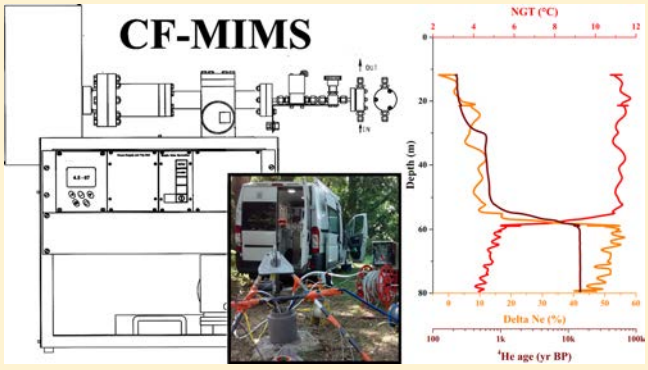

INTRODUCTION

Dissolved gas concentrations in groundwater originate mainly from atmosphere−water equilibria existing at the water table during aquifer recharge. These equilibria are governed by physical laws allowing the calculation of dissolved gas equilibrium concentrations (solubilities) as a function of the gas partial pressure in the air (z_i), the atmospheric pressure (P), the water temperature (T) and salinity (S).[1−8] Therefore, the combined determination of any dissolved gas concentration unaltered from recharge equilibrium enables the reconstruction of recharge conditions (T, S, P) as long as the gas partial pressures at the time of recharge are known. Consequently, several studies have been using dissolved noble gases[9−11] sometimes combined to dissolved nitrogen[12,13] to derive past and present climatic conditions through the determination of noble gas temperatures (NGTs i.e. recharge temperatures), the extent of the excess air phenomenon (EA) and recharge elevations. Therefore, dissolved noble gases (and dissolved nitrogen) are valuable tools for the study of groundwater origins, paleoclimates and climate changes.

Contrary to other noble gases, dissolved ^{4}He concentrations in groundwater can increase quite rapidly (over a hundred years) due to in situ production by radioactive decay of uranium and thorium rich minerals of aquifer rocks. As a result, dissolved radiogenic ^{4}He accumulates over time in aquifers and its production creates an excess He that can be typically quantified for residence time larger than hundred years. The determination of dissolved radiogenic He concentrations enables the characterization of groundwater residence times as long as ^{4}He production rates are known.[14−17]

Dissolved reactive gases (N_2, CO_2, O_2, CH_4, N_2O and H_2) originate initially from atmospheric equilibria. However, their concentrations in natural waters can be significantly altered by biogeochemical reactions that typically occur in aquatic environments.[18] Therefore, the measurement of these reactive dissolved gases is critical to the understanding of the biogeochemical reactivity of aquatic environments.[19−25]

All these applications need precise dissolved gas measurements with various requirements in terms of spatial and

Received: July 24, 2016
Revised: December 4, 2016
Accepted: December 12, 2016
Published: December 12, 2016

DOI: 10.1021/acs.est.6b03706
Environ. Sci. Technol. 2017, 51, 846−854

temporal distribution in the field. Currently, most of the available analytical techniques are based on field sampling and laboratory analysis performed from a few hours or several days after sampling. Therefore, ensuring sample preservation and representativeness is crucial for the determination of accurate actual dissolved gas concentrations. For instance, groundwater sampling in wells is not an easy task due to the risk of sample contamination with atmospheric air, mixing processes naturally occurring in the well (natural flows) or induced by the sampling process (renewal of the well water, pumping, movement of mobile samplers) that would bias water samples.[26] Furthermore, preservation of dissolved gas samples is a crucial stake particularly for the measurement of dissolved reactive gases such as O_2, N_2, N_2O and H_2 in reactive environments.

In order to solve the issues related to sampling, field measurement techniques such as membrane inlet mass spectrometers (MIMS) received great attention from environmental scientists for their capacity of rapid evaluation of dissolved gases in water.[27−32] MIMS technology was first developed for the measurement of organic compounds in environmental water samples.[33,34] Later, Ketola, et al.[35] proposed a review of the applications and improvements of this technique. Kana et al.[36] optimized a MIMS for quasi-continuous determination of major dissolved gases (O_2, N_2, Ar) in water samples in order to study biological activity.[37−40] MIMS systems were also miniaturized for oceanographic studies in order to create dissolved gas profiles in seawater.[41−44]

Recently, developments of MIMS have been realized for groundwater studies. Mächler, et al.[45] developed a portable GE-MIMS for field and laboratory measurements. This stand-alone system allows the quasi-continuous monitoring of dissolved He, Ar, Kr, N_2, and O_2 every 12 min over several days. Similarly, Visser et al.[46] developed also their own portable NG-MIMS for quasi-continuous measurements of the whole suite of dissolved noble gases. However, the NG-MIMS remains sensitive to the sampling conditions as it requires the collection of water samples that are sequentially analyzed (every 5 min). Furthermore, the available field quasi-continuous techniques (GE-MIMS and NG-MIMS) do not allow so far the measurement of all major dissolved gases.

We propose here a new approach for the continuous field measurement of dissolved gases in aquatic environments with a CF-MIMS (Continuous Flow Membrane Inlet Mass Spectrometer). Through this technique, natural waters (surface water or groundwater) are directly brought to a semipermeable membrane at a constant flow rate for the continuous measurement of dissolved gases. With an original calibration procedure, the CF-MIMS allows the continuous monitoring of dissolved noble and reactive gases (He, Ne, Ar, Kr, Xe, N_2, CO_2, O_2, CH_4, and N_2O) over a large concentration range. After presenting the details of the analytical development, the capabilities of the CF-MIMS are evaluated through two field applications: two groundwater tracer tests with dissolved ^4He and a well-logging of dissolved gases.

MATERIALS AND METHODS

System Description. Many MIMS systems are currently available on the market for different applications. The design and conception of the CF-MIMS (HPR-40) was carried out by the private supplier Hiden Analytical. According to the specification requirements, the instrument dimensions (0.150 m^3), weight (55 kg) and shielding (reinforced frame mounted on Silent Bloc) make the CF-MIMS a mobile and resistant tool designed for field experiments.

Although its robustness, the CF-MIMS consists in a leading-edge analytical instrument for dissolved gas measurements. Equipped with a membrane inlet connected to the vacuum of a Quadrupole Mass Spectrometer (QMS around 10^{-5} Torr), the CF-MIMS shown in Figure 1 allow the direct permeation of

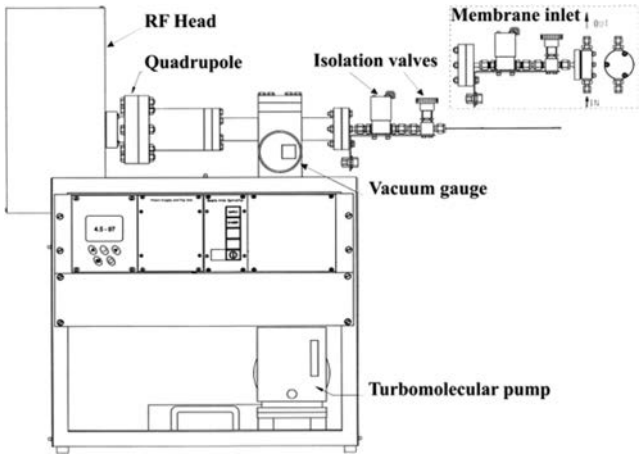

Figure 1. Representation of the CF-MIMS adapted from Hiden Analytical HPR40 manual.

dissolved gases from liquids to the mass spectrometer. Inside the QMS, dissolved gases are ionised using an oxide coated iridium filament allowing the selection of ionization energies (between 4 and 150 eV) and emission intensities (between 20 and 5000 μA). Once ionised, dissolved gases are separated by the quadrupole according to their mass to charge ratios (m/z ratios). Then, the detection of dissolved gases is performed either by a Faraday cup or a single channel electron multiplier (SCEM). Finally, the CF-MIMS allows a direct and continuous measurement of dissolved gases at the high frequency of 1 dissolved gas measurement every 2 s.

Optimisation Techniques. *Membrane.* The originality of MIMS systems lies in the inlet that uses a semipermeable membrane to measure directly the dissolved gases of the water. The choice of a suitable membrane is therefore essential to ensure the maximal permeation of the targeted dissolved gases. Laboratory experiments have been carried out at Hiden Analytical to select or create the best membrane for our purposes by comparing different types of membrane (PDMS, Biaxially oriented PET, X44 polymer). With an enhanced noble gas permeability and a suitable gas exchange surface (16 cm^2), the membrane X44 has been selected for our CF-MIMS. This membrane inlet system (Figure 1) allows a continuous flow measurement of dissolved gases.

Water Vapor Entrapment. In order to enhance the sensitivity of MIMS systems to low abundant gases a water trap can be installed just between the membrane inlet and the mass spectrometer.[46] However, the water trap requires a long stabilization time to remove the totality of the water vapor from the signal and uses lots of electrical power that is hardly available in the field. Since this water entrapment did not significantly enhance signal/noise ratios in our CF-MIMS we chose not to use it.

Ionization. Inside the mass spectrometer, optimization of ionization procedures can be performed to improve the signal/noise ratio by optimization of the emission intensity (flow of

DOI: 10.1021/acs.est.6b03706
Environ. Sci. Technol. 2017, 51, 846−854

ionizing electrons) or, to a lower extent, by experimental determination of optimal ionization energies. In the CF-MIMS, the standard ionization procedure (250 μA, 70 eV) has been optimized by increasing the emission intensity in order to enhance the sensitivity to low abundant gases such as Kr and Xe (see Supporting Information (SI)).

Calibration. In order to convert the partial pressures measured by the CF-MIMS into gas concentrations it is necessary to define a proper calibration procedure. In order to account for the different membrane interactions with dissolved gas concentrations, the system is directly calibrated on water flows of known concentration. For the purpose, a calibration chamber has been built in order to saturate a water volume with different standard gas mixtures of known composition while preventing from any atmospheric exchange (see SI). The Standard Gas Equilibrated Water (SGEW) is continuously brought from the calibration chamber to the membrane using a low voltage impeller pump allowing the monitoring of water saturation until equilibrium is reached.

Measured partial pressures for each gas can be converted into gas concentrations using either an internal or external calibration procedure. The internal calibration consists in the calculation of dissolved gas equilibrium concentrations of different SGEWs using the laws of gas solubility in water.[1−8] The parameters required for the calculation of equilibrium concentrations such as air pressure, water temperature and salinity are continuously monitored in the calibration chamber. In addition, the calibration chamber includes an outlet valve allowing an external calibration by sampling each SGEW for control analysis using classical gas-chromatography techniques (GC-TCD or GC−MS).

The calibration procedure is performed after connecting the membrane inlet to the mass spectrometer and should be implemented when the partial pressure baselines are stable (requiring almost 2 h to establish an equilibrium between the permeation of gases through the membrane and the mass spectrometer vacuum). Calibration temporal stability has been investigated through a laboratory test that did not indicate any sign of instrumental drift over the 38 h experiment. Therefore, when the calibration is achieved and as long as the membrane inlet remains connected, the CF-MIMS does not require any additional calibration. Nevertheless, regular sampling (for analysis with classical techniques) always ensures the validity of the calibration for long-term monitoring experiments.

The CF-MIMS calibration is performed at the same flow and temperature as the measurements because membrane permeability to dissolved gases depends on water temperature and flow. Water flow is controlled by an impeller/submersible pump serving the membrane (Q: 4L/min). Calibrations and measurements are performed in a mobile laboratory conditioned at a controlled temperature close to the temperature of the monitored water. However, when natural waters (in a river or in a borehole) show temperature variations while monitoring, the signals measured with the CF-MIMS must be corrected from temperature effects on the membrane permeability.

Temperature Sensitivity. Laboratory experiments have been carried out to determine the influence of the water temperature on the permeability of the membrane X44. The results (see SI) show that the membrane permeability to gases increases substantially with temperature. Small temperature variations ($\Delta T \pm 2$ °C) can modify the signal acquired at 17 °C from 2.5% to 11.0% depending on the gas considered (He is less sensitive than H_2O to temperature variations). However, the fitted curves allow the calculation of effective permeability coefficients β_T^i of the gas i at the temperature T of measurement expressed in eq 1 as the ratio of the partial pressure of the gas i at the temperature T on the partial pressure of the same gas i at the temperature of calibration (T_{calib}).

$$\beta_T^i = \frac{P_T^i}{P_{T\,calib}^i} \quad (1)$$

The effective permeability coefficients are used when postprocessing the data to correct temperature effects on the membrane permeability for the different gases measured with the CF-MIMS.

Spectral Overlaps. In MIMS systems, the simplest case consists in measuring dissolved gases directly at their corresponding m/z. For instance, the partial pressures of He, Ar, Kr, Xe, and O_2 can be respectively associated with the m/z at 4, 40, 84, 132, and 32. However, in mass spectrometry, spectral overlaps are issues frequently encountered.

The objective of the CF-MIMS is to measure the full suite of noble gases (He, Ne, Ar, Kr, Xe) as well as the most common dissolved gases (N_2, O_2, CO_2, CH_4, and N_2O). These dissolved species coexist in natural waters and unfortunately some of them occur at m/z ratio overlapping with other gases as shown in Table 1. Most of the time, the overlapping gases are also among the targeted ones which inhibits the use of traps and getters[46] to remove the overlapping N_2, CO_2, CH_4, N_2O and Ar.

Table 1. Spectral overlaps occurring at measured mass-to-charge ratios

m/z	targeted gas	main overlap	second overlap
12	**CO_2**	CH_4	
14	**N_2**	N_2O	
15	**CH_4**	N_2	
20	**Ne**	Ar	H_2O
22	**Ne**	CO_2	N_2O
28	**N_2**	N_2O	CO_2
44	**CO_2/N_2O**		

Without traps and getters, the other way to remove overlapping species at a particular m/z ratio is to optimize ionization energies. For instance, laboratory tests have been carried out to distinguish Ne signals from $^{20}(Ar_{(II)})$ and $^{20}(H_2O)$ or from $^{22}(CO_{2(II)})$ and $^{22}(N_2O_{(II)})$ using lower ionization energies to avoid the second ionization of overlapping gases at m/z 20 and 22 respectively. Although ^{20}Ne and $^{20}(Ar_{(II)})$ could be separated from $^{20}(H_2O)$, the attempts to fully discriminate (with ionization energies) Ne signals from $^{20}(Ar_{(II)})$, $^{22}(CO_{2(II)})$ or $^{22}(N_2O_{(II)})$ were unsuccessful despite the information reported in other works on similar QMS systems.[47,48]

Therefore, we choose to overcome the issue of spectral overlaps by calibrating the CF-MIMS with a variety of suitable standard gases allowing the quantification of these overlaps. The idea here is to quantify the distribution of a given gas on the different m/z ratios of interest. For instance, CO_2 is found at m/z 12, 22, 28, and 44 (Table 1) and its distribution over each of these m/z ratios can be measured and expressed as polynomials (see Supporting Information). This is performed by monitoring the partial pressures at these m/z ratios when

DOI: 10.1021/acs.est.6b03706
Environ. Sci. Technol. 2017, 51, 846−854

saturating a volume of water in the calibration chamber with pure CO_2 and desaturating it with another pure gas (N_2, Ar, He, etc.). The same rationale applies for N_2 at m/z 14, 15, 28 and for Ar at m/z 20 and 40. The polynomials linking the partial pressures P_k^i and P_l^i of the gas i measured respectively at m/z k and l are expressed in eq 2:

$$P_k^i = f(P_l^i) = \sum_{n=0}^{N} \alpha_n (P_l^i)^n \quad (2)$$

Once fitted to the data, the resulting polynomials allow the determination of relationships between each m/z ratios due to each gas (CO_2, N_2 and Ar) over a large concentration range. As a result, any significant partial pressure change away from the fitted polynomials indicates an overlap attributable either to Ne, N_2O or CH_4 depending on the considered m/z. In this case, the partial pressure (P_k^j) attributed to the overlapping gas j can be calculated as the difference between the total partial pressure (P_k) measured at m/z k and the partial pressure (P_k^i) of the gas i at m/z k as expressed in eq 3:

$$P_k^j = P_k - P_k^i = P_k - \sum_{n=0}^{N} \alpha_n (P_l^i)^n \quad (3)$$

This method relies on multiple measurements at different m/z ratios of the same targeted gas to guarantee a better precision (the gas is measured twice or thrice) and a better confidence respect to overlaps (the different m/z ratios of a gas usually do not undergo the same overlap).

After calibration and measurement, the data files provided by the CF-MIMS are postprocessed using a data processing program implemented in Matlab that calculates the partial pressure $P_{m/z}^i$ of the gas i at m/z using the spectral overlap polynomials and the effective permeability coefficients β_T following eq 4:

$$P_{m/z}^i = \beta_T^i * [P_{m/z} - \sum_j (\beta_T^j \times \sum_{n=0}^{N} \alpha_n (P_{m/z}^j)^n)] \quad (4)$$

Dissolved gases undergoing overlaps are hence calculated as the difference between the measured partial pressure at a given m/z and the sum of partial pressures produced by the overlapping species j weighted by their effective permeability coefficients (β_T^j). Therefore, it is essential to properly assess the different overlap polynomials.

Finally, the data processing program calculates and compiles the partial pressures of each gas free from overlaps, determines internal or external calibration coefficients for each gas and provides the dissolved gas concentrations that are delivered as a spreadsheet.

Analytical Performances. For each dissolved gas, laboratory experiments have been carried out to evaluate the analytical precisions of the CF-MIMS (expressed as the relative standard deviation, RSD) and the detection limits (DL) for reactive (N_2, O_2, CO_2, CH_4, N_2O) and noble (He, Ne, Ar, Kr, Xe) gases. Table 2 shows the details of the analytical performances of the CF-MIMS measured from three series of monitoring (2 h) of an AEW kept at a constant temperature (17 °C). The analytical frequency of the instrument allows the measurement of a m/z ratio every two seconds (the measurement of gas can require more than one m/z measurement). Therefore, a measurement cycle of the 10 gases listed in the Table 2 takes about 26 s.

Table 2. Experimental Assessment of the CF-MIMS Gas Measurement Precisions (RSD) and Estimated Detection Limits (DL)[a]

gas	RSD (%)	DL (× 10^{-9} ccSTP/g)
N_2	0.3	750
O_2	0.3	2
CO_2	0.3	2000
CH_4	2.0	800*
N_2O	0.3	900*
He	1.0	0.01
Ne	2.5	6*
Ar	0.3	200
Kr	1.2	0.5
Xe	7.5	4

[a]Asterisks refer to DL estimations performed on the basis of 3 × RSD of the most abundant gas at the measured m/z for typical concentrations obtained with an AEW (CO_2 = 4.3 × 10^{-4} ccSTP/g; N_2 = 1.4 × 10^{-2} ccSTP/g).

As Ne, CH_4, and N_2O are measured at overlapped m/z ratios, their detection limits depend also on the analytical uncertainty of the main overlapping gas at these m/z ratios (respectively $^{22}(CO_2)$, $^{15}(N_2)$ and $^{44}(CO_2)$). Table 2 displays an example of the detection limits calculated for Ne, CH_4 and N_2O for an air equilibrated water ($[CO_2]_{atm}$ = 0.04% and $[N_2]_{atm}$ = 78.08%) expressed as three RSD of the main overlapping gas. As a result, higher levels of N_2 or CO_2 would increase proportionally the detection limits of Ne, CH_4, and N_2O.

FIELD APPLICATIONS

Groundwater Tracer Test with Dissolved ^{4}He. In hydrogeology, groundwater introduced tracer tests are usually performed with salts or fluorescent dyes in order to derive the transport properties of aquifers.[49−51] Although little used so far in tracer tests, dissolved noble gases are inert tracers of the physical processes governing conservative transport in aquifers such as advection, dispersion, and diffusion.[52−55] Where classical tracers may possibly entail flaws such as toxicity, sorption, degradation, or density effects,[56−58] dissolved noble gases can represent a valuable alternative especially when implementing tracer tests in drinking water supply areas.[59] As a result, we decided to evaluate the potential of the CF-MIMS to perform continuous and field measurements through a groundwater tracer test using dissolved ^{4}He.

The groundwater tracer test was carried out in a fractured aquifer located at the experimental site of Ploemeur (H+ observatory network, Brittany, France) at the contact zone between a granitic formation and the overlying micaschist.[60] This vertical tracer test was performed in a single well (B3) and consisted in the combined pulse injection of dissolved ^{4}He (60 L of He saturated water) and a fluorescent dye called amino-G acid (7-amino-1,3-naphthalenedisulfonic acid) in a fracture crossing the borehole at 44.9m (B3.2) while pumping in an hydraulically connected fractured zone (B3.1) found in the same well at 34.0m. Tracer path was constrained into the fracture network using low flow injections (6 L/min) below a single packer placed in the borehole between the two connected fractures.

Figure 2 shows the ^{4}He and amino-G acid (AG) breakthrough curves produced respectively by the CF-MIMS and the fluorimeter over two tracer tests performed with two pumping

DOI: 10.1021/acs.est.6b03706
Environ. Sci. Technol. 2017, 51, 846−854

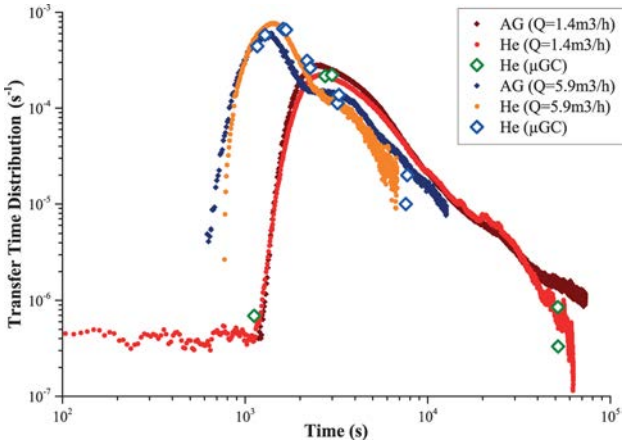

Figure 2. ^{4}He and AG acid breakthrough curves obtained with two different pumping conditions (1.4 and 5.9 m^3/h). The transfer time distribution curves (s^{-1}) refer to the tracer mass flux (g/s) divided by the recovered mass of tracer (g).

rates (1.4 and 5.9 m^3/h). For these short tracer tests, ^{4}He and AG show similar breakthrough curves (although ^{4}He systematically peaks late) as well as similar fitted transport parameters (see SI) using a semianalytical solution developed by Becker and Charbeneau.[49] For longer tracer tests, the differences between the two breakthrough curves are expected to increase with time due to a higher He diffusion.

This groundwater tracer tests show that the CF-MIMS is able to measure dissolved gas concentrations in situ over experiments of several hours and to record large concentration gradients with high temporal resolution. The CF-MIMS measurements are directly validated by control sampling performed during the two tracer tests and indirectly by AG breakthrough curves produced by the fluorimeter.

Well-Logging of Dissolved Gases. Classically, a first order characterization of groundwater geochemistry is achieved using a multiparameter probe allowing the vertical measurement of the field parameters in wells (temperature, electrical conductivity, pH, redox potential, and dissolved oxygen). More detailed investigations require additional measurements that are usually performed through the sampling of targeted dissolved species (gases, ions, stable isotopes, etc.). The results of such geochemical characterization are hardly available on the field and rely inherently on substantial uncertainties associated with sampling (representativeness, contamination, and preservation of the sample). Besides, due to practical constrains the exhaustiveness (number of measured parameters, spatial, and temporal distribution) of classical geochemical characterization is often limited in view of the variety and variability of biogeochemical processes in time and space.

In order to test the method developed here, we have investigated the potential of performing a well-log of dissolved gases with the CF-MIMS in a borehole (Pz6) drilled in a schist bedrock and located nearby our laboratory in Rennes (H+ observatory, Brittany, France). The transportation and power supply of the CF-MIMS has been made possible thanks to the mobile laboratory arranged in an all-terrain truck (CRITEX Lab). This simple experiment consisted in coupling a multiparameter probe (OTT Hydrolab) to the well-pump (Grundfos MP1) serving the CF-MIMS in order to measure the evolution with depth of dissolved gases concentrations (He, Ne, Ar, Kr, Xe, N_2, O_2, CO_2, CH_4), temperature (T), pH, electrical conductivity (σ), and redox potential (Eh). The pumping rate (3 L/min) and the logging velocity (2.5 m/min) have been adjusted to the borehole diameter, the number of measured dissolved gases and hence to the measurement frequency of the CF-MIMS (12 m/z every 24 s for 1 measure every meter).

The Figure 3 shows the profiles that were obtained at Pz6 for the field parameters (Figure 3a), the reactive dissolved gases (Figure 3b) and the dissolved noble gases (Figure 3c). This well-log consists in two contrasted groundwater bodies and two transition zones: (80−60m) high pH and conductivity, high

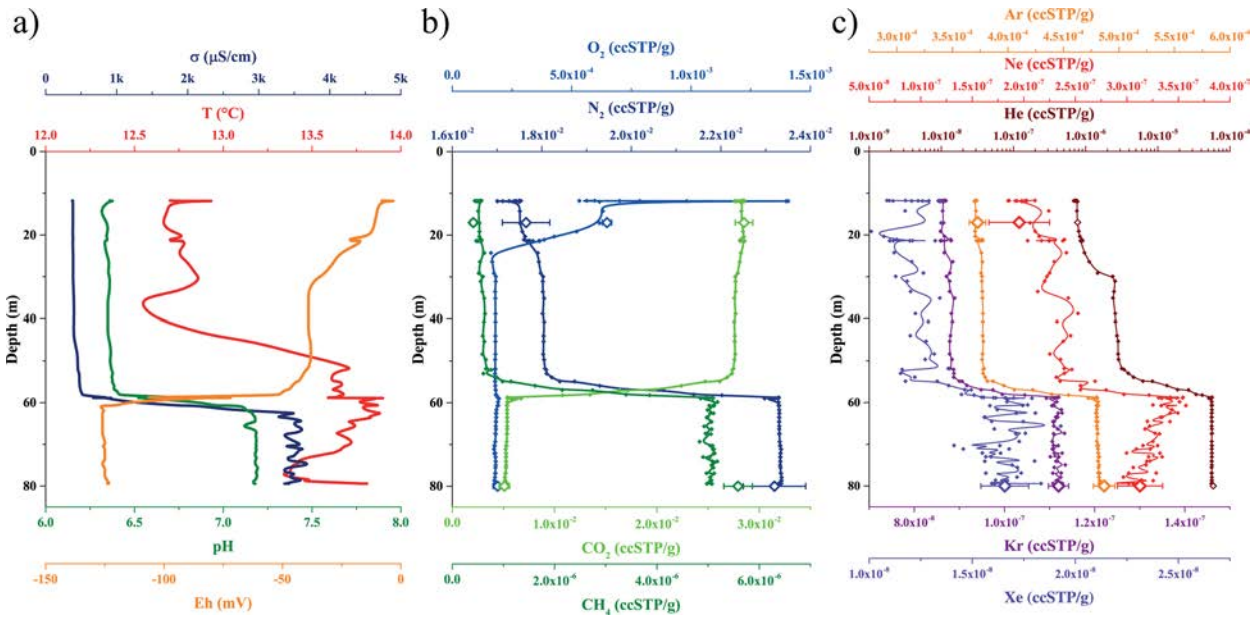

Figure 3. Well-logs performed at Pz6 for (a) water temperature (T), electrical conductivity (σ), pH and redox potential (Eh); (b) reactive dissolved gases (N_2, O_2, CO_2, CH_4); (c) dissolved noble gases (He, Ne, Ar, Kr, Xe). The large dots in (b) and (c) refer to samples collected at 17 m and 80 m. Continuous lines refer to a spline fit of the data points shown as small dots in the figure.

DOI: 10.1021/acs.est.6b03706
Environ. Sci. Technol. 2017, 51, 846−854

Table 3. Comparison of CF-MIMS Measurements with Measurements of Dissolved Gases in Pz6 Conducted Either (*) at the University of Rennes by Gas-Chromatography[61,62] or (#) in Situ by Mass-Spectrometry with a NG-MIMS.[46]

depth (m)	gas*#	sample (ccSTP/g)	sample RSD (%)	CF-MIMS (ccSTP/g)	CF-MIMS RSD (%)	relative difference (%)
17	N_2*	1.76×10^{-2}	3.0	1.75×10^{-2}	0.3	0.5
	O_2*	6.48×10^{-4}	3.0	6.21×10^{-4}	1.3	3.0
	CO_2*	2.85×10^{-2}	3.0	2.84×10^{-2}	0.3	0.5
	CH_4*	4.11×10^{-7}	15.0	5.29×10^{-7}	3.0	17.5
	He*	7.75×10^{-7}	3.0	1.19×10^{-6}	3.5	1.0
	Ne*	1.96×10^{-7}	10.0	2.11×10^{-7}	5.0	5.5
	Ar*	3.73×10^{-4}	2.5	3.71×10^{-4}	0.1	0.5
80	N_2*	2.32×10^{-2}	3.0	2.33×10^{-2}	0.1	0.5
	O_2*	1.90×10^{-4}	10.0	1.77×10^{-4}	0.6	5.0
	CO_2*	5.09×10^{-3}	10.0	5.24×10^{-3}	2.1	2.0
	CH_4*	5.59×10^{-6}	5.0	5.05×10^{-6}	0.7	7.0
	He#	5.88×10^{-5}	2.0	5.82×10^{-5}	1.3	3.0
	Ne#	3.13×10^{-7}	6.5	3.04×10^{-7}	4.8	2.0
	Ar#	4.87×10^{-4}	2.0	4.83×10^{-4}	0.1	0.5
	Kr#	1.12×10^{-7}	2.0	1.12×10^{-7}	0.7	0.5
	Xe#	1.66×10^{-8}	6.5	1.66×10^{-8}	5.2	0.5

reactive and noble gas concentrations except CO_2 and low Eh and O_2; (60−55m) a mixing zone where almost all the parameters change; (55−30m) lower pH, conductivity and dissolved gas concentrations except CO_2 that increases, low O_2 and higher Eh. The shallowest part of the well (30−12m) shows a transition toward an atmospheric dissolved gas composition.

During the well-logging experiment discrete samples were collected and analyzed using accepted analytical protocols.[46,61,62] A comparison of these analyses with the CF-MIMS measurements is shown in Table 3. Both measurements agree for all dissolved gases analyzed within the error of the respective methods.

The field measurement of dissolved noble gas concentrations allow to derive profiles of groundwater recharge conditions[63] and the amount of nonatmospheric ^{4}He produced by radiogenic U and Th of the rocks. With no mantle He and using a production rate of 4×10^{-9} ccSTP/g/yr for ^{4}He calibrated on ^{14}C ages,[64] the groundwater residence time can be assessed for regional groundwater circulations using ^{4}He dating.[17] Figure 4 shows the field determination of the distribution with depth of noble gas temperatures (NGTs i.e. recharge temperatures), amounts of excess air (commonly expressed as the $\Delta Ne = ((CNe_{meas}/CNe_{eq}) - 1) \times 100$) and ^{4}He ages.

Similarly to the previous profiles, the Figure 4 shows three groundwater layers: (80−60m) low NGTs (≈5 °C) associated with large ΔNe (≈50%) and ^{4}He ages (≈14 000 yr BP); (60−55m) mixing zone; (55−12m) NGTs around 11 °C associated with smaller ΔNe (≈ 10%) and ^{4}He ages (≈ 500 yr BP). The shallowest part of this layer (30−12m) shows decreasing ΔNe (0% in average) and ^{4}He ages (≈200 yr BP) toward the water table.

This field experiment illustrates the usefulness of field measurements of dissolved gases for the characterization of groundwater chemistry and the determination of groundwater origins. The field continuous measurements performed with the CF-MIMS make available a quantity of valuable distributed information so far inaccessible during field works.

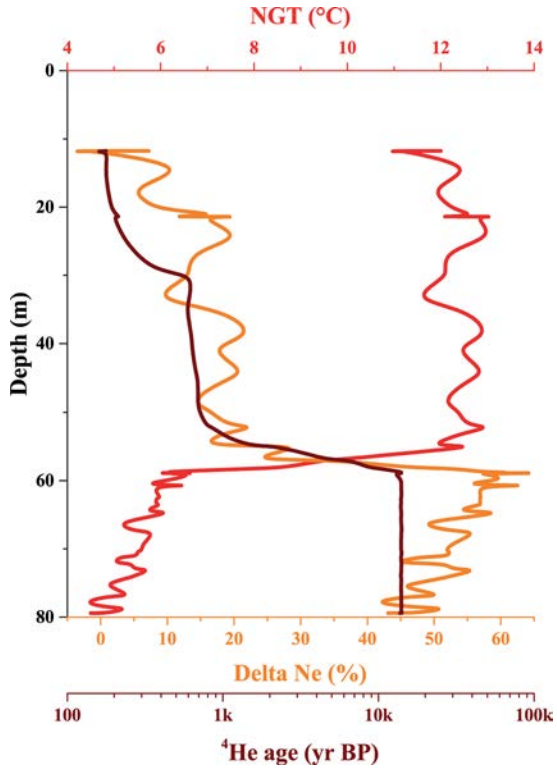

Figure 4. Profile of noble gas temperature (NGT), ΔNe, and ^{4}He age distribution with depth.

DISCUSSION

Calibration. Precise dissolved gas measurements with a CF-MIMS can only be achieved with a proper calibration procedure which is not so trivially accomplished because it is performed on SGEWs (a precise determination of their composition is essential) with a water flow and temperature dependent membrane permeability (a precise determination of these effects is also necessary). In addition, calibration of Ne, CH_4, and N_2O require a special care (use of additional SGEWs) in order to overcome spectral overlap issues.

DOI: 10.1021/acs.est.6b03706
Environ. Sci. Technol. 2017, 51, 846−854

When the calibration procedure is properly achieved and as long as the membrane inlet remains connected to the mass spectrometer, the CF-MIMS allow a continuous monitoring of dissolved gases over relatively long experiments (days or weeks) without additional calibration (standard bracketing). The latter would alter the benefits of the continuous measurements since the CF-MIMS measurements require as much stability as possible. For long monitoring experiments we thus recommend a regular sampling to ensure the validity of the calibration. So far, biogeochemical clogging of the membrane has not been observed which might be explained by the nature of the membrane X44.

Capabilities of the CF-MIMS. First, the dissolved gas tracer tests demonstrate the ability of the CF-MIMS to perform field dissolved gas measurements accurate enough to produce appropriate breakthrough curves during groundwater tracer tests. This experiment exhibits the instrument capabilities for high-frequency measurements and its rapidity to quantify large concentration gradients. The CF-MIMS offer new perspectives for groundwater tracer tests enabling the use of new tracers (noble and reactive gases) and allowing a combined injection of several tracers of different nature (salts, fluorescent tracers, dissolved gases, etc.).

As for tracer tests, the well-logging experiment demonstrates the ability of the CF-MIMS to work at high-frequency in situ and provide accurate environmental measurements allowing in this case the determination of groundwater recharge conditions, groundwater residence time, and redox conditions profiles. These field continuous measurements do not only solve the problems associated with sampling (representativeness, contamination or preservation of samples) but also, taken as a whole, improve the quality of the information carried by each value of the data set (enhanced representativeness with distributed measurements and enhanced precision with several replicates). Therefore, the CF-MIMS gives access to spatially and temporally distributed data of great significance that represents an important breakthrough for environmental measurements.

In addition, the CF-MIMS ability to produce field continuous measurements allows the scientist to visualize and interpret the data directly on site allowing a better definition of field experiment strategies and a higher flexibility when implementing them. Finally, the rationale behind the CF-MIMS technology consists in bringing back environmental scientists on the field to get a much more thorough understanding of the site structure and properties all along the experiments.

Potential Applications. Once installed in the mobile laboratory, the CF-MIMS has the required mobility to perform in situ measurements in a large diversity of accessible areas (boreholes, rivers, vadose zone, sea or lake shores, wetlands). In these sites, the high-frequency and multitracer measurements offered by this instrument allow the observation of a variety of stable to highly transitory physical, chemical or biological phenomena modifying dissolved gases concentrations (water flow, mixing, degassing, biochemical consumption/production of one or more gas(es)). Therefore, the CF-MIMS is a valuable tool for the field characterization of biogeochemical reactivity in aquatic systems, aquifer and river transport properties, groundwater recharge conditions, groundwater residence time (^{4}He, ^{40}Ar) and aquifer−river exchanges.

■ ASSOCIATED CONTENT

Supporting Information

The Supporting Information is available free of charge on the ACS Publications website at DOI: 10.1021/acs.est.6b03706.

Measurement settings, Instrumental drift, Temperature Sensitivity, Calibration standard gases, Overlap extents, Tracer test details, Part List (PDF)

■ AUTHOR INFORMATION

Corresponding Author

*Phone: (+33) 223 233 725; e-mail: eliot.chatton@gmail.com.

ORCID

Eliot Chatton: 0000-0002-8234-1479

Notes

The authors declare no competing financial interest.

■ ACKNOWLEDGMENTS

This study was funded by the CRITEX program (ANR-11-EQPX-0011). The ANR projects CRITEX and Stock-en-Socle also coprovided financial support to fund the Ph.D. of E.C. We thank Hiden Analytical especially Thomas Gaudy and Peter Hatton for the high quality of their customer service. We are also grateful to Christophe Petton and Nicolas Lavenant for their technical help in the conception and building of the calibration chamber. MicroGC dissolved gas analysis were performed within the CONDATE-EAU analytical platform. We also thank Ate Visser for allowing us to use his data of the G-DAT 2012. Finally, we thank the two anonymous reviewers for their careful revision of the manuscript.

■ REFERENCES

(1) Clever, H. L. Helium and Neon - Gas Solubilities. *Solubility data Ser.* **1979**, *1*, 393.

(2) Clever, H. L. Krypton, Xenon and Radon - Gas-Solubilities. *Solubility data Ser.* **1979**, *2*, 357.

(3) Clever, H. L. Argon. *Solubility data Ser.* **1980**, *4*, 331.

(4) Smith, S. P.; Kennedy, B. M. The solubility of noble gases in water and in NaCl brine. *Geochim. Cosmochim. Acta* **1983**, *41* (1), 503−515.

(5) Weiss, R. F. The solubility of nirogen, oxygen and argon in water and seawater. *Deep-Sea Res. Oceanogr. Abstr.* **1970**, *17*, 721−735.

(6) Weiss, R. F. Carbon dioxide in water and seawater: the solubility of a non-ideal gas. *Mar. Chem.* **1974**, *2*, 203−215.

(7) Weiss, R. F.; Price, B. A. Nitrous oxide solubility in water and seawater. *Mar. Chem.* **1980**, *8*, 347−359.

(8) Wiesenburg, D. A.; Guinasso, N. L. Equilibrium solubilities of methane, carbon monoxide, and hydrogen in water and sea water. *J. Chem. Eng. Data* **1979**, *24* (4), 356−360.

(9) Aeschbach-Hertig, W.; Peeters, F.; Beyerle, U.; Kipfer, R. Interpretation of dissolved atmospheric noble gases in natural waters. *Water Resour. Res.* **1999**, *35* (9), 2779−2792.

(10) Aquilina, L.; Vergnaud-Ayraud, V.; Armandine Les Landes, A.; Pauwels, H.; Davy, P.; Petelet-Giraud, E.; Labasque, T.; Roques, C.; Chatton, E.; Bour, O.; Ben Maamar, S.; Dufresne, A.; Khaska, M.; Le Gal La Salle, C.; Barbecot, F. Impact of climate changes during the last 5 million years on groundwater in basement aquifers. *Sci. Rep.* **2015**, *5*, 14132.

(11) Stute, M.; Schlosser, P. Principles and applications of the noble gas paleothermometer. In *Geophys. Monogr.*, **1993**, *78*.8910.1029/GM078p0089

(12) Chatton, E.; Aquilina, L.; Petelet-Giraud, E.; Cary, L.; Bertrand, G.; Labasque, T.; Hirata, R.; Martins, V.; Montenegro, S.; Vergnaud, V.; Aurouet, A.; Kloppmann, W.; Pauwels, H. Glacial recharge,

salinization and anthropogenic contamination in the coastal aquifers of Recife (Brazil). *Sci. Total Environ.* **2016**, *569−570*, 1114−1125.
(13) Plummer, L. N.; Eggleston, J. R.; Andreasen, D. C.; Raffensperger, J. P.; Hunt, A. G.; Casile, G. C. Old groundwater in parts of the upper Patapsco aquifer, Atlantic Coastal Plain, Maryland, USA: evidence from radiocarbon, chlorine-36 and helium-4. *Hydrogeol. J.* **2012**, *20* (7), 1269−1294.
(14) Andrews, J. N.; Davis, S. N.; Fabryka-Martin, J.; Fontes, J. C.; Lehman, B. E.; Loosli, H. H.; Michelot, J. L.; Moser, H.; Smith, B.; Wolf, M. The in situ production of radioisotopes in rock matrices with particular reference to the Stripa granite. *Geochim. Cosmochim. Acta* **1989**, *53*, 1803−1815.
(15) Méjean, P.; Pinti, D. L.; Larocque, M.; Ghaleb, B.; Meyzonnat, G.; Gagné, S. Processes controlling 234U and 238U isotope fractionation and helium in the groundwater of the St. Lawrence Lowlands, Quebec: The potential role of natural rock fracturing. *Appl. Geochem.* **2016**, *66*, 198−209.
(16) Solomon, D. K.; Hunt, A. G.; Poreda, R. J. Source of radiogenic helium 4 in shallow aquifers: Implications for dating young groundwater. *Water Resour. Res.* **1996**, *32* (6), 1805−1813.
(17) Wei, W.; Aeschbach-hertig, W.; Chen, Z. Identification of He sources and estimation of He ages in groundwater of the North China Plain. *Appl. Geochem.* **2015**, *63*, 182−189.
(18) Boisson, A.; De Anna, P.; Bour, O.; Le Borgne, T.; Labasque, T.; Aquilina, L. Reaction chain modeling of denitrification reactions during a push-pull test. *J. Contam. Hydrol.* **2013**, *148*, 1−11.
(19) Abbott, B. W.; Jones, J. B.; Godsey, S. E.; Larouche, J. R.; Bowden, W. B. Patterns and persistence of hydrologic carbon and nutrient export from collapsing upland permafrost. *Biogeosciences* **2015**, *12* (12), 3725−3740.
(20) Beaulieu, J. J.; Tank, J. L.; Hamilton, S. K.; Wollheim, W. M.; Hall, R. O.; Mulholland, P. J.; Peterson, B. J.; Ashkenas, L. R.; Cooper, L. W.; Dahm, C. N.; Dodds, W. K.; Grimm, N. B.; Johnson, S. L.; McDowell, W. H.; Poole, G. C.; Maurice Valett, H.; Arango, C. P.; Bernot, M. J.; Burgin, A. J.; Crenshaw, C. L.; Helton, A. M.; Johnson, L. T.; O'Brien, J. M.; Potter, J. D.; Sheibley, R. W.; Sobota, D. J.; Thomas, S. M. Nitrous oxide emission from denitrification in stream and river networks. *Proc. Natl. Acad. Sci. U. S. A.* **2011**, *108* (1), 214−219.
(21) Gardner, J. R.; Fisher, T. R.; Jordan, T. E.; Knee, K. L. Balancing watershed nitrogen budgets: accounting for biogenic gases in streams. *Biogeochemistry* **2016**, *127* (2−3), 231−253.
(22) Kling, G. W.; Kipphut, G. W.; Miller, M. C. Arctic Lakes and Streams as Gas Conduits to the Atmosphere: Implications for the Tundra Carbon Budgets. *Science* **1991**, *251* (4991), 298−301.
(23) Mächler, L.; Brennwald, M. S.; Tyroller, L.; Livingstone, D. M.; Kipfer, R. Conquering the outdoors with on-site mass spectrometry. *Chimia* **2014**, *68* (3), 155−159.
(24) Peter, S.; Mächler, L.; Kipfer, R.; Wehrli, B.; Durisch-Kaiser, E. Flood-Controlled Excess-Air Formation Favors Aerobic Respiration and Limits Denitrification Activity in Riparian Groundwater. *Front. Environ. Sci.* **2015**, *3*, 75.
(25) Riley, A. J.; Dodds, W. K. Whole-stream metabolism: strategies for measuring and modeling diel trends of dissolved oxygen. *Freshw. Sci.* **2013**, *32* (1), 56−69.
(26) Reilly, T. E.; LeBlanc, D. R. Experimental Evaluation of Factors Affecting Temporal Variability of Water Samples Obtained from Long-Screened Wells. *Groundwater* **1998**, *36* (4), 566−576.
(27) Cowie, G.; Lloyd, D. Membrane inlet ion trap mass spectrometry for the direct measurement of dissolved gases in ecological samples. *J. Microbiol. Methods* **1999**, *35* (1), 1−12.
(28) Kotiaho, T. On-site environmental and in situ process analysis by mass spectrometry. *J. Mass Spectrom.* **1996**, *31* (1), 1−15.
(29) Lloyd, D.; Scott, R. I. Direct measurement of dissolved gases in microbiological systems using membrane inlet mass spectrometry. *J. Microbiol. Methods* **1983**, *1* (6), 313−328.
(30) Takahata, N.; Igarashi, G.; Sano, Y. Continuous monitoring of dissolved gas concentrations in groundwater using quadrupole mass spectrometer. *Appl. Geochem.* **1997**, *12* (4), 377−382.
(31) Virkki, V. T.; Ketola, R. A.; Ojala, M.; Kotiaho, T.; Komppa, V.; Grove, A.; Facchetti, S. On-Site Environmental Analysis by Membrane Inlet Mass Spectrometry. *Anal. Chem.* **1995**, *67* (8), 1421−1425.
(32) White, A. J.; Blamire, M. G.; Corlett, C. A.; Griffiths, B. W.; Martin, D. M.; Spencer, S. B.; Mullock, S. J. Development of a portable time-of-flight mebrane inlet mass spectrometer for environmental analysis. *Rev. Sci. Instrum.* **1998**, *69*, 565.
(33) Hemond, H. F. A backpack-portable mass spectrometer for measurement of volatile compounds in the environment. *Rev. Sci. Instrum.* **1991**, *62*, 1420.
(34) Lauritsen, F. R.; Bohatka, S.; Degn, H. A Membrane-inlet Tandem Mass Spectrometer for Continuous Monitoring of Volatile Organic Compounds. *Rapid Commun. Mass Spectrom.* **1990**, *4* (10), 401−403.
(35) Ketola, R. A.; Kotiaho, T.; Cisper, M. E.; Allen, T. M. Environmental applications of membrane introduction mass spectrometry. *J. Mass Spectrom.* **2002**, *37* (5), 457−476.
(36) Kana, T. M.; Darkangelo, C.; Hunt, M. D.; Oldham, J. B.; Bennett, G. E.; Cornwell, J. C. Membrane inlet mass spectrometer for rapid high-precision determination of N2, O2, and Ar in environmental water samples. *Anal. Chem.* **1994**, *66* (23), 4166−4170.
(37) An, S.; Gardner, W. S.; Kana, T. M. Simultaneous Measurement of Denitrification and Nitrogen Fixation Using Isotope Pairing with Membrane Inlet Mass Spectrometry Analysis. *Appl. Environ. Microbiol.* **2001**, *67* (3), 1171−1178.
(38) Bohatka, S.; Futo, I.; Gal, I.; Gal, J.; Langer, G.; Molnar, J.; Paal, A.; Pinter, G.; Simon, M.; Szadai, J.; Szekely, G. Quadrupole mass spectrometer system for fermentation monitoring. *Vacuum* **1993**, *44* (5−7), 669−671.
(39) Degn, H. Membrane inlet mass spectrometry in pure and applied microbiology. *J. Microbiol. Methods* **1992**, *15* (3), 185−197.
(40) Eschenbach, W.; Well, R. Online measurement of denitrification rates in aquifer samples by an approach coupling an automated sampling and calibration unit to a membrane inlet mass spectrometry system. *Rapid Commun. Mass Spectrom.* **2011**, *25* (14), 1993−2006.
(41) Bell, R. J.; Short, R. T.; Van Amerom, F. H. W.; Byrne, R. H. Calibration of an in situ membrane inlet mass spectrometer for measurements of dissolved gases and volatile organics in seawater. *Environ. Sci. Technol.* **2007**, *41* (23), 8123−8128.
(42) Gentz, T.; Schlüter, M. Underwater cryotrap-membrane inlet system (CT-MIS) for improved in situ analysis of gases. *Limnol. Oceanogr.: Methods* **2012**, *10*, 317−328.
(43) Short, R. T.; Fries, D. D.; Kerr, M. L.; Lembke, C. E.; Toler, S. K.; Wenner, P. G.; Byrne, R. H. Underwater mass spectrometers for in-situ chemical analysis of the hydrosphere. *J. Am. Soc. Mass Spectrom.* **2001**, *12* (1), 676−682.
(44) Tortell, P. D. Dissolved gas measurements in oceanic waters made by membrane inlet mass spectrometry. *Limnol. Oceanogr.: Methods* **2005**, *3*, 24−37.
(45) Mächler, L.; Brennwald, M. S.; Kipfer, R. Membrane Inlet Mass Spectrometer for the Quasi-Continuous On-Site Analysis of Dissolved Gases in Groundwater. *Environ. Sci. Technol.* **2012**, *46*, 8288−8296.
(46) Visser, A.; Singleton, M. J.; Hillegonds, D. J.; Velsko, C. A.; Moran, J. E.; Esser, B. K. A membrane inlet mass spectrometry system for noble gases at natural abundances in gas and water samples. *Rapid Commun. Mass Spectrom.* **2013**, *27*, 2472−2482.
(47) Hamme, R. C.; Emerson, S. R. Measurement of dissolved neon by isotope dilution using a quadrupole mass spectrometer. *Mar. Chem.* **2004**, *91*, 53−64.
(48) Manning, C. C.; Stanley, R. H. R.; Lott, D. E. Continuous Measurements of Dissolved Ne, Ar, Kr, and Xe Ratios with a Field-Deployable Gas Equilibration Mass Spectrometer. *Anal. Chem.* **2016**, *88* (6), 3040−3048.
(49) Becker, M. W.; Charbeneau, R. J. First-passage-time transfer functions for groundwater tracer tests conducted in radially convergent flow. *J. Contam. Hydrol.* **2000**, *40* (4), 299−310.
(50) Becker, M. W.; Shapiro, A. M. Tracer transport in fractured crystalline rock: Evidence of nondiffusive breakthrough tailing. *Water Resour. Res.* **2000**, *36* (7), 1677−1686.

DOI: 10.1021/acs.est.6b03706
Environ. Sci. Technol. 2017, 51, 846−854

(51) Kang, P.; Le Borgne, T.; Dentz, M.; Bour, O.; Juanes, R. Impact of velocity correlation and distribution on transport in fractured media: Field evidence and theoretical model. *Water Resour. Res.* **2015**, *51* (2), 940−959.
(52) Gupta, S. K.; Stephen Lau, L.; Moravcik, P. S. Ground-Water Tracing with Injected Helium. *Groundwater* **1994**, *32* (1), 96−102.
(53) Gupta, S. K.; Moravcik, P. S.; Stephen Lau, L. Use of Injected Helium as a Hydrological Tracer. *Hydrol. Sci. J.* **1994**, *39* (2), 109−119.
(54) Sanford, W. E.; Shropshire, R. G.; Solomon, D. K. Dissolved gas tracers in groundwater: Simplified injection, sampling, and analysis. *Water Resour. Res.* **1996**, *32* (6), 1635−1642.
(55) Visser, A.; Singleton, M. J.; Esser, B. K. Xenon Tracer Test at Woodland Aquifer Storage and Recovery Well. *Lawrence Livermore Natl. Lab. Rep.* **2014**, DOI: 10.2172/1162248.
(56) Laidlaw, I. M. S.; Smart, P. L. An Evaluation of Some Fluorescent Dyes for Water Tracing. *Water Resour. Res.* **1977**, *13* (1), 15−33.
(57) Magal, E.; Weisbrod, N.; Yakirevich, A.; Yechieli, Y. The use of fluorescent dyes as tracers in highly saline groundwater. *J. Hydrol.* **2008**, *358*, 124−133.
(58) Shakas, A.; Linde, N.; Baron, L.; Bochet, O.; Bour, O.; Le Borgne, T. Hydrogeophysical characterization of transport processes in fractured rock by combining push-pull and single-hole ground penetrating radar experiments. *Water Resour. Res.* **2016**, *52* (2), 938−953.
(59) Uddin, M. K.; Dowd, J. F.; Wenner, D. B. Krypton Tracer Test to Characterize the Recharge of Highly Fractured Aquifer in Lawrenceville, Georgia. *Proc. Georg. Water Resour. Conf.* **1999**, 516−519.
(60) Le Borgne, T.; Bour, O.; Riley, M. S.; Gouze, P.; Pezard, P. A.; Belghoul, A.; Lods, G.; Le Provost, R.; Greswell, R. B.; Ellis, P. A.; Isakov, E.; Last, B. J. Comparison of alternative methodologies for identifying and characterizing preferential flow paths in heterogeneous aquifers. *J. Hydrol.* **2007**, *345*, 134−148.
(61) Labasque, T.; Aquilina, L.; Vergnaud, V.; Hochreutener, R.; Barbecot, F.; Casile, G. C. Inter-comparison exercises on dissolved gases for groundwater dating - (1) Goals of the exercise and site choice, validation of the sampling strategy. *Appl. Geochem.* **2014**, *40*, 119−125.
(62) Sugisaki, R.; Taki, K. Simplified analyses of He, Ne, and Ar dissolved in natural waters. *Geochem. J.* **1987**, *21*, 23−27.
(63) Aeschbach-Hertig, W.; Peeters, F.; Beyerle, U.; Kipfer, R. Palaeotemperature reconstruction from noble gases in ground water taking into account equilibration with entrapped air. *Nature* **2000**, *405* (6790), 1040−1044.
(64) Ayraud, V.; Aquilina, L.; Labasque, T.; Pauwels, H.; Molenat, J.; Pierson-Wickmann, A. C.; Durand, V.; Bour, O.; Tarits, C.; Le Corre, P.; Fourre, E.; Merot, P.; Davy, P. Compartmentalization of physical and chemical properties in hard-rock aquifers deduced from chemical and groundwater age analyses. *Appl. Geochem.* **2008**, *23* (9), 2686−2707.

DOI: 10.1021/acs.est.6b03706
Environ. Sci. Technol. 2017, 51, 846−854

4. Discussion and perspectives

This chapter first describes different commonly implemented analytical techniques for the measurement of dissolved gases in aquatic environments. So far these techniques have been our eyes in the observation of environmental systems and delivered very informative information. Today, research efforts are now focused towards the development of very advanced analytical techniques for the precise measurement of new dissolved gas tracers (noble gas radioisotopes). Despite limited analytical capacities (in terms of number of samples), these novel techniques are rightly rising great interests in the field of hydrology and particularly in the characterisation of large groundwater systems.

On the other hand, this chapter points out the complementary need for a better distribution of observation data and thus presents the development of an innovative instrument for the continuous field measurement of dissolved gases. The CF-MIMS technique is shown to be a valuable tool for the field characterisation of biogeochemical reactivity, transport properties of aquatic environments, groundwater recharge, groundwater residence time as well as surface-ground water exchanges from few hours to several weeks experiments.

This innovative tool approaches the concept of “operational hydrology” which aims to enhance both the spatio-temporal distribution and the quality of environmental data for a thorough exploration of the Hydrosphere. The rationale behind this concept has already forged many instruments alike fiber-optics for distributed temperature sensing (J. S. Selker et al. 2006; J. Selker et al. 2006; Read et al. 2013; Read et al. 2014; de La Bernardie et al. 2017) and could be more widely applied to the measurement of any other observable (physical, chemical or biological) quantity of the CZ.

Chapter III: Assessment of natural dynamics and anthropogenic impacts on aquifer functioning using dissolved gases: example of the coastal aquifers of the metropolitan region of Recife (Brazil)

1. Introduction

The work presented in this section aims to demonstrate the interest of the use of dissolved gases in a multi-tracer approach at the catchment scale in order to infer both the natural dynamics of complex aquifer systems and the anthropogenic footprint of their exploitation. These investigations focused on the coastal aquifers of the metropolitan region of Recife (RMR, Pernambuco, Brazil) which was identified as a typical "hot-spots" where global climatic and societal pressures on water resources converge and intensify.

Owing to a tremendous population growth amplified by several drought periods, the RMR (3.7 million inhabitants) underwent remarkable water and land use changes increasing the pressure on water resources. Over the last decades, these pressures gave rise to many environmental consequences on groundwater quantity and quality, such as the dramatic decline of water tables as well as groundwater salinization and contamination.

In this context, the investigations presented in this section took place as part of the French-Brazilian research project COQUEIRAL. This multidisciplinary project consisted in (1) the analysis of the pressures on the groundwater resources and their societal and structural reasons (P. Cary et al. 2015) (2) the identification of the sources and mechanisms of groundwater quality and quantity degradation (L. Cary, Petelet-Giraud, et al. 2015; Chatton et al. 2016; Bertrand et al. 2016; Bertrand et al. 2017) and (3) the assessment of the regional impact of global changes on water resources (Petelet-Giraud et al. 2017).

Among these three lines of research, the following study investigates the processes potentially affecting groundwater residence times and flow paths using a multi-tracer approach (CFCs, SF_6, dissolved noble gases, ^{14}C, Cl^-, ^{2}H and ^{18}O). With respect to the previous section, when studies classically operate high-precision analyses on a few samples, the present investigation chose to implement relatively simple analytical techniques for dissolved gas measurements favouring both the on-site analysis of a large number of samples and a better spatial distribution of the dataset.

2. Article: Glacial recharge, salinisation and anthropogenic contamination in the coastal aquifers of Recife (Brazil)

Science of the Total Environment 569–570 (2016) 1114–1125

Contents lists available at ScienceDirect

Science of the Total Environment

journal homepage: www.elsevier.com/locate/scitotenv

Glacial recharge, salinisation and anthropogenic contamination in the coastal aquifers of Recife (Brazil)

E. Chatton [a,*], L. Aquilina [a], E. Pételet-Giraud [b], L. Cary [b], G. Bertrand [c], T. Labasque [a], R. Hirata [c], V. Martins [c], S. Montenegro [d], V. Vergnaud [a], A. Aurouet [e], W. Kloppmann [b], Pauwels [b]

[a] Géosciences Rennes, Université Rennes 1-CNRS, UMR 6118, adress: 263 av du général Leclerc, Campus de Beaulieu, bat 15, 35042 Rennes Cedex, France
[b] Bureau de Recherches Géologiques et Minières (BRGM), adress: 3 avenue Claude-Guillemin, BP 36009, 45060 Orléans Cedex 2, France
[c] Instituto de Geociências, CEPAS (Groundwater Research Center), University of São Paulo, adress: Rua do lago 562, 05508-080 Sao Paulo, Brazil
[d] Civil Engineering Department, Universidade Federal Pernambuco, adress: Avenida Professor Moraes Rego, n° 1235, bairro Cidade Universitária, Recife, Brazil
[e] GeoHyd, adress: Parc technologique du Clos du Moulin, 101 rue Jacques Charles, 45160 Olivet, France

HIGHLIGHTS

- Study of anthropogenic impacts on the dynamics of coastal aquifers in urban areas.
- A multi-tracer approach was used to assess processes potentially affecting groundwater residence times and flow paths.
- Natural dynamics of deep groundwater systems were reconstructed showing large residence times and paleoclimate characterisation.
- These deep aquifers show a Pleistocene seawater intrusion.
- Present-day mixing with saline surface water and contaminated shallow groundwater has been identified in the deep aquifers.

GRAPHICAL ABTRACT

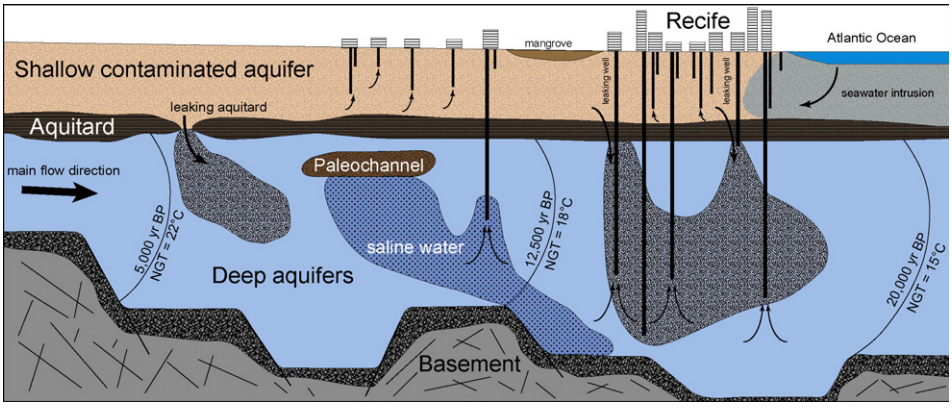

ARTICLE INFO

Article history:
Received 22 February 2016
Received in revised form 29 May 2016
Accepted 21 June 2016
Available online 4 July 2016

Editor: D. Barcelo

Keywords:
Groundwater

ABSTRACT

Implying large residence times and complex water origins deep coastal aquifers are of particular interest as they are remarkable markers of climate, water use and land use changes. Over the last decades, the Metropolitan Region of Recife (Brazil) went through extensive environmental changes increasing the pressure on water resources and giving rise to numerous environmental consequences on the coastal groundwater systems. We analysed the groundwater of the deep aquifers Cabo and Beberibe that are increasingly exploited. The processes potentially affecting groundwater residence times and flow paths have been studied using a multi-tracer approach (CFCs, SF6, noble gases, 14C, 2H and 18O). The main findings of these investigations show that: (1) Groundwaters of the Cabo and Beberibe aquifers have long residence times and were recharged about 20,000 years ago. (2) Within these old groundwaters we can find palaeo-climate evidences from the last glacial

Abbreviations: BP, Before present; EA, excess air amount; GMWL, global meteoric water line; LMWL, local meteoric water line; LGM, last glacial maximum; MAT, mean annual temperature; NGT, noble gas temperature; pMC, percentage of modern carbon; RMR, Metropolitan Region of Recife; RT, residence time; SST, sea surface temperature; STP, Standard Temperature and Pressure; UA, Unfractionated excess Air; ΔT, cooling estimate.

* Corresponding author.
E-mail addresses: eliot.chatton@gmail.com (E. Chatton), luc.aquilina@univ-rennes1.fr (L. Aquilina), e.petelet@brgm.fr (E. Pételet-Giraud), l.cary@brgm.fr (L. Cary), guillaume353@gmail.com (G. Bertrand), thierry.labasque@univ-rennes1.fr (T. Labasque), rhirata@usp.br (R. Hirata), veridian@usp.br (V. Martins), suzanam@ufpe.br (S. Montenegro), virginie.vergnaud@univ-rennes1.fr (V. Vergnaud), axel.aurouet@anteagroup.com (A. Aurouet), w.kloppmann@brgm.fr (W. Kloppmann), h.pauwels@brgm.fr (Pauwels).

http://dx.doi.org/10.1016/j.scitotenv.2016.06.180
0048-9697/

Residence time
Salinisation
Contamination
Palaeoclimate
Noble gases
Chlorofluorocarbons
Radiocarbon
Stable isotopes.

period at the tropics with lower temperatures and dryer conditions than the present climate. (3) Recently, the natural slow dynamic of these groundwater systems was significantly affected by mixing processes with contaminated modern groundwater coming from the shallow unconfined Boa Viagem aquifer. (4) The large exploitation of these aquifers leads to a modification of the flow directions and causes the intrusion through palaeo-channels of saline water probably coming from the Capibaribe River and from the last transgression episodes. These observations indicate that the current exploitation of the Cabo and Beberibe aquifers is unsustainable regarding the long renewal times of these groundwater systems as well as their ongoing contamination and salinisation. The groundwater cycle being much slower than the human development rhythm, it is essential to integrate the magnitude and rapidity of anthropogenic impacts on this extremely slow cycle to the water management concepts.

1. Introduction

Accounting for approximately 10% of the Earth's surface the coastal zones host more than half of the world population and human activities. In coastal zones, the social and economic development relies heavily on the availability of water resources for drinking water, agriculture and industry. In many countries, coastal water resources are limited and when surface water fails to meet the demand in terms of resource quality or quantity, groundwater turns out to be a valuable alternative. However, the rhythm at which human activities develop i.e. at which the water demand increases is usually much faster than the renewal times associated to the groundwater cycle and makes groundwater systems particularly vulnerable to environmental changes and human pressure.

Deep coastal groundwater systems are of particular interest as they usually imply large residence times and complex water origins that make these aquifers remarkable archives of climate, water use and land use changes (Edmunds and Milne, 2001). Furthermore, these aquifers are also highly sensitive to salinisation due to their proximity to the ocean and salinisation may be emphasised by aquifer exploitation. Therefore, the study of deep coastal aquifers allows the analysis of the link between anthropogenic pressures and hydrogeological processes which is critical to understand the dynamics and the resilience of coastal groundwater systems for a sustainable management of coastal groundwater resources (Araújo et al., 2015; Vengosh and Rosenthal, 1994).

In order to study groundwater dynamics and anthropogenic impacts for a given aquifer system, the combined use of environmental tracers is usually a fruitful strategy. Atmospheric tracers such as the CFCs and SF_6 are commonly used to study modern groundwater dynamics (<60 yr) and mixing processes as well as the impacts of environmental changes on groundwater systems (Ayraud et al., 2008; Bohlke and Denver, 1995; Cook et al., 1995; Koh et al., 2006). These anthropogenic gases have been released in the atmosphere since the 1950′s and are subsequently found in natural waters through atmospheric equilibria that allow dating groundwater by the means of their atmospheric concentrations chronicles. In addition to tracers of modern recharge, radiocarbon dating is a valuable tool to assess slower groundwater dynamics associated with larger residence times (1000 to 40,000 yr) which are found in many aquifers (Corcho Alvarado et al., 2007). To understand the resilience of groundwater systems, impacts of changes in the climate and recharge conditions have been commonly assessed using dating tools combined with noble gases and/or stable isotopes δ^2H and $\delta^{18}O$ (Aeschbach-Hertig et al., 2002; Beyerle et al., 1998; Castro et al., 2012; Corcho Alvarado et al., 2011; Gastmans et al., 2010; Plummer et al., 2012; Stute et al., 1995). Finally, processes of mixing and salinisation have been largely investigated using conservative geochemical tracers such as chloride and bromide (Aquilina et al., 2015; Cary et al., 2015; Vengosh et al., 1999).

In a context of declining precipitation and increasing demographic pressure the dry North-East of Brazil has been identified as an area of particular interest for the study of climate change and its effects on hydrological services (Bates et al., 2008). Over the last decades, the Metropolitan Region of Recife (RMR, Pernambuco, Brazil) underwent remarkable water and land use changes increasing the pressure on water resources and giving rise to numerous environmental consequences (Melo, 2013). Over the last three decades, the insufficient public water supply and repeated droughts (1998–1999 and 2012–2013) led to the development of a large and uncontrolled groundwater abstraction with 13,000 private wells (Costa et al., 2002). Recently, the dramatic decline of water tables and the ascertainment of local groundwater salinisation and contamination initiated the abandonment of shallow wells drilled in the superficial aquifers and the construction of new wells in the deep aquifers (Costa et al., 2002; Costa Filho et al., 1998). Despite the limited information about hydraulic connections between aquifers, the ongoing excessive groundwater exploitation is expected to induce significant aquifer exchanges (Costa Filho et al., 1998).

This work aims to address the need for a better understanding on groundwater systems in coastal population growing areas. This study will focus on the investigation of the processes potentially affecting groundwater flow paths and residence times in the deep aquifers of the RMR using a multi-tracer approach (noble gases, CFCs, SF_6, ^{14}C, δ^2H, $\delta^{18}O$ and Cl^-).

2. Materials and methods

2.1. Study area

The RMR is an urban area located on the Atlantic coast of the Pernambuco State in north-eastern Brazil with a population of 1.538 million inhabitants (IBGE and E., 2011). The city of Recife was built on the estuary of the Capibaribe River that comprises smaller rivers and a mangrove threatened by recent urbanisation (Melo, 2013).

The RMR knows a hot and humid tropical climate with a mean annual temperature (MAT) of 25.5 °C and an average rainfall of 1600 mm/yr (Silva and de P.R., 2004). While temperatures show low seasonal variations, precipitations are characterised by two distinct seasons: a dry season (September–February, <100 mm/month) and a rainy season (March–August, >200 mm/month).

Surrounded by hills of about 100 m above sea level, the Recife coastal plain is located on two major Mesozoic sedimentary basins divided by an E-W structure called the Pernambuco Lineament. As shown in Fig. 1, the Pernambuco and the Paraíba sedimentary basins are found respectively south and north of the lineament and are underlying Cenozoic sediments that occur all across the plain of Recife.

The Pernambuco basin has a graben and horst structure (de Lima Filho et al., 2006; Maia et al., 2012) and hosts the Cabo Formation (Aptian–Albian) that overlies the crystalline basement of gneisses and granites. The Cabo Formation has mainly a continental origin (de Lima Filho, 1998) and consists of conglomerates of 90 m of average thickness. This formation is topped by arkosean sandstones alternating with discontinuous clay layers that separate the lower Cabo from the sandy upper Cabo. Then a marine transgression led to the formation of limestones deposits of the Estiva Formation (Late Cretaceous).

At the bottom of the Paraíba basin, the Beberibe Formation (Santonian–Campanian) overlies a crystalline basement of highly fractured granites, gneisses, schists and migmatites (de Lima Filho et al., 2006). With an average thickness of 200 m, the Beberibe Formation

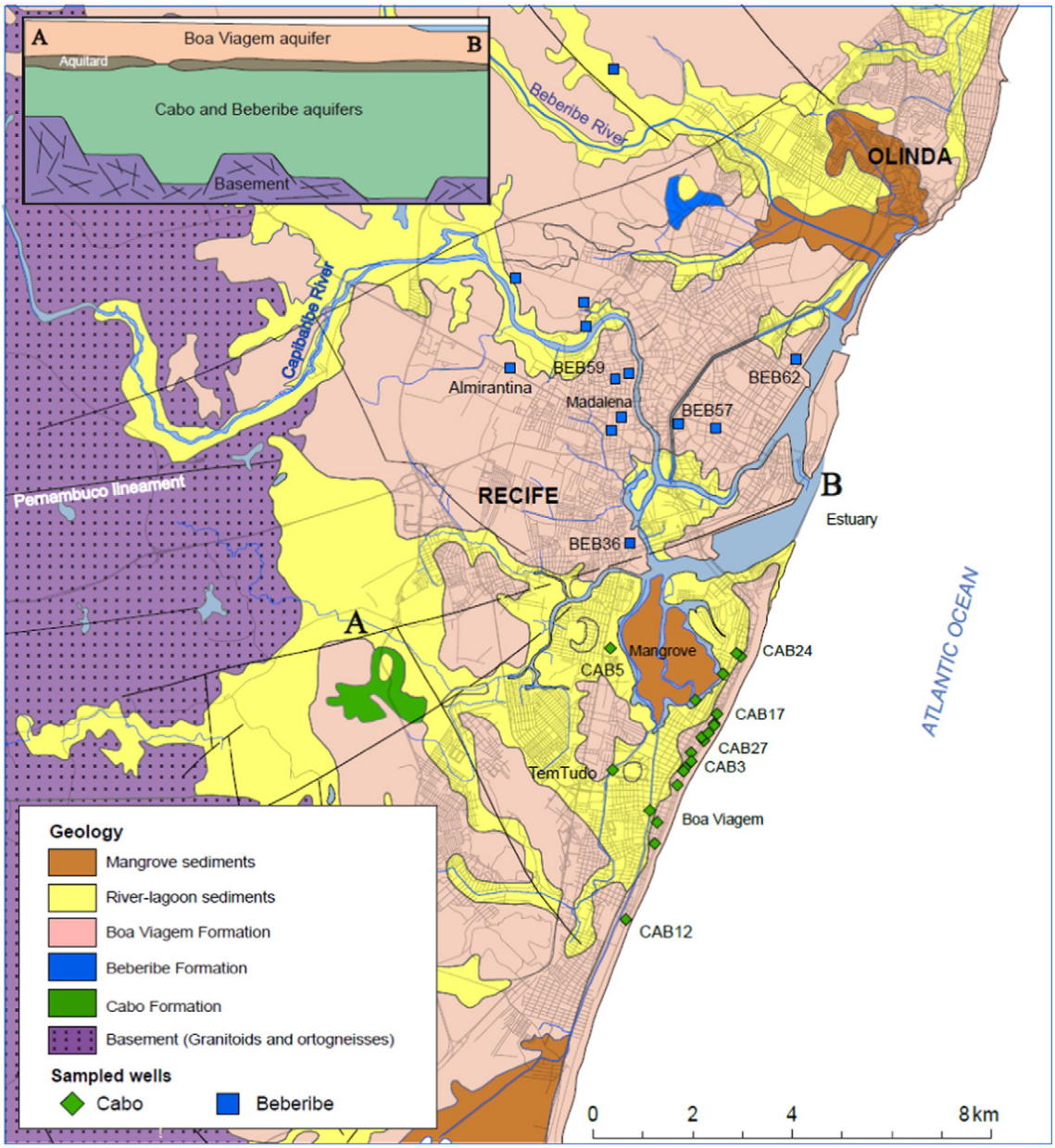

Fig. 1. Geology and hydrogeology of the study area.

consists of continental sandstones and argillaceous deposits (Beurlen, 1967) that are underlying the Campanian–Maastrichtian estuarine and lagoonal deposits of the Itamaracá Formation and the limestones with thin interbedded clays of the Gramame Formation (Barbosa et al., 2003). Then a marine transgression led to the formation of Palaeocene and Eocene limestones deposits of the Maria Farinha Formation (Mabesoone et al., 1968).

Finally, fluvial deposits of the Barreiras Formation (Plio-Pleistocene) and the quaternary sediments cover the two Mesozoic sedimentary basins. With an average thickness of 40 m, the Boa Viagem Formation consists mainly of Pleistocene and Holocene marine terraces originating from the last transgression episodes at 123,000, 5100, 3600 and 2500 yr BP (Dominguez et al., 1990; Martin et al., 1996). It also includes tidal lagoon and alluvial deposits, sandstone, reefs, freshwater swamps and mangroves.

In Recife, the public water supply relies mainly on surface waters and dams. Nevertheless, the contemporaneous rise in water demand due to population growth and the repeated droughts led to an increase in groundwater abstraction.

The coastal plain of Recife hosts three main aquifers: the shallow unconfined Boa Viagem aquifer and two deep confined aquifers within the Beberibe and Cabo formations. The Boa Viagem aquifer is the most vulnerable water resource in terms of pollution due to its connection to the mangrove, the estuary and urbanised areas (Leal, 1994). Over the last decades, the dramatic decline of piezometric levels and groundwater quality induced the abandonment of some wells of the Boa Viagem aquifer and led to the drilling of numerous private wells in the deep aquifers (Cabo and Beberibe).

According to the lithological description of the wells, the Cabo and Beberibe aquifers are confined by several clay layers of spatially varying thickness (Cary et al., 2015). However, this aquitard gives locally way to sandy levels where the two deep aquifers are consequently locally unconfined. Despite the limited information about hydraulic connections between aquifers, the ongoing excessive groundwater exploitation is

expected to induce significant aquifer exchanges (Costa Filho et al., 1998).

2.2. Sampling and analyses

Forty wells were sampled in the three aquifers (Boa Viagem, Cabo and Beberibe) during a sampling campaign that took place after the rainy season in March 2013 (except 3 samples in September 2013). All the samples were analysed for dissolved gases, chemistry and the stable isotopes ^{18}O and ^{2}H. Some samples of the Cabo and Beberibe aquifers were selected for radiocarbon analysis according to their hydrochemical characteristics and spatial distribution.

Stable isotopes (^{18}O and ^{2}H) and anion analyses were performed respectively at the University of São Paulo and BRGM laboratory (Orléans, France) following the procedures detailed in Cary et al. (2015). The uncertainty is $\pm 0.09‰$ for $\delta^{18}O$ and $\pm 0.9‰$ for $\delta^{2}H$.

The SF_6 and CFCs (CFC-11, CFC-12 and CFC-113) were sampled in steel ampoules (300 mL and 40 mL respectively) and analysed quickly after the sampling campaign using a Purge-and-trap GC-ECD (Perkin-Elmer) at Geosciences Rennes gas laboratory (Rennes, Brittany, France). An uncertainty of 3% applies to the values above 0.1 pmol/kg for CFCs and 0.1 fmol/kg for SF_6 and rises to 20% for lower values (Labasque et al., 2014). The detection limits are 0.06 fmol/L for SF_6, 0.05 pmol/L for CFC-11, 0.02 pmol/L for CFC-12 and 0.015 pmol/L for CFC-113.

Major and noble gases were measured throughout the sampling campaign using a GC-TCD (Agilent 3000A Micro-GC) after headspace extraction following the Sugisaki and Taki method (1987) with an analytical precision of 2.5% for Ar, 4% for N_2 and 10% for Ne.

2.3. Noble gas temperature modelling

Based on the work of Aeschbach-Hertig et al. (1999) an inverse model was developed to infer the recharge conditions of the aquifers. This model has been adapted to use the available dissolved Ne, Ar and N_2 concentrations in cm^3STP/g (Standard Temperature and Pressure) to model the noble gas temperature (NGT) and the amount of excess air (EA) that is commonly used to correct atmospheric tracer concentrations (CFC-12 and SF_6).

Conceptual models have been proposed to describe the excess air component in order to infer recharge conditions from the dissolved noble gas concentrations (Aeschbach-Hertig et al., 2000; Aeschbach-Hertig and Solomon, 2013; Freundt et al., 2013; Stute et al., 1995). Given the limited number of available dissolved gases (Ne, N_2 and Ar) and their related analytical uncertainty this study considers a simple model of excess air formation to determine the recharge conditions of the aquifers of Recife.

Among these simple conceptual models, the Unfractionated excess Air model (UA model) assumes a total dissolution of unfractionated excess air. In the UA model, the dissolved noble gas concentrations are assumed to depend only on the recharge temperature (also called noble gas temperature, NGT), the volume of unfractionated excess air (EA), the altitude of recharge (H) and the recharge salinity (S). Since H and S are well known only two free parameters (NGT and EA) remain to be determined using the inverse model with a degree of freedom $\nu = 1$.

The UA model has already been implemented with N_2 and Ar concentrations measured in gas-chromatography by Plummer et al. (2012) to infer the recharge conditions of an old groundwater system in the Atlantic Coastal Plain, USA. As Plummer et al. found N_2—Ar recharge temperatures in good agreement with NGTs predicted with the full suite of noble gases using a more complex conceptual model, the UA model appears to be a suitable choice for the determination of the recharge conditions of the aquifers of Recife.

The uncertainties associated with the model predictions are given by Monte-Carlo simulation that takes into account the analytical uncertainties to derive the model uncertainties on each NGT and EA. For the described configuration (3 noble gases to infer the NGT and EA of the UA model), the typical calculated uncertainties $\sigma_{NGT} = 2.5$ °C and $\sigma_{EA} = 0.0013$ cm^3STP/g are significant and were balanced by the large number of samples collected on the field.

The average NGT calculated for the Boa Viagem aquifer $NGT_{BOV} = 22.6 \pm 0.6$ °C is slightly lower than the MAT (25.5 °C) and was considered as the current recharge temperature for the region. In the following sections the calculated ΔT of a sample represents the temperature difference between the apparent modern recharge temperature (NGT_{BOV}) and the sample NGT.

2.4. Radiocarbon dating

Radiocarbon analyses were performed on selected samples of the Cabo and Beberibe aquifers. This selection was mainly based on the distribution of NGTs and chloride concentrations as well as the spatial distribution of the samples.

The preparation and measurements of the $^{13}C/^{12}C$ ratio and ^{14}C activity were performed by Beta Analytic Inc. The dissolved inorganic carbon was extracted by acidification (with H_3PO_4) under vacuum and then cryogenically purified. An aliquot was used for the measurement by mass spectrometry of the $^{13}C/^{12}C$ ratio. The CO_2 was reduced to graphite to be analysed. The ^{14}C activity was measured by Accelerator Mass Spectrometry. The ^{14}C activity was measured relative to the modern carbon reference and is expressed in % of modern carbon (pMC) and normalised taking into account the value of $\delta^{13}C$. Radiocarbon dating was performed through the software NETPATH (Plummer et al., 1994) using the revised Fontes and Garnier model (Han and Plummer, 2013) to derive ^{14}C ages expressed in years before present (yr BP). The uncertainty associated to the radiocarbon age of each sample is calculated as the standard deviation of the radiocarbon ages given by different radiocarbon dating models available in NETPATH: Vogel, Tamers, Eichinger, Mook, Ingerson, Fontes and Garnier. These uncertainties vary between 500 and 1500 yr.

As in the case of many studies the $\delta^{13}C$ of rock matrixes were not available. Therefore, the commonly used value of 1‰ has been selected in NETPATH for $\delta^{13}C$ of the rock matrix. Similarly, there is no information on $\delta^{13}C$ of the soil CO_2 and this value is often guessed by the authors. Usually, the soil CO_2 is fractionated by the soil plants and thus shows the isotopic signature of either C_4 plants (-10 to $-15‰$) or C_3 plants (around $-25‰$). Nowadays, C_4 plants are very abundant in Northeastern Brazil (Powell and Still, 2009) however, low $\delta^{13}C$ of the DIC have been measured in sample of the RMR (most are found between $-15‰$ and $-20‰$) indicating that at the time of the recharge the $\delta^{13}C$ of the soil CO_2 was probably more influenced by C_3 plants than it is now. Therefore the value of $-25‰$ was selected in NETPATH for the $\delta^{13}C$ of the soil CO_2.

2.5. Interpolations

The two-dimensional interpolations used in this article are based on a biharmonic spline interpolation implemented in the software MATLAB® (griddata v4 method).

3. Results

3.1. Noble gases and NGTs

Noble and major gas analysis shows a clear distinction between the shallow aquifer Boa Viagem and the two deep underlying aquifers Cabo and Beberibe. Fig. 2a shows that the Boa Viagem aquifer presents low concentrations in Ne, Ar and N_2 while Cabo and Beberibe have significantly higher gas concentrations.

Groundwaters may show *in-situ* production of N_2 through denitrification processes (Boisson et al., 2013). Such activity usually induces high contents of NO_2, N_2O when the reaction is not complete or high N_2/Ar ratios when the reaction is total. In this study, no evidences of

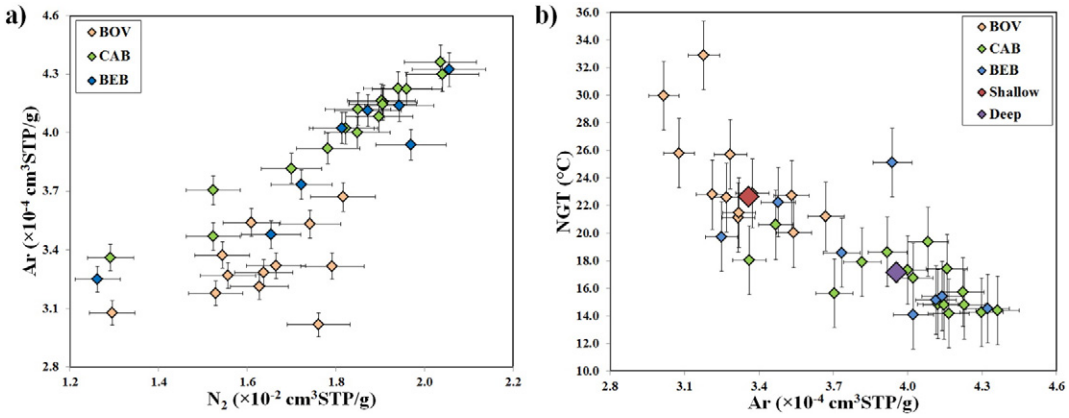

Fig. 2. Measured N_2 and Ar concentrations (2a) and modelled NGTs (2b) for the Boa Viagem (BOV), Cabo (CAB) and Beberibe (BEB) aquifers.

non-atmospheric sources of N_2 were found in the deep aquifers (Cabo and Beberibe). Fig. 2a shows that Cabo and Beberibe aquifers have relatively low N_2/Ar ratios and their N_2 contents are proportional to Ar contents ($[N_2] = 45.98_*[Ar]$; $R^2 = 0.85$). This trend is characteristic of physical processes defining gas concentrations in groundwater such as solubility and excess air. Therefore, the observed N_2 concentrations of the deep aquifers will be assumed to originate only from the atmosphere and hence reflect the characteristics of the aquifers recharge.

The concentrations in Ne, Ar and N_2 were implemented in the inverse model described earlier in order to derive the recharge temperature (NGT) and the amount of excess air (EA) for each sample. The results presented in Fig. 2b show that the NGTs are inversely proportional to Ar contents according to the laws of gas solubility. On the one hand, the Boa Viagem aquifer displays high NGTs (with low Ar concentrations) with an average recharge temperature of 22.6 ± 0.6 °C. On the other hand, the Cabo and Beberibe aquifers show low recharge temperatures (with high Ar concentrations) with an average value of 17.1 ± 1.2 °C. However, the Cabo and Beberibe samples cannot be distinguished on the basis of their noble gas contents or NGTs.

Since the noble gases Ne and Ar only have negligible non-atmospheric sources and N_2 production has been excluded in the deep aquifers, the high dissolved gas concentrations observed in the Cabo and Beberibe samples as well as their corresponding low NGTs have to be explained by other processes.

3.2. Radiocarbon dating

Thirteen samples from the Cabo and Beberibe aquifers were analysed for radiocarbon and provided ^{14}C residence times (RTs) for groundwater. The results presented in Fig. 3 show that the RTs of the deep aquifers vary over a large time period ranging from 2000 to 16,500 yr BP.

Fig. 3 also shows that the NGTs of the deep aquifers decrease with increasing RTs. Hence, the lowest recharge temperatures are measured for the samples with the largest RTs while the "modern" ones provide warmer NGTs close to the current recharge temperatures (NGT_{BOV}). Between 16,500 and 11,500 yr BP the NGTs remain relatively stable close to the value of 15.0 °C. Then, from 11,500 yr BP and present time the NGTs continue to increase slowly to reach the current recharge temperature ($NGT_{BOV} = 23.0 \pm 0.6$ °C).

3.3. Stable isotopes of water

Stable isotopes of water were analysed for the Boa Viagem, Cabo and Beberibe aquifers. The results presented in Fig. 4 show that all the samples present a trend similar to the global meteoric water line (GMWL: $\delta^2H = 8.0 \times \delta^{18}O + 10.0$, Rozanski et al., 1993) indicating a meteoric origin. Regarding each aquifer, two main trends may be delineated. On the one hand, the Cabo and Beberibe samples gather along a line which is slightly steeper than the modern local meteoric water line (LMWL:

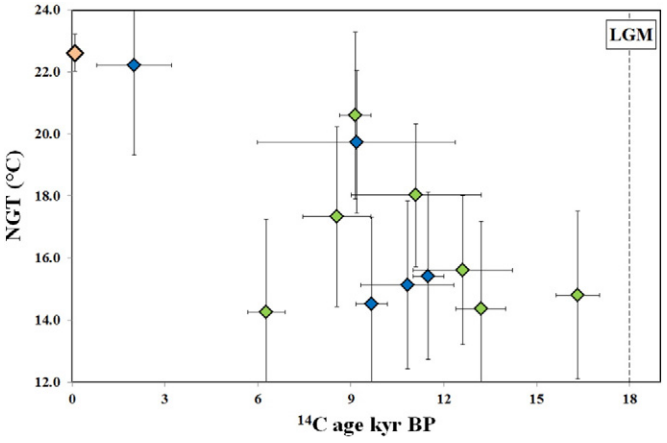

Fig. 3. Evolution of the NGTs with residence times (^{14}C ages) in the Boa Viagem (BOV), Cabo (CAB) and Beberibe (BEB) aquifers.

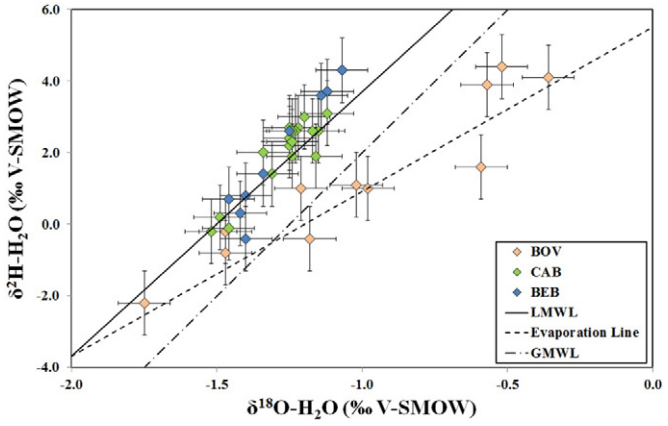

Fig. 4. Measured δ^2H and $\delta^{18}O$ for Boa Viagem (BOV), Cabo (CAB) and Beberibe (BEB) aquifers.

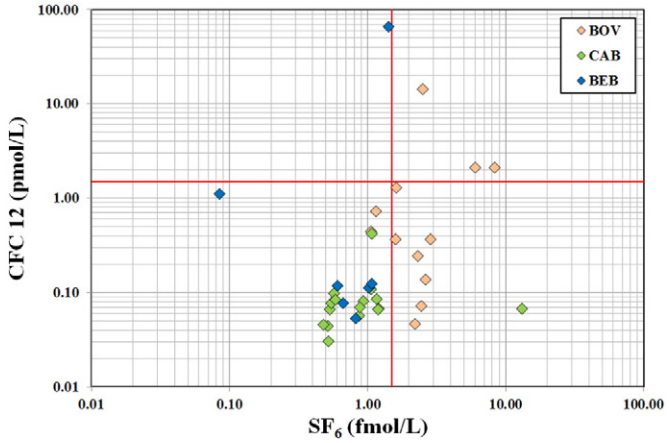

Fig. 5. Measured SF_6 and CFC-12 concentrations for Boa Viagem (BOV), Cabo (CAB) and Beberibe (BEB) aquifers. The red lines show the equilibrium concentrations of each tracer with the atmosphere of the Southern Hemisphere 2010.

$\delta^2H = 7.4 \times \delta^{18}O + 11.1$, Cary et al., 2015). On the other hand, samples from the Boa Viagem aquifer clearly plot along the dotted line that characterises evaporation processes or mixing with evaporated surface waters (Cary et al., 2015). Once again, there is a distinction between shallow Boa Viagem samples affected by evaporation and the deep Cabo and Beberibe samples plotting along a meteoric water line thus showing no evaporation influence.

3.4. CFCs and SF_6

Chlorofluorocarbon and sulphur hexafluoride analyses were performed on 40 samples of the Boa Viagem, Cabo and Beberibe aquifers. Fig. 5 shows that for the Cabo and Beberibe aquifers, the results are relatively homogeneous with very low CFCs and low SF_6 concentrations. On the contrary, Boa Viagem samples show a large variability of CFC contents which are generally greater than the deep aquifers values and sometimes exceed atmospheric equilibria (especially for CFC-113) represented by red lines in Fig. 5. The SF_6 concentrations show less variability than CFCs in the Boa Viagem aquifer but remain higher than the values observed for the Cabo and Beberibe.

According to the previous sections, the Cabo and Beberibe aquifers do not clearly differ on the basis of their NGTs, RTs, stable isotopic signatures and atmospheric tracer contents. Therefore, we will consider in the following sections that these two deep aquifers behave similarly and record the same physical processes.

4. Discussion

4.1. Quantification of mixing processes

The different tracers used in this study give complementary information that can be combined to understand the mixing processes occurring in the deep aquifers of Recife.

Table 1
End-members characteristics considered for the ternary mixing problem.

End-member	^{14}C activity (pMC)	Cl^- (mg/L)
Boa Viagem aquifer	90	30–150
Capibaribe River	90	2500
Pleistocene Seawater	0	19,000
Palaeo-recharge	To be inferred	10

Table 2
Palaeo-recharge residence time and mixing extents inferred for each end-member for Cabo and Beberibe samples. The saline components percentages refer to mixing processes occurring either with Pleistocene Seawater (P-S) or Capibaribe River (C-R).

Sample	Modern component (%)	Saline component (%)	Palaeo-recharge component (%)	Palaeo-recharge ^{14}C age (kyr BP)
CAB-002	10.0	0.0	90.0	
CAB-003	5.0	0.0	95.0	19.5
CAB-004	9.0	1.0 (P-S)	90.0	
CAB-005	19.0	7.0 (P-S)	74.0	14.8
CAB-010	11.0	1.5 (P-S)	87.5	
CAB-011	7.0	0.0	93.0	
CAB-012	5.0	0.0	95.0	8.7
CAB-013	7.0	2.5 (P-S)	90.5	
CAB-017	11.0	4.0 (P-S)	85.0	6.7
CAB-020	16.0	0.0	84.0	
CAB-022	9.0	0.0	91.0	
CAB-023	38.0	2.0 (P-S)	60.0	
CAB-024	30.0	9.0 (P-S)	61.0	20.0
CAB-026	19.0	0.0	81.0	
CAB-027	11.0	0.0	89.0	17.8
CAB-101	25.0	0.0	75.0	
CAB-102	19.0	0.0	81.0	
CAB-114	16.0	2.5 (P-S)	81.5	
TTD-094	9.0	3.0 (P-S)	88.0	11.1
TTD-110	7.0	2.5 (P-S)	90.5	14.3
BEB-047	22.0	0.0	78.0	
BEB-050	21.0	8.0 (C-R)	71.0	
BEB-051	35.0	8.0 (C-R)	57.0	
BEB-057	10.0	8.0 (C-R)	82.0	13.5
BEB-059	12.0	8.0 (C-R)	80.0	4.6
BEB-060	93.0	7.0 (C-R)	0.0	
BEB-062	12.0	1.0 (P-S)	87.0	14.5
BEB-036	17.0	1.0 (P-S)	82.0	16.0
ALM-073	17.0	6.0 (C-R)	77.0	8.4

On the one hand, considering the large RTs (beyond the CFCs and SF_6 dating range) deduced from ^{14}C measurements in the Cabo and Beberibe aquifers, such "old" groundwater should not contain any tracer of modern recharge or at least only close to the recharge areas. However, the Cabo and Beberibe aquifers show CFCs and SF_6 contents all over the plain of Recife. Furthermore, the presence of these atmospheric tracers is not a punctual phenomenon as they are spatially distributed in the deep aquifers. Therefore, it is reasonable to assume that the CFCs and SF_6 concentrations observed in the Cabo and Beberibe aquifers originate from mixing with the Boa Viagem shallow groundwater rather than from direct exchanges with surface sources (atmosphere or urban contamination).

On the other hand, some chloride concentrations measured in the deep aquifers exceed the maximum concentrations observed in the

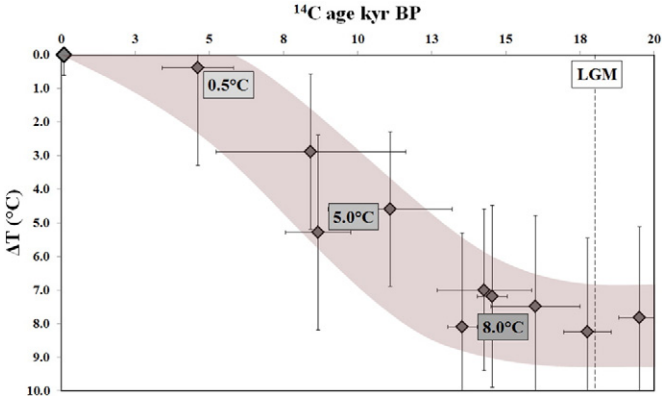

Fig. 6. Evolution of the temperature cooling (ΔT) with residence time (^{14}C age).

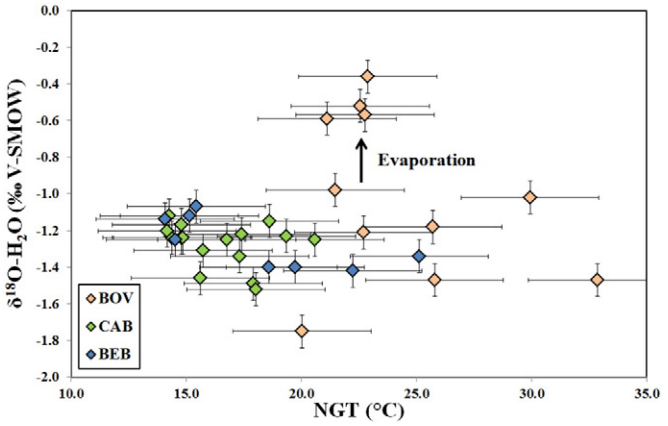

Fig. 7. Evolution of the $\delta^{18}O$ as a function of the NGT.

Boa Viagem aquifer. Therefore, the chemical composition of the Cabo and Beberibe aquifers cannot be explained by a single binary mixing with the Boa Viagem aquifer. Accordingly, the quantification of the mixing processes that takes place in the deep aquifers of Recife consists in solving a ternary mixing between a palaeo-recharge, a saline end-member and a modern end-member (Boa Viagem aquifer).

In order to characterise the modern end-member, we considered local averages of the Boa Viagem samples for each deep aquifer (BOV-113 for the southern Cabo aquifer, an average of BOV-014, BOV-019, BOV-100 and BOV-110 for the northern Cabo aquifer and an average of BOV-030, BOV-033, BOV-034, BOV-046 and BOV-130 for the Beberibe aquifer). Samples presenting signs of lithogenic production of SF_6 or punctual extreme values of one of the CFCs were excluded from the average Boa Viagem composition. Then, a binary mixing problem between an "old" end-member (free from CFCs and SF_6) and the local averages of the Boa Viagem was solved to derive the proportions of modern groundwater in the deep aquifers. For each Cabo and Beberibe sample, the percentage of modern end-member varied from a tracer to another, however, when at least 3 tracers provided mixing values with a standard deviation <0.1, an average mixing percentage was considered. This first step allowed quantifying the proportion of modern groundwater (<60 years old) in the Cabo and Beberibe aquifers. The next steps consisted in identifying older end-members (free from CFCs and SF_6) involved in the mixing processes according to their chloride contents and radiocarbon activity.

Given the existing saline bodies in the RMR and the transgression-regression history of the region, several saltwater sources are likely to affect the groundwater chemistry in Recife. Considering the assumptions formulated by Cary et al. (2015) based on chemical and isotopic data and allowing for the spatial distribution of salt concentrations in the deep aquifers, a salinisation by modern seawater was excluded and two saline end-members have been considered: the Capibaribe River and the palaeo-seawater from the Pleistocene transgression (123,000 yr BP) recorded in the Boa Viagem Formation (Dominguez et al., 1990; Martin et al., 1996).

Table 1 shows the characteristics of the different end-members considered in the ternary mixing problem. Chloride contents were measured by Cary et al. (2015) except the palaeo-seawater that was assumed to have a chloride composition close to the modern seawater. The radiocarbon activity was assumed to be 90 pMC for modern end-members and 0 pMC for the Pleistocene seawater.

At this stage, the information given by the partial identification of the palaeo-recharge (radiocarbon activity is still unknown), the complete identification of the other end-members and the determination of the modern end-member proportions allows solving the ternary mixing problem. In a chloride versus radiocarbon activity diagram,

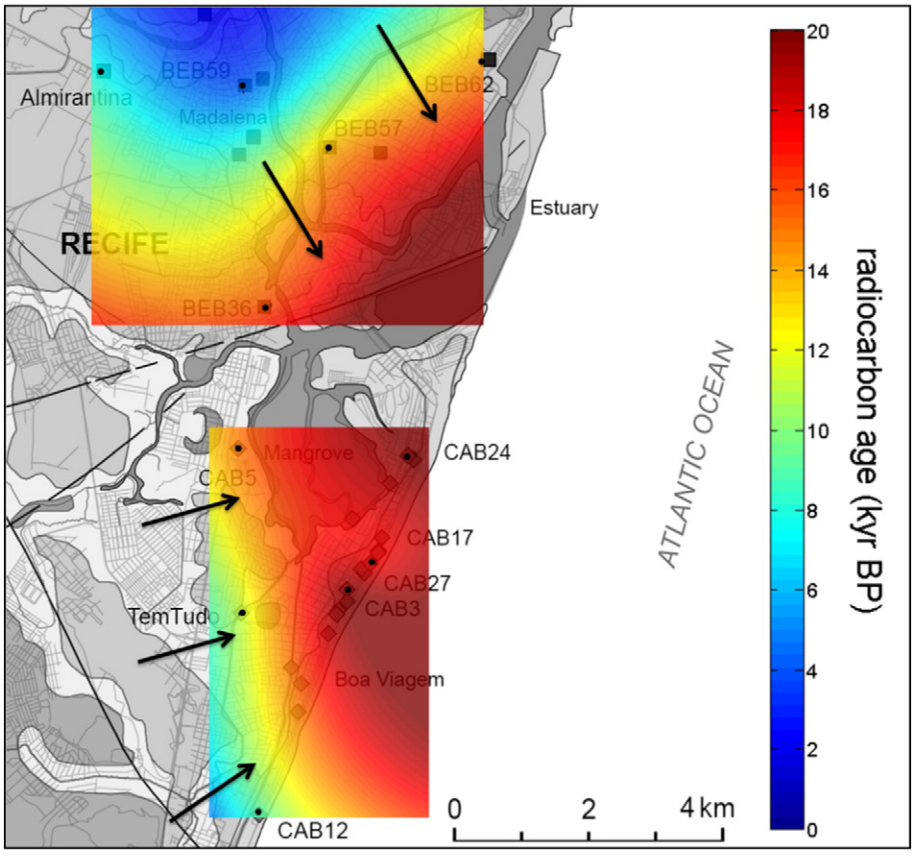

Fig. 8. Spatial interpolation of residence times (^{14}C ages) in the Cabo and Beberibe aquifers. Black arrows show natural flow directions coming from the edge of the plain to the estuary and the Atlantic Ocean. Black dots show the location of sampled wells used for the interpolation.

setting the known characteristics of each end-member and the percentage of modern component enables to determine by trial and error the radiocarbon activity of the palaeo-recharge and the two last mixing proportions. Table 2 summarises the mixing extents of the considered end-members for each Cabo and Beberibe samples. In the end, the resolution of the mixing problem enables to study independently the three components involved in the mixing processes.

4.2. Climate reconstruction

4.2.1. Recharge temperatures

This part of the discussion focuses on the palaeo-recharge component inferred in the previous section. Fig. 6 shows the evolution of the cooling estimate (ΔT) as a function of the residence time of the palaeo-recharge i.e. the radiocarbon age of the sample calculated from the radiocarbon activity corrected from mixing (using $RT = 5730/\ln(2) \times \ln(90/a_{corrected})$). Contrary to radiocarbon activities, the inferred NGTs have not been corrected from mixing as the corrections on gas concentrations seem uncertain and risk to alter the information of the dataset. In Fig. 6, two outliers have been removed from this figure due to either an excessive mixing extent affecting the sample NGT (CAB-024) or a radiocarbon dating bias (incoherence with the neighbouring samples) that underestimated the sample RT (CAB-017).

The palaeo-recharge component shows RTs ranging from 4600 to 19,500 yr BP that are somewhat larger than the modelled ^{14}C ages of the deep samples before correction for mixing (results section). These differences do not affect the general trend observed earlier between recharge temperatures and residence times. Once more, there is an increase in ΔTs (decrease in NGTs) with increasing RTs, starting from 0.4 ± 2.9 °C at 4600 yr BP to 8.0 ± 2.7 °C close to the last glacial maximum (LGM around 18,000 yr BP). Fig. 6 also shows that the transition between Late-Glacial and present day recharge temperatures is a relatively rapid process (1 °C/1000 yr) that takes place between 13,500 and 5000 yr BP.

The residence times observed in the Cabo and Beberibe aquifers refer to Late-Pleistocene and Holocene periods. Over the last decades, the temperature cooling of the region during this period has been documented in the literature including noble gas data, pollen data, speleothem data and oceanographic data (Aeschbach-Hertig et al., 2002; Behling, 1995; Behling and Lichte, 1997; Behling, 1998; Behling et al., 2002; Bush et al., 2007; Ledru et al., 1996; Ledru et al., 2009; Santos et al., 2013; Santos et al., 2014; Stute et al., 1995; Wang et al., 2004). These studies observed that the Late-Pleistocene and Holocene periods recorded a dry and cold phase at the LGM in north-eastern Brazil and a global warming towards the present day warmer and wetter climate. Therefore, this study produces a temperature trend over time that is consistent with the previous observations.

The beginning of the recharge temperatures transition described earlier is also consistent with a previous palaeoclimate data review (Bush et al., 2007). These authors highlight the persistence and, in some cases, the peak abundance of cold resistant taxa in eastern Amazonia and coastal Brazil until 14,000 yr BP while western Amazonia and the Andes were already recording a considerable warming of the climate (Bush et al., 2007). However, the rapidity and time of the transition has not yet been precisely documented for the region (Behling, 1995; Ledru et al., 1996). Nevertheless, the recorded NGT transition period (Fig. 5) concurs with the short time gap in the NGT record published by Stute et al. (Stute et al., 1995) that separates cool Pleistocene recharge temperatures (24.2 °C) from warm Late-Holocene NGTs (29.6 °C) measured in the Piaui province, Brazil.

Another synthesis of terrestrial palaeoclimate data was carried out for tropical climates at the LGM (Farrera et al., 1999). These authors show that over the past two decades many studies have attempted to produce regional cooling estimates at the LGM. If the ΔTs differ from a

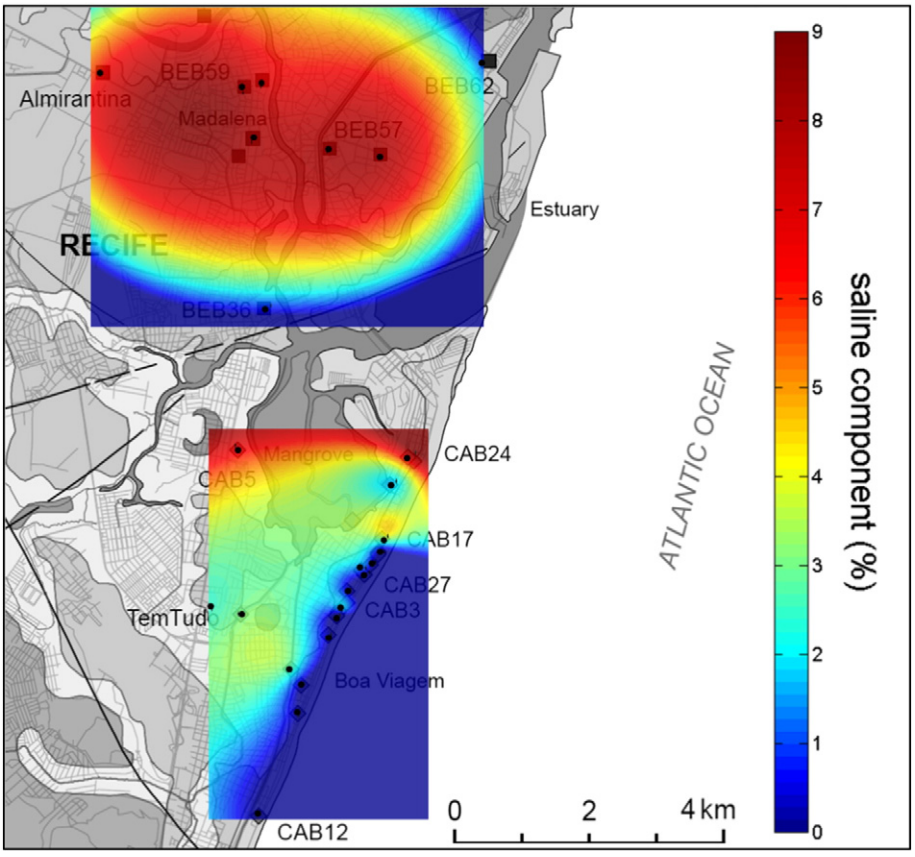

Fig. 9. Spatial interpolation of the percentage of saline component (Capibaribe River or Pleistocene Seawater) in the Cabo and Beberibe aquifers. Black dots show the location of sampled wells used for the interpolation.

study to another depending on the site location and the palaeoclimate proxy, the values suggested in the literature lie in a range of 4 °C to 7 °C (Farrera et al., 1999). In the plain of Recife the predicted cooling estimate reach the value of 8.0 ± 2.7 °C that slightly exceeds the values reported for tropical Brazil. These cooler recharge temperatures carry substantial uncertainties and might reflect the limits of the simple method employed here that seems to underestimate the NGTs.

4.2.2. Precipitation pattern

The predicted temperature change at LGM (ΔT) does not seem to be recorded by the stable isotopes of water as shown in the Fig. 7. In the case of a large cooling, the samples of the deep aquifers would have undergone a stronger fractionation and would appear more depleted in heavy isotopes than the shallow aquifer (Jasechko et al., 2015). On the contrary, Fig. 7 shows that the oldest and coldest samples of the deep aquifers show less isotopic fractionation ($\delta^{18}O$ varying from −1.25 to −1.05‰) than the youngest and warmest ones ($\delta^{18}O$ varying from −1.34 to −1.52‰). The reasons of these discrepancies can be explained by the following: (1) There is a lack of correlation between $\delta^{18}O$ and temperature when the MATs (≈NGTs) are larger than 20 °C because of the amount effect observed in the tropics (Rozanski et al., 1993). (2) The sea surface temperatures (SST) of the region documented for the Late-Pleistocene and Holocene periods did not vary as much as in the continent (ΔT = 2 °C, Santos et al., 2013). Since the plain of Recife is a coastal area and receives its precipitation directly from the ocean, the stable isotopic signatures would just reflect the Rayleigh distillation happening at the sea surface at a quasi-non-contrasted temperature. (3) Another possibility would be that the ocean water presented higher isotopic values during the LGM. The global cooling led to ice formation and subsequent higher ^{16}O sequestration in continental ice, favouring therefore ^{18}O enrichment in the remaining ocean water by a range of about 1‰ for $\delta^{18}O$ (Baker and Fritz, 2015). Such a change in the oceanic source of vapour would lead, despite of the regional air cooling, to richer isotopic signatures of the resulting precipitation.

4.3. Assessment of natural dynamics and anthropogenic impacts

Apart from palaeo-climate record, the study of the palaeo-recharge component informs on the natural flows occurring in the deep aquifers of Recife. Fig. 8 shows that the RTs increase from 4000 yr BP close to the high topographic areas surrounding the plain to 20,000 yr BP on the coastline. Hence, the study of the palaeo-recharge evidences natural flows starting from recharge areas located at the edges of the plain that are moving slowly (≈0.7 m/yr) to the estuary and the sea (discharge areas).

With a better understanding of the natural dynamics of the deep aquifers of Recife, this section will now consider the impacts of the saline and modern components involved in the mixing processes shown respectively in the Figs. 9 and 10.

In the southern part of the plain, most of the wells located close the Atlantic Ocean (East of the plain) show very low chloride contents while the salinised samples can be found further inland to the West. This observation supports that a modern seawater intrusion is not directly involved in the ongoing salinisation of the Cabo aquifer. Considering the geological and climate history of the region as well as the assumptions made by Cary et al. (2015) based on Sr and B isotopic data, the salty groundwater found in the Cabo aquifer and in some wells of the Beberibe aquifer (BEB-036 and 062) most probably originates from the Pleistocene marine transgression that occurred at 123,000 yr BP. As shown in Table 2 and Fig. 9, this old saline component affects a dozen of wells of the Cabo and Beberibe aquifer that show between 1 and 9% mixing with the Pleistocene seawater.

In the northern part of the plain of Recife, the Fig. 9 shows that most of the samples of the Beberibe aquifer are affected by infiltration of 6 to

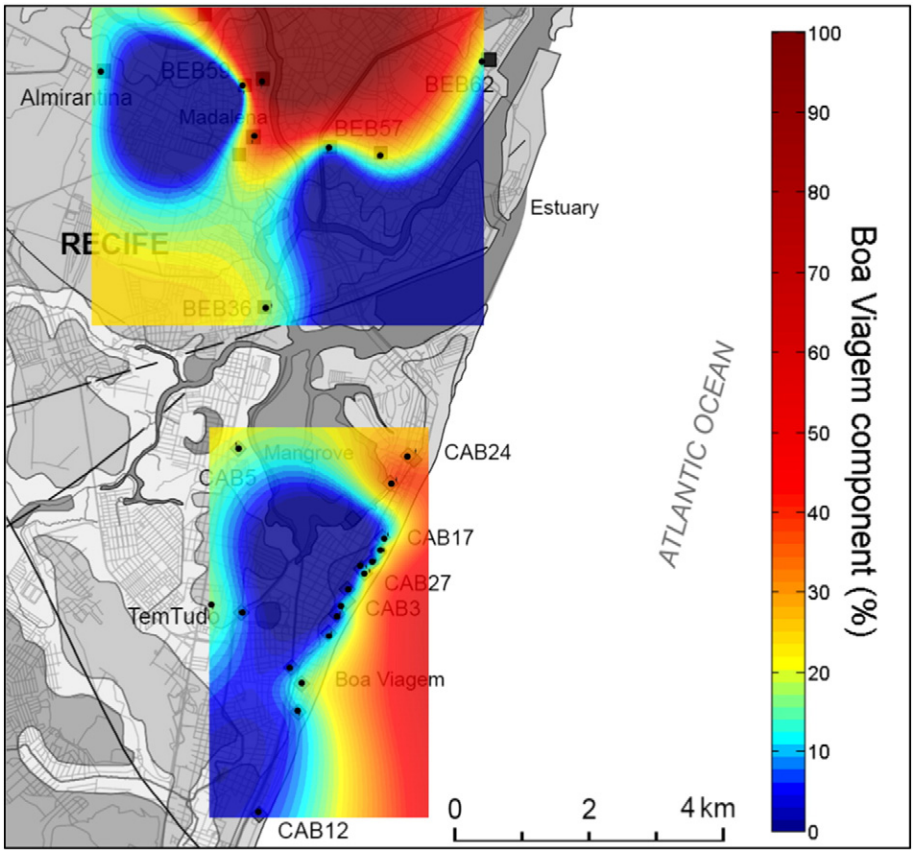

Fig. 10. Spatial interpolation of the percentage of Boa Viagem component leaking in the Cabo and Beberibe aquifers. Black dots show the location of sampled wells used for the interpolation.

8% of salty water coming from the Capibaribe River (BEB-050, 051, 057, 059, 060 and ALM). Recently drawn by large groundwater abstraction, these saline waters reach the deep aquifer system using the present-day Capibaribe River channel and the palaeo-channels that were evidenced by Cary et al. with boron isotopes (Cary et al., 2015).

In addition to salinisation processes, Table 2 and Fig. 10 highlight the presence in variable proportions (5 to 93%) in the deep aquifers of Recife of a modern component i.e. shallow contaminated groundwater from the Boa Viagem aquifer. Fig. 10 also shows that these leakages from the Boa Viagem aquifer are the largest in the high well density areas (in the Madalena neighbourhood for the Beberibe aquifer and on the coastline for the Cabo aquifer) where flow direction measurements carried out in March 2014 evidenced downward flows around the mangrove (CAB-005 and 006) and in the Boa Viagem neighbourhood (coastline). These observations support the assumption that large drawdowns related to important deep groundwater abstraction and associated with the construction of improperly sealed wells induced a significant modification of groundwater flows.

As a result, the Cabo and Beberibe aquifers have become more vulnerable to contamination and salinisation and the ongoing mixing with contaminated shallow groundwater (Boa Viagem aquifer) and saline surface water (Capibaribe River) is severely threatening the quality of the groundwater resource of Recife.

5. Conclusion

Over the last decades, the Metropolitan Region of Recife went through remarkable water and land use changes increasing the pressure on water resources and giving rise to numerous environmental consequences on the coastal groundwater systems.

We analysed the groundwater of the deep aquifers Cabo and Beberibe that are increasingly exploited. The processes potentially affecting groundwater residence times and flow paths have been studied using a multi-tracer approach (CFCs, SF_6, noble gases, ^{14}C, ^{2}H and ^{18}O). The main findings of these investigations show that:

(1) Groundwaters of the Cabo and Beberibe aquifers have long residence times and were recharged about 20,000 years ago.
(2) Within these old groundwaters we can find palaeo-climate evidences from the last glacial period at the tropics with lower temperatures and dryer conditions than the present climate.
(3) Recently, the natural slow dynamic of these groundwater systems was significantly affected by mixing processes with contaminated modern groundwater coming from the shallow unconfined Boa Viagem aquifer.
(4) The large exploitation of these aquifers leads to a modification of the flow directions and causes the intrusion through palaeo-channels of saline water probably coming from the Capibaribe River and from the last transgression episodes.

These observations indicate that the current exploitation of the Cabo and Beberibe aquifers is unsustainable regarding the long renewal times of these groundwater systems as well as their ongoing contamination and salinisation. The groundwater cycle being much slower than the human development rhythm, it is essential to integrate this extremely slow cycle to the water management concepts. Finally, if the magnitude of environmental changes is comparable to the anthropic pressure exerted on natural systems, the contrasting rapidity at which such large and permanent changes can occur in slow dynamic systems has to be emphasised.

Acknowledgements

This work is part of the multidisciplinary French–Brazilian research project COQUEIRAL financed by ANR CEP&S (ANR-11-CEPL-012)/FACEPE (APQ-0077-3.07/11)/FAPESP (2011/50553-0) and accredited by the French competitiveness cluster DREAM. The consortium is constituted by BRGM, CeRIES Lille 3 University, Géosciences Rennes 1 University, GEO-HYD, UFPE, USP, APAC (Water and Climate Agency of Pernambuco), CPRM, INPE. The authors are grateful to all colleagues and students from UFPE, USP and CPRM for their help during the sampling campaign. This work was also supported by the projects CRITEX and ANR Stock-en-Socle that funded the PhD of E. Chatton. We thank the two anonymous reviewers for their careful revision of the manuscript.

Appendix A

Table A
Summary of the SF_6, CFCs, noble gas and chloride concentrations as well as the $\delta^{18}O$ and $\delta^{2}H$ measured in the Boa Viagem, Cabo and Beberibe aquifers. Recharge conditions modelling (NGT and EA) is based on the UA model that uses either Ne, Ar and N_2 concentrations (UA3) or only Ne and Ar concentrations (UA2). The error is 3% on CFCs and SF_6, 2.5% on Ar, 4% on N_2, 10% on Ne, 0.09‰ on $\delta^{18}O$ and 0.9‰ on $\delta^{2}H$.

	SF_6	CFC-12	CFC-11	CFC-113	Ne	Ar	N_2	Model	NGT	σ_{NGT}	EA	σ_{EA}	ΔT	Cl^-	$\delta^{18}O$	$\delta^{2}H$
					$\times 10^{-7}$	$\times 10^{-4}$	$\times 10^{-2}$				$\times 10^{-3}$	$\times 10^{-3}$			‰	‰
Units	fmol/L	pmol/L	pmol/L	pmol/L	ccSTP/g	ccSTP/g	ccSTP/g		°C	°C	ccSTP/g	ccSTP/g	°C	mg/L	V-SMOW	V-SMOW
BOV-014	2.53	14.39	0.28	0.31	2.58	3.02	1.76	UA2	29.9	3.5	4.73	1.49		267.2	−1.02	1.1
BOV-019	2.85	0.37	0.22	0.30	2.34	3.21	1.63	UA2	22.8	3.1	3.01	1.5		62.3	−0.57	3.9
BOV-030	1.62	1.29	0.46	0.11	2.74	3.29	1.64	UA2	25.7	3.8	5.43	1.75		70.5	−1.18	−0.4
BOV-033	1.16	0.73	1.07	0.07	2.71	3.54	1.61	UA2	20.0	3.1	4.84	1.69		18.3	−1.75	−2.2
BOV-034	1.06	0.44	0.11	0.19	2.8	3.67	1.82	UA3	21.2	3.0	7.38	1.28		14.5	n.a.	n.a.
BOV-046	2.21	0.05	0.10	0.11	2.68	3.53	1.74	UA3	22.7	3.0	6.83	1.21		110.6	−1.21	1.0
BOV-100	2.63	0.14	0.10	1.48	1.98	3.32	1.79	UA3	21.1	2.5	4.37	1.03		173.6	−0.59	1.6
BOV-110	2.31	0.24	0.11	0.50	2.55	3.37	1.54	UA3	22.9	2.9	4.99	1.13		89.4	−0.36	4.1
BOV-112	1.59	0.37	0.19	0.39	2.42	3.32	1.67	UA2	21.5	3.0	3.38	1.54		2826.8	−0.98	1.0
BOV-113	6.00	2.11	0.89	0.30	2.43	3.27	1.56	UA2	22.6	3.1	3.52	1.54		856.9	−0.52	4.4
BOV-115	2.46	0.07	0.13	0.07	3.56	3.18	1.53	UA3	32.9	2.5	7.75	0.93		17.8	−1.47	−0.8
BOV-130	8.35	2.11	1.74	0.62	2.46	3.08	1.30	UA3	25.8	2.8	3.16	1.00		26.4	−1.47	−0.2
CAB-002	1.06	0.11	0.09	0.03	3.42	4.02	1.82	UA3	16.8	2.8	7.61	1.40	5.9	38.3	−1.25	2.7
CAB-003	0.53	0.07	0.14	0.08	3.52	4.23	1.94	UA3	14.8	2.7	8.36	1.46	7.8	23.5	−1.24	1.9
CAB-004	0.54	0.08	0.13	0.08	3.67	4.22	1.96	UA3	15.7	2.9	9.00	1.50	6.9	206.8	−1.31	1.4
CAB-005	n.a.	0.09	0.35	0.04	n.a.	n.a.	n.a.	n.a.	n.a.	n.a.	n.a.	n.a.	n.a.	1402.7	−1.16	1.9
CAB-010	0.58	0.10	0.17	0.11	3.50	3.92	1.78	UA3	18.6	3.0	7.76	1.38	4.0	290.0	−1.15	2.6
CAB-011	0.52	0.03	0.11	0.01	4.04	4.16	1.91	UA3	17.4	3.1	9.31	1.50	5.2	28.4	−1.22	2.7
CAB-012	13.21	0.07	0.07	0.01	3.33	4.00	1.85	UA3	17.3	2.9	7.87	1.39	5.3	17.7	−1.34	2.0
CAB-013	n.a.	0.06	0.10	0.02	n.a.	n.a.	n.a.	n.a.	n.a.	n.a.	n.a.	n.a.	n.a.	502.3	−1.24	2.3

(continued on next page)

Table A (*continued*)

	SF_6	CFC-12	CFC-11	CFC-113	Ne	Ar	N_2	Model	NGT	σ_{NGT}	EA	σ_{EA}	ΔT	Cl^-	$\delta^{18}O$	δ^2H
Units	fmol/L	pmol/L	pmol/L	pmol/L	$\times10^{-7}$ ccSTP/g	$\times10^{-4}$ ccSTP/g	$\times10^{-2}$ ccSTP/g		°C	°C	$\times10^{-3}$ ccSTP/g	$\times10^{-3}$ ccSTP/g	°C	mg/L	‰ V-SMOW	‰ V-SMOW
CAB-017	0.52	0.04	0.08	0.07	3.41	4.30	2.04	UA3	14.3	2.7	8.92	1.50	8.4	724.1	−1.12	3.1
CAB-020	1.08	0.42	0.09	0.00	3.10	3.82	1.70	UA3	17.9	2.7	6.28	1.29	4.7	34.4	−1.49	0.2
CAB-022	n.a.	0.05	0.13	0.03	n.a.	n.a.	n.a.	n.a.	n.a.	n.a.	n.a.	n.a.	n.a.	23.4	−1.25	2.2
CAB-023	0.93	0.08	0.08	0.51	4.16	4.08	1.90	UA3	19.4	3.3	9.8	1.52	3.3	377.1	−1.23	2.6
CAB-024	0.87	0.06	0.06	0.46	2.61	3.47	1.52	UA3	20.6	2.7	4.49	1.12	2.0	1674.6	−1.25	2.4
CAB-026	1.21	0.07	0.14	0.06	3.33	4.12	1.85	UA3	14.8	2.6	7.25	1.38	7.8	56.4	−1.24	2.3
CAB-027	1.20	0.07	0.09	0.03	3.74	4.36	2.04	UA3	14.4	2.8	9.47	1.55	8.2	19.6	−1.24	2.6
CAB-101	n.a.	0.07	0.21	0.08	n.a.	n.a.	n.a.	n.a.	n.a.	n.a.	n.a.	n.a.	n.a.	80.8	n.a.	n.a.
CAB-102	0.88	0.07	0.15	0.08	3.20	4.17	1.90	UA3	14.2	2.6	7.34	1.38	8.4	48.3	−1.20	3.0
CAB-114	1.16	0.09	0.13	0.07	3.26	4.15	1.91	UA3	14.8	2.7	7.62	1.42	7.8	454.4	−1.17	2.6
TTD-094	0.48	0.05	0.13	0.04	2.29	3.36	1.29	UA3	18.0	2.3	1.32	1.00	4.6	537.1	−1.52	−0.2
TTD-110	0.59	0.08	0.09	0.02	2.62	3.70	1.52	UA3	15.6	2.4	3.39	1.15	7.0	468.0	−1.46	−0.1
BEB-036	1.03	0.11	0.13	0.17	3.31	4.11	1.87	UA3	15.1	2.7	7.48	1.42	7.5	186.1	−1.12	3.7
BEB-047	n.a.	1.40	0.27	0.03	n.a.	n.a.	n.a.	n.a.	n.a.	n.a.	n.a.	n.a.	n.a.	27.3	−1.46	0.7
BEB-050	1.08	0.12	0.22	0.14	2.86	4.02	1.81	UA3	14.1	2.4	5.92	1.30	8.5	205.8	−1.14	3.6
BEB-051	1.41	65.50	0.10	0.09	2.81	3.73	1.72	UA3	18.6	2.7	6.13	1.25	4.0	219.4	−1.40	0.8
BEB-057	0.66	0.08	0.05	0.07	3.53	4.32	2.05	UA3	14.5	2.8	9.33	1.51	8.1	204.6	−1.25	2.6
BEB-059	0.32	n.a.	0.12	0.04	2.60	3.48	1.65	UA3	22.2	2.9	5.88	1.16	0.4	210.9	−1.42	0.3
BEB-060	0.08	1.12	0.90	0.33	4.30	3.94	1.97	UA3	25.1	3.9	11.89	1.57	−2.5	189.1	−1.34	1.4
BEB-062	0.61	0.12	0.11	0.02	3.26	4.14	1.94	UA3	15.4	2.7	8.12	1.41	7.2	206.6	−1.07	4.3
ALM-073	0.82	0.05	0.04	0.03	2.25	3.25	1.26	UA3	19.7	2.3	1.35	0.98	2.9	170.5	−1.40	−0.4

Table B
Data summary on temperature, pH, $\delta^{13}C$, radiocarbon activity as well as major anion and cation concentrations measured in the Boa Viagem, Cabo and Beberibe aquifers

	$\delta^{13}C$	^{14}C activity	σ_{14C}	T	pH	HCO_3^-	Cl^-	NO_3^-	SO_4^{2-}	Na^+	K^+	Ca^{2+}	Mg^{2+}
Units	‰ PDB ± 0.1	pMC	pMC	°C		mg/L	mg/L	mg/L	mg/L	mg/L	mg/L	mg/L	mg/L
CAB-003	−18.8	12.8	0.11	31.3	6.3	74.8	23.5	0.2	8.2	43.6	6.7	3.4	3.3
CAB-005	−14.9	27.9	0.10	30.4	6.5	91.6	1402.7	0.8	170.9	589.4	23.7	130.6	119.4
CAB-012	−11.4	34.4	0.10	30.5	6.0	41.0	17.7	0.3	15.6	34.8	7.8	1.5	1.7
CAB-017	−19.5	44.0	0.22	30.8	6.1	33.8	724.1	0.6	88.5	298.5	20.2	60.5	55.3
CAB-024	−17.7	31.6	0.15	31.2	6.0	39.2	1674.6	0.3	41.8	120.4	19.8	25.7	22.7
CAB-027	−17.1	19.3	0.10	32.1	6.3	63.9	19.6	0.2	10.3	39.5	6.2	3.7	3.5
TTD-094	−19.5	28.9	0.10	30.5	6.9	70.8	537.1	n.a.	169.1	323.0	13.3	47.3	61.5
TTD-110	−18.1	20.9	0.10	30.6	6.6	65.3	468.0	n.a.	142.2	281.2	13.3	47.3	56.4
BEB-036	−11.4	26.0	0.10	30.0	6.2	38.6	186.1	0.6	28.9	84.5	16.6	26.5	22.5
BEB-057	−19.7	30.3	0.19	31.3	5.9	28.9	204.6	0.2	32.5	57.3	24.5	41.3	28.6
BEB-059	−7.2	59.1	0.21	29.7	6.1	109.7	210.9	1.0	11.4	115.5	30.8	20.0	25.3
BEB-062	−15.6	24.4	0.15	32.8	5.9	28.9	206.6	0.2	11.4	19.7	11.5	3.9	3.6
ALM-073	−10.1	46.2	0.30	30.2	6.8	308.1	170.5	n.a.	2.9	164.8	21.5	44.1	39.9

References

Aeschbach-Hertig, W., et al., 2002. Excess Air in Groundwater as a Potential Indicator. IAEA, pp. 174–183.

Aeschbach-Hertig, W., et al., 1999. Interpretation of dissolved atmospheric noble gases in natural waters. Water Resour. Res. 35 (9), 2779–2792.

Aeschbach-Hertig, W., et al., 2000. Palaeotemperature reconstruction from noble gases in ground water taking into account equilibration with entrapped air. Nature 405 (6790), 1040–1044.

Aeschbach-Hertig, W., Solomon, D.K., 2013. Noble Gas Thermometry in Groundwater Hydrology. The Noble Gases as Geochemical Tracers, pp. 81–122 http://dx.doi.org/10.1007/978-3-642-28836-4_5 (Available at:).

Aquilina, L., et al., 2015. Impact of climate changes during the last 5 million years on groundwater in basement aquifers. Sci. Report. 5, 14132.

Araújo, R.S., et al., 2015. Water resource management: a comparative evaluation of Brazil, Rio de Janeiro, the European Union, and Portugal. Sci. Total Environ. 511, 815–828 (Available at: http://www.sciencedirect.com/science/article/pii/S0048969714016994).

Ayraud, V., et al., 2008. Compartmentalization of physical and chemical properties in hard-rock aquifers deduced from chemical and groundwater age analyses. Appl. Geochem. 23 (9), 2686–2707.

Baker, P.A., Fritz, S.C., 2015. Nature and causes of Quaternary climate variation of tropical South America. Quat. Sci. Rev. 124, 31–47.

Barbosa, J.A., et al., 2003. A estratigrafia da bacia Paraíba: uma reconsideraçâo. Estud. Geol. 13, 89–108.

Bates, B.C., et al., 2008. Climate change and water.

Behling, H., 1995. Investigations into the Late Pleistocene and Holocene history of vegetation and climate in Santa-Catarina (S Brazil). Veg. Hist. Archaeobot. 4 (3), 127–152.

Behling, H., 1998. Late Quarternary vegetational and climatic changes in Brazil. Rev. Palaeobot. Palynol. 99, 143–156.

Behling, H., et al., 2002. Late Quaternary vegetational and climate dynamics in northeastern Brazil, interferences from marine core GeoB 3104-1. Quat. Sci. Rev. 19, 981–994.

Behling, H., Lichte, M., 1997. Evidence of dry and cold climatic conditions at glacial times in tropical southeastern Brazil. Quat. Res. 48 (3), 348–358.

Beurlen, K., 1967. Estratigrafia da faixa sedimentar costeira Recife-João Pessoa. Bol. Geol. 16 (1), 43–53.

Beyerle, U., et al., 1998. Climate and groundwater recharge during the last glaciation in an ice-covered region. Science 282 (5389), 731–734.

Bohlke, J.K., Denver, J.M., 1995. Combined use of ground- water dating, chemical, and isotopic analyses to resolve the history and fate of nitrate contamination in two agricultural watersheds, Atlantic coastal Plain, Maryland. Water Resour. Res. 31 (9), 2319–2339.

Boisson, A., et al., 2013. Reaction chain modeling of denitrification reactions during a push–pull test. J. Contam. Hydrol. 148, 1–11.

Bush, M.B., Gosling, W.D., Colinvaux, P.A., 2007. Climate Change in the Lowlands of the Amazon Basin. Tropical Rainforest Responses to Climate Change, second ed., pp. 55–76.

Cary, L., et al., 2015. Origins and processes of groundwater salinization in the urban coastal aquifers of Recife (Pernambuco, Brazil): a multi-isotope approach. Sci. Total Environ. 530-531, 411–429.

Castro, M.C., et al., 2012. A late Pleistocene-mid-Holocene noble gas and stable isotope climate and subglacial record in southern Michigan. Geophys. Res. Lett. 39 (19), 1–6.

Cook, P.G., et al., 1995. Chlorofluorocarbons as tracers of groundwater transport processes in a shallow, silty sand aquifer. Water Resour. Res. 31 (3), 425–434.

Corcho Alvarado, J.A., et al., 2007. Constraining the age distribution of highly mixed groundwater using 39Ar: a multiple environmental tracer (3H/3He, 85Kr, 39Ar, and 14C) study in the semiconfined Fontainebleau Sands aquifer (France). Water Resour. Res. 43 (3), 1–16.

Corcho Alvarado, J.A., et al., 2011. Reconstruction of past climate conditions over Central Europe from groundwater data. Quat. Sci. Rev. 30, 3423–3429.

Costa Filho, W.D., et al., 1998. Concentração Salina das águas subterrâneas na planície do Recife. Proc. III Simpósio de Hidrogeologia do Nordeste, pp. 124–131.

Costa, W.D., Costa Filho, W.D., Monteiro, A.B., 2002. A sobre-explotaçao dos aquiferos costeiros em Recife-PE. Groundwater and Human Development.

Dominguez, J.M.L., et al., 1990. Geologia do Quaternário Costeiro do Estado de Pernambuco. Rev. Bras. Geosci. 20 (1–4), 208–215.
Edmunds, W.M., Milne, C.J., 2001. Palaeowaters in coastal Europe: evolution of groundwater since the late Pleistocene. J. Quat. Sci.
Farrera, I., et al., 1999. Tropical climates at the Last Glacial Maximum: a new synthesis of terrestrial paleoclimate data. I. Vegetation, lake levels, and geochemistry. Clim. Dyn. 15 (11), 823–856.
Freundt, F., Schneider, T., Aeschbach-Hertig, W., 2013. Response of noble gas partial pressures in soil air to oxygen depletion. Chem. Geol. 339, 283–290.
Gastmans, D., Chang, H.K., Hutcheon, I., 2010. Stable isotopes (H-2, O-18 and C-13) in groundwaters from the northwestern portion of the Guarani Aquifer System (Brazil). Hydrogeol. J. 18 (6), 1497–1513.
Han, L.F., Plummer, L.N., 2013. Revision of Fontes & Garnier's model for the initial ^{14}C content of dissolved inorganic carbon used in groundwater dating. Chem. Geol. 351, 105–114.
IBGE, I.B., E., d.G.e., 2011. Sinopse do censo demográfico. p. 2010.
Jasechko, S., et al., 2015. Late-glacial to late-Holocene shifts in global precipitation δ18O. Clim. Past 11, 1375–1393.
Koh, D.C., et al., 2006. Application of environmental tracers to mixing, evolution, and nitrate contamination of ground water in Jeju Island, Korea. J. Hydrol. 327 (1–2), 258–275.
Labasque, T., et al., 2014. Inter-comparison exercises on dissolved gases for groundwater dating - (1) goals of the exercise and site choice, validation of the sampling strategy. Appl. Geochem. 40, 119–125.
Leal, O., 1994. Vulnerabilidade das Águas Subterrâneas da Região Metropolitana do Recife.
Ledru, M.P., et al., 1996. The last 50,000 years in the Neotropics (Southern Brazil): evolution of vegetation and climate. Palaeogeogr. Palaeoclimatol. Palaeoecol. 123, 239–257.
Ledru, M.P., Mourguiart, P., Riccomini, C., 2009. Related changes in biodiversity, insolation and climate in the Atlantic rainforest since the last interglacial. Palaeogeogr. Palaeoclimatol. Palaeoecol. 271, 140–152.
de Lima Filho, M., 1998. Análise Estratigráfica e Estrutural da bacia Pernambuco. Instituto de Geociências. USP, p. 180.
de Lima Filho, M., Barbosa, J.A., Souza, E.M., 2006. Eventos tectonicos e sedimentares nas bacias de Pernambuco e da paraiba: Implicaçoes no quebramento do gondwana e correlação com a bacia do Rio Muni. Geociencias 25 (1), 117–126.
Mabesoone, J.M., Tinoco, I.M., Coutinho, P.N., 1968. The Mesozoic–Tertiary boundary in northeastern Brazil. Palaeogeogr. Palaeoclimatol. Palaeoecol. 4 (3), 161–185.
Maia, M.F.B., et al., 2012. Estudos Geológicos. Estud. Geol. 22 (1), 55–75 (22 (1) , 2012 55).
Martin, L., et al., 1996. Quaternary Sea-level History and Variation in Dynamics along the Central Brazilian Coast: Consequences on Coastal Plain Construction.
Melo, A.M., 2013. Recettes identiques, impacts contrastés: La Planification stratégique à Lille et à Recife. Ségrégation et fragmentation dans les métropoles, perspectives internationales, pp. 217–240.
Plummer, L.N., et al., 2012. Old groundwater in parts of the upper Patapsco aquifer, Atlantic Coastal Plain, Maryland, USA: evidence from radiocarbon, chlorine-36 and helium-4. Hydrogeol. J. 20 (7), 1269–1294.
Plummer, L.N., Prestemon, E.C., Parkhurst, D.L., 1994. An interactive code (NETPATH) for modeling net geochemical reactions along a flow path, version 2.0. Water-Resour. Investig. Rep.
Powell, R.L., Still, C.J., 2009. Biogeography of C3 and C4 vegetation on South America. Anais do XIV Simpósio Brasileiro de Sensoriamento Remoto, pp. 2935–2942.
Rozanski, K., Araguas-Araguas, L., Gonfiantini, R., 1993. Isotopic Patterns in Modern Global Precipitation. In: Swart, P.K., et al. (Eds.), Climate Change in Continental Isotopic Records.
Santos, T.P., et al., 2013. Millennial- to centennial-scale changes in sea surface temperature in the tropical South Atlantic throughout the Holocene. Palaeogeogr. Palaeoclimatol. Palaeoecol. 392, 1–8.
Santos, T.P., et al., 2014. Paleoceanographic reconstruction of the western equatorial Atlantic during the last 40 kyr. Palaeogeogr. Palaeoclimatol. Palaeoecol. 415, 14–20.
Silva, d., de P.R., V., 2004. On climate variability in Northeast of Brazil. J. Arid Environ. 58 (4), 575–596.
Stute, M., et al., 1995. Cooling of tropical Brazil (5{degrees}C) during the Last Glacial Maximum. Science 269, 379–383.
Sugisaki, R., Taki, K., 1987. Simplified analyses of He, Ne, and Ar dissolved in natural waters. Geochem. J. 21, 23–27.
Vengosh, A., et al., 1999. Geochemical and boron, strontium, and oxygen isotopic constraints on the origin of the salinity in groundwater from the Mediterranean coast of Israel. Water Resour. Res. 35 (6), 1877–1894.
Vengosh, A., Rosenthal, E., 1994. Saline groundwater in Israel: its bearing on the water crisis in the country. J. Contam. Hydrol. 156, 389–430.
Wang, X., et al., 2004. Wet periods in northeastern Brazil over the past 210 kyr linked to distant climate anomalies. Nature 432 (7018), 740–743.

3. Discussion and perspectives

This chapter demonstrates the usefulness of the implementation of a multi-tracer approach at the catchment scale for the assessment of the evolution of aquifer recharge conditions (noble gases, ^{2}H and ^{18}O), the characterisation of past (^{14}C) and modern (CFCs and SF_6) groundwater dynamics, and the identification of the sources and pathways of groundwater contamination and salinisation (CFCs, SF_6 and Cl^-). This approach gives important insights adding to the outcomes of the COQUEIRAL project on the origin and biogeochemical processes of groundwater contamination and salinisation in urbanised coastal areas (L. Cary, Petelet-Giraud, et al. 2015; Bertrand et al. 2016). As a matter of fact, the analysis of subsurface impacts of water resource mismanagement enables understanding the complex responses of groundwater systems to anthropogenic pressures. However, the identification at the surface of societal and structural reasons of water management failures provides more important indications to the stakeholders on the origins of the problems (P. Cary et al. 2015). Together, these investigations exhibit the various causes and consequences of groundwater overexploitation and anticipate the effects of global changes on water resources in densely populated regions (Petelet-Giraud et al. 2017).

Despite the relative simplicity of the analytical technique and modelling method employed, the information conveyed by the distributed dissolved gas dataset is highly valuable in these investigations. In fact, the low CFC and high noble gas contents of the Cabo and Beberibe aquifers were the first key evidences of the existence of an old groundwater system carrying the record of a past climate that became subsequently refined by radiocarbon dating.

In this respect and owing to the past and modern climate dynamics, the investigation of recharge conditions (especially temperature) with dissolved noble gas data could enable or assist in the evaluation of groundwater residence times, using thus noble gases as event markers. In addition, the so far poorly understood phenomenon of excess air could recently be associated to the amplitude of water table fluctuations or to the structure and depth of the unsaturated zone (Aeschbach-Hertig et al. 2002). These progresses in the conceptualisation and modelling of the excess air component offer new perspectives in the application of noble gases in groundwater (Andrews & Lee 1979; Heaton & Vogel 1981; Stute, Forster, et al. 1995; Kipfer et al. 2002; Aeschbach-Hertig et al. 2002; Lippmann et al. 2003; Mercury et al. 2004; Hall et al. 2005; Sun et al. 2008).

As pointed out by scientists of the groundwater dating community, the widely implemented radiocarbon dating method is often subject to many uncertainties due to the high reactivity of dissolved inorganic carbon (carbonate and gypsum dissolution or isotopic exchanges). Alongside, recent progresses in the advanced technique of atom trap trace analysis now enable the use of ^{85}Kr, ^{39}Ar and ^{81}Kr to properly constrain the timescales of aquifer dynamics and overcome the issues

associated to other dating methods (Loosli 1992; Chen 1999; Collon et al. 2000; Du et al. 2003). However, these novel techniques require for each sample the field extraction of dissolved gases from very large volumes of water (several hundred litres). The collected gas samples are subsequently analysed by means of quite complex and expensive analytical systems (not commercially available). As a result, few laboratories possess such equipment and the application of noble gas radionuclide dating methods has been so far relatively limited.

In the spirit of simplicity used so far, the simple measurement of dissolved He concentrations in groundwater (mainly ^{4}He) allows the evaluation of groundwater residence time distribution through the ^{4}He dating method (Andrews & Lee 1979; Andrews et al. 1982; Andrews 1985; Torgersen & Clarke 1985; Torgersen & Ivey 1985; Torgersen & Clarke 1987). This technique based on the subsurface accumulation of ^{4}He through rock U-Th decay enables the integration of timescales ranging from a hundred to million years (Stute et al. 1992; Solomon et al. 1996; Castro et al. 2000; Lehmann et al. 2003; Morikawa et al. 2005; Mahara et al. 2009; Plummer et al. 2012; Corcho Alvarado et al. 2013; Wei et al. 2015; Méjean et al. 2016). The ^{4}He method consists therefore in one of the most simple and integrative groundwater dating methods. Nevertheless, its implementation require more detailed investigations on the mechanisms of the subsurface ^{4}He production and transport particularly in fractured media (Neretnieks 1980; Andrews et al. 1982; Neretnieks 2013; Méjean et al. 2016; Labasque et al. 2017).

In essence, the integrative information derived from dissolved gas tracers allow the identification of groundwater mixing and pathways, the characterisation of groundwater residence time distribution (timescales from days to million years) and the record of recharge conditions (water origins, past climates). The collection and analysis of these data provide important information for the management of the quantity and quality of water resources (water supply, contamination/salinisation management, ecosystem protection) and also for the investigation of the Earth's climate through its past changes. Most dissolved gas tracer applications require the use of advanced sampling and analytical techniques that make them unfortunately inaccessible for most stakeholders. On the other hand, this chapter shows that implementing relatively simple analytical techniques can deliver useful information on complex groundwater systems provided an adequate sampling is ensured (number of samples, data spatio-temporal distribution). Naturally, these simple techniques necessitate continuous improvements to reduce the detection/precision gaps with respect to more advanced techniques. Along with the choice of simplicity, the staff of our gas laboratory will continue to stand for a wider availability of research outcomes to all water management stakeholders through the CONDATE analytical platform. Finally, the investigations of the COQUEIRAL project demonstrate the benefits of the combined "hydro-sociological" approaches to provide exhaustive (and hopefully comprehensive) insights to decision makers and to the other water management stakeholders.

Chapter IV: Combined characterisation of conservative and reactive transport in fractured media with a new experimental setup

1. Introduction

Predicting contaminant migration and attenuation in aquifers is essential for the management of the environment and the groundwater resources. For instance, these estimates are useful for the management and prevention of point and non-point source contaminations or for the selection of waste repositories. Additionally, the identification and characterisation of the subsurface biogeochemical reactions potentially affecting groundwater flow and heat exchange surfaces are particularly interesting for the geothermal energy development. However, characterising dominant solute transport processes as well as the subsurface biogeochemical reactivity remains challenging in fractured media (Berkowitz 2002; Bodin et al. 2003).

The particularity of fractured media lies in their ability to transfer groundwater through highly localised areas (single fractures and fracture networks), which represents only a small part of the total rock volume (low porosity but high permeability). These fractured areas result in a vast heterogeneity of groundwater flows and imply both fast transfers by preferential paths of high permeability and very slow transfers in areas of low permeability (Tsang & Neretnieks 1998; Becker & Shapiro 2003). The complex structure of fractures and the geometry of the networks they form in the subsurface have therefore a crucial impact on solute transport (Berkowitz 2002; Bodin et al. 2003).

For a non-reactive solute, mass transport in fractured media is the result of a superposition of different physical processes such as the solute advection at the mean fluid velocity, the hydrodynamic dispersion due to local fluctuations of the fluid velocity, the solute spreading by heterogeneous advection as a result of existing adjacent advective pathways (channelling) and finally, the solute diffusion in the immobile zones (rock matrix pores and fracture network dead-ends). On the other hand, the transport of reactive solutes can be additionally affected by several biogeochemical reactions between the groundwater solutes, the subsurface microorganisms and the solid interfaces (minerals of the fracture walls and the rock matrix).

The most common approach to characterise the physical and biogeochemical transport processes is to implement groundwater tracer tests directly in fractured media. Classically, field tracer experiments are performed by injecting known quantities of one or more tracers into a fracture or a fracture network. The injected tracers are constrained in the geological formation by a forced or natural hydraulic gradient while measuring their concentrations at one or more observation points. The

temporal evolution of the concentration of a given tracer at an observation point is called the breakthrough curve (BTC), from which transport parameters can be derived by fitting a suitable transport model.

Over the last decades, several transport models have been developed based on various simplifying assumptions on the flow field and on the dominant transport processes to infer solute transport parameters in fractured media. Depending on the geological context, the experimental setup or the injected tracers, these assumptions are not always appropriate and can produce erroneous interpretations. Besides, different transport processes can have the same effects on tracer breakthrough. For instance, breakthrough tailing (tailing effects) appear to be a common feature of both channelling and matrix diffusion (Bodin et al. 2003). As a result, the identification of the respective impact of matrix diffusion and channelling on anomalous transport in fractured media remains challenging.

In this regard, different tracer experiments have been implemented with tracers of different diffusivities to investigate the actual impact of matrix diffusion on solute breakthrough tailing (Maloszewski & Zuber 1990; Moench 1995; Hadermann & Heer 1996; Jardine et al. 1999; Callahan et al. 2000; Becker & Shapiro 2000; Becker & Shapiro 2003; Sanford et al. 2002). Most of these studies demonstrate the importance of matrix diffusion on solute transport as tracers of different diffusivities exhibit considerably different BTCs. In particular, Hadermann and Heer (Hadermann & Heer 1996) show that BTCs with power law slopes of $t^{-3/2}$ are characteristic of matrix diffusion processes. On the other hand, the experiments carried out by Becker and Shapiro (Becker & Shapiro 2000) give a counter example, where all tracers have similar late-time behaviours showing thus no significant impact of matrix diffusion. Subsequently, the authors demonstrate that this anomalous transport rather results from the processes of heterogeneous advection which can be characterised by BTCs with power law slope of t^{-2} (Becker & Shapiro 2003). Therefore, the injection of tracers of different physico-chemical properties is useful for the selection of a suitable transport model and the characterisation of the major transport processes in fractured media.

For this purpose, noble gases consist in a formidable family of inert elements whose physical and geochemical properties vary more or less smoothly from light to heavy gases (Ozima & Podosek 2002). Therefore, when introduced in aquatic environments, these dissolved tracers show no toxicity, no reactivity, no effect on water density and encompass different diffusivities. These characteristics make noble gases outstanding tools for the characterisation of surface and ground water transport properties. So far, field experiments using dissolved noble gas tracers are quite exceptional owing to the scarce availability of suitable analytical techniques (Eikenberg et al. 1992; Gupta, Moravcik, et al. 1994; Gupta, Stephen Lau, et al. 1994; Sanford et al. 1996; Jardine et al. 1999; Uddin et al. 1999; McNeill et al. 2001; Sanford et al. 2002; Richter et al. 2008; Visser et al. 2014). However, if most

these studies used noble gases as non-toxic tracers in drinking water supply areas, some of them highlight the potential of noble gases to characterise matrix diffusion (Eikenberg et al. 1992; Jardine et al. 1999; McNeill et al. 2001; Sanford et al. 2002). As mentioned earlier, the combined use of tracers of differing diffusivity allows the detailed investigation of physical transport processes provided the different tracers do not interact with each other. In this respect, the inert behaviour of noble gases makes them ideal for a combined injection of several conservative and/or reactive tracers.

The use of combined conservative and reactive tracers is particularly essential for the study of biogeochemical reactions in the subsurface. For instance, the reduction of nitrates by denitrification is a very common reaction in groundwater which results from the widespread release of high nitrate concentrations in natural waters (Korom 1992; Mariotti 1986). The latter stems from the intensive application of nitrogen fertilisers in agriculture and contributed to the rise of environmental and human health concerns. Characterising nitrate transport and denitrification kinetics is therefore essential to predict the migration and the attenuation of nitrate concentrations in the environment. To this end, field experiments must use both inert and reactive tracers to account respectively for the physical and biogeochemical transport processes.

The reaction of denitrification consists in the sequential reduction of nitrates ($NO_{3\,(aq)}^-$) to nitrogen gas ($N_{2(g)}$) and occurs under anaerobic conditions according to this chain reaction (Betlach & Tiedje 1981; Boisson et al. 2013):

$$NO_{3\,(aq)}^- \overset{k_1}{\rightarrow} NO_{2\,(aq)}^- \overset{k_2}{\rightarrow} NO_{(g)} \overset{k_3}{\rightarrow} N_2O_{(g)} \overset{k_4}{\rightarrow} N_{2\,(g)}$$

(Eq. 22)

Owing to the complexity of fractured media and the subsequent difficulty of reproducing natural conditions in laboratory, field measurements of biogeochemical reactions are required to characterise reactive transport in the subsurface. As a result, different tracer experiments have been carried out to study the mechanisms of denitrification in aquifers (Istok et al. 1997; Pauwels et al. 1998; Addy et al. 2002; McGuire et al. 2002; Kim et al. 2005; Boisson et al. 2013). Many of these studies have been carried out in anaerobic sites with important organic carbon contents (electron donors) favouring heterotrophic denitrification. However, most aquifers have low organic carbon content and can nonetheless be the scene of denitrification reactions. As a matter of fact, autotrophic microorganisms can also mediate denitrification reactions under anaerobic conditions using rock minerals instead of organic carbon. For instance, autotrophic denitrification has already been evidenced in crystalline aquifers via the oxidation of sulphur-bearing minerals such as pyrite (FeS_2) according to the equation 23 below (Pauwels et al. 1998; Tarits et al. 2006; Aquilina et al. 2012; Boisson et al. 2013):

$$5FeS_{2\,(s)} + 14NO_{3\,(aq)}^- + 4H_{(aq)}^+ \rightarrow 7N_{2\,(g)} + 10SO_{4\,(aq)}^{2-} + 5Fe_{(aq)}^{2+} + 2H_2O_{(aq)}$$

(Eq. 23)

These studies demonstrate both that crystalline aquifers are significant contributors of nitrate fluxes in agricultural catchments but also that autotrophic denitrification is an important mechanism of nitrate removal in groundwater systems (Pauwels et al. 1998; Tarits et al. 2006; Aquilina et al. 2012). As denitrification reactions are biologically mediated, the rates at which they occur depend not only on the presence of nitrates and electron donors but also on the availability and repartition of denitrifying communities in the aquifer (Becker et al. 2003; Philippot et al. 2009). Therefore, these reactions can be very complex in heterogeneous media such as crystalline aquifers and thus require the implementation of suitable field investigation techniques.

In this study, we propose to characterise simultaneously the physical and the biogeochemical processes controlling solute transport in a fractured media using forced-gradient tracer experiments. In this respect, a radially convergent tracer test is conducted using a combined slug injection of dissolved noble gas tracers for the investigation of physical transport processes, and nitrates for the characterisation of subsurface reactivity. This approach is complemented by an intensive sampling which allows the continuous monitoring of the suite of denitrification by-products; groundwater anions, cations and trace elements; stable isotopes of nitrate and sulphate as well as the microorganism community (metagenomic analyses). This study consist therefore in an original experiment opening new opportunities for the simultaneous characterisation of the physical, chemical and biological controls on solute transport in heterogeneous porous media.

2. Experimental site

The experimental site is located in the Coët-Dan drainage basin (Brittany, France) in an intensive agricultural catchment where agricultural activities (pig-stock breeding, temporary pastures, maize and wheat farming) cover about 90% of the 1193 ha of land (Pauwels et al. 1998). The geology of the catchment comprises a Brioverian pyrite-bearing schist (530 Ma) dominated by silt, clay or sandstone which is overlain by a weathered facies. The schist mineralogy was determined from F80 cores and F1 cuttings which comprise mainly biotite and muscovite (~41.5%), quartz (~25.5%), albite (~15%), chlorite (~11%), sanidine (~1.5%) and secondary phases including illite and smectite (~5%). Pyrite is the main accessory mineral and varies in the schist between 0.3 and 5‰ of the dry rock weight (Pauwels et al. 1998).

Hydrogeological observations (especially pumping tests) show that the site configuration comprises a shallow compartment with interstitial porosity having a storage role and a lower compartment with fissure and fracture porosity which has a transmissive role (Pauwels et al. 1998). Pauwels et al (Pauwels et al. 2000) showed that if the hydraulic connection between the two aquifer compartments is rather poor, the piezometric and chemical monitoring indicated significant influence of the vertical flow component. This monitoring also showed that the agricultural activities used to be responsible for

the release of high amounts of nitrate reaching up to 200 mg of NO_3^-/L in the streams and the shallow groundwater (< 10m) while nitrate concentrations in the fractured compartment varied seasonally between 10 mg/L and below the detection limits (Pauwels et al. 1998; Pauwels et al. 2000). This spatio-temporal distribution of nitrate concentrations in the aquifer is interpreted as a result of the combined effects of seasonal changes in input fluxes, vertical flow directions as well as denitrification processes.

Two convergent tracer tests have already carried out between the injection well F1 and the pumping well DNS1 using injections of Br^-, NO_3^- and TiO_2 nanoparticles over the whole height of the injection well (Pauwels et al. 1998; L. Cary, Pauwels, et al. 2015). The bromide BTCs were interpreted as a result of a transfer in a dual-porosity aquifer with two compartments comprising a fractured medium and a highly-fissured medium. The 26% difference between Br^- and NO_3^- recovery rates was interpreted as a result of nitrate removal by autotrophic denitrification and could be described by a first-order reaction model with a half-life of 7.9 days for the fractured medium and only 2.1 days for the highly-fissured medium.

3. Materials and methods

Experimental setup

For the purposes of this study, the tracer injection was only constrained in the deep fractured system rather than using the whole aquifer. Due to the alteration of the hydraulic connection between F1 and DNS1, the reproduction of anterior tracer test setups (Pauwels et al. 1998; L. Cary, Pauwels, et al. 2015) could not be considered and a new borehole F80 was drilled in the experimental site 8 meters away from F1. Hydrogeological observations such as pumping tests, cross-borehole flowmeter tests and well-logs evidenced a connection between the wells F1 and F80. Equipped with casings, F1 and F80 prevent the use of packers for the injection procedure which usually allow to constrain efficiently the injected tracers in the targeted fractured zone.

Contrary to F1, F80 comprise only one flow zone identified between 53 and 61 m depth. This characteristic prevents from accidental tracer injection in different flow zones since it is usually difficult to fully constrain the injectate in the geological formation without packers. As a result, the slug injection was performed in the injection well F80 using a ballasted polytetrafluoroethylene tube (φ=12mm) screened at the bottom where a rubber half-sphere closes the immersed tube edge and partially prevents the injectate from falling in the bottom of the borehole. On the other side, the tube was connected to the injection pump placed in an airtight 150 L tank.

Since solute transport can potentially be affected by diffusion processes, this experiment uses the combined injection of tracers of different diffusion coefficients that are shown in table 2.

Table 2: Free water diffusion coefficients of the injected tracers at T=12.3°C.

Tracer	D_w (m^2/s) at T=12.3°C	D_w^i/D_w^{NaNO3}
$NaNO_3$	1.50×10^{-9}	1.0
KBr	1.93×10^{-9}	1.3
O_2	1.27×10^{-9}	0.8
He	5.91×10^{-9}	3.9
Ar	2.10×10^{-9}	1.4
Xe	1.00×10^{-9}	0.7

The injectate was prepared using 120 L of F1 groundwater to which dissolved He, Ar, Xe, O_2, KBr and $NaNO_3$ salts were admixed (table 3).

Table 3: Concentration of tracers in the injected solution.

Element	Concentration (mol/L)	C/C_{F80}
Na^+	7.36×10^{-1}	843
K^+	3.55×10^{-2}	94
Mg^{2+}	2.70×10^{-5}	0.9
Ca^{2+}	3.63×10^{-4}	1.3
Fe^{2+}	9.53×10^{-5}	2.0
Cl^-	8.13×10^{-4}	1.0
Br^-	3.50×10^{-2}	27702
F^-	1.67×10^{-5}	0.9
NO_3^-	7.35×10^{-1}	26820
SO_4^{2-}	3.00×10^{-4}	0.9
O_2	1.94×10^{-4}	124
He	2.81×10^{-5}	3275
Ar	7.19×10^{-4}	39
Xe	6.38×10^{-6}	12756

Subsequently, the slug injection procedure consisted in the injection of 110 L of the solution containing the tracers at the rate of 5.50 L/min while pumping in the well F1 at the rate of 0.95 m^3/h (15.8 L/min). This pumping rate was established 24h before the injection and kept stable all along the experiment.

Sampling and analysis

During the experiment a continuous monitoring of the dissolved gases (N_2, N_2O, CO_2, CH_4, O_2, H_2, He, Ar and Xe) was carried out using a CF-MIMS (Chatton et al. 2017) and the control analyses of a gas chromatograph (Agilent® Micro-GC TCD 3000A) both installed in a mobile laboratory (CRITEX

Lab). This continuous monitoring of dissolved gases has been performed using the equipment and the services of staff members of the CONDATE analytical platform (OSUR).

The field parameters such as the temperature (T), dissolved oxygen, electrical conductivity (σ), pH and redox potential (Eh) were continuously monitored in the well F1 with a multiparameter probe (Idronaut® Ocean Seven). In addition, nitrate and dissolved organic carbon (DOC) concentrations were continuously measured using a spectrometer probe (S::CAN® spectro::lyser). Field NH4+ measurements were performed with an ISE sensor (Hach® ISENH4).

This intensive monitoring of the pumping well was complemented by a frequent sampling of anions (Cl^-, Br^-, F^-, NO_3^-, NO_2^-, SO_4^{2-}), cations (Na^+, K^+, Mg^{2+}, Ca^{2+}, Fe^{2+}, Mn^{2+}, Si^{4+}), trace elements (Li, B, Rb, Sr, Sb, U), dissolved organic and inorganic carbon (DOC and DIC), stable isotopes of the nitrate and sulphate molecules ($^{15}N/^{14}N$, $^{18}O/^{16}O$, $^{34}S/^{32}S$) as well as samples for microorganism diversity analysis.

Cation and trace elements as well as dissolved carbon analyses were performed after field sample filtration (0.22µm) at the University of Rennes (GEM service) with respectively an ICP-MS (Agilent® 7700) and a total organic carbon analyser (Shimadzu® TOC-5050A). Anion analyses were performed at the LERES laboratory (Laboratoire d'Etude et de Recherche en Environnement et Santé) in Rennes.

Metagenomic analyses were performed on samples collected in the injection well (F80) and throughout the experiment in the pumping well (F1). These samples consist in filters (0.22µm) obtained in triplicates after the filtration of 5 L of groundwater, momentarily stored in RNAlater-filled Eppendorf tubes in the CRITEX Lab fridge at 4°C and finally flash frozen in liquid nitrogen and stored at -20°C. A total DNA extraction was then performed for each sample with the NucleoSpin® gDNA Clean-up kit (Macherey-Nagel) and the DNA was fragmented with the M220 Focused-ultrasonicator TM (Covaris, Inc). All libraries of metagenomics DNA were prepared with the NEBNextR UltraDNA Library Prep Kit for Illumina and the NEBNextR Multiplex Oligos for Illumina Index (New England Biolabs, Inc) and pooled after DNA quantification with Quantifluor (Promega). Pooled libraries were sequenced with a 2x250pb paired-end MiSeq run (Illumina INC) at the Human and Environmental Genomics facility of the University of Rennes 1. Read quality was analysed with FastQC-v0.11.5 (www.bioinformatics.babraham.ac.uk/projects/fastqc) and the reads were quality filtered and trimmed with FastQ QC-Trimmer (Galaxy tool shed, https://toolshed.g2.bx.psu.edu/repository?repository_id=ef54ec2068e06fbe). After the filtering step, metagenomic reads were compared to the NCBI NR database with DIAMOND-BLASTx v0.7.9 (Buchfink et al. 2015). Blastx results were analyzed with MEGAN community Edition v6.4 (Huson et al. 2016) to obtain taxonomic profiles for each sample. Finally, these metagenomic analyses were performed by Lorine Bethencourt as part of her PhD project on the abundance, diversity and activity of iron-oxidising communities in groundwater systems.

Modelling approach

The combined use of different conservative tracers enables the selection of a suitable solute transport model and allows the determination of a greater variety of transport parameters. In this regard, dissolved noble gas BTCs (He, Ar and Xe) were concurrently modelled using a set of transport parameters of the analytical solution developed by Moench (Moench 1995) coupled to an inverse model based on root mean squared errors (RMSE) developed by the author on the software Matlab®.

The selected transport model accounts for the convergent radial advection and dispersion of the solute in a fracture system allowing for the solute diffusion into a matrix system. Although not used in this study, Moench's solution can also take into account the effects of fracture skin and linear adsorption on solute transport.

Once the set of transport parameters determined, the theoretical unreactive nitrate BTC was modelled serving as a reference curve for the interpretation of nitrate losses. Subsequently, a reactive transport model was fitted to the actual measure nitrate BTC assuming a first order reaction.

4. Conservative transport

The dissolved noble gas tracer BTCs are represented in figure 29 as the ratio (C/C_0) of the tracer concentration above the background levels (C) to the tracer concentration in the injected solution (C_0). Figure 29 shows that dissolved gas tracers arrived simultaneously at the pumping well around 3h after the injection. Their BTCs show distinctive shapes whose characteristics shown in table 4 and figure 29 range from the relatively sharp Xe curve (in orange) to the relatively smooth He curve (in dark red).

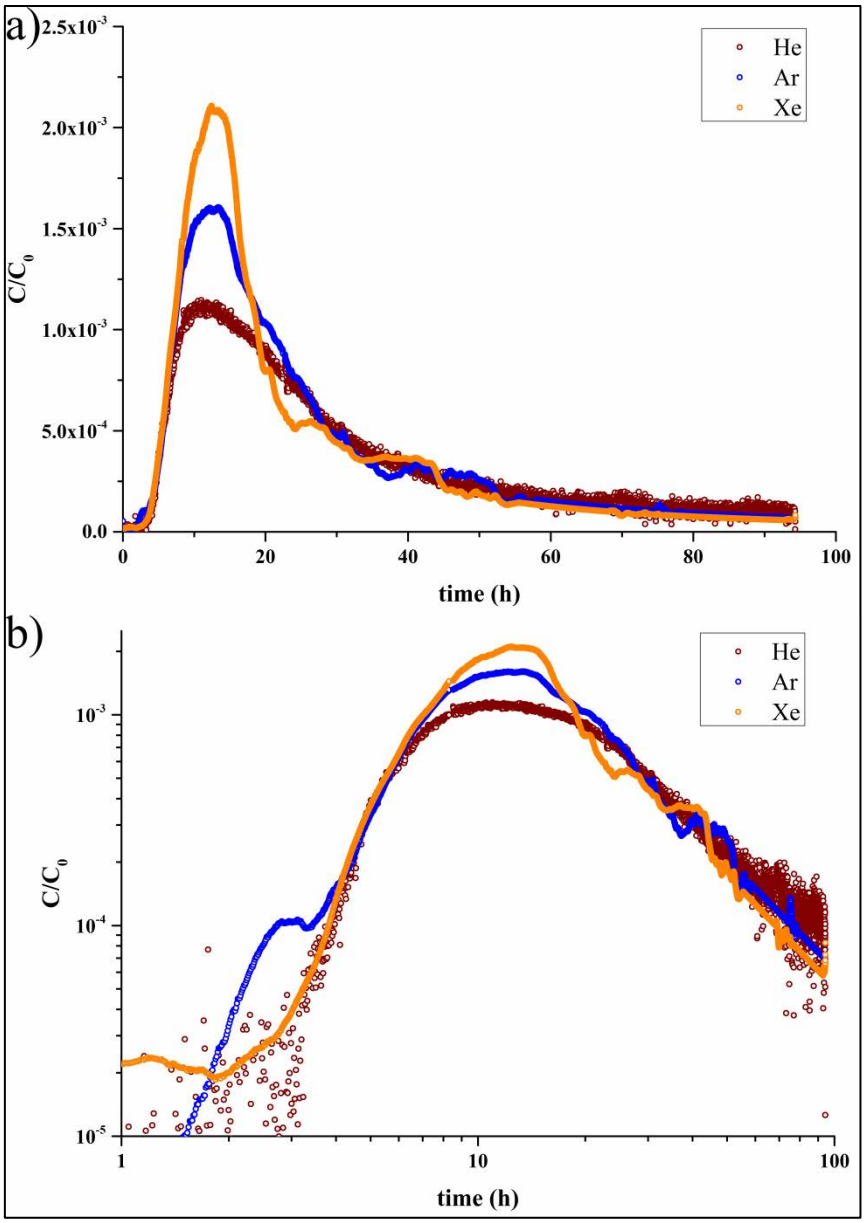

Figure 29: Dissolved He, Ar and Xe breakthrough curves obtained simultaneously using a radial convergent tracer test between F80 (injection well) and F1 (pumping well, Q = 0.95 m^3/h) at the Naizin site. Tracer BTCs are represented as the ratio of the measured tracer concentration C on the injected tracer concentration C0 on linear a) and log-log b) scales.

For instance, He peak dilution appears higher than the Ar one which is in turn more diluted than the Xe one. This trend describes a power law increase of the peak dilution with tracer diffusivity (figure 30). After the peak arrival, the tracer concentration decay with different power law slopes ranging from $t^{-1.8}$ for Xe to $t^{-1.5}$ for He. These slopes appear to attenuate exponentially with increasing tracer diffusivity. Finally, the relatively low tracer recovery rates are quite similar from a tracer to another (between 29 and 34% of the injected mass) although they appear to decrease linearly with increasing tracer diffusivity.

Table 4: Tracer breakthrough shape parameters as a function of the free water diffusion coefficient.

Tracer	D_w (m^2/s) at T=12.3°C	C_{max}/C_0	Recovery (%)	Power law exponent
He	5.91×10^{-9}	872	29.8	-1.48
Ar	2.10×10^{-9}	623	33.0	-1.72
Xe	1.00×10^{-9}	475	33.5	-1.80

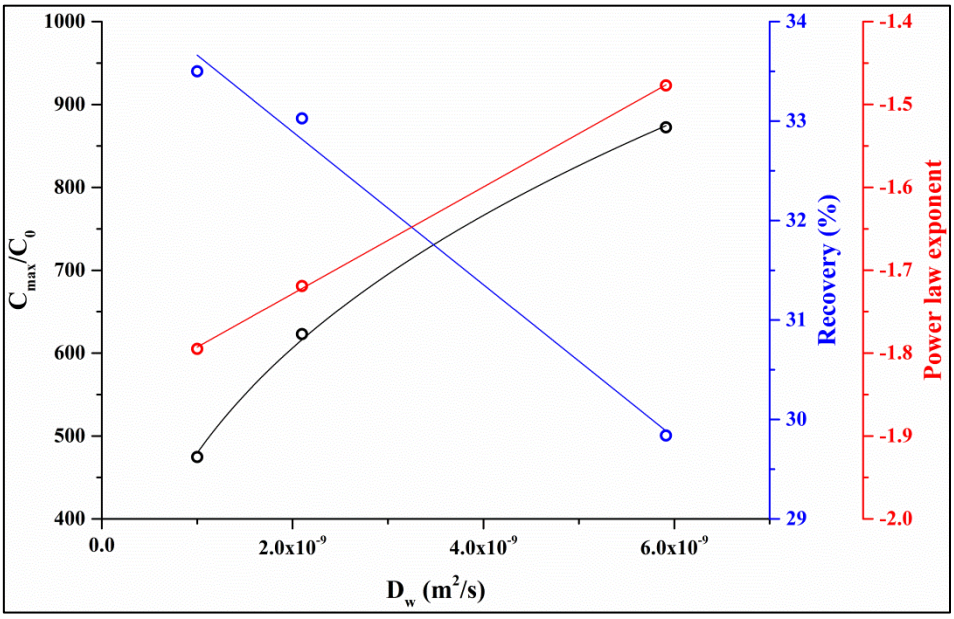

Figure 30: Evolution of tracer breakthrough shape parameters as a function of the free water diffusion coefficient.

5. Reactive transport

The nitrate and bromide BTCs are represented in figure 31 as the ratio (C/C_0) which shows a delay (36 min) between noble gases and nitrate/bromide arrival times at the pumping well. This delay is accompanied by a nitrate and bromide recovery deficit compared to the noble gas tracers (table 5).

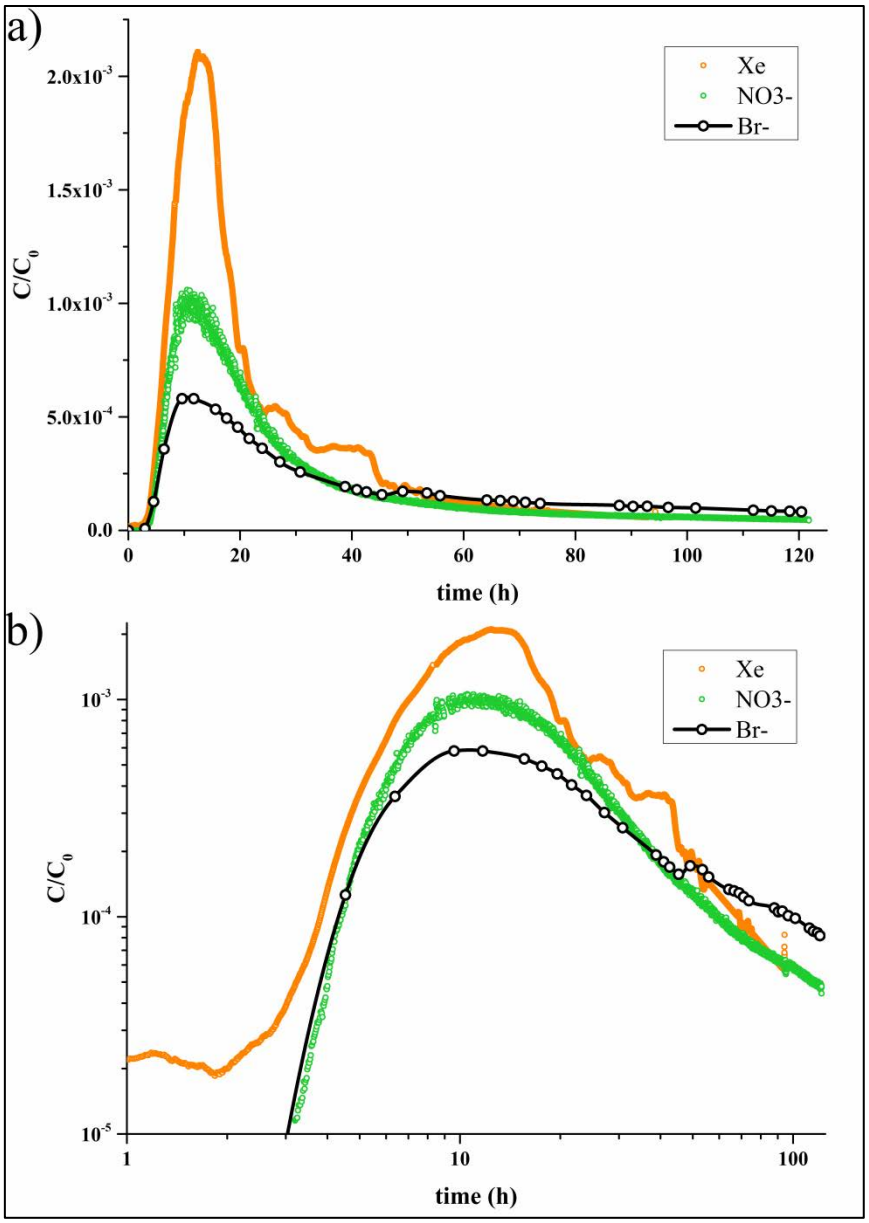

Figure 31: Dissolved xenon, bromide and nitrate breakthrough curves obtained simultaneously using a radial convergent tracer test between F80 (injection well) and F1 (pumping well, Q = 0.95 m^3/h) at the Naizin site. Tracer BTCs are represented as the ratio of the measured tracer concentration C on the injected tracer concentration C_0 on linear a) and log-log b) scales.

The nitrate peak is followed by the progressive and concomitant apparition of NO_2^-, N_2O and NH_4^+ in the pumping well as shown in figure 32. This increase in nitrogen-bearing molecules is also associated to the rise of N_2 concentrations above the natural N_2 background levels. After about 50h of experiment, the concentrations of the measured N-bearing molecules (NO_2^-, N_2O, N_2 and NH_4^+) begin to decrease as progressively as they rose.

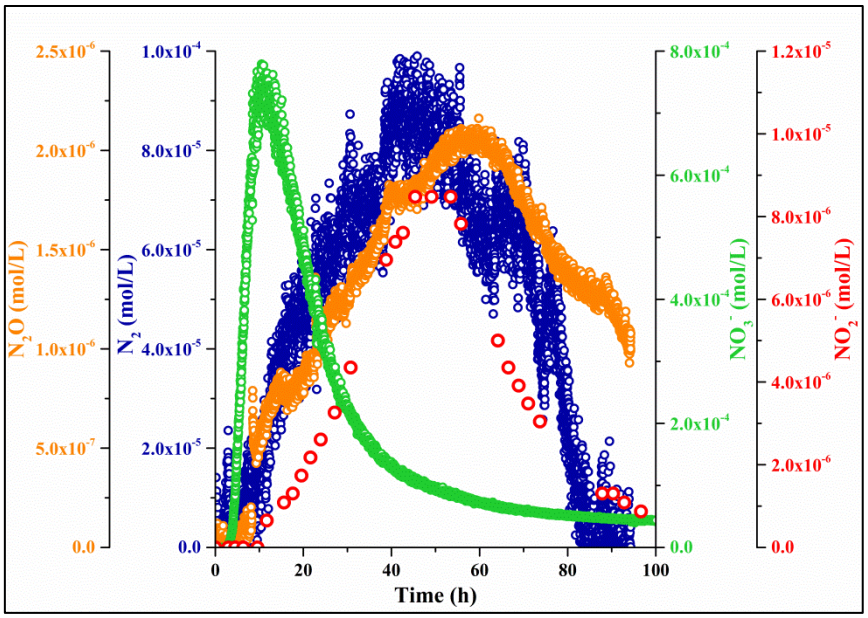

Figure 32: Evolution of nitrate (NO_3^-), nitrite (NO_2^-), nitrous oxide (N_2O) and nitrogen gas (N_2) concentrations in F1 throughout the tracer experiment.

To account for the actual amounts of nitrogen that N-bearing molecules represent, a mass balance is calculated over the whole experiment. Table 5 shows the significance of the different N-bearing molecules relative to the amount of nitrogen injected (N_{inj}). Among these N-bearing molecules, NO_3^- is the most important followed by N_2. In comparison, the remaining NH_4^+, NO_2^- and N_2O concentrations account for relatively negligible amounts of nitrogen-N bringing the total measured N to around 34% of N_{inj} which is comparable to the noble gas tracer recovery.

Table 5: Summary of tracer recovery rates.

Tracer	Recovery (%)	Recovery (% N_{inj})
Br^-	19.6	-
NO_3^-	22.1	22.1
NO_2^-	-	0.5
N_2O	-	0.3
N_2	-	10.5
NH_4^+	-	0.6
Total N	-	33.9

The frequent sampling of anions, cations and trace elements indicate a rise of SO_4^{2-}, Mg^{2+}, Fe^{2+}, Mn^{2+}, Si^{4+}, Li^+, B, Sb and U concentrations above background levels as shown in figure 33. For most elements, this concentration increase begins 24 to 72h after the tracer injection and follows a linear trend. Uranium (U) and antimony (Sb) are the only elements having a non-linear trend which somewhat follows the evolution of N-bearing molecule concentrations. The total organic carbon

analysed in the different samples taken throughout the experiment shows stable concentrations close to the low value of 0.40 mg/L, the dissolved organic carbon levels were always below the detection limits.

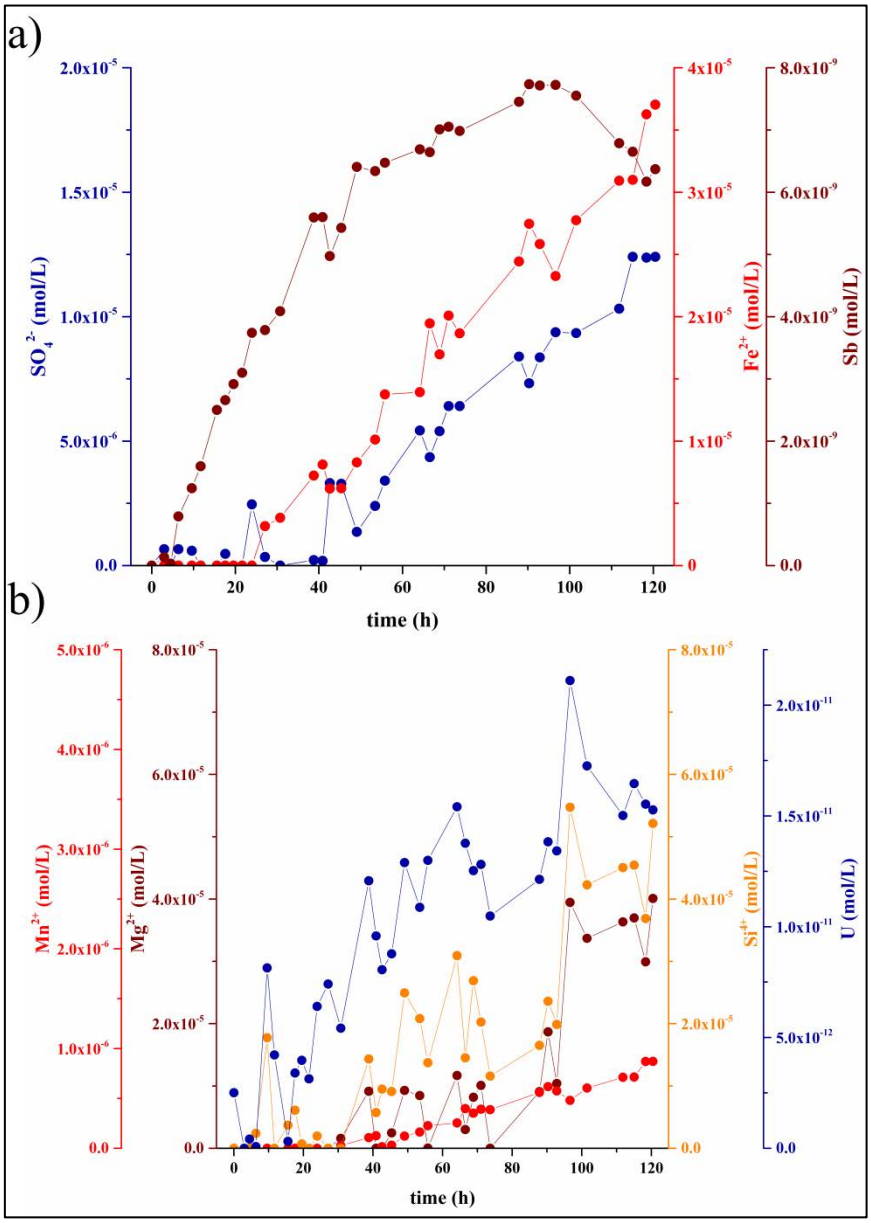

Figure 33: Evolution of the concentrations in a) sulphate (SO_4^{2-}), iron (Fe), antimony (Sb) and b) magnesium (Mg^{2+}), silicon (Si^{4+}), manganese (Mn^{2+}), uranium (U) in F1 throughout the tracer experiment.

Figure 34 shows the results of the microorganism diversity analysis where the coloured bands denote the different taxonomic genera identified in the sample and where the thickness of each coloured band refers to the genus relative abundance in the sample.

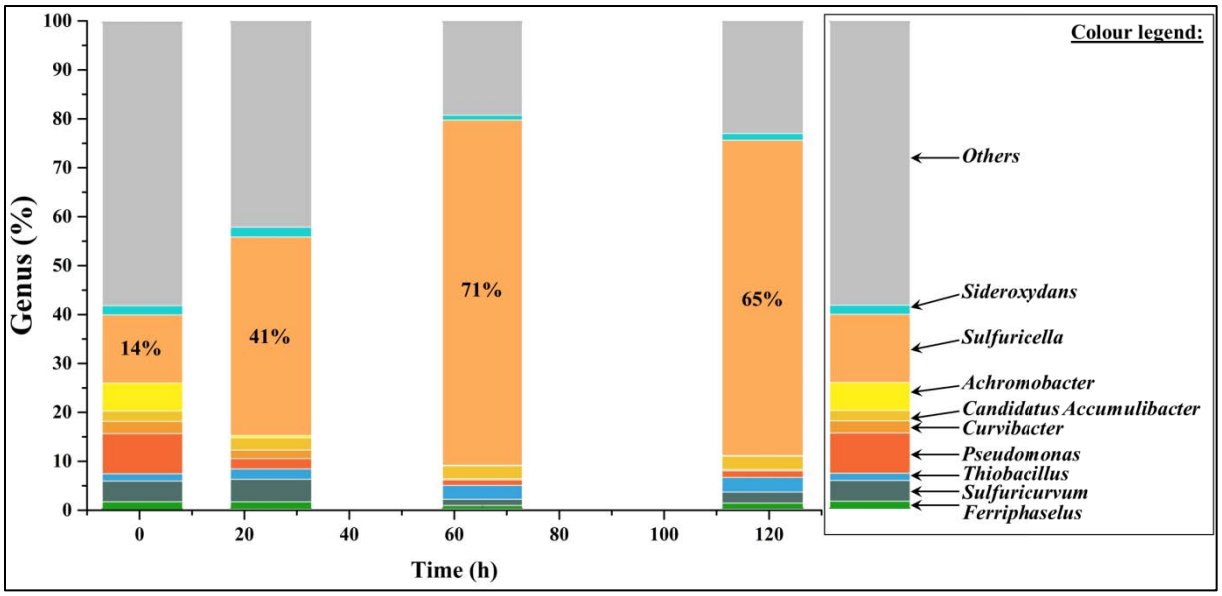

Figure 34: Evolution of main microorganism genera abundances in F1 throughout the experiment.

Two series of samples were collected in the pumping well (F1) before the injection: one when arriving at the experimental site and another after the 24h pumping preceding the injection. These sample series were analysed and showed no effect of the pumping on the microorganism community. Before the injection, the most abundant genera consist mainly in denitrifying, sulphur oxidising or iron oxidising bacteria such as *Sulfuricella* (14.0%, orange), *Pseudomonas* (8.3%, dark orange), *Achromobacter* (5.8%, yellow), *Sulfuricurvum* (4.5%, dark grey), *Curvibacter* (2.4%, orange), *Candidatus Accumulibacter* (2.1%, dark yellow), *Sideroxydans* (2.1%, cyan), *Ferriphaselus* (1.5%, green), *Thiobacillus* (1.4%, light blue), *Gallionella* (3.9%, fig.35 appendix dark orange), *Acidovorax* (2.5%, fig.35 appendix light green), *Geothrix* (2.5%, fig.35 appendix orange), *Geobacter* (2.5%, fig.35 appendix blue), *Burkholderia* (1.6%, fig.35 appendix light orange) or *Dechloromonas* (1.4%, fig.35 appendix light orange).

After the nitrate injection, the microorganism community changes considerably alike the *Sulfuricella* abundance rising rapidly from 14 to 71% after 65h and then decreasing slowly to 65% at the end of the experiment. Similarly, *Thiobacillus* abundance rises from 1.4% to 3.0% after 65h and then remains constant until the end of the experiment. As a consequence, some genera abundances decrease alike *Pseudomonas* (from 8.3 to 1.1%), *Achromobacter* (5.8% to 0.1%), *Sulfuricurvum* (from 4.5 to 1.2%) and *Ferriphaselus* (from 1.5 to 0.6%). On the other hand, several genera abundances do not change significantly during the experiment alike *Gallionella*, *Candidatus Accumulibacter* and *Sideroxydans*.

Finally, the growth of small orange rounded biofilms was observed from about 110h after the injection of nitrate until the end of the experiment.

6. Discussion

6.1. Physical transport model

According to the results, the simultaneously injected He, Ar and Xe exhibit different BTCs whose shape appear to vary with the dissolved gas free water diffusion coefficient (table 4, figure 30). Therefore, the different behaviours displayed by dissolved noble gas tracers highlight the control of diffusion processes on their transport in the fractured media. The latter is supported by the tracer breakthrough power law slopes which are comprised between the characteristic matrix diffusion slope ($t^{-1.5}$) for He and an intermediate behaviour driven by both matrix diffusion and channelling for Ar and Xe ($t^{-2.0} < t^{-x} < t^{-1.5}$).

In this respect, a transport model accounting for the both advection-dispersion processes in the fractured system and the solute diffusion in the matrix system was selected to fit the dissolved noble gas BTCs. The chosen analytical solution developed by Moench (Moench 1995) was implemented in the software Matlab® to derive solute transport parameters using an inverse model based on the model RMSEs to fit simultaneously the different tracer BTCs. The results of this modelling approach are shown in the table 6 and the figures 36 and 37 in the appendix.

Table 6: Fitted transport parameters using dissolved noble gas BTCs to constrain Moench's solution.

Property	Guessed value	Fitted value	Calculated value
h (m)	100	-	-
κ/τ^2	0.2	-	-
φ_f (%)	-	0.07	-
α (m)	-	1.14	-
φ_m (%)	-	1.50	-
b_m (m)	-	0.53	-
a (mm)	-	-	70
Ss (m^{-1})	-	-	5.66

Table 6 shows that Moench's solution is constrained by six dimensioned parameters among which the aquifer thickness (h) and the matrix geometric factor (κ/τ^2) are paradoxically either easily assessed or hardly evaluated. Setting these two parameters allows the determination of the remaining four such as the fracture system porosity (φ_f), the dispersivity (α), the matrix system porosity (φ_m) and the radius of the matrix sphere-shaped blocks (b_m). As a result, an apparent fracture aperture ($a = h \times \varphi_f$) and the specific surface of the fracture system ($Ss = (3/b_m)*(1- \varphi_f)$) can be calculated. This transport model fits relatively well the tracer BTCs and delivers acceptable parameter estimates. Under the assumptions formulated in the derivation of Moench's solution, the use of several tracers of different properties

allow to constrain physical properties essential for reactive transport characterisation. For instance, the specific surface of the fracture system is scarcely evaluated although this parameter controls the availability of reactive solid surfaces in the fracture system.

The combined use of dissolved noble gas tracers coupled to this modelling approach allows the identification of dominant transport processes in fractured media as well as the determination of transport parameters for the prediction of solute migration in the subsurface.

On the other hand, Br^- is considered as a conservative tracer and has been used in many field tracer tests. In comparison with dissolved noble gas tracers, the bromide BTC displays a retard (36 min), a peak dilution (C_0/C_{max}=1725), a power law slope ($t^{-0.9}$) and a recovery deficit (around 12%) that cannot be explained by diffusion processes.

The same applies to the nitrate BTC which has the same retard as the bromide one displaying however a steeper power law slope ($t^{-1.4}$). Nevertheless, nitrate recovery deficit (around 11%) and peak dilution (C_0/C_{max}= 944) are lower than the bromide ones.

The modelling of bromide and nitrate data therefore requires the consideration of additional transport processes and parameters which are presented in the next section.

6.2. Biogeochemical reactivity

According to the results, the transit of high nitrate concentrations in the investigated fractured media was followed by the formation of N-bearing molecules which are also known as denitrification by-products (except ammonium). Furthermore, this formation of N-bearing molecules is accompanied by a nitrate recovery deficit and the release of SO_4^{2-}, Mg^{2+}, Fe^{2+}, Mn^{2+}, Si^{4+} and trace elements in a low organic carbon environment which represent clearly the characteristics of an ongoing autotrophic denitrification.

The detected NH_4^+ concentrations indicate that other nitrate reducing reactions took place during the experiment such as for instance the dissimilatory reduction of nitrate to ammonia (DNRA). However, regarding the small amounts of nitrogen at stake, these reactions are negligible with respect to the autotrophic denitrification detailed in this study.

The reaction of autotrophic denitrification can be modelled as a first order reaction (Pauwels et al. 1998; Boisson et al. 2013). In the present experiment, this requires the modelling of theoretical unreactive nitrate BTC using $NaNO_3$ diffusion coefficient and the findings of the previous section. Since nitrate concentrations appeared to be delayed compared to the noble gases, an additional retardation parameter (R>1) was required for the modelling of the theoretical nitrate BTC. Afterwards, the denitrification of the theoretical nitrate BTC was modelled using a first order kinetic constant (k)

to fit the measured nitrate BTC. As a result, a combined determination of R and k was implemented in Matlab® using Moench's solution.

Subsequently, a reactive transport model was fitted to the nitrate BTC (figure 38 in the appendix) using a retardation factor R = 1.11 and a kinetic constant k = 0.0085 h^{-1} corresponding to a nitrate half-life of about 3.4 days. This nitrate half-life is about two times smaller than the 7.9 days previously predicted for the low-porosity fractured medium and remains close to the 2.1 days predicted for the high-porosity weathered medium (Pauwels et al. 1998). As a matter of fact, the late-time behaviour of the nitrate BTC could not be accurately explained by the fitted transport model which means that the lone use of a retardation factor does not fully describe the processes behind the differential transport between nitrates and noble gases. Alike the bromide BTC, the retard and tailing of the nitrate BTC could be the result of density effects rather than a linear sorption reaction simulated here with R>1. However, according to the literature (Istok & Humphrey 1995; Becker 2003), the evaluation of density effects on tracer buoyancy is not trivial especially in such heterogeneous media. More investigations based on the bromide BTC are necessary to predict accurately late-time nitrate transport. Nevertheless, the present reactive transport model predicts reaction kinetics in good agreement with the literature even though a faster denitrification rate was measured in the fractured media.

The analysis of denitrification by-products shows that nitrite (NO_2^-) and nitrous oxide (N_2O) are very unstable in reducing environments. These N-bearing molecules are thus rapidly transformed into nitrogen gas (N_2) as it was shown with the denitrification kinetics inferred by Boisson et al (Boisson et al. 2013).

The subsequent production of SO_4^{2-} and Fe^{2+} probably results from pyrite (FeS_2) oxidation as previously evidenced by Pauwels et al (Pauwels et al. 1998) on the experimental site. Furthermore, the additional release of cations such as Fe^{2+}, $Mg^{2+}$and Si^{4+} indicate the weathering of silicate minerals and most probably biotite ($K(Fe,Mg)_3[Si_3AlO_{10}(OH,F)_2]$) as showed in crystalline media by Aquilina et al (Aquilina et al. 2017) and Roques et al (Roques et al. 2017). However, the amount of nitrate reduced by denitrification during the experiment (9.08 mol) is much higher than the quantity of produced SO_4^{2-} (0.57 mol), Fe^{2+} (1.75 mol), Mg^{2+} (1.42 mol) and Si^{4+} (2.38 mol). For instance, using equation 23 such amount of reduced nitrate should be balanced by the production of at least ten times the recovered sulphate (6.48 mol). The absence of H_2S gas in the collected samples indicates that this deficit in sulphate recovery cannot be attributed to the SO_4^{2-} reduction but rather to a precipitation of secondary sulphate minerals (jarosite $KFe_3(SO_4)_2(OH)_6$) as advocated by Pauwels et al (Pauwels et al. 1998). On the other hand, the steady linear increase of SO_4^{2-}, Fe^{2+}, $Mg^{2+}$and Si^{4+} concentrations until the end of the experiment suggests that mineral weathering reactions were still ongoing when the experiment was stopped which leads to an underestimation of SO_4^{2-}, Fe^{2+}, $Mg^{2+}$and Si^{4+} productions.

6.3. Response of the microorganism community

The analysis of the microorganism community throughout the experiment exhibited a clear evolution of this subsurface ecosystem. Since the genus abundances are expressed as a fraction of the total number of microorganisms, the analysis of the different abundances can only remain qualitative. Nevertheless, the observed strong increase of *Sulfuricella* and *Thiobacillus* abundances can probably be more attributed to the rapid growth of these genera (and also of the total number of microorganism) rather than a fast decay of the others. The dynamics of these denitrifying and sulphur-oxidising bacteria are intrinsically correlated to the other observed hydrogeochemical evidences of autotrophic denitrification. Therefore, the observed response of the microorganism community to a nitrate contamination is rapid and ample.

Even though the injection of nitrates in the aquifer seems to specialise the microorganism community and threaten its diversity, the late-time slight decrease of *Sulfuricella* could be interpreted as a broader acclimatisation of the rest of the community to the induced disturbance. The latter could be supported by the observation of biofilm growth at the end of the experiment which has already been attributed to the development of iron-oxidising communities (*Gallionella*, *Ferriphaselus*) in fractured media (Bochet et al. 2017).

In this regard, the constant abundance displayed by *Gallionella*, *Candidatus Accumulibacter* and *Sideroxydans* does not necessarily mean that their respective population remained constant during the experiment. For instance, in case of an increase of the total number of microorganisms due to the enhanced nutrient availability, a constant genus abundance would actually indicate a population growth at the same rate as the total community. The same applies for genera of decreasing abundance (*Pseudomonas*, *Achromobacter*, *Sulfuricurvum* and *Ferriphaselus*) which, in this case, could indicate a population growth at a slower rate than the rest of the community, a stable population or an actually decreasing population.

In other words, the rapid growth of denitrifying and sulphur-oxidising bacteria (*Sulfuricella* and *Thiobacillus*) shortly after the injection of nitrates might have been followed by a growth of iron oxidising bacteria (*Gallionella* and *Sideroxydans*) under the assumption of a rise of the total microorganism population in response to the sudden provision of nutrients.

More investigations are required to determine quantitatively the impacts of the nitrate contamination on the microorganism community. Nevertheless, the observations made in this study show a strong response of microorganism communities along the experiment. These changes occur rapidly and show that the injection of nitrates in the anoxic fractured medium mostly influenced the denitrifying and sulphur-oxidising communities. It is highly likely that the total microorganism population increased during the experiment in response to the sudden availability of nutrients. The latter would indicate a

broader and more complex response of the subsurface ecosystem involving varying rates of genus growth or decay depending on the interactions taking place inside microorganism community in response to nutrient availability.

7. Conclusion and perspectives

Using the simultaneous injection of conservative and reactive tracers combined to a continuous field monitoring of the aquifer biogeochemistry, this study proposes a new field experiment for the characterisation of the physical, chemical and biological controls on solute transport in heterogeneous porous media. This approach is based on a single injection of dissolved noble gases and nitrates and a continuous monitoring of the dissolved gases, anions, cations, trace elements, stable isotopes and the microorganism community.

Dissolved noble gas data enabled the characterisation of the dominant physical transport properties of a fractured media using a double porosity model. These findings enabled the subsequent modelling of the nitrate breakthrough curve and the derivation of a reactive transport model based on a first order kinetic reaction of denitrification. The continuous monitoring of groundwater chemistry and microbiology allowed the identification of pyrite and biotite as reactive minerals involved in the denitrification reaction which is mediated by autotrophic microorganisms. The sudden availability of nutrients in the anoxic fractured media resulted in significant modifications in microorganism communities particularly a fast and ample growth of denitrifying and sulphur-oxidising bacteria.

This ongoing work requires more investigation for a better prediction of nitrate late-time behaviour as well as the quantitative characterisation of the dynamics of microorganism communities. Nevertheless, this experiment releases new opportunities for the study of solute transport in porous media particularly the study of diffusive processes in heterogeneous media, the investigation of the role heterogeneity on biogeochemical reactions and the assessment of subsurface ecosystem resilience.

Chapter V: Conclusion and perspectives

The general objective of this thesis was to describe the interest and the potentials which reside in the measurements of dissolved gases, particularly their field measurements, to characterise of groundwater hydrobiogeochemical dynamics at different scales. In order to complete this ambition, our investigations focused on the development of an innovative instrumentation, the implementation of novel tracers in original experimental setups and the acquisition, processing, analysis and interpretation of various dissolved gas datasets.

Firstly, this thesis consisted in the development of an innovative tool enabling the continuous field measurements of several dissolved gases. Owing to the potentials and the versatility these tracers, the CF-MIMS was shown to be a valuable tool for the field characterisation of biogeochemical reactivity, groundwater transport properties, groundwater origins and residence time distribution. This innovative technique improves the spatio-temporal distribution and the quality of dissolved gas data and makes a contribution of hydrogeochemistry to the concept of "operational hydrology". This novel instrument is now to be more widely implemented in the CZ for the field characterisation of biogeochemical reactivity, solute transport properties in aquatic environments, water residence time distribution as well as surface-ground water exchanges and their impacts from few hours to several weeks experiments.

Secondly, this thesis also comprised the characterisation of the natural dynamics of a coastal groundwater system and the anthropogenic footprint of its exploitation at the catchment scale. The integrative information derived from dissolved gas tracers allowed the identification of groundwater mixing and pathways, the characterisation of groundwater residence time distribution and the record of recharge conditions. The collection and analysis of these environmental data provide important information for the management of the quantity and quality of water resources (water supply, contamination/salinisation management, ecosystem protection) and also for the investigation of the Earth's climate through its past changes. This thesis shows that implementing relatively simple multi-tracer approach can deliver useful information on complex groundwater systems provided an adequate sampling is ensured (number of samples, data spatio-temporal distribution). Naturally, these approaches necessitate continuous analytical improvements without altering their simplicity and may integrate a larger variety of fairly accessible tracers (such as ^{4}He). In addition, the different investigations of the COQUEIRAL project demonstrate the benefits of the integrated "hydro-sociological" approach to provide exhaustive insights to decision makers and to the layperson especially when water management is deficient. In the end, it appears now essential for academic research to understand and accept part of the "responsibility for the stewardship of Earth" by standing for a wider availability of research outcomes to all environmental management stakeholders.

This thesis finally involved the simultaneous characterisation of the physical and biogeochemical processes controlling solute transport in heterogeneous aquifers at the fracture scale using dissolved gas tracers. Dissolved noble gas data enabled the characterisation of the dominant physical transport properties of the fractured media and the prediction of the reactive transport of nitrates in the fracture network. The continuous monitoring of groundwater chemistry and microbiology allowed the identification of the reactive minerals involved in the denitrification reaction mediated by autotrophic microorganisms. The sudden availability of nutrients in the anoxic fractured media resulted in significant modifications in microorganism communities particularly a fast and ample growth of denitrifying and sulphur-oxidising bacteria. This ongoing work already opens new opportunities for the study of solute transport in aquatic environments particularly the study of diffusive processes, the investigation of the impact of aquatic biogeochemical reactions in the global sulphur, carbon and nitrogen cycle and the evaluation of the response of microorganism community to natural and anthropogenic stresses.

To conclude, among the different families of tracers, dissolved gases comprise many advantages. Owing to the versatility of their physical and biogeochemical properties they enable the understanding of various physical, chemical and biological processes occurring at different spatial and temporal scales in the Hydrosphere. Many of these dissolved gas tracers can be measured with the same monitoring techniques which now benefit from key technological advances that allow geochemists to leave the laboratory and converge with the rest of the environmental science community towards the thorough exploration of the CZ. From now on, to observe the CZ, if our instruments are eyes that become sharper, if our measurements are images that become clearer, then all that remains is to take a walk and turn our head in the right direction (what an adventure!).

References

Abelin, H. et al., 1994. Channeling experiments in crystalline fractured rocks. *Journal of Contaminant Hydrology*, 15(3), pp.129–158.

Adams, E.E. & Gelhar, L.W., 1992. Field Study of Dispersion in a Heterogeneous Aquifer: Moments Analysis. *Water Resources Research*, 28(12), pp.3293–3307.

Addy, K. et al., 2002. In Situ Push – Pull Method to Determine Ground Water Denitrification in Riparian Zones. *Journal of Environmental Quality*, 31, pp.1017–1024.

Adler, P.M., Thovert, J.F. & Mourzenko, V. V., 2012. *Fractured porous media*, Oxford University Press.

Aeschbach-Hertig, W. et al., 2002. Excess Air in Groundwater As a Potential Indicator of Past Environmental Changes. *IAEA*, pp.174–183.

Aeschbach-Hertig, W. et al., 1999. Interpretation of dissolved atmospheric noble gases in natural waters. *Water Resources Research*, 35(9), pp.2779–2792.

Aeschbach-Hertig, W. et al., 2000. Palaeotemperature reconstruction from noble gases in ground water taking into account equilibration with entrapped air. *Nature*, 405(6790), pp.1040–1044.

Aeschbach-Hertig, W. & Gleeson, T., 2012. Regional strategies for the accelerating global problem of groundwater depletion. *Nature Geoscience*, 5(12), pp.853–861. Available at: http://www.nature.com/doifinder/10.1038/ngeo1617.

Aeschbach-Hertig, W. & Solomon, D.K., 2013. Noble Gas Thermometry in Groundwater Hydrology. In *The Noble Gases as Geochemical Tracers*. pp. 81–122. Available at: http://dx.doi.org/10.1007/978-3-642-28836-4_5.

Amiotte Suchet, P., Probst, J.-L. & Ludwig, W., 2003. Worldwide distribution of continental rock lithology: Implications for the atmospheric/soil CO2 uptake by continental weathering and alkalinity river transport to the oceans. *Global Biogeochemical Cycles*, 17(2). Available at: http://doi.wiley.com/10.1029/2002GB001891.

Andersson, P. et al., 2004. In situ tracer tests to determine retention properties of a block scale fracture network in granitic rock at the Äspö Hard Rock Laboratory, Sweden. *Journal of Contaminant Hydrology*, 70(3–4), pp.271–297.

Andrews, J.N. et al., 1982. Radioelements, radiogenic helium and age relationships for groundwaters from the granites at Stripa, Sweden. *Geochimica et Cosmochimica Acta*, 46(9), pp.1533–1543.

Andrews, J.N., 1985. The isotopic composition of radiogenic helium and its use to study groundwater movement in confined aquifers. *Chemical Geology*, 49(1–3), pp.339–351.

Andrews, J.N. & Lee, D.J., 1979. Inert gases in groundwater from the Bunter Sandstone of England as indicators of age and palaeoclimatic trends. *Journal of Hydrology*, 41(3–4), pp.233–252.

Aquilina, L. et al., 2017. Denitrification processes in crystalline pumped aquifers (1) : Geochemical and microbiological mechanisms (submitted). *Submitted to Science of the Total Environment*, (1).

Aquilina, L. et al., 2012. Nitrate dynamics in agricultural catchments deduced from groundwater dating and long-term nitrate monitoring in surface- and groundwaters. *Science of the Total Environment*, 435–436, pp.167–178. Available at: http://dx.doi.org/10.1016/j.scitotenv.2012.06.028.

Aquilina, L. et al., 2004. Porosity and fluid velocities in the upper continental crust (2 to 4 km) inferred from injection tests at the Soultz-sous-Forêts geothermal site. *Geochimica et Cosmochimica Acta*, 68(11), pp.2405–2415.

Ashley, G.M., 1998. Where are we headed ? Soft rock research into the new millenium. *Geological Society of America*, 30(7), p.148.

Ayraud, V. et al., 2008. Compartmentalization of physical and chemical properties in hard-rock aquifers deduced from chemical and groundwater age analyses. *Applied Geochemistry*, 23(9), pp.2686–2707.

Banwart, S. a. et al., 2013. *Sustaining Earth' s Critical Zone: Basic Science and Interdisciplinary Solutions for Global Challenges*,

Becker, M.W. et al., 2003. Bacterial Transport Experiments in Fractured Crystalline Bedrock. *Ground Water*, 41(5), pp.682–689.

Becker, M.W., 2003. Effect of tracer buoyancy on tracer experiments conducted in fractured crystalline bedrock. *Geophysical Research Letters*, 30(3), pp.7–10.

Becker, M.W. & Shapiro, A.M., 2003. Interpreting tracer breakthrough tailing from different forced-gradient tracer experiment configurations in fractured bedrock. *Water Resources Research*, 39(1), pp.1–13. Available at: http://doi.wiley.com/10.1029/2001WR001190.

Becker, M.W. & Shapiro, A.M., 2000. Tracer transport in fractured crystalline rock: Evidence of nondiffusive breakthrough tailing. *Water Resources Research*, 36(7), pp.1677–1686.

Bense, V.F. et al., 2013. Fault zone hydrogeology. *Earth-Science Reviews*, 127, pp.171–192. Available at: http://dx.doi.org/10.1016/j.earscirev.2013.09.008.

Berkowitz, B., 2002. Characterizing flow and transport in fractured geological media: A review. *Advances in Water Resources*, 25(8–12), pp.861–884.

Berkowitz, B. et al., 2000. Scaling of fracture connectivity in geological formations Brian. *Geophysical Research Letters*, 27(14), pp.2061–2064.

Berkowitz, B., Emmanuel, S. & Scher, H., 2008. Non-Fickian transport and multiple-rate mass transfer in porous media. *Water Resources Research*, 44(3), pp.1–16.

Bertrand, G. et al., 2016. Groundwater contamination in coastal urban areas: Anthropogenic pressure and natural attenuation processes. Example of Recife (PE State, NE Brazil). *Journal of Contaminant Hydrology*, 192, pp.165–180. Available at: http://dx.doi.org/10.1016/j.jconhyd.2016.07.008.

Bertrand, G. et al., 2017. Groundwater isotopic data as potential proxy for Holocene paleohydroclimatic and paleoecological models in NE Brazil. *Palaeogeography, Palaeoclimatology, Palaeoecology*, 469, pp.92–103.

Betlach, M.R. & Tiedje, J.M., 1981. Kinetic Explanation for Accumulation of Nitrite, Nitric Oxide, and Nitrous Oxide during Bacterial Denitrification. *Applied and Environmental Microbiology*, 42(6), pp.1074–1084.

Beyerle, U. et al., 2000. A Mass Spectrometric System for the Analysis of Noble Gases and Tritium from Water Samples. *Environmental Science and Technology*, 34(10), pp.2042–2050.

Beyerle, U. et al., 1998. Climate and groundwater recharge during the last glaciation in an ice-covered region. *Science*, 282(5389), pp.731–734.

Bochet, O. et al., 2017. Fractures sustain dynamic microbial hotspots in the deep subsurface. *submitted to Nature Geoscience*. Available at: http://arxiv.org/abs/1708.09645.

Bodin, J., Delay, F. & de Marsily, G., 2003. Solute transport in a single fracture with negligible matrix permeability: 1. Fundamental mechanisms. *Hydrogeology Journal*, 11, pp.418–433.

Bohlke, J.K. & Denver, J.M., 1995. Combined use of ground- water dating, chemical, and isotopic analyses to resolve the history and fate of nitrate contamination in two agricultural watersheds, atlantic coastal Plain, Maryland. *Water Resources Research*, 31(9), pp.2319–2339.

Boisson, A. et al., 2013. Reaction chain modeling of denitrification reactions during a push-pull test.

Journal of Contaminant Hydrology, 148, pp.1–11.

Bonnet, E. et al., 2001. Scaling of fracture systems in geological media. *Reviews of Geophysics*, 39(3), pp.347–383.

Le Borgne, T. et al., 2006. Assessment of preferential flow path connectivity and hydraulic properties at single-borehole and cross-borehole scales in a fractured aquifer. *Journal of Hydrology*, 328, pp.347–359.

Bour, O. et al., 2002. A statistical scaling model for fracture network geometry, with validation on a multiscale mapping of a joint network (Hornelen Basin, Norway). *Journal of Geophysical Research*, 107, p.2113. Available at: http://doi.wiley.com/10.1029/2001JB000176.

Bour, O. & Davy, P., 1999. Clustering and size distributions of fault patterns: theory and measurements. *Geophysical Research Letters*, 26(13), pp.2001–2004.

Bour, O. & Davy, P., 1997. Connectivity of random fault networks following a power law fault length distribution. *Water Resources Research*, 33(7), pp.1567–1583.

Bour, O. & Davy, P., 1998. On the connectivity of three-dimensional fault networks. *Water Resources Research*, 34(10), pp.2611–2622.

Bourke, S.A. et al., 2014. Characterisation of hyporheic exchange in a losing stream using radon-222. *Journal of Hydrology*, 519, pp.94–105. Available at: http://dx.doi.org/10.1016/j.jhydrol.2014.06.057.

Brantley, S.L. et al., 2017. Designing a network of critical zone observatories to explore the living skin of the terrestrial Earth. *Earth Surface Dynamics Discussions*.

Brantley, S.L., Goldhaber, M.B. & Vala Ragnarsdottir, K., 2007. Crossing disciplines and scales to understand the critical zone. *Elements*, 3(5), pp.307–314.

Brennwald, M.S., Hofer, M. & Kipfer, R., 2013. Simultaneous analysis of noble gases, sulfur hexafluoride, and other dissolved gases in water. *Environmental Science and Technology*, 47(15), pp.8599–8608.

Buchfink, B., Xie, C. & Huson, D.H., 2015. Fast and sensitive protein alignment using DIAMOND. *Nature Methods*, 12(1), pp.59–60. Available at: http://www.nature.com/doifinder/10.1038/nmeth.3176.

Burnard, P., 2013. *The Noble Gases as Geochemical Tracers*,

Busenberg, E. & Plummer, L.N., 2000. Dating young groundwater with sulfur hexafluoride: Natural

and anthropogenic sources of sulfur hexafluoride. *Water Resources Research*, 36(10), pp.3011–3030.

Busenberg, E. & Plummer, L.N., 1992. Use of Chlorofluorocarbons (CCl3F and CCl2F2) as Hydrologic Tracers and Age-Dating Tools: The Alluvium and Terrace System of Central Oklahoma. *Water Resources Research*, 28(9), pp.2257–2283.

Callahan, T.J. et al., 2000. Using multiple experimental methods to determine fracture/matrix interactions and dispersion of nonreactive solutes in saturated volcanic tuff. *Water Resources Research*, 36(12), pp.3547–3558.

Canfield, D.E. & Thamdrup, B., 2009. Towards a consistent classification scheme for geochemical environments, or, why we wish the term "suboxic" would go away: Editorial. *Geobiology*, 7(4), pp.385–392.

Cary, L., Pauwels, H., et al., 2015. Evidence for TiO2 nanoparticle transfer in a hard-rock aquifer. *Journal of Contaminant Hydrology*, 179, pp.148–159. Available at: http://dx.doi.org/10.1016/j.jconhyd.2015.06.007.

Cary, L., Petelet-Giraud, E., et al., 2015. Origins and processes of groundwater salinization in the urban coastal aquifers of Recife (Pernambuco, Brazil): A multi-isotope approach. *Science of the Total Environment*, 530–531, pp.411–429.

Cary, P. et al., 2015. Vivre avec la pénurie d'eau à Recife. *Espace populations sociétés*. Available at: http://eps.revues.org/5824.

Castro, M.C. et al., 2012. A late Pleistocene-Mid-Holocene noble gas and stable isotope climate and subglacial record in southern Michigan. *Geophysical Research Letters*, 39(19), pp.1–6.

Castro, M.C. et al., 2007. A new noble gas paleoclimate record in Texas - Basic assumptions revisited. *Earth and Planetary Science Letters*, 257(1–2), pp.170–187.

Castro, M.C., Jambon, A., et al., 1998. Noble gases as natural tracers of water circulation in the Paris Basin: 1. Measurements and discussion of their origin and mechanisms of vertical transport in the basin. *Water Resources Research*, 34(10), pp.2443–2466.

Castro, M.C., Goblet, P., et al., 1998. Noble gases as natural tracers of water circulation in the Paris Basin 2. Calibration of a groundwater flow model using noble gas isotope data. *Water Resources Research*, 34(10), pp.2467–2483.

Castro, M.C., Stute, M. & Schlosser, P., 2000. Comparison of 4He ages and 14C ages in simple aquifer systems: Implications for groundwater flow and chronologies. *Applied Geochemistry*,

15(8), pp.1137–1167.

Charlson, R.J. et al., 1987. Oceanic phytoplankton, atmospheric sulphur, cloud albedo and climate. *Nature*, 326(16), pp.655–661.

Chatton, E. et al., 2017. Field Continuous Measurement of Dissolved Gases with a CF-MIMS: Applications to the Physics and Biogeochemistry of Groundwater Flow. *Environmental Science and Technology*, 51, p.846−854.

Chatton, E. et al., 2016. Glacial recharge, salinisation and anthropogenic contamination in the coastal aquifers of Recife (Brazil). *Science of the Total Environment*, 569–570, pp.1114–1125.

Chen, C.Y., 1999. Ultrasensitive Isotope Trace Analyses with a Magneto-Optical Trap. *Science*, 286(5442), pp.1139–1141. Available at: http://www.sciencemag.org/cgi/doi/10.1126/science.286.5442.1139.

Christiansen, J.R., Outhwaite, J. & Smukler, S.M., 2015. Comparison of CO2, CH4 and N2O soil-atmosphere exchange measured in static chambers with cavity ring-down spectroscopy and gas chromatography. *Agricultural and Forest Meteorology*, 211–212, pp.48–57. Available at: http://dx.doi.org/10.1016/j.agrformet.2015.06.004.

Clark, I., 2015. *Groundwater Geochemistry and Isotopes*, CRC Press.

Clauser, C., 1992. Permeability of crystalline rocks. *Eos, Transactions American Geophysical Union*, 73(21), pp.233–238.

Clever, H.L., 1980. Argon. *Solubility data series (IUPAC)*, 4, p.331.

Clever, H.L., 1979a. Helium and Neon - Gas Solubilities. *Solubility data series (IUPAC)*, 1, p.393.

Clever, H.L., 1979b. Krypton, Xenon and Radon - Gas-Solubilities. *Solubility data series (IUPAC)*, 2, p.357.

Collon, P. et al., 2000. 81Kr in the Great Artesian Basin, Australia: A new method for dating very old groundwater. *Earth and Planetary Science Letters*, 182(1), pp.103–113.

Condon, L.E., Maxwell, R.M. & Gangopadhyay, S., 2013. The impact of subsurface conceptualization on land energy fluxes. *Advances in Water Resources*, 60, pp.188–203. Available at: http://dx.doi.org/10.1016/j.advwatres.2013.08.001.

Cook, P.G. et al., 1995. Chlorofluorocarbons as Tracers of Groundwater Transport Processes in a Shallow, Silty Sand Aquifer. *Water Resources Research*, 31(3), pp.425–434.

Cook, P.G. & Böhlke, J.K., 2000. Determining timescales for groundwater flow and solute transport. In *Environmental Tracers in Subsurface Hydrology*.

Cook, P.G. & Herczeg, A.L., 2000. *Environmental Tracers in Subsurface Hydrology*,

Cook, P.G. & Solomon, D.K., 1997. Recent advances in dating young groundwater: Chlorofluorocarbons, 3H/3He and 85Kr. *Journal of Hydrology*, 191(1–4), pp.245–265.

Corcho Alvarado, J.A. et al., 2007. Constraining the age distribution of highly mixed groundwater using 39Ar: A multiple environmental tracer (3H/3He, 85Kr, 39Ar, and 14C) study in the semiconfined Fontainebleau Sands Aquifer (France). *Water Resources Research*, 43(3), pp.1–16.

Corcho Alvarado, J.A. et al., 2009. European climate variations over, the past half-millennium reconstructed from groundwater. *Geophysical Research Letters*, 36(15), pp.1–5.

Corcho Alvarado, J.A. et al., 2011. Reconstruction of past climate conditions over central Europe from groundwater data. *Quaternary Science Reviews*, 30, pp.3423–3429.

Corcho Alvarado, J.A., Pačes, T. & Purtschert, R., 2013. Dating groundwater in the Bohemian Cretaceous Basin: Understanding tracer variations in the subsurface. *Applied Geochemistry*, 29, pp.189–198.

Cranswick, R.H., Cook, P.G. & Lamontagne, S., 2014. Hyporheic zone exchange fluxes and residence times inferred from riverbed temperature and radon data. *Journal of Hydrology*, 519, pp.1870–1881. Available at: http://dx.doi.org/10.1016/j.jhydrol.2014.09.059.

Cuthbert, M.O. et al., 2017. Modelling the role of groundwater hydro-refugia in East African hominin evolution and dispersal. *Nature Communications*, 8, pp.1–11. Available at: http://www.nature.com/doifinder/10.1038/ncomms15696.

Darcel, C. et al., 2003. Connectivity properties of two-dimensional fracture networks with stochastic fractal correlation. *Water Resources Research*, 39(10), pp.1–13. Available at: http://doi.wiley.com/10.1029/2002WR001628.

Darcy, H., 1856. *Exposition et Application des Principes à Suivre et des Formules à Employer dans les Questions de Distribution d'Eau*, Available at: http://ogst.ifpenergiesnouvelles.fr/articles/ogst/abs/2008/01/ogst07042/ogst07042.html.

Davy, P. et al., 2010. A likely universal model of fracture scaling and its consequence for crustal hydromechanics. *Journal of Geophysical Research*, 115(10), pp.1–13.

Davy, P. et al., 2006. Flow in multiscale fractal fracture networks. In *Fractal Analysis for Natural*

Hazards. The Geological Society of London, pp. 31–45. Available at: http://sp.lyellcollection.org/lookup/doi/10.1144/GSL.SP.2006.261.01.03.

Dawkins, R., 2006. *The Selfish Gene*, Oxford University Press.

Delbart, C. et al., 2014. Investigation of young water inflow in karst aquifers using SF6-CFC-3H/He-85Kr-39Ar and stable isotope components. *Applied Geochemistry*, 50, pp.164–176. Available at: http://dx.doi.org/10.1016/j.apgeochem.2014.01.011.

DeWayne Cecil, L. & Green, J.R., 2000. Radon-222. In *Environmental Tracers in Subsurface Hydrology*. pp. 175–194.

Döll, P. et al., 2012. Impact of water withdrawals from groundwater and surface water on continental water storage variations. *Journal of Geodynamics*, 59–60, pp.143–156. Available at: http://dx.doi.org/10.1016/j.jog.2011.05.001.

Doolittle, W.F., 1981. *Is Nature Motherly ?*, The CoEVOLUTION QUARTERLY.

de Dreuzy, J.-R., Davy, P. & Bour, O., 2001. Hydraulic properties of two-dimensional random fracture networks following power law distributions 1. Effective connectivity. *Water Resources Research*, 37(8), pp.2065–2078. Available at: http://doi.wiley.com/10.1029/2001WR001009.

de Dreuzy, J.-R., Davy, P. & Bour, O., 2002. Hydraulic properties of two-dimensional random fracture networks following power law distributions of length and aperture. *Water Resources Research*, 38(12), pp.12-1-12–9. Available at: http://doi.wiley.com/10.1029/2001WR001009.

de Dreuzy, J.R., Davy, P. & Bour, O., 2001. Hydraulic properties of two-dimensional random fracture networks following a power law length distribution 2. Permeability of networks based on lognormal distribution of apertures. *Water Resources Research*, 37(8), pp.2079–2095.

de Dreuzy, J.R., Méheust, Y. & Pichot, G., 2012. Influence of fracture scale heterogeneity on the flow properties of three-dimensional discrete fracture networks (DFN). *Journal of Geophysical Research*, 117(11), pp.1–21.

Le Druillennec, T. et al., 2010. Hydrogeological and geochemical control of the variations of 222Rn concentrations in a hard rock aquifer: Insights into the possible role of fracture-matrix exchanges. *Applied Geochemistry*, 25(3), pp.345–356.

Du, X. et al., 2003. A New Method of Measuring 81Kr and 85Kr Abundances in Environmental Samples. *Geophysical Research Letters*, 30(20), p.2068. Available at: http://arxiv.org/abs/physics/0311118.

Dykhuizen, R.C., 1992. Diffusive Matrix Fracture Coupling Including the Effects of Flow Channeling. *Water Resources Research*, 28(9), pp.2447–2450.

Eikenberg, J. et al., 1992. On-line detection of stable helium isotopes in migration experiments. *Tracer Hydrology*, pp.77–84.

Ekwurzel, B. et al., 1994. Dating of shallow groundwater: Comparison of the transient tracers 3H/3He, chlorofluorocarbons, and 85Kr. *Water Resources Research*, 30(6), pp.1693–1708.

Faybishenko, B., Witherspoon, P.A. & Benson, S.M., 2000. *Dynamics of Fluids in Fractured Rock*,

Fetter, C.W., 2014. *Applied Hydrogeology*,

Fetter, C.W., 1993. *Contaminant Hydrogeology*,

Fontes, J.C., 1992. Chemical and isotopic constraints on 14C dating of groundwater. In *Radiocarbon After Four Decades an interdisciplinary perspective*. pp. 242–261.

Foster, S.S.D. & Chilton, P.J., 2003. Groundwater: the processes and global significance of aquifer degradation. *Philosophical Transactions of the Royal Society of London B: Biological Sciences*, 358(1440), pp.1957–1972. Available at: http://rstb.royalsocietypublishing.org/cgi/doi/10.1098/rstb.2003.1380.

Freeze, R.A. & Cherry, J.A., 1979. *Groundwater*, Prentice-Hall.

Gardner, P. & Solomon, D.K., 2009. An advanced passive diffusion sampler for the determination of dissolved gas concentrations. *Water Resources Research*, 45(6), pp.1–12.

Gelhar, L.W., Welty, C. & Rehfeldt, K.R., 1992. A Critical Review of Data on Field-Scale Dispersin in Aquifers. *Water Resources Research*, 28(7), pp.1955–1974.

Giardino, J.R. & Houser, C., 2015. Principles and Dynamics of the Critical Zone. *Developments in Earth Surface Processes*, 19.

Gleeson, T. et al., 2010. Groundwater sustainability strategies. *Nature Geoscience*, 3(6), pp.378–379. Available at: http://www.nature.com/doifinder/10.1038/ngeo881.

Gleeson, T. et al., 2011. Mapping permeability over the surface of the Earth. *Geophysical Research Letters*, 38(2), pp.1–6.

Gleeson, T. et al., 2012. Water balance of global aquifers revealed by groundwater footprint. *Nature*, 488(7410), pp.197–200. Available at: http://www.nature.com/doifinder/10.1038/nature11295.

Grisak, G.E. & Pickens, J.F., 1981. An analytical solution for solute transport through fractured media

with matrix diffusion. *Journal of Hydrology*, 52, pp.47–57.

Guihéneuf, N., 2014. *Structure des écoulements et propriétés de transport des aquifère cristallins fracturés et altérés: Application au site de Choutuppal (Inde du Sud)*. Univerité de Rennes 1.

Gupta, S.K., Moravcik, P.S. & Stephen Lau, L., 1994. Use of Injected Helium as a Hydrological Tracer. *Hydrological Sciences Journal*, 39(2), pp.109–119.

Gupta, S.K., Stephen Lau, L. & Moravcik, P.S., 1994. Ground-Water Tracing with Injected Helium. *Ground Water*, 32(1), pp.96–102.

Hadermann, J. & Heer, W., 1996. The Grimsel (Switzerland) migration experiment: Integrating field experiments, laboratory investigations and modelling. *Journal of Contaminant Hydrology*, 21(1–4), pp.87–100.

Haggerty, R. & Gorelick, S.M., 1995. Multiple-rate mass transfer for modeling diffusion and surface reactions in media with pore-scale heterogeneity. *Water Resources Research*, 31(10), pp.2383–2400.

Haggerty, R., McKenna, S. a & Meigs, L.C., 2000. On the late-time behaviour of tracer breakthrough curves. *Water Resources Research*, 36(12), pp.3467–3479.

Hall, C.M. et al., 2005. Noble gases and stable isotopes in a shallow aquifer in southern Michigan: Implications for noble gas paleotemperature reconstructions for cool climates. *Geophysical Research Letters*, 32(18), pp.1–4.

Heaton, T.H.E. & Vogel, J.C., 1981. "Excess air" in groundwater. *Journal of Hydrology*, 50, pp.201–216.

Herczeg, A.L. & Edmunds, W.M., 2000. Inorganic ions as tracers. In *Environmental Tracers in Subsurface Hydrology*. pp. 31–78.

Hsieh, P.A., 1998. Scale effects in Fluid Flow through Fractured Geologic Media. In *Scale dependence and scale invariance in hydrology*. pp. 335–353.

Hubbard, S.S. & Linde, N., 2010. Hydrogeophysics. In *Treatise on Water Science*. pp. 1–106.

Huson, D.H. et al., 2016. MEGAN Community Edition - Interactive Exploration and Analysis of Large-Scale Microbiome Sequencing Data. *PLoS Computational Biology*, 12(6), pp.1–12.

IAEA, 2001. *Environmental Isotopes in the Hydrological Cycle: Principles and Applications*,

IAEA, 2013. *Isotope methods for dating old groundwater*,

Istok, J.D. et al., 1997. Single-well, “Push-Pull” Test for In Situ Determination of Microbial Activities. *Ground Water*, 35(4), pp.619–631.

Istok, J.D. & Humphrey, M.D., 1995. Laboratory Investigation of Buoyancy-Induced Flow (Plume Sinking) During Two-Well Tracer Tests. *Ground Water*, 33(4), pp.597–604.

Jardine, P.M. et al., 1999. Quantifying diffusive mass transfer in fractured shale bedrock. *Water Resources Research*, 35(7), pp.2015–2030.

Juanes, R., MacMinn, C.W. & Szulczewski, M.L., 2010. The footprint of the CO2 plume during carbon dioxide storage in saline aquifers: Storage efficiency for capillary trapping at the basin scale. *Transport in Porous Media*, 82(1), pp.19–30.

Kalin, R.M., 2000. Radiocarbon dating of groundwater systems. In *Environmental Tracers in Subsurface Hydrology*. pp. 111–144.

Kampbell, D.H., Wilson, J.T. & Vandegrift, S.A., 1989. Dissolved oxygen and methane in water by a gc headspace equilibration technique. *International Journal of Environmental Analytical Chemistry*, 36(4), pp.249–257.

Kang, P. et al., 2015. Impact of velocity correlation and distribution on transport in fractured media: Field evidence and theoretical model. *Water Resources Research*, 51(2), pp.940–959.

Kharaka, Y.K. et al., 2006. Gas-water-rock interactions in Frio Formation following CO2 injection: Implications for the storage of greenhouse gases in sedimentary basins. *Geology*, 34(7), pp.577–580.

Kim, Y. et al., 2005. A single well push-pull test method for in situ determination of denitrification rates in a nitrate-contaminated groundwater aquifer. *Water Science and Technology*, 52(8), pp.77–86.

Kipfer, R. et al., 2002. Noble Gases in Lakes and Ground Waters. *Reviews in Mineralogy and Geochemistry*, 47(1), pp.615–700. Available at: http://rimg.geoscienceworld.org/cgi/doi/10.2138/rmg.2002.47.14.

Kirchner, J.W., 1989. The Gaia Hypothesis: Can It Be Tested ? *Reviews of Geophysics*, 27(2), pp.223–235.

Kirchner, J.W., 2002. The Gaia hypothesis: Fact, theory, and wishful thinking. *Climatic Change*, 52(4), pp.391–408.

Korom, S.F., 1992. Natural denitrification in the saturated zone: A review. *Water Resources Research*,

28(6), pp.1657–1668.

de La Bernardie, J. et al., 2017. Thermal retardation in fractured media : theory and field evidence through heat and solute tracer experiments. *submitted to Geothermics*.

Labasque, T. et al., 2017. 4He as a tool for groundwater age estimation in fractured aquifers: validation using CFCs, 3H/He and 14C data. *in prep*.

Lapcevic, P. a., Novakowski, K.S. & Sudicky, E. a., 1999. The interpretation of a tracer experiment conducted in a single fracture under conditions of natural groundwater flow. *Water Resources Research*, 35(8), p.2301.

Latour, B., 2014. Some advantages of the notion of "Critical Zone" for Geopolitics. *Procedia Earth and Planetary Science*, pp.3–6. Available at: http://dx.doi.org/10.1016/j.proeps.2014.08.002.

Lehmann, B.E. et al., 2003. A comparison of groundwater dating with 81Kr, 36Cl and 4He in four wells of the Great Artesian Basin, Australia. *Earth and Planetary Science Letters*, 211(3–4), pp.237–250.

Leibundgut, C., Maloszewski, P. & Külls, K., 2009. *Tracers in Hydrology*, Wiley-Blackwell.

Leung, L.R. et al., 2011. Climate-soil-vegetation control on groundwater table dynamics and its feedbacks in a climate model. *Climate Dynamics*, 36(1), pp.57–81.

Lippmann, J. et al., 2003. Dating ultra-deep mine waters with noble gases and 36Cl, Witwatersrand Basin, South Africa. *Geochimica et Cosmochimica Acta*, 67(23), pp.4597–4619.

Loosli, H.H., 1992. Applications of 37Ar, 39Ar and 85Kr in hydrology, oceanography and atmospheric studies: Current state of the art. In *IAEA*. pp. 73–85.

Loosli, H.H., 2000. Noble gas radioisotopes 37Ar, 85Kr, 39Ar, 81Kr. In *Environmental Tracers in Subsurface Hydrology*. pp. 379–396.

Lovelock, J.. E., Maggs, R.J. & Rasmussen, R.A., 1972. Atmospheric dimethyl sulfide and the natural sulfur cycle. *Nature*, 237, pp.452–453.

Lovelock, J.E., 1958. A Sensitive Detector for Gas Chromatography. *Journal of Chromatography*, 1, pp.35–46.

Lovelock, J.E., 1972. Gaia as seen through the atmosphere. *Atmospheric Environment*, 6(8), pp.579–580.

Lovelock, J.E., 2003. The Living Earth. *Nature*, 426, pp.769–770. Available at:

http://linkinghub.elsevier.com/retrieve/pii/S0140673600486757.

Lovelock, J.E., Maggs, R.J. & Wade, R.J., 1973. Halogenated Hydrocarbons in and over the Atlantic. *Nature*, 241(5386), pp.194–196.

Lovley, D.R., Chapelle, F.H. & Woodward, J.C., 1994. Use of Dissolved H2 Concentrations To Determine Distribution of Microbially Catalyzed Redox Reactions in Anoxic Groundwater. *Environmental Science and Technology*, 28(7), pp.1205–1210.

Lu, Z.T. et al., 2014. Tracer applications of noble gas radionuclides in the geosciences. *Earth-Science Reviews*, 138, pp.196–214.

Lu, Z.T. & Wendt, K.D.A., 2003. Laser-based methods for ultrasensitive trace-isotope analyses. *Review of Scientific Instruments*, 74, pp.1169–1179.

Ben Maamar, S. et al., 2015. Groundwater isolation governs chemistry and microbial community structure along hydrologic flowpaths. *Frontiers in Microbiology*, 6, pp.1–13.

Mahara, Y. et al., 2009. Groundwater dating by estimation of groundwater flow velocity and dissolved 4He accumulation rate calibrated by 36Cl in the Great Artesian Basin, Australia. *Earth and Planetary Science Letters*, 287(1–2), pp.43–56. Available at: http://dx.doi.org/10.1016/j.epsl.2009.07.034.

Maiss, M. et al., 1996. Sulfur hexafluoride--A powerful new atmospheric tracer. *Atmospheric Environment*, 30(10–11), pp.1621–1629. Available at: http://www.sciencedirect.com/science/article/pii/1352231095004254.

Maloszewski, P. & Zuber, A., 1990. Mathematical modeling of tracer behavior in short-term experiments in fissured rocks. *Water Resources Research*, 26(7), pp.1517–1528.

Maloszewski, P. & Zuber, A., 1993. Tracer experiments in fractured rocks: Matrix diffusion and the validity of models. *Water Resources Research*, 29(8), pp.2723–2735.

Małoszewski, P. & Zuber, A., 1982. Determining the turnover time of groundwater systems with the aid of environmental tracers. 1. Models and their applicability. *Journal of Hydrology*, 57(3–4), pp.207–231.

Małoszewski, P. & Zuber, A., 1985. On the theory of tracer experiments in fissured rocks with a porous matrix. *Journal of Hydrology*, 79(3–4), pp.333–358.

Margulis, L. & Lovelock, J.E., 1974. Biological modulation of the Earth's atmosphere. *Icarus*, 21(4), pp.471–489.

Mariotti, A., 1986. La dénitrification dans les eaux souterraines, principes et méthodes de son identification: une revue. *Journal of Hydrology*, 88, pp.1–23.

de Marsily, G. et al., 1977. Nuclear Waste Disposal : Can the Geologist Guarantee Isolation ? *Science*, 197(4303), pp.519–527.

McGuire, J.T. et al., 2002. Evaluating behavior of oxygen, nitrate, and sulfate during recharge and quantifying reduction rates in a contaminated aquifer. *Environmental Science and Technology*, 36(12), pp.2693–2700.

McNeill, G.W. et al., 2001. Krypton gas as a novel applied tracer of groundwater flow in a fissured sandstone aquifer. *New Approaches to Characterizing Groundwater Flow. Volume 1*, (November 2016), pp.143–148.

Méjean, P. et al., 2016. Processes controlling 234U and 238U isotope fractionation and helium in the groundwater of the St. Lawrence Lowlands, Quebec: The potential role of natural rock fracturing. *Applied Geochemistry*, 66, pp.198–209.

Mercury, L., Pinti, D.L. & Zeyen, H., 2004. The effect of the negative pressure of capillary water on atmospheric noble gas solubility in ground water and palaeotemperature reconstruction. *Earth and Planetary Science Letters*, 223(1–2), pp.147–161.

Moench, A.F., 1995. Convergent radial dispersion in a double-porosity aquifer with fracture skin: Analytical solution and application to a field experiment in fractured chalk. *Water Resources Research*, 31(8), pp.1823–1835.

Molina, M.J. & Rowland, F.S., 1974. Stratospheric sink for chlorofluoromethanes: chlorine atom-catalysed destruction of ozone. *Nature*, 249(5460), pp.810–812. Available at: http://www.nature.com/doifinder/10.1038/249810a0.

Mongstad Hope, S. et al., 2015. Topological impact of constrained fracture growth. *Frontiers in Physics*, 3(September), pp.1–10. Available at: http://journal.frontiersin.org/Article/10.3389/fphy.2015.00075/abstract.

Moreno, L. et al., 1988. Flow and tracer transport in a single fracture: A stochastic model and its relation to some field observations. *Water Resources Research*, 24(12), pp.2033–2048.

Moreno, L. & Neretnieks, I., 1993a. Flow and nuclide transport in fractured media: The importance of the flow-wetted surface for radionuclide migration. *Journal of Contaminant Hydrology*, 13, pp.49–71.

Moreno, L. & Neretnieks, I., 1993b. Fluid and Solute Transport in a Network of Channels. *Journal of*

Contaminant Hydrology, 14, pp.163–192.

Morikawa, N. et al., 2005. Estimation of groundwater residence time in a geologically active region by coupling 4He concentration with helium isotopic ratios. *Geophysical Research Letters*, 32(2), pp.1–4.

National Research Council, 2001. *Basic research opportunities in Earth Science*, National Academy Press.

Neretnieks, I., 1980. Diffusion in the Rock Matrix: An Important Factor in Radionuclide Retardation? *Journal of Geophysical Research*, 85(2), pp.4379–4397.

Neretnieks, I., 2013. Some aspects of release and transport of gases in deep granitic rocks : possible implications for nuclear waste repositories. *Hydrogeology Journal*, 21, pp.1701–1716.

Neretnieks, I., Eriksen, T. & Tähtinen, P., 1982. Tracer movement in a single fissure in granitic rock: Some experimental results and their interpretation. *Water Resources Research*, 18(4), pp.849–858.

Neretnieks, I. & Rasmuson, A., 1984. An Approach to Modelling Radionuclide Migration in a Medium With Strongly Varying Velocity and Block Sizes Along the Flow Path. *Water & Environment Newsletter*, 20(12), pp.1823–1836.

Neuman, S.P., 2005. Trends, prospects and challenges in quantifying flow and transport through fractured rocks. *Hydrogeology Journal*, 13(1), pp.124–147.

Neuman, S.P., 1990. Universal Scaling of Hydraulic Conductivities and Dispersivities in Geologic Media. *Water Resources Research*, 26(8), pp.1749–1758.

Novakowski, K.S. et al., 1995. Preliminary interpretation of tracer experiments conducted in a discrete rock fracture under conditions of natural flow. *Geophysical Research Letters*, 22(11), pp.1417–1420.

Novakowski, K.S. & Bogan, J.D., 1999. A semi-analytical model for the simulation of solute transport in a network of fractures having random orientations. *International Journal for Numerical and Analytical Methods in Geomechanics*, 23, pp.317–333.

Novakowski, K.S. & Lapcevic, P.A., 1994. Field measurement of radial solute transport in fractured rock. *Water Resources Research*, 30(1), pp.37–44.

Ohlsson, Y. & Neretnieks, I., 1995. *Literature survey of matrix diffusion theory and of experiments and data including natural analogues*,

Olsson, O., 1992. *Site characterization and validation - Final Report - Stripa Project*,

Oster, H. & Sonntag, C., 1996. Groundwater age dating with chlorofiuorocarbons. *Water Resources Research*, 32(10), pp.2989–3001.

Ozima, M. & Podosek, F.A., 2002. *Noble Gas Geochemistry*, Cambridge.

Pauwels, H. et al., 1998. Field tracer test for denitrification in a pyrite-bearing schist aquifer. *Applied Geochemistry*, 13(6), pp.767–778.

Pauwels, H., Foucher, J.C. & Kloppmann, W., 2000. Denitrification and mixing in a shist aquifer : influence on water chemistry and isotopes. *Chemical Geology*, 168(3), pp.307–324.

Petelet-Giraud, E. et al., 2017. Global change and its impact on water resources in a southern metropolis: When will it be already too late? Crossed analysis in Recife, NE Brazil. *Science of the Total Environment*.

Petford, N. & Mccaffrey, K., 2003. Hydrocarbons in crystalline rocks: an introduction. In *Hydrocarbons in Crystalline Rocks*. The Geological Society of London, pp. 1–5. Available at: http://sp.lyellcollection.org/cgi/doi/10.1144/GSL.SP.2003.214.01.14.

Philippot, L. et al., 2009. Mapping field-scale spatial patterns of size and activity of the denitrifier community. *Environmental Microbiology*, 11(6), pp.1518–1526.

Plummer, L.N. et al., 2012. Old groundwater in parts of the upper Patapsco aquifer, Atlantic Coastal Plain, Maryland, USA: evidence from radiocarbon, chlorine-36 and helium-4. *Hydrogeology Journal*, 20(7), pp.1269–1294.

Plummer, L.N. & Sprinkle, C.L., 2001. Radiocarbon dating of dissolved inorganic carbon in groundwater from confined parts of the Upper Floridan aquifer, Florida, USA. *Hydrogeology Journal*, 9(2), pp.127–150.

Rasmuson, A. & Neretnieks, I., 1981. Migration of radionuclides in fissured rock — The influence of micropore diffusion and longitudinal dispersion. *Journal of Geohpysical Research*, 86, pp.3749–3758.

Rasmuson, A. & Neretnieks, I., 1986. Radionuclide Transport in Fast Channels in Crystalline Rock. *Water Resources Research*, 22(8), pp.1247–1256.

Raven, K.G., Novakowski, K.S. & Lapcevic, P.A., 1988. Interpretation of field tracer tests of a single fracture using a transient solute storage model. *Water Resources Research*, 24(12), pp.2019–2032.

Read, T. et al., 2014. Active-distributed temperature sensing to continuously quantify vertical flow in boreholes. *Water Resources Research*, 50(5), pp.3706–3713.

Read, T. et al., 2013. Characterizing groundwater flow and heat transport in fractured rock using fiber-optic distributed temperature sensing. *Geophysical Research Letters*, 40(10), pp.2055–2059.

Reimus, P.W. et al., 2003. Testing and parameterizing a conceptual solute transport model in saturated fractured tuff using sorbing and nonsorbing tracers in cross-hole tracer tests. *Journal of Contaminant Hydrology*, 62–63, pp.613–636.

Richter, F.., Whittier, R.B.. b & El-Kadi, A.I.., 2008. Use of dissolved helium as an environmental water tracer. *Journal of Hydraulic Engineering*, 134(5), pp.672–675. Available at: http://www.scopus.com/inward/record.url?eid=2-s2.0-42449138801&partnerID=40&md5=f50d6ef3a75f93a5b8d44c485401b02d.

Roques, C. et al., 2017. Denitrification processes in crystalline aquifers revealed by short- and long-term experiments: (2) Mixing and denitrification dynamic during long-term pumping. *Submitted to Science of the Total Environment*.

Roques, C., 2013. *Hydrogéologie des zones de faille du socle cristallin: implications en terme de ressources en eau pour le Massif Armoricain*. Université de Rennes 1.

Roubinet, D., De Dreuzy, J.R. & Tartakovsky, D.M., 2012. Semi-analytical solutions for solute transport and exchange in fractured porous media. *Water Resources Research*, 48(1), pp.1–10.

Sánchez-Vila, X., Carrera, J. & Girardi, J.P., 1996. Scale effects in transmissivity. *Journal of Hydrology*, 183, pp.1–22.

Sanford, W.E., Cook, P.G. & Dighton, J.C., 2002. Analysis of a Vertical Dipole Tracer Test in Highly Fractured Rock. *Ground Water*, 40(5), pp.535–542.

Sanford, W.E., Shropshire, R.G. & Solomon, D.K., 1996. Dissolved gas tracers in groundwater: Simplified injection, sampling, and analysis. *Water Resources Research*, 32(6), pp.1635–1642.

Schlosser, P. et al., 1988. Tritium/3He dating of shallow groundwater. *Earth and Planetary Science Letters*, 89(3–4), pp.353–362.

Schuite, J., 2016. *Apports des mesures de déformation de surface et de l'inclinométrie à la caractérisation pluriéchelle des réservoirs géologiques fracturés*. Université de Rennes 1.

Selker, J. et al., 2006. Fiber optics opens window on stream dynamics. *Geophysical Research Letters*, 33(24), pp.27–30.

Selker, J.S. et al., 2006. Distributed fiber-optic temperature sensing for hydrologic systems. *Water Resources Research*, 42(12), pp.1–8.

Shiklomanov, I.A., 2000. International Water Resources Association Appraisal and Assessment of World Water Resources. *Water International*, 25(11), pp.250–8060. Available at: http://www.tandfonline.com/action/journalInformation?journalCode=rwin20%5Cnhttp://www.tandfonline.com/loi/rwin20%5Cnhttp://dx.doi.org/10.1080/02508060008686794.

Singhal, B.B.S. & Gupta, R.P., 2010. *Applied Hydrogeology of Fractured Rocks*, Kluwer Academic Publishers. Available at: https://books.google.no/books?id=k5HtCAAAQBAJ&printsec=frontcover&dq=Applied+Hydrogeology+of+Fractured+Rocks&hl=no&sa=X&ved=0ahUKEwiLjo6XlebOAhVIApoKHb10ALsQ6AEIHTAA#v=onepage&q=Applied Hydrogeology of Fractured Rocks&f=false.

Smethie, W.M. et al., 1992. Tracing groundwater flow in the Borden aquifer using krypton-85. *Journal of Hydrology*, 130(1–4), pp.279–297.

Smith, R.L. et al., 2004. Assessing denitrification in groundwater using natural gradient tracer tests with 15N: In situ measurement of a sequential multistep reaction. *Water Resources Research*, 40(7), pp.1–17. Available at: http://doi.wiley.com/10.1029/2003WR002919.

Smith, R.L., Garabedian, S.P. & Brooks, M.H., 1996. Comparison of denitrification activity measurements in groundwater using cores and natural-gradient tracer tests. *Environmental Science and Technology*, 30(12), pp.3448–3456.

Smith, S.P. & Kennedy, B.M., 1983. The solubility of noble gases in water and in NaCl brine. *Geochimica et Cosmochimica Acta*, 41(1), pp.503–515.

Solomon, D.K. et al., 1992. Tritium and Helium 3 as Groundwater Age Tracers in the Borden Aquifer. *Water Resources Research*, 28(3), pp.741–755.

Solomon, D.K. & Cerling, T.E., 1987. The annual carbon dioxide cycle in a montane soil: Observations, modeling, and implications for weathering. *Water Resources Research*, 23(12), pp.2257–2265.

Solomon, D.K. & Cook, P.G., 2000. 3H and 3He. In *Environmental Tracers in Subsurface Hydrology*. pp. 397–424.

Solomon, D.K., Hunt, A.G. & Poreda, R.J., 1996. Source of radiogenic helium 4 in shallow aquifers: Implications for dating young groundwater. *Water Resources Research*, 32(6), pp.1805–1813.

Sophocleous, M., 2002. Interactions between groundwater and surface water: The state of the science.

Hydrogeology Journal, 10(1), pp.52–67.

Spalding, B.P. & Watson, D.B., 2006. Measurement of dissolved H2, O2, and CO2 in groundwater using passive samplers for gas chromatographic analyses. *Environmental science and technology*, 40(24), pp.7861–7. Available at: http://www.ncbi.nlm.nih.gov/pubmed/17256539.

Spalding, B.P. & Watson, D.B., 2008. Passive sampling and analyses of common dissolved fixed gases in groundwater. *Environmental Science and Technology*, 42(10), pp.3766–3772.

Sparkman, D.O., 2011. *Gas chromatography and mass spectrometry: a practical guide*,

Van Stempvoort, D. et al., 2005. Oxidation of fugitive methane in ground water linked to bacterial sulfate reduction. *Ground Water*, 43(2), pp.187–199.

Stewart, M.K. & Morgenstern, U., 2016. Importance of tritium-based transit times in hydrological systems. *Wiley Interdisciplinary Reviews*, 3(2), pp.145–154. Available at: http://doi.wiley.com/10.1002/wat2.1134.

Sturchio, N.C. et al., 2004. One million year old groundwater in the Sahara revealed by krypton-81 and chlorine-36. *Geophysical Research Letters*, 31(5), pp.1–4. Available at: http://doi.wiley.com/10.1029/2003GL019234.

Stute, M., Clark, J.F., et al., 1995. A 30,000 yr Continental Paleotemperature Record Derived from Noble Gases Dissolved in Groundwater from the San Juan Basin, New Mexico. *Quaternary Research*, 43, pp.209–220.

Stute, M., Forster, M., et al., 1995. Cooling of Tropical Brazil (5°C) During the Last Glacial Maximum. *Science*, 269, pp.379–383.

Stute, M. et al., 1992. Helium in deep circulating groundwater in the Great Hungarian Plain: Flow dynamics and crustal and mantle helium fluxes. *Geochimica et Cosmochimica Acta*, 56(5), pp.2051–2067.

Stute, M. & Schlosser, P., 1993. Principles and applications of the noble gas paleothermometer. In *Geophysical Monograph Series*. p. 1993.

Sudicky, E.A. & Frind, E.O., 1982. Contaminant transport in fractured porous media: Analytical solutions for a system of parallel fractures. *Water Resources Research*, 18(6), pp.1634–1642. Available at: http://dx.doi.org/10.1029/WR018i006p01634.

Sun, T. et al., 2008. Excess air in the noble gas groundwater paleothermometer: A new model based on diffusion in the gas phase. *Geophysical Research Letters*, 35(19), pp.1–5.

Tang, D.H., Frind, E.O. & Sudicky, E.A., 1981. Contaminant Transport in Fractured Porous Media: Analytical Solution for a Single Fracture. *Water Resources Research*, 20(7), p.1021.

Tarits, C. et al., 2006. Oxido-reduction sequence related to flux variations of groundwater from a fractured basement aquifer (Ploemeur area, France). *Applied Geochemistry*, 21(1), pp.29–47.

Taylor, R.G. et al., 2012. Ground water and climate change. *Nature Climate Change*, 3(4), pp.322–329. Available at: http://www.nature.com/doifinder/10.1038/nclimate1744.

Torgersen, T., Benoit, J. & Mackie, D., 1990. Controls on groundwater Rn-222 concentrations in fractured rock. *Geophysical Research Letters*, 17(6), pp.845–848.

Torgersen, T. & Clarke, W.B., 1985. Helium accumulation in groundwater, I: An evaluation of sources and the continental flux of crustal 4He in the Great Artesian Basin, Australia. *Geochimica et Cosmochimica Acta*, 49, pp.1211–1218.

Torgersen, T. & Clarke, W.B., 1987. Helium accumulation in groundwater, III. Limits on helium transfer across the mantle-crust boundary beneath Australia and the magnitude of mantle degassing. *Earth and Planetary Science Letters*, 84, pp.345–355.

Torgersen, T. & Ivey, G.N., 1985. Helium accumulation in groundwater. II: A model for the accumulation of the crustal 4He degassing flux. *Geochimica et Cosmochimica Acta*, 49, pp.2445–2452.

Touchard, F., 1999. *Caractérisation hydrogéologique d'un aquifère en socle fracturé*. Université de Rennes 1.

Trudell, M.R., Gillham, R.W. & Cherry, J.A., 1986. An in-situ study of the occurrence and rate of denitrification in a shallow unconfined sand aquifer. *Journal of Hydrology*, 83(3–4), pp.251–268.

Tsang, C. & Neretnieks, I., 1998. Flow channeling in heterogeneous fractured rocks. *Reviews of Geophysics*, 36(2), pp.275–298.

Tsang, Y.W. et al., 1988. Flow and tracer transport in fractured media: A variable aperture channel model and its properties. *Water Resources Research*, 24(12), pp.2049–2060.

Uddin, M.K., Dowd, J.F. & Wenner, D.B., 1999. Krypton Tracer Test to Characterize the Recharge of Highly Fractured Aquifer in Lawrenceville, Georgia. *Proceedings of the 1999 Georgia Water Resources Conference*, 1, pp.516–519.

Vengosh, A. & Rosenthal, E., 1994. Saline groundwater in Israel: its bearing on the water crisis in the country. *Journal of Contaminant Hydrology*, 156, pp.389–430.

Visser, A., Singleton, M.J. & Esser, B.K., 2014. Xenon Tracer Test at Woodland Aquifer Storage and Recovery Well. *Lawrence Livermore National Laboratory Report*, LLNL-TR-65, pp.1–24.

Vogel, J.C., Talma, A.S. & Heaton, T.H.E., 1981. Gaseous nitrogen as evidence for denitrification in groundwater. *Journal of Hydrology*, 50, pp.191–200.

Wei, W., Aeschbach-hertig, W. & Chen, Z., 2015. Identification of He sources and estimation of He ages in groundwater of the North China Plain. *Applied Geochemistry*, 63, pp.182–189. Available at: http://dx.doi.org/10.1016/j.apgeochem.2015.08.010.

Werner, A.D. et al., 2013. Seawater intrusion processes, investigation and management: Recent advances and future challenges. *Advances in Water Resources*, 51, pp.3–26. Available at: http://dx.doi.org/10.1016/j.advwatres.2012.03.004.

Wilde, K.D. & Engewald, W., 2014. *Practical Gas Chromatography: A Comprehensive Reference*,

Winberg, A. et al., 2000. *Äspö Hard Rock Laboratory. Final report of the first stage of the Tracer Retention Understanding Experiments*,

Wolfbeis, O.S., 2008. Fiber-Optic Chemical Sensors and Fiber-Optic Bio-Sensors. *Analytical Chemistry*, 80, pp.4269–4283. Available at: http://www.mdpi.com/1424-8220/15/10/25208/htm.

Yokochi, R., 2016. Recent developments on field gas extraction and sample preparation methods for radiokrypton dating of groundwater. *Journal of Hydrology*, 540, pp.368–378. Available at: http://dx.doi.org/10.1016/j.jhydrol.2016.06.020.

Zhou, Q. et al., 2007. Field-scale effective matrix diffusion coefficient for fractured rock: Results from literature survey. *Journal of Contaminant Hydrology*, 93(1–4), pp.161–187.

Appendix

1. Supporting information for Chapter 2

Supporting information for:

Field continuous measurement of dissolved gases with a CF-MIMS: Applications to the physics and biogeochemistry of groundwater flow

Eliot Chatton [a,*], Thierry Labasque [a], Jérôme de La Bernardie [a], Nicolas Guihéneuf [a,b], Olivier Bour [a], Luc Aquilina [a]

[a] *OSUR-UMR6118 Géosciences Rennes, Université de Rennes 1 and Centre National de la Recherche Scientifique, Rennes, France*

[b] *University of Guelph, 50 Stone Road East Guelph, Ontario, Canada.*

* *E-mail: eliot.chatton@gmail.com*

Content: 8 pages, 6 tables, 5 figures, 1 part list.

Measurement Settings

Table S1: Settings used for the measurements of reactive and noble gases with the CF-MIMS. (*)Helium is usually measured with the SCEM detector however the Faraday can sometimes be more suited for environments with higher He levels (> 2.5×10^{-5} ccSTP/g).

m/z	Targeted gas	Electron Energy (eV)	Emission (µA)	Detector
4(*)	He	70	250	Faraday/SCEM
12	CO_2	70	250	Faraday
14	N_2	70	250	Faraday
15	CH_4	70	250	Faraday
18	H_2O	70	250	Faraday
20	Ne	70	250	Faraday
22	Ne	70	250	Faraday
28	N_2	70	250	Faraday
32	O_2	70	250	Faraday
40	Ar	70	250	Faraday
44	CO_2/N_2O	70	250	Faraday
84	Kr	70	1000	SCEM
132	Xe	100	1500	SCEM

Instrumental drift

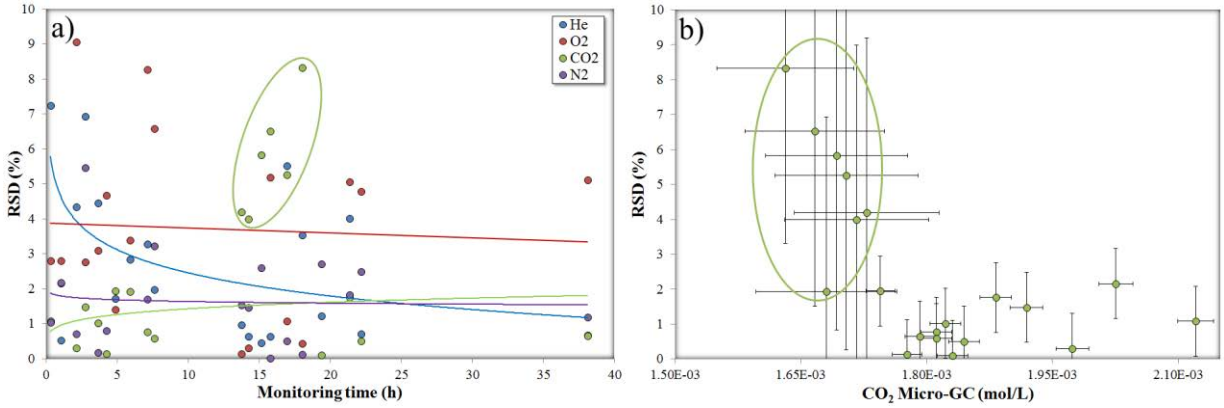

Figure S1: Evolution of the RSD(%) with operation time over a 38 hours experiment. The RSD calculations are based on CF-MIMS measurements and samples analysed by gas chromatography at the University of Rennes. The green ellipse refers to values of RSD increasing over monitoring time due to a lower accuracy of the gas chromatograph (b).

Temperature Sensitivity

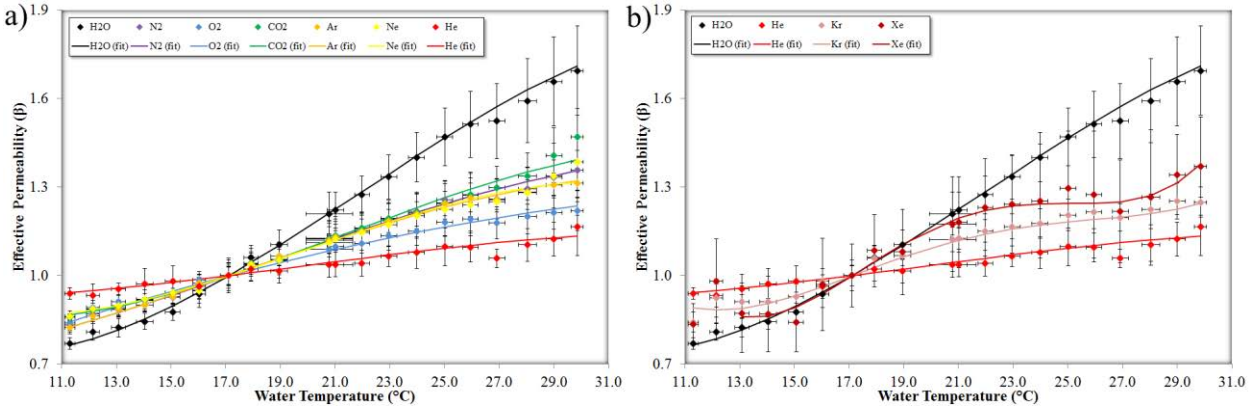

Figure S2: Membrane X44® effective permeability coefficients β as a function of the water temperature. As the effective permeability changes non-linearly with the absolute temperature, the coefficient β is expressed as a function of the effective permeability obtained at the room temperature (17°C). The dots refer to the averaged data points obtain after repeating 4 times the experiment. The dots refer to the polynomials that were fitted directly on the bulk data.

Standard gases used for calibration

Table S2: Standard gases used for calibration of the CF-MIMS. The number of standard gases used varies depending on the application and the targeted dissolved gases (N_2, O_2, CO_2, CH_4, He, Ar, Kr and Xe can be calibrated only with Air&STDB). The saturation of the water in the calibration chamber takes about 15 min for each standard gas.

Gas (mole fraction)	Air	STD A	STD B	STD Ar	STD CO_2	STD N_2
N_2	7.81×10^{-1}	7.88×10^{-1}	9.39×10^{-1}	-	-	1
O_2	2.09×10^{-1}	2.00×10^{-1}	1.00×10^{-2}	-	-	-
CO_2	3.95×10^{-4}	5.00×10^{-4}	5.00×10^{-4}	-	1	-
CH_4	1.89×10^{-7}	5.00×10^{-4}	1.00×10^{-4}	-	-	-
N_2O	-	2.50×10^{-4}	-	-	-	-
He	5.24×10^{-6}	-	1.00×10^{-4}	-	-	-
Ne	1.82×10^{-5}	2.00×10^{-5}	1.00×10^{-4}	-	-	-
Ar	9.34×10^{-3}	1.00×10^{-2}	5.00×10^{-2}	1	-	-
Kr	1.14×10^{-6}	-	1.00×10^{-5}	-	-	-
Xe	8.70×10^{-8}	-	1.00×10^{-5}	-	-	-

Overlap extents for different SGEWs

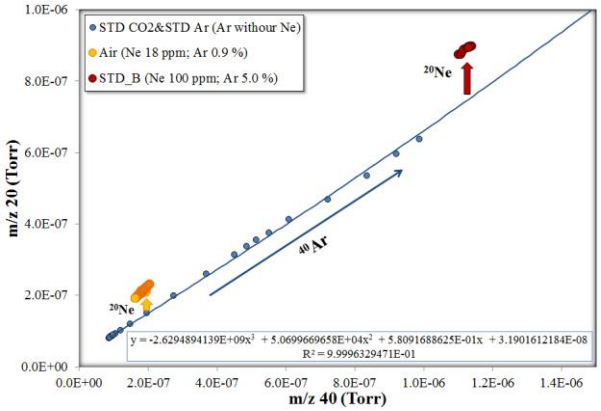

Figure S3: Example of calibration of ^{20}Ne overcoming $^{40}Ar_{(II)}$ overlap using Air, STD B, STD CO_2 and STD Ar.

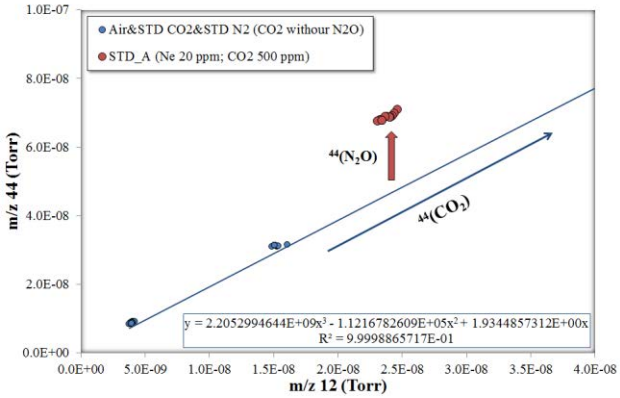

Figure S4: Example of calibration of CO_2 and N_2O overcoming the overlap using Air, STD CO_2, STD N_2 and STD A.

Table S3: Estimated overlap extents for an AEW. In this case, the signals measured at m/z 12 and 44 refer directly to the partial pressure of CO_2 and the signals measured at m/z 14, 15 and 28 refer directly to the partial pressure of N_2.

m/z	% gas 1	% gas 2	% gas 3
12	CO_2 (100)	CH_4 (0)	-
14	N_2 (100)	N_2O (0)	-
15	N_2 (100)	CH_4 (0)	-
22	Ne (50)	N_2O (0)	CO_2 (50)
28	N_2 (100)	N_2O (0)	CO_2 (0)
44	CO_2 (100)	N_2O (0)	-

Table S4: Approximated overlap extents for an SGEW (standard air composition: [N_2]=78.8%, [CO_2]=500ppm, [N_2O]=250ppm, [CH_4]=500ppm, [Ne]=20ppm).

m/z	% gas 1	% gas 2	% gas 3
12	CO_2 (50)	CH_4 (50)	-
14	N_2 (90)	N_2O (10)	-
15	N_2 (15)	CH_4 (85)	-
22	Ne (25)	N_2O (50)	CO_2 (25)
28	N_2 (90)	N_2O (10)	CO_2 (0)
44	CO_2 (40)	N_2O (60)	-

Tracer Test

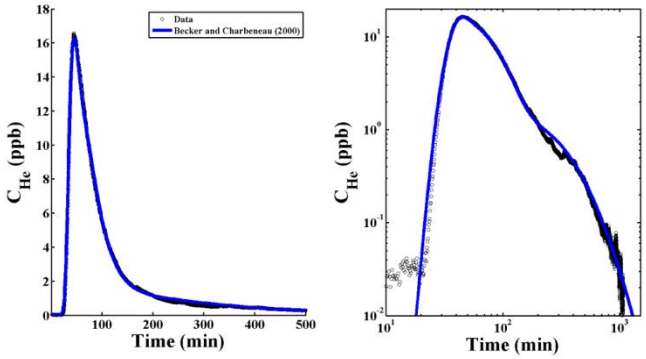

Figure S5: Fitted ^{4}He breakthrough curve (5.9 m^3/h) using the solution developed by Becker and Charbeneau (2000).

Table S5: Comparison of CF-MIMS measurements with measurements of dissolved gases in B3 conducted at the University of Rennes by gas-chromatography.

Q (m^3/h)	Sample (ccSTP/g)	CF-MIMS (ccSTP/g)	Relative difference (%)
5.9	3.97×10^{-6}	3.61×10^{-6}	6.7
	4.24×10^{-6}	4.01×10^{-6}	3.8
	4.10×10^{-6}	4.28×10^{-6}	3.0
	3.90×10^{-6}	4.23×10^{-6}	5.8
	3.00×10^{-6}	3.23×10^{-6}	5.2
	2.93×10^{-6}	3.09×10^{-6}	3.8
	2.72×10^{-6}	2.65×10^{-6}	1.6
	2.72×10^{-6}	2.73×10^{-6}	0.1
	2.52×10^{-6}	2.65×10^{-6}	3.6
1.4	3.19×10^{-6}	3.28×10^{-6}	2.1
	9.46×10^{-5}	9.24×10^{-5}	1.6
	9.26×10^{-5}	9.48×10^{-5}	1.7
	3.33×10^{-6}	3.35×10^{-6}	0.4
	3.29×10^{-6}	3.13×10^{-6}	3.6

Table S6: Derived transport parameters obtained with ^{4}He and Amino-G acid (AG) breakthrough curves interpreted as the superposition of two or three paths. For each path, the distribution of recovered mass is determined as well as the dispersivity (α) and the volume equivalent aperture (h).

	^{4}He	AG	^{4}He	AG
Q (m^3/h)	1.4		5.9	
Recovery (%)	54.2	95.0	75.7	99.0
Mass in Path 1 (%)	16.0	27.4	68.0	46.5
α_1 (m)	0.20	0.17	0.37	0.30
h_1 (mm)	2.5	2.5	4.7	4.0
Mass in Path 2 (%)	58.0	36.8	-	-
α_2 (m)	0.75	0.35	-	-
h_2 (mm)	4.4	4.0	-	-
Mass in Path 3 (%)	26.0	35.8	32.0	53.5
α_3 (m)	1.50	1.2	0.75	1.00
h_3 (mm)	18.0	6.5	13.5	13.0

Part List

CF-MIMS:

Mechanical specifications:

Dimensions: 52cm × 53cm × 54cm.

Weight: 55kg.

Vacuum system:

Primary pump (70 L/s turbomolecular pump).

Backing pump (2.5 m3/h dry scroll pump).

Inlet system:

Housing: stainless steel (φ: 3 inches)

Membrane: X44® polymer film (surface area: 16 cm^2; thickness: 0.05mm, proprietary Hiden Analytical).

Typical water flow: 4 L/min.

Mass spectrometer:

Type: Triple Filter Quadrupole.

Mass range: 0.40 to 200.00 amu (resolution: 0.01 amu).

Filaments: Oxide Coated Iridium.

Electron Energy: 4.0 to 150.0 eV (resolution: 0.1 eV).

Emission: 20.000 to 5000.000 μA (resolution: 0.001 μA).

Detectors: Faraday and SCEM.

Electrical specifications:

Voltage: 220/240 V.

Frequency: 50/60 Hz.

Power: 900 W.

Cold trap

Copper tube (φ: 1/8 inch).

Cryogenic storage Dewar filled with pure ethanol.

Immersion cooler (Huber TC100E, T: -100°C)

Calibration chamber

Chamber: polymethyl methacrylate tube (L: 300mm; φ: 100mm) equipped with a polyvinyl chloride screwable cover.

Water and gas circulation: ×4 ball valves for water inflow, water outflow, gas inflow and gas outflow.

Water pump: low voltage impeller pump (Q: 4L/min, 12V/1A, 12W).

Gas introduction: flexible aquarium air diffuser.

Temperature and Pressure monitoring: MiniDiver®.

Mobile laboratory (CRITEX Lab):

Mechanical specifications:

All-terrain truck

Inside dimensions (Lab): 1930×3120×1910mm (H×L×W)

Facilities:

Sinewave Inverter 12V/220V (3000W), autonomy 3 hours (for typical CF-MIMS operation).

Electric generator (2800W, 230V, 50Hz, 12.2A), autonomy 8 hours (for typical mobile laboratory operation).

Air conditioner (1800W).

Refrigerator for sample storage.

Lab benches.

Sink.

Freshwater tank (120L).

Wastewater tank (120L).

Storage spaces (shelves, cupboards).

Electrical plugs.

Light-spots (LED) for indoor and outdoor work.

Lateral awning to protect from the sun of Brittany.

2. Supporting information for Chapter 4

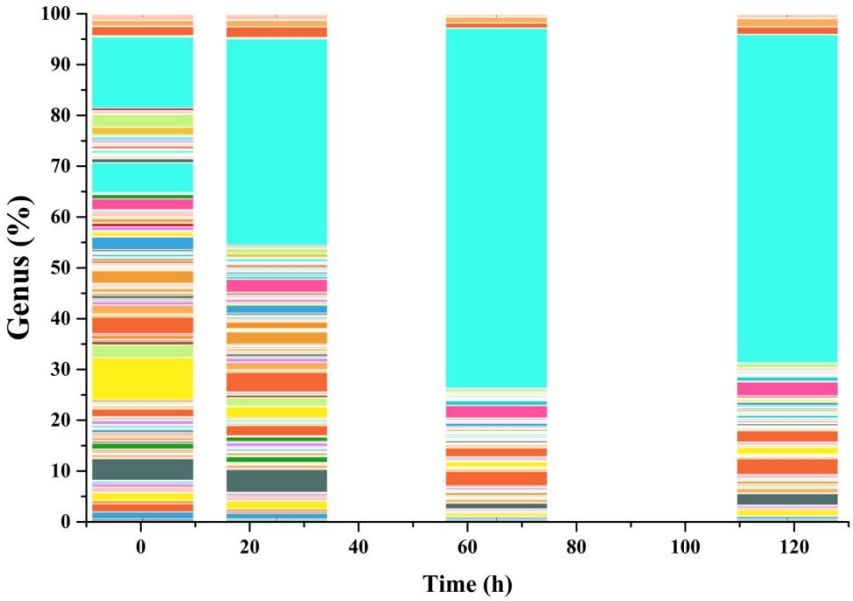

Figure 35: Evolution of all microorganism genera abundances in F1 throughout the experiment.

Table 7: Legend of the figure 35.

TABLEAU PRESENTANT LA LEGENDE (DU GRAPHIQUE EN LIEN) ET DES STATISTIQUES DESCRIPTIVES DE L'ABONDANCE RELATIVE DE CHAQUE TAXON:

(La couleur correspond a la couleur du taxon sur le graphique, sachant que la premiere ligne du tableau correspond au taxon le plus proche de l'axe des abscisses)

Taxon	Abondance relative minimale	Abondance relative maximale	Moyenne	Variance	Ecart-type
Methylobacillus	0.104657247514	0.292321116928	0.212600593357	0.0051357106724	0.0716638728538
Ferrovum	0.192150646107	0.355834641549	0.279725042247	0.00564705659845	0.0751469001253
Polaromonas	0.423211169284	1.38147566719	0.831645324536	0.172206757099	0.41497802002
Sphingobium	0.065445026178	1.64311878598	0.538956776093	0.421332669262	0.649101432183
Clostridioides	0.0	0.565149136578	0.283344277668	0.0657790206824	0.25647421056
Candidatus Cloacimonas	0.0	0.0	0.0	0.0	0.0
Ferriphaselus	0.629293365999	1.50706436421	1.17265412003	0.117413946805	0.342657185544
Herminiimonas	0.156985871272	0.466841186736	0.289137463557	0.0135726820035	0.116501854077
Sandaracinus	0.0	0.0209314495029	0.00523286237572	8.21485459297e-05	0.00906358350376
unclassified Caulobacteraceae	0.0	0.0	0.0	0.0	0.0
Levilinea	0.0	0.0	0.0	0.0	0.0
Thermodesulfovibrio	0.0	0.94191522763	0.42206004559	0.160081897131	0.400102358318
Caulobacter	0.0	0.0	0.0	0.0	0.0
Cupriavidus	0.269010904549	0.722135007849	0.421032931559	0.0312246410945	0.176704954923
Acidithiobacillus	0.213787085515	0.282211835259	0.235603585544	0.000763669378045	0.0276345685337
Smithella	0.0240188307633	0.397697540555	0.16702325725	0.0218845811387	0.147934381192
Desulfotomaculum	0.0	0.0837257980115	0.0209314495029	0.00131437673487	0.036254334015
Candidatus Magnetoovum	0.0	0.0	0.0	0.0	0.0
Oxalobacter	0.0	0.052914719111	0.0132286797778	0.000524993905987	0.0229127454921
Sulfuricurvum	1.18653023971	4.58594232296	3.07388422076	1.99884086358	1.41380368636
Rhodoluna	0.0	0.0	0.0	0.0	0.0
Bacteriovorax	0.014411298458	0.230245944532	0.130300611861	0.00609616922035	0.0780779688539
Flavihumibacter	0.0	0.0209314495029	0.00523286237572	8.21485459297e-05	0.00906358350376
Chloroflexus	0.0	0.0	0.0	0.0	0.0
Rhodopseudomonas	0.0	0.0209314495029	0.00523286237572	8.21485459297e-05	0.00906358350376
Methylobacter	0.408163265306	0.876963350785	0.665795866403	0.0281475859825	0.167772423189
Pelobacter	0.0	0.104657247514	0.0261643118786	0.00205371364824	0.0453179175188
Neisseria	0.0	0.312244799923	0.151141479213	0.0228933658817	0.151305538173
Desulfobacca	0.0	0.230245944532	0.0818140657255	0.00891250786036	0.0944060795731
Nocardia	0.0	0.0	0.0	0.0	0.0
unclassified Planctomycetaceae	0.0	0.0	0.0	0.0	0.0
Pelomonas	0.0240188307633	0.125588697017	0.0702640695763	0.00139220718618	0.0373122926953
Perlucidibaca	0.0	0.167451596023	0.0418628990058	0.0052575069395	0.0725086680301
Azohydromonas	0.0	0.0	0.0	0.0	0.0
Desulfobulbus	0.0	0.355834641549	0.130849479683	0.0215523496634	0.146807185326
Azospira	0.10907504363	0.185201516889	0.151674833392	0.000980559096505	0.0313138802531
Magnetospirillum	0.287958115183	1.18262689691	0.732723054416	0.179538979167	0.423720402113

Afipia	0.0	0.282574568289	0.0948962216648	0.0133095542422	0.115367041404
Pseudoalteromonas	0.0	0.021815008726	0.0150961744831	7.83874369375e-05	0.00885366799341
Desulfatibacillum	0.0	0.240711669283	0.0689970371726	0.0100360432935	0.10018005437
Nitrosomonas	0.538021809098	0.628272251309	0.583197487952	0.0010472773244	0.0323616644257
Sunxiuqinia	0.0	0.0	0.0	0.0	0.0
Paludibacter	0.0	0.0	0.0	0.0	0.0
Desulfomonile	0.0	0.303506017792	0.10012908404	0.0153558927057	0.123918895677
Rubrivivax	0.0	0.0	0.0	0.0	0.0
Alistipes	0.0	0.0	0.0	0.0	0.0
unclassified Oxalobacteraceae	0.0	0.157068062827	0.0769087324746	0.00388671683099	0.0623435388071
Mariprofundus	0.0	0.0	0.0	0.0	0.0
Thiomonas	0.0	0.0261780104712	0.0113482687705	0.000134843530969	0.0116122147314
Desulfotignum	0.0	0.0418628990058	0.0104657247514	0.000328594183719	0.0181271670075
Candidatus Solibacter	0.0	0.282574568289	0.0993057815907	0.0133865313707	0.115700178784
Lamprocystis	0.0	0.00960753230533	0.00240188307633	1.73071269371e-05	0.00416018352205
Mycobacterium	0.0	0.324437467295	0.114157787178	0.0171130198302	0.130816741399
Planctomyces	0.0	0.0	0.0	0.0	0.0
Candidatus Jettenia	0.0	0.0	0.0	0.0	0.0
Micromonospora	0.0	0.0	0.0	0.0	0.0
Pedosphaera	0.0	0.586080586081	0.221679768374	0.0579285240161	0.240683451895
Cystobacter	0.0	0.0	0.0	0.0	0.0
Leeia	0.0	0.087260034904	0.0422310148748	0.00178737303378	0.0422773347526
Agromyces	0.0	0.0567190226876	0.0189835218246	0.000536192459794	0.023155829931
Bordetella	0.211658876444	0.313971742543	0.253737697626	0.00139094846642	0.0372954215209
Verminephrobacter	0.0	0.0523286237572	0.0298841768913	0.000459644337526	0.021439317562
Flavobacterium	0.0087260034904	0.397697540555	0.161529151238	0.0257131439151	0.160353184923
Desulfospira	0.0	0.0	0.0	0.0	0.0
Klebsiella	0.0	0.0	0.0	0.0	0.0
Candidatus Scalindua	0.0	0.251177394035	0.095866047953	0.0109571708849	0.104676505888
Nitrospina	0.0	0.0	0.0	0.0	0.0
Methylotenera	0.355478695297	0.740806067554	0.561933415748	0.0310549246143	0.176224075013
Azonexus	0.0	0.200698080279	0.100632387531	0.00618709397365	0.0786580826975
Asinibacterium	0.0	0.0	0.0	0.0	0.0
Pedobacter	0.0	0.251177394035	0.095866047953	0.0109571708849	0.104676505888
Gemmata	0.0	0.0	0.0	0.0	0.0
Novosphingobium	0.0828970331588	0.899550224888	0.363092176572	0.10091651263	0.317673594481
Comamonas	0.00960753230533	0.188383045526	0.0913419055733	0.00624729776874	0.0790398492454
Chlorobium	0.0	0.104657247514	0.0482121115082	0.00235829904227	0.04856232122
Thiobacillus	1.41287284144	3.01483420593	2.36463293754	0.437740892108	0.661619900024
Desulfosarcina	0.0	0.251177394035	0.0716134683605	0.0109551394677	0.104666802128
Thauera	0.450026164312	0.485051591851	0.462277489876	0.000195946954735	0.0139981053981
Gemmatimonas	0.0	0.0418628990058	0.0104657247514	0.000328594183719	0.0181271670075
Phenylobacterium	0.0	0.0418628990058	0.0104657247514	0.000328594183719	0.0181271670075
Arcobacter	0.0	0.0176382397037	0.00440955992592	5.83326562208e-05	0.00763758183071
Devosia	0.0	0.0	0.0	0.0	0.0
Ardenticatena	0.0	0.0	0.0	0.0	0.0

Methylovorus	0.0	0.0785340314136	0.0196335078534	0.00115642389189	0.0340062331329
Rhizobacter	0.0	0.0	0.0	0.0	0.0
Paraburkholderia	0.100879089206	0.167563277185	0.135151501075	0.00104874456384	0.0323843258976
Chondromyces	0.0	0.0418628990058	0.0104657247514	0.000328594183719	0.0181271670075
Bdellovibrio	0.0	0.388041273481	0.187715549315	0.032302945336	0.179730201513
Skermanella	0.0	0.0418628990058	0.0104657247514	0.000328594183719	0.0181271670075
Sulfurospirillum	0.0240188307633	0.10907504363	0.069226726617	0.000912417248318	0.0302062451873
Thiomargarita	0.0	0.0	0.0	0.0	0.0
Haloferula	0.0	0.0	0.0	0.0	0.0
Acidihalobacter	0.0	0.0959860383944	0.0556335186756	0.00160197326605	0.0400246582252
Variovorax	0.10907504363	0.3663003663	0.220424188176	0.0124292307206	0.111486459808
Thiocystis	0.0	0.00960753230533	0.00240188307633	1.73071269371e-05	0.00416018352205
Leptolyngbya	0.0	0.0	0.0	0.0	0.0
Pseudomonas	1.07123985204	8.32025117739	3.22958840939	8.81946282141	2.96975804089
Salmonella	0.0	0.0418628990058	0.01705678555	0.000244004304184	0.0156206371248
Marinobacter	0.0209314495029	0.0881911985184	0.0651486751349	0.000695146815669	0.0263656370238
Curvibacter	0.270506108202	2.41758241758	1.17700390893	0.837599104753	0.915204405995
Ruminiclostridium	0.0	0.0	0.0	0.0	0.0
Chthoniobacter	0.0	0.0523286237572	0.0130821559393	0.00051342841206	0.0226589587594
unclassified Comamonadaceae	0.213787085515	0.701203558346	0.400844309758	0.0404977803518	0.201240603139
Neochlamydia	0.0	0.309773123909	0.19178479879	0.0164578145545	0.128288014072
Desulfuromonas	0.0	0.240711669283	0.10427351658	0.0113902481684	0.106725105614
Candidatus Omnitrophus	0.0	0.230245944532	0.0641758260218	0.0093097600664	0.0964870979271
Desulforegula	0.0	0.680272108844	0.200934946692	0.0791287495885	0.281298328449
Aquabacterium	0.00960753230533	0.345368916797	0.147993822191	0.0150569290804	0.122706679037
unclassified Rhodospirillaceae	0.0	0.0	0.0	0.0	0.0
Bryobacter	0.0	0.0209314495029	0.00523286237572	8.21485459297e-05	0.00906358350376
Rhodopirellula	0.0	0.0	0.0	0.0	0.0
Gallionella	1.72935581496	3.90687009436	2.78864516339	0.726999331193	0.852642557695
Pseudogulbenkiania	0.0	0.0741710296684	0.0409664404155	0.00107289756544	0.0327551151035
Azoarcus	0.244992073786	0.352764794074	0.295337789845	0.00239347167846	0.048923120081
Candidatus Magnetomorum	0.0	0.251177394035	0.0914564880271	0.0106943045833	0.103413270828
Rhodoferax	0.270506108202	1.76870748299	0.956654160934	0.437241194645	0.661242160366
unclassified Desulfuromonadaceae	0.0	0.0	0.0	0.0	0.0
Methylophilus	0.0	0.0	0.0	0.0	0.0
Propionibacterium	0.0	0.0627943485086	0.0229042363562	0.000668864031343	0.0258624057532
Thioflavicoccus	0.0	0.0672527261373	0.0320836876425	0.00103412270768	0.0321577783387
Stenotrophomonas	0.0	0.0352764794074	0.00881911985184	0.000233330624883	0.0152751636614
Sulfuritalea	0.187609075044	0.802539906517	0.449944347001	0.0719171150769	0.26817366589
Sorangium	0.0174520069808	0.21978021978	0.0939749038996	0.00675099585056	0.0821644439558
Chromobacterium	0.0	0.0741710296684	0.0277560834957	0.000775016791458	0.027839123396
Desulfobacterium	0.0	0.0837257980115	0.0209314495029	0.00131437673487	0.036254334015

unclassified Desulfovibrionaceae	0.0	0.021815008726	0.0102575183342	0.000106061646051	0.0102986235027
Hydrogenophaga	0.028822596916	0.272108843537	0.130235963736	0.0100106670578	0.100053321073
Janthinobacterium	0.389105058366	0.617477760335	0.492984266992	0.00733429545001	0.0856405012247
Erwinia	0.0	0.0418628990058	0.0104657247514	0.000328594183719	0.0181271670075
Legionella	0.115290387664	0.313971742543	0.200704413258	0.00750713028594	0.0866436973238
Opitutus	0.0	0.0392670157068	0.0260726382574	0.000234820876021	0.015323866223
Thiothrix	0.0	0.052914719111	0.0291603324972	0.000361924954209	0.0190243253286
Paenibacillus	0.0	0.261643118786	0.0984824791409	0.0117904309208	0.108583750722
Holophaga	0.0	0.795395081109	0.339954687907	0.122237663894	0.349625033277
Geopsychrobacter	0.0	0.0	0.0	0.0	0.0
Methyloversatilis	0.087260034904	0.188383045526	0.126198403429	0.00145286770763	0.0381165017758
Noviherbaspirillum	0.0	0.0	0.0	0.0	0.0
Lautropia	0.0	0.0176382397037	0.00440955992592	5.83326562208e-05	0.00763758183071
unclassified Desulfobulbaceae	0.0	0.303506017792	0.128791223559	0.0176416664375	0.132821935077
Fimbriimonas	0.0	0.0	0.0	0.0	0.0
Ramlibacter	0.0	0.191972076789	0.0800242345009	0.0059390417174	0.0770651783713
Methylibium	0.115122972266	0.178883071553	0.146401384272	0.000757891396895	0.027529827404
Vibrio	0.0528414276793	0.177917320774	0.102736362267	0.00267226600263	0.0516939648569
Pirellula	0.0	0.0	0.0	0.0	0.0
Ralstonia	0.198848770277	0.283595113438	0.233178560721	0.000971099672968	0.0311624721896
Hymenobacter	0.0	0.0176382397037	0.00440955992592	5.83326562208e-05	0.00763758183071
Azospirillum	0.0	0.0	0.0	0.0	0.0
Chromohalobacter	0.0	0.07205649229	0.0311031283081	0.00101591816196	0.0318734711314
Geothrix	0.043630017452	2.48037676609	1.27235891628	1.44638027438	1.20265550944
Nevskia	0.0	0.0741710296684	0.0269493481843	0.000931751116267	0.0305245985439
Kouleothrix	0.0	0.0	0.0	0.0	0.0
Desulfatitalea	0.0	0.230245944532	0.0575614861329	0.00993997405749	0.0996994185414
Aromatoleum	0.0	0.44502617801	0.208587777668	0.0255950141458	0.159984418447
Acinetobacter	0.153720516885	0.324437467295	0.241381004456	0.00476924753565	0.0690597388907
unclassified Opitutaceae	0.0	0.209314495029	0.061147743609	0.00752520040866	0.0867479129931
unclassified Acidobacteriaceae	0.0192150646107	0.14652014652	0.0721843268123	0.0022996422974	0.0479545857807
Lentimicrobium	0.0	0.0	0.0	0.0	0.0
Limnohabitans	0.0192150646107	0.188383045526	0.0914458923253	0.00408725214507	0.0639316208544
Ignavibacterium	0.0	0.0	0.0	0.0	0.0
Nocardioides	0.0	0.29304029304	0.0732600732601	0.0161011150022	0.126890169053
Sphingomonas	0.161431064572	1.27877237852	0.567690824758	0.204178871153	0.451861561933
Singulisphaera	0.0	0.0	0.0	0.0	0.0
Pediococcus	0.0	0.00960753230533	0.00458338394893	2.11045450548e-05	0.00459396833411
Candidatus Brocadia	0.0	0.282574568289	0.108124901443	0.0138904815649	0.117857887156
Chlamydia	0.0	0.0	0.0	0.0	0.0
Desulfatirhabdium	0.0	0.14652014652	0.03663003663	0.00402527875055	0.0634450845263
Bacillus	0.14411298458	0.29304029304	0.204788863713	0.0036958135052	0.0607932027878
unclassified Rhodobacteraceae	0.0	0.0174520069808	0.00676488482153	5.34556395154e-05	0.00731133637001

Methyloglobulus	0.0	0.0959860383944	0.046420192597	0.00152430700616	0.0390423744944
Thermithiobacillus	0.0	0.43630017452	0.228220327596	0.027800373512	0.16673444009
unclassified Rhodocyclaceae	0.283422203007	0.460491889063	0.373707360324	0.00737811642685	0.0858959628088
Desulfocapsa	0.0	0.0418628990058	0.0104657247514	0.000328594183719	0.0181271670075
Achromatium	0.0	0.0	0.0	0.0	0.0
unclassified Methylococcaceae	0.0	0.0	0.0	0.0	0.0
Desulfosporosinus	0.0	0.0209314495029	0.00523286237572	8.21485459297e-05	0.00906358350376
Prolixibacter	0.0	0.0418628990058	0.0104657247514	0.000328594183719	0.0181271670075
Bacteroides	0.0	0.177917320774	0.0532984500455	0.00538402598049	0.0733759223485
Nitrosococcus	0.0	0.0916230366492	0.0523379882763	0.00161705243782	0.0402125905385
Mesorhizobium	0.0	0.211658876444	0.115280986601	0.00771496051037	0.0878348479271
Caldilinea	0.0	0.0	0.0	0.0	0.0
Xanthomonas	0.057645193832	0.10034904014	0.0750401652867	0.000277962420081	0.0166722050156
Herbaspirillum	0.269010904549	0.33512655437	0.313294194155	0.000726329832343	0.0269505070888
Geobacter	0.59566700293	2.48037676609	1.33182835554	0.623579505262	0.789670504237
Methylogaea	0.0	0.0	0.0	0.0	0.0
Tepidiphilus	0.0	0.0352764794074	0.0140519822276	0.000223180689894	0.0149392332432
Arthrobacter	0.0	0.188383045526	0.0470957613815	0.0066540322203	0.0815722515339
Sulfurimonas	0.182543113801	0.879120879121	0.506475211463	0.0635320440994	0.252055636912
Streptococcus	0.0	0.0	0.0	0.0	0.0
Syntrophobacter	0.0	0.115122972266	0.0287807430665	0.00248499351437	0.0498497092707
Hyphomicrobium	0.0	0.0	0.0	0.0	0.0
Draconibacterium	0.0	0.0	0.0	0.0	0.0
Dehalogenimonas	0.0	0.0418628990058	0.0104657247514	0.000328594183719	0.0181271670075
Fusibacter	0.0	0.0	0.0	0.0	0.0
Bradyrhizobium	0.177739347649	0.868655154369	0.491497631191	0.0977188559238	0.312600153429
Candidatus Saccharimonas	0.0	0.690737833595	0.172684458399	0.0894597665174	0.299098255624
Intrasporangium	0.0	0.0	0.0	0.0	0.0
Rhodanobacter	0.0523286237572	0.07205649229	0.0639817457333	5.99988581873e-05	0.00774589298837
Prevotella	0.0	0.0	0.0	0.0	0.0
Thiohalocapsa	0.0	0.00960753230533	0.00240188307633	1.73071269371e-05	0.00416018352205
Halomonas	0.0	0.0176382397037	0.00440955992592	5.83326562208e-05	0.00763758183071
Methylococcus	0.0	0.057645193832	0.0275003036936	0.000759763621972	0.0275638100046
Fluviicola	0.0	0.136054421769	0.0340136054422	0.00347077606553	0.0589132927745
Syntrophus	0.0	0.701203558346	0.223806048772	0.0822434619629	0.286781209222
Pandoraea	0.0	0.0209314495029	0.00523286237572	8.21485459297e-05	0.00906358350376
Nitrobacter	0.0	0.0305410122164	0.0136399607449	0.000191365885487	0.0138335059
Treponema	0.0	0.167451596023	0.0462724589317	0.00494664567204	0.0703323941868
Ktedonobacter	0.0	0.0	0.0	0.0	0.0
Candidatus Koribacter	0.0	0.0352764794074	0.00881911985184	0.000233330624883	0.0152751636614
Syntrophorhabdus	0.0	0.125588697017	0.0358067341802	0.00273878486693	0.0523334010641
unclassified Syntrophaceae	0.0	0.816326530612	0.330739606109	0.110362635801	0.332208723247
Nitrosospira	0.29304029304	0.396860393333	0.345982615041	0.00140618699332	0.0374991599015

unclassified Peptococcaceae	0.0	0.115122972266	0.0287807430665	0.00248499351437	0.0498497092707
Rhizobium	0.028822596916	0.114648558074	0.0655252417408	0.00125727604599	0.0354580885835
Herpetosiphon	0.0	0.0	0.0	0.0	0.0
Aeromonas	0.0	0.115122972266	0.0331903029924	0.00228950534807	0.0478487758262
Candidatus Accumulibacter	2.13500784929	2.75741710297	2.50239716405	0.051611158995	0.227180894872
Rhodococcus	0.00960753230533	0.879120879121	0.241978564342	0.13571174045	0.368390744251
Leptothrix	0.0	0.0	0.0	0.0	0.0
Zavarzinella	0.0	0.0	0.0	0.0	0.0
Brevundimonas	0.0176382397037	0.104657247514	0.0420323316768	0.00131254454233	0.0362290566028
Rickettsiella	0.0	0.0	0.0	0.0	0.0
Microcystis	0.0	0.0	0.0	0.0	0.0
Ornatilinea	0.0	0.0	0.0	0.0	0.0
Enterobacter	0.0	0.0	0.0	0.0	0.0
unclassified Hydrogenophilaceae	0.21978021978	0.912715569006	0.629127993218	0.0818945334811	0.286172209484
Gemmatirosa	0.0	0.00960753230533	0.00458338394893	2.11045450548e-05	0.00459396833411
Pseudorhodobacter	0.0	0.0	0.0	0.0	0.0
Dyella	0.0	0.00960753230533	0.00240188307633	1.73071269371e-05	0.00416018352205
Segetibacter	0.0	0.0	0.0	0.0	0.0
Myxococcus	0.0	0.0418628990058	0.0104657247514	0.000328594183719	0.0181271670075
Ideonella	0.0	0.0	0.0	0.0	0.0
Achromobacter	0.120094153817	5.82940868655	1.63254200129	5.88877113857	2.42667903493
Shewanella	0.0209314495029	0.043630017452	0.0309641942814	8.19782304465e-05	0.00905418303584
Deinococcus	0.0	0.0418628990058	0.012647225624	0.000297209046535	0.0172397519279
Spirosoma	0.0	0.0	0.0	0.0	0.0
Streptomyces	0.043233895374	0.774463631606	0.317749398479	0.0854686727482	0.292350256966
Alkanindiges	0.0	0.0837257980115	0.0209314495029	0.00131437673487	0.036254334015
Desulfobacula	0.0	0.230245944532	0.0575614861329	0.00993997405749	0.0996994185414
Pyrinomonas	0.0	0.0	0.0	0.0	0.0
Methylobacterium	0.0	0.0418628990058	0.0104657247514	0.000328594183719	0.0181271670075
Clostridium	0.0	0.240711669283	0.0954543967281	0.010351705075	0.101743329388
Sphingopyxis	0.0	0.167563277185	0.0763763900151	0.00359563827267	0.0599636412559
Calothrix	0.0	0.043630017452	0.0169122120538	0.000334097746971	0.018278340925
Collimonas	0.167451596023	0.196954412259	0.179941148308	0.0001422099426	0.0119251810301
Cellulomonas	0.0	0.0523286237572	0.0130821559393	0.00051342841206	0.0226589587594
Candidatus Magnetoglobus	0.0	0.0313971742543	0.00784929356358	0.000184834228342	0.0135953752556
Verrucomicrobium	0.0	0.0	0.0	0.0	0.0
Microbacterium	0.0	0.14652014652	0.03663003663	0.00402527875055	0.0634450845263
Anaerolinea	0.0	0.0523286237572	0.0130821559393	0.00051342841206	0.0226589587594
Massilia	0.196335078534	0.554683411826	0.323768056664	0.0194001716375	0.139284498913
Caldimonas	0.0	0.00960753230533	0.00240188307633	1.73071269371e-05	0.00416018352205
Desulfobacter	0.0	0.156985871272	0.0392464678179	0.00462085570854	0.0679768762782
Chryseobacterium	0.0	0.0732600732601	0.0315436980928	0.0010467465688	0.0323534630109
Candidatus Entotheonella	0.0	0.0418628990058	0.0104657247514	0.000328594183719	0.0181271670075

Tetrasphaera	0.0	0.136054421769	0.0340136054422	0.00347077606553	0.0589132927745
unclassified Gallionellaceae	0.134505452275	0.555604550666	0.350265027482	0.0241869105561	0.155521415104
Nitrospira	0.0261780104712	0.177917320774	0.0937030645611	0.00404886893235	0.0636307231796
Pelosinus	0.0	0.0	0.0	0.0	0.0
Desulfatiglans	0.0	0.0209314495029	0.00523286237572	8.21485459297e-05	0.00906358350376
Candidatus Symbiobacter	0.0698080279232	0.167451596023	0.108393051654	0.00143257199184	0.0378493327794
Candidatus Magnetobacterium	0.0	0.198848770277	0.0827838920137	0.00740698479982	0.0860638414192
Staphylococcus	0.0	0.0418628990058	0.0104657247514	0.000328594183719	0.0181271670075
Corynebacterium	0.0	0.0	0.0	0.0	0.0
Caldithrix	0.0	0.0	0.0	0.0	0.0
Marinobacterium	0.0	0.0384301292213	0.0161520349231	0.000279652533891	0.0167228147718
Desulfococcus	0.0	0.387231815803	0.121060533543	0.0251842174783	0.158695360607
Deferrisoma	0.0	0.272108843537	0.090075010514	0.0123417200378	0.111093294297
Methylomonas	0.264207138397	0.648874934589	0.440298493326	0.0298883410331	0.172882448598
Caballeronia	0.0	0.0	0.0	0.0	0.0
Halobacteriovorax	0.0	0.0	0.0	0.0	0.0
Pseudorhodoferax	0.0	0.0	0.0	0.0	0.0
Spirochaeta	0.0	0.0349040139616	0.0223654566333	0.000196573365122	0.0140204623719
Delftia	0.0	0.0	0.0	0.0	0.0
Thioalkalivibrio	0.124897919969	0.167563277185	0.138325737068	0.000301703398499	0.0173696113514
Leptospira	0.0	0.21978021978	0.0902215343524	0.00891363098827	0.0944120277733
unclassified Geobacteraceae	0.201758178412	1.52799581371	0.67658709666	0.291806099897	0.54019079953
Frankia	0.0	0.0	0.0	0.0	0.0
Methylocaldum	0.0	0.0	0.0	0.0	0.0
Schlesneria	0.0	0.0	0.0	0.0	0.0
Acidovorax	0.682134793678	2.51177394035	1.27347249691	0.525754437686	0.725089261874
Melioribacter	0.0	0.0418628990058	0.0104657247514	0.000328594183719	0.0181271670075
Anaeromyxobacter	0.0	0.586080586081	0.237113228115	0.0607837565518	0.246543619978
Leptolinea	0.0	0.0	0.0	0.0	0.0
Labilithrix	0.0	0.094191522763	0.0235478806907	0.00166350805508	0.0407861257669
Desulfovibrio	0.0672527261373	0.470957613815	0.20491931108	0.0270072369273	0.164338787045
Sulfuricella	14.0136054422	70.8699620502	47.5662800621	502.439274781	22.4151572553
Macellibacteroides	0.0	0.0	0.0	0.0	0.0
Polynucleobacter	0.0	0.156985871272	0.0745229472253	0.0055851912791	0.0747341373075
Roseiflexus	0.0	0.0	0.0	0.0	0.0
Candidatus Tenderia	0.0	0.0705529588147	0.0357387099072	0.000976033333954	0.031241532196
Beggiatoa	0.0	0.0418628990058	0.0104657247514	0.000328594183719	0.0181271670075
Sideroxydans	0.984772061296	2.09895052474	1.58112534461	0.169322021202	0.411487571139
Niastella	0.0	0.0523286237572	0.0130821559393	0.00051342841206	0.0226589587594
Leifsonia	0.0	0.0209314495029	0.00523286237572	8.21485459297e-05	0.00906358350376
Actinoplanes	0.0	0.0	0.0	0.0	0.0
Burkholderia	1.1198325484	1.55759162304	1.29249314042	0.0273471472935	0.165369729073
Andreprevotia	0.0	0.0816640245953	0.0378680131296	0.00145155700052	0.0380993044624
Duganella	0.0	0.105829438222	0.0441234070458	0.00148501271769	0.0385358627474

Candidatus Contendobacter	0.0	0.0523560209424	0.0271060974668	0.000397543295301	0.0199384877887
Dechloromonas	0.59566700293	1.37100994244	1.0305333314	0.0926122193239	0.304322558027

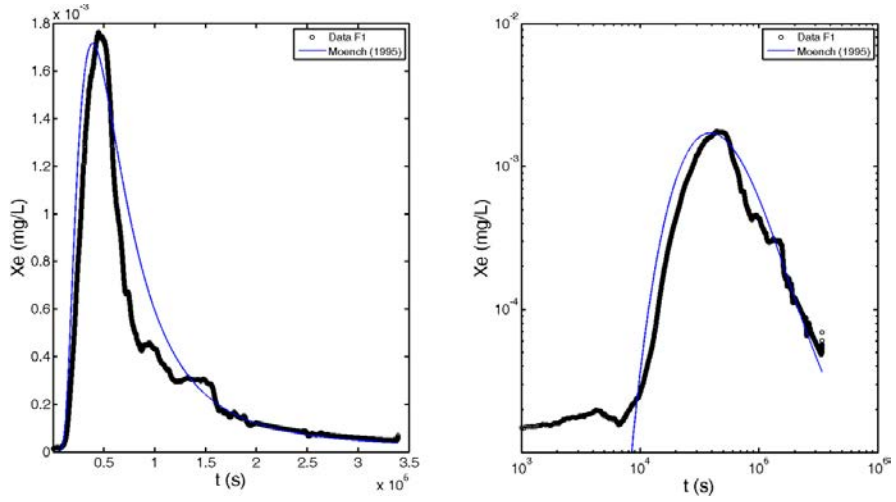

Figure 36: Fitted transport model to Xe BTC using Moench' solution.

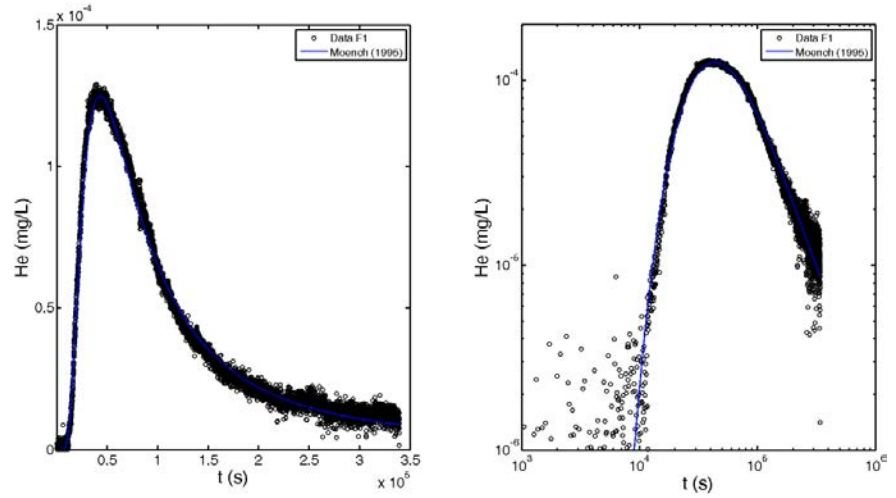

Figure 37: Fitted transport model to He BTC using Moench' solution.

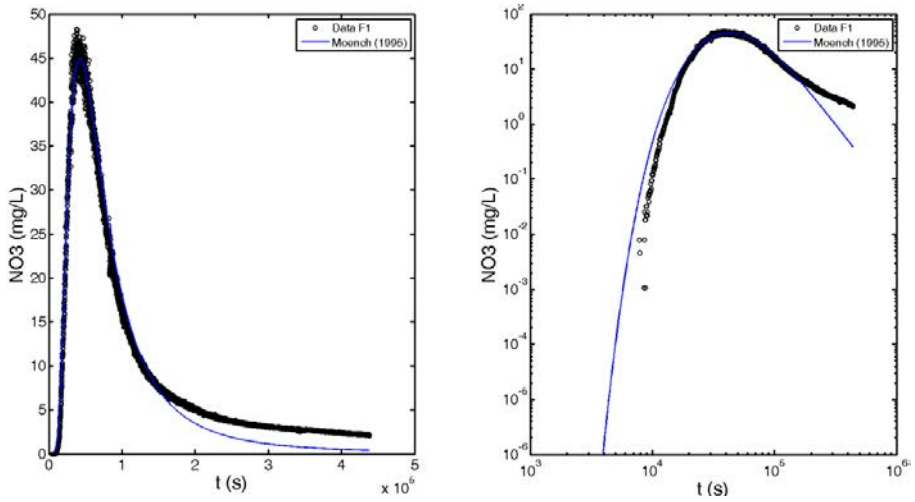

Figure 38: Fitted reactive transport model to nitrate BTC using Moench's solution combined with a first order kinetic reaction.

Abstract:

For more than a century, global change has led to a profound modification of our societies, our lifestyles and, of course, our environment. This trajectory followed willy-nilly by all mankind has consequences for natural systems and already seems to lead the future generations ahead of serious challenges. In order not to compromise our ability to meet these future ordeals, and because of the urgent need for action, part of the scientific community has chosen to concentrate on the near-surface environment that supports terrestrial life: the Critical Zone. The emergence of this concept underlines the need to develop multidisciplinary scientific approaches integrating a wide variety of temporal and spatial scales. As the link between the different compartments of the Critical Zone (Atmosphere, Biosphere, Hydrosphere, Lithosphere and Pedosphere), water is an essential molecule controlling the exchanges of energy and matter whose dynamics require special attention. In view of the diversity and spatiotemporal variability of water and matter transfers arising in aquatic environments, new methods of investigation are needed.

The general objective of this thesis is to describe the interest and the potential lying in the use of dissolved gases, especially when they are measured at high frequency in the field, in order to characterise the hydrobiogeochemical dynamics of the natural waters of the Critical Zone at different spatial and temporal scales. To perfect this ambition, this work focused first on the development of an innovative instrumentation, then, on the implementation of novel tracers integrated into original experimental setups and finally, on the acquisition, processing and analysis of dissolved gas datasets focusing on groundwater.

This thesis therefore provides new tools for observing and understanding the functioning of aquatic environments including the origin of water masses, their residence time, the potential exchanges between hydrological compartments as well as solute transport and biogeochemical reactions occurring in aquatic environments.

Résumé:

Depuis plus d'un siècle, les changements globaux sont à l'origine de profondes modifications de nos sociétés, nos modes de vie et il en va bien sûr de même pour notre environnement. Cette trajectoire empruntée, bon gré mal gré, par l'ensemble de l'humanité n'est pas sans conséquences pour les systèmes naturels et semble déjà mener les générations futures au-devant de grands défis. Afin de ne pas compromettre notre capacité à relever ces épreuves futures et, devant l'urgence du besoin d'action, une partie de la communauté scientifique a choisi de concentrer ses efforts sur la couche superficielle de notre planète qui soutient la vie terrestre : la Zone Critique. L'émergence de ce concept souligne la nécessité de développer des approches scientifiques pluridisciplinaires intégrant une large variété d'échelles de temps et d'espace. En tant que lien entre les différents compartiments de la Zone Critique (Atmosphère, Biosphère, Hydrosphère, Lithosphère et Pédosphère), l'eau est une molécule essentielle aux échanges d'énergie et de matière dont la dynamique requiert une attention particulière. Compte tenu de la diversité et de la variabilité spatiotemporelle des transferts d'eau et de matière dissoute dans les milieux aquatiques, de nouvelles méthodes d'investigations sont nécessaires.

L'objectif général de cette thèse est de décrire l'intérêt et le potentiel qui résident dans l'utilisation des gaz dissous, en particulier lorsqu'ils sont mesurés à haute fréquence sur le terrain, afin de caractériser la dynamique hydrobiogéochimique des eaux naturelles de la Zone Critique à différentes échelles spatiales et temporelles. Pour parfaire cette ambition, ce travail s'est tout d'abord attaché au développement d'une instrumentation innovante puis, au déploiement de nouveaux traceurs intégrés dans des dispositifs expérimentaux originaux et enfin, à l'acquisition, au traitement et à l'analyse de jeux de données de gaz dissous en se focalisant sur les eaux souterraines.

Cette thèse apporte donc de nouveaux outils d'observation et de compréhension du fonctionnement des milieux aquatiques notamment l'origine des masses d'eau, leur temps de résidence, les échanges entre compartiments hydrologiques, le transport d'éléments et les réactions biogéochimiques qui se produisent dans les milieux aquatiques.

Contribution des Gaz Dissous à la Compréhension de la Dynamique Hydrobiogéochimique des Eaux Souterraines

Depuis plus d'un siècle, les changements globaux sont à l'origine de profondes modifications de nos sociétés, nos modes de vie et il en va bien sûr de même pour notre environnement. Cette trajectoire empruntée, bon gré mal gré, par l'ensemble de l'humanité n'est pas sans conséquences pour les systèmes naturels et semble déjà mener les générations futures au-devant de grands défis. Afin de ne pas compromettre notre capacité à relever ces épreuves futures et, devant l'urgence du besoin d'action, une partie de la communauté scientifique a choisi de concentrer ses efforts sur la couche superficielle de notre planète qui soutient la vie terrestre : la Zone Critique. L'émergence de ce concept souligne la nécessité de développer des approches scientifiques pluridisciplinaires intégrant une large variété d'échelles de temps et d'espace. En tant que lien entre les différents compartiments de la Zone Critique (Atmosphère, Biosphère, Hydrosphère, Lithosphère et Pédosphère), l'eau est une molécule essentielle aux échanges d'énergie et de matière dont la dynamique requiert une attention particulière. Compte tenu de la diversité et de la variabilité spatiotemporelle des transferts d'eau et de matière dissoute dans les milieux aquatiques, de nouvelles méthodes d'investigations sont nécessaires.

L'objectif général de cette thèse est de décrire l'intérêt et le potentiel qui résident dans l'utilisation des gaz dissous, en particulier lorsqu'ils sont mesurés à haute fréquence sur le terrain, afin de caractériser la dynamique hydrobiogéochimique des eaux naturelles à différentes échelles spatiales et temporelles. Pour parfaire cette ambition, ce travail s'est tout d'abord attaché au développement d'une instrumentation innovante puis, à la mise en place de nouveaux traceurs intégrés dans des dispositifs expérimentaux originaux et enfin, à l'acquisition, au traitement, à l'analyse et à l'interprétation de différents jeux de données de gaz dissous en se focalisant sur un objet : les réservoirs d'eaux souterraines aussi appelés aquifères.

Dans un premier temps, cette thèse a consisté à développer un outil innovant permettant la mesure en continu sur le terrain d'une grande variété de gaz dissous. En raison du potentiel et de la polyvalence de ces traceurs, le CF-MIMS s'est avéré un outil utile pour la caractérisation *in situ* de l'origine des eaux souterraines, de la distribution de leurs temps de résidence, de leur réactivité biogéochimique et des propriétés de leur transport dans les aquifères. Cette technique innovante améliore à la fois la distribution spatio-temporelle et la qualité des données de gaz dissous et apporte une contribution de l'hydrogéochimie au concept d'hydrologie opérationnelle. Cette nouvelle technique de mesure haute fréquence de terrain est maintenant plus largement déployée dans la Zone Critique sur des expériences de quelques heures à plusieurs semaines pour caractériser les milieux aquatiques à travers leur réactivité biogéochimique, leur propriétés de transport, leur distribution de temps de résidence ainsi que les échanges entre les eaux de surface et les eaux souterraines.

Dans un second temps, cette thèse a consisté à caractériser la dynamique naturelle d'un système aquifère côtier en milieu urbain ainsi que l'impact anthropique de son exploitation à l'échelle du bassin versant. L'information intégrative dérivée des traceurs gazeux dissous a permis l'identification des chemins d'écoulement et du mélange des eaux souterraines ainsi que la caractérisation de la distribution de leur temps de résidence et l'enregistrement de leurs conditions de recharge. La collecte et l'analyse de ces données environnementales fournissent des informations importantes pour la gestion de la quantité et de la qualité des ressources en eau (approvisionnement en eau, gestion de la contamination/salinisation, protection des écosystèmes) et pour l'étude du climat et de son évolution. Ce travail montre que la mise en œuvre d'une approche multi-traceurs relativement simple peut fournir des informations utiles sur des systèmes aquifères complexes à condition qu'un échantillonnage adéquat soit assuré (nombre d'échantillons, distribution spatio-temporelle des données). Naturellement, ces approches nécessitent un perfectionnement continuel des techniques analytiques sans altérer leur simplicité ainsi que l'intégration d'une plus grande variété de traceurs relativement accessibles (tels que l'^{4}He). De plus, les résultats des différentes investigations du projet COQUEIRAL démontrent les avantages d'une approche «hydro-sociologique» intégrée pour fournir des informations exhaustives aussi bien aux gestionnaires de l'eau qu'aux reste des utilisateurs, en particulier lorsque la gestion de l'eau est déficiente. En fin de compte, il semble maintenant essentiel que la recherche académique comprenne et accepte une part de la «responsabilité de l'intendance de la planète» en assurant une plus grande disponibilité des

résultats de la recherche pour le public et tous les responsables de la gestion environnementale.

Enfin, cette thèse a porté sur la caractérisation simultanée des processus physiques et biogéochimiques contrôlant le transport de solutés dans des aquifères hétérogènes à l'échelle de la fracture à l'aide de traceurs gazeux dissous. Les données de gaz nobles dissous ont permis de caractériser les propriétés de transport physiques dominantes des milieux fracturés et de prédire le transport réactif des nitrates dans un réseau de fractures. La surveillance continue de la chimie des eaux souterraines et de la microbiologie a permis d'identifier les minéraux réactifs impliqués dans la réaction de dénitrification induite par des microorganismes autotrophes. La disponibilité soudaine de nutriments dans le milieu fracturé anoxique a entraîné des modifications significatives des communautés de microorganismes, en particulier une croissance rapide et abondante de bactéries dénitrifiantes et oxydantes du soufre. Ce travail en cours ouvre déjà de nouvelles opportunités pour l'étude du transport de solutés en milieux aquatiques notamment l'étude des processus diffusifs, l'étude de l'impact des réactions biogéochimiques aquatiques dans le cycle global du soufre, du carbone et de l’azote ainsi que l'évaluation de la réponse des microorganismes aux stress naturels et anthropiques.

En conclusion, parmi les différentes familles de traceurs, les gaz dissous comportent de nombreux avantages. En raison de la polyvalence de leurs propriétés physiques et biogéochimiques, ils permettent la compréhension de divers processus physiques, chimiques et biologiques se produisant à différentes échelles spatiales et temporelles dans l'Hydrosphère. Bon nombre de ces traceurs gazeux dissous peuvent être mesurés avec les mêmes techniques analytiques qui bénéficient maintenant de progrès technologiques clés qui permettent aux géochimistes de quitter le laboratoire et de converger avec le reste de la communauté scientifique environnementale vers l'exploration approfondie de la ZC. Dorénavant, dans l’observation de la Zone Critique, si nos instruments sont des yeux qui deviennent plus perçants, si nos mesures sont des images qui deviennent plus nettes, alors il ne reste plus qu'à se promener et tourner la tête dans la bonne direction.

Mots clés : Hydrogéologie ; Géochimie ; Zone Critique ; Eaux souterraines ; Milieux fracturés ; Hydrochronologie ; Traçage ; Datation ; Transport ; Réactivité biogéochimique ; Gaz dissous ; Gaz nobles ; Instrumentation innovante ; Mesure haute fréquence ; Mesure in situ.